A NOVEL FRP ANCHOR FOR PREVENTING DELAMINATION IN FRP STRENGTHENED CONCRETE BEAMS

By

AHMED ABO EL-KHAIR BAYOUMY MOSTAFA
B.Sc., M.A. Sc., P.Eng.

A Thesis

Submitted to the School of Graduate Studies

in Partial Fulfillment of the Requirements

for the Degree

Doctor of Philosophy

McMaster University

October 2010

DOCTOR OF PHILOSOPHY (2010) McMaster University

(Civil Engineering) Hamilton, Ontario

TITLE: A Novel FRP Anchor for Preventing Delamination in FRP Strengthened Concrete Beams

AUTHOR: Ahmed Abo El-Khair Bayoumy Mostafa,
B.Sc. (Ain Shams University)
M.A.Sc (Carleton University)

ADVISOR:Dr. A.G.Razaqpur

NUMBER OF PAGES: xviii, 288.

ABSTRACT

To delay the delamination of the externally bonded Fiber Reinforced Polymer (FRP) laminate from the concrete surface and to ensure that after initial delamination the FRP continue to carry some load, a new FRP mechanical anchor system was developed and tested to delay complete delamination in RC beams externally strengthened with FRP laminate. The anchor will be akin to a nail with a relatively flat and wide head and a small diameter shank. It will be inserted into epoxy-filled drilled holes in the concrete while its head will rest on the surface of the FRP laminate and will be adhesively bonded to it. The advantage of this anchor is the ease with which it can be used in different structural elements involving flexural and/or shear strengthening with FRP laminates. The salient feature of the anchor is its wide head to resist high interfacial shear stresses and its shanks that are inserted inside the concrete to provide mechanical anchorage and to resist pullout.

A number of full scale RC beams, retrofitted with FRP sheets or laminates will be tested to verify the validity of the concept and the effectiveness of the proposed anchor in delaying/preventing delamination. Different oriented models will be used to calculate the capacity of the tested beams. Finally, a modified model to predict the interfacial shear and normal stresses with and without tension stiffness is presented. The proposed anchor system can eliminate the delamination problem in beams retrofitted for increased flexural strength. It could increase the delamination load and allowed the FRP laminate to reach its full ultimate strength.

DEDICATIONS

To my Mother & Father.

To my Brother and Sister.

ACKNOWLEDGMENTS

All praise and gratitude be to
ALLAH the Most Gracious, the Most Compassionate and the Most Merciful
with the blessings of Whom the good deeds are fulfilled.

I wish to express my deep gratitude to my supervisor Dr. A. Ghani Razaqpur for his interest, insight throughout this research, advices, encouragement, patience, and endless support throughout the research steps and innovative ideas. I am especially grateful for our long discussions that significantly impacted the quality of the dissertation. I believe this research would not have been completed in this way without his sincere guidance and continuous support. Also, I would like to thank him for the funding provided throughout this research.

Special thanks are due to my supervisory committee members, Dr. K.S. (Siva) Sivakumaran and Dr. Wael W. El-Dakhakhni, Dr. Philip. Koshy and Dr. Michael J. Tait for their valuable advice and suggestions. Their helpful comments and discussions during our meetings are greatly appreciated

A word of thanks is due to the Applied Dynamics Laboratory team Mr. David Perrett and Mr. Kent Wheeler for their unwavering help, support and flexibility during my experimental program. I would also like to thank all of my friends and colleagues, Marawan Shedid, Amr Nasr, Badr Abou Zeid, Bennett Banting, Joe Wizbeski, Kevin Hughes,Tom Kasparik for their help and useful discussions during all stages of my experimental and analytical studies. A special thanks to Manuel Campidelli for his valuable and tremendous help to learn Matlab.

I would like to give the administrative assistance and my colleagues in the Civil Department warm thanks for their support and help whenever asked for. Words are not enough to thank my family, especially my parents, brother and sister for their patience, care, support and for everything they did, and are still doing for me. Without their continuous support, love, prayer and encouragement throughout my life I would have never been the one I am now. Many thanks to my Uncle, Dr. Saaid

Osman and his wife Annette Poirier for their care and support since I arrived to Canada.

TABLE OF CONTENTS

CHAPTER 1- Introduction

CHAPTER 2- Literature Review

CHAPTER 3- Experimental Program

CHAPTER 4- Experimental Results

LIST OF TABLES

LIST OF FIGURES

CHAPTER 1
INTRODUCTION

1.1 General

The need for new strengthening techniques has emerged as a result of increased live load on bridges over the past few decades or due to more stringent design requirements for earthquake and other severe loads acting on structures. Strengthening of reinforced concrete members by externally bonded Fiber Reinforced Polymer (FRP) laminates is now an established practice, but premature delamination of the FRP from the concrete surface is a concern. The phenomenon is complicated since it is affected by various factors, such as concrete cracking and stress concentrations at the concrete-FRP interface which makes it difficult to predict the ultimate strength of FRP retrofitted structures.

The numerous advantages of using FRP include ease of application, high ultimate strength, which greatly exceeds that of steel rebars, and lack of corrosion. The high strength and stiffness of FRP make it possible to use it as reinforcement for concrete members. Unlike steel rebars, FRP materials, particularly carbon FRP (CFRP), are unaffected by electrochemical deterioration and they can resist acids, salts, and similar aggressive chemicals under a wide range of temperatures and other severe conditions. The specific gravity of the FRP is generally one-fourth that of the steel which allows reduction in the transportation costs and easier handling on construction site.

The failure modes of FRP-strengthened beams can be broadly divided into two main types: sectional failures and debonding failures. The sectional failure consists of either compression failure of concrete, once the concrete strain reaches its limiting strain or rupture of the FRP laminate once it reaches its ultimate strength. Both cases can be easily predicted using the conventional beam theory in conjunction with strain compatibility. The debonding failure is considered more difficult to predict due to the complexity of the failure mechanisms. These include delamination at the FRP laminate epoxy adhesive interface, the adhesive-concrete interface, the separation of the concrete cover at the reinforcement level. These mechanisms are triggered by a complex set of mixed stresses at the above mentioned interfaces and in the concrete cover. Quantifying these stresses is quite difficult due to the stress risers occurring at cracks and flaws at the interfaces and the brittle nature of the materials involved. When FRP is used for post-strengthening and repair of deficient reinforced concrete members, it is generally in the form of sheets/laminates adhesively bonded to the concrete surface. The adhesive is generally epoxy-based while the sheets/laminates comprise either carbon or glass fibres. The effectiveness of this retrofit technique depends mainly on the stress transfer performance and strength of the FRP-concrete interface. Premature failure at the interface causes delamination at the epoxy- concrete, or epoxy-FRP interface, and in both cases once delamination initiates, it propagates rapidly, the FRP separates from the concrete and becomes ineffective. To prevent, or rather delay, delamination, different techniques are being used and/or developed. Currently, FRP U-shape straps, akin to U-stirrups in conventional reinforced concrete, are glued to the tension face and sides of beams. Such a system works relatively well, provided the surface concrete is undamaged and is able to transfer the resulting shear and normal stresses.

For members where the surface concrete is weathered and/or damaged, this method may not be feasible because the interface between the concrete and the epoxy will fail at relatively low loads. In the latter case, it may be more appropriate to use mechanical anchors which can be embedded deep inside the beam in the more sound concrete. Steel stud anchors have already been effectively used by some researchers for this purpose, but the disadvantage of steel studs is their vulnerability to corrosion in severe environments. Other techniques such as mechanical fasteners, fan and spike anchors have been used in many investigations. These techniques have shown increase in the capacity of retrofitted beams in some cases while in other cases they have had a negligible effect on the delamination load.

A requirement for applying such anchors in practice is the development of a simple and relatively accurate method to predict the stresses at the interface between the concrete and the FRP laminate. To date, many methods have been proposed but none of these can be used to determine the number and disposition of the anchors, even if the anchor mechanical properties and strength were given. In the opinion of the writer, the development of a simple, design oriented, method for finding interfacial stresses is essential for dealing with the delamination problem.

1.2 Problem Definition

To be able to identify the problem, let us consider the simply supported beam, loaded in four point bending, with the corresponding bending moment and shear force diagrams shown in Fig.1-1

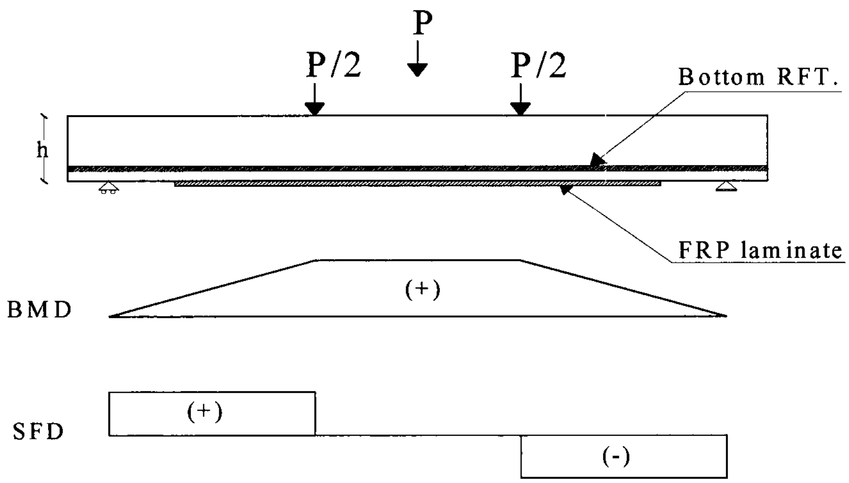

Fig.1-1: Bending moment and shear force diagrams for beam loaded in four point bending

The shear stress τ at the interface between the concrete and the FRP laminate can be calculated based on elastic theory as:

$$\tau = \frac{VQ}{Ib} \qquad \text{Eq.1-1}$$

where V is the shear force , Q is the first moment of area, I is the second moment of area and b is the cross section width. The shear force in the zone of maximum moment is zero; therefore, based on this simple theory the shear stress is also zero. Notice that the elastic theory does not take into account the crack locations and the local stresses associated with crack opening, or the so-called stress concentrations at the crack tip. Furthermore, the tensile stress in the concrete after cracking is considered equal to zero. The shear stress in the zone of maximum moment is zero which makes it hard to relate delamination at the zone of maximum moment to the interfacial shear stresses due to external loading. This makes the intermediate crack debonding phenomena hard to explain and even harder to predict.

To be able to identify the reasons for delamination in the zone of maximum moment, consider element A in Fig.1-2 between two cracks in the zone of maximum moment. The tensile stresses in the concrete at the crack are zero since it is a free surface and in between the cracks, they vary in a parabolic fashion reaching a maximum between the two cracks. These tensile stresses are transferred by bond stresses between the reinforcement and the concrete and the phenomenon is referred to as tension stiffening.

A similar situation exists at the interface between the concrete and the FRP. The shear stress distribution between the cracks rises rapidly, depending on the tensile stress variation between the cracks. The local stresses may be significantly different from the average stress and it is believed that due to the brittle nature of the materials involved, these local stress concentrations lead to delamination.

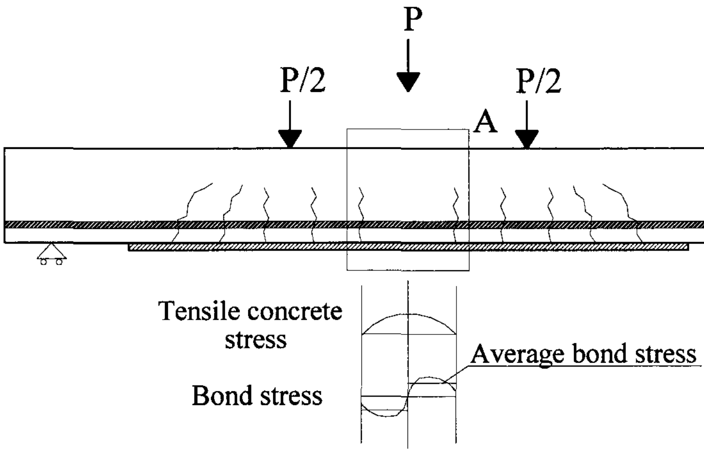

Fig.1-2: Tensile and bond stresses distribution between two adjacent cracks

Cracks appear in the zone of maximum moment, and with increased loading, the crack width increases. Two movements may be considered at the crack location: crack opening and sliding. Relative displacement or slip between the two faces of the crack cause shear stress at the interface of the FRP and concrete. Since concrete is considered the weakest element in the concrete, FRP and epoxy system, when the shear stress exceeds the shear strength of concrete, failure occurs. The normal forces at the interface might arise from the rigid body rotation of concrete, causing local normal stress concentration at the crack face as shown in Fig.1-3. Both the horizontal and vertical crack displacements cause stress concentration and tend to initiate delamination. None of the available elastic theories consider the effect of crack spacing and crack movements on delamination.

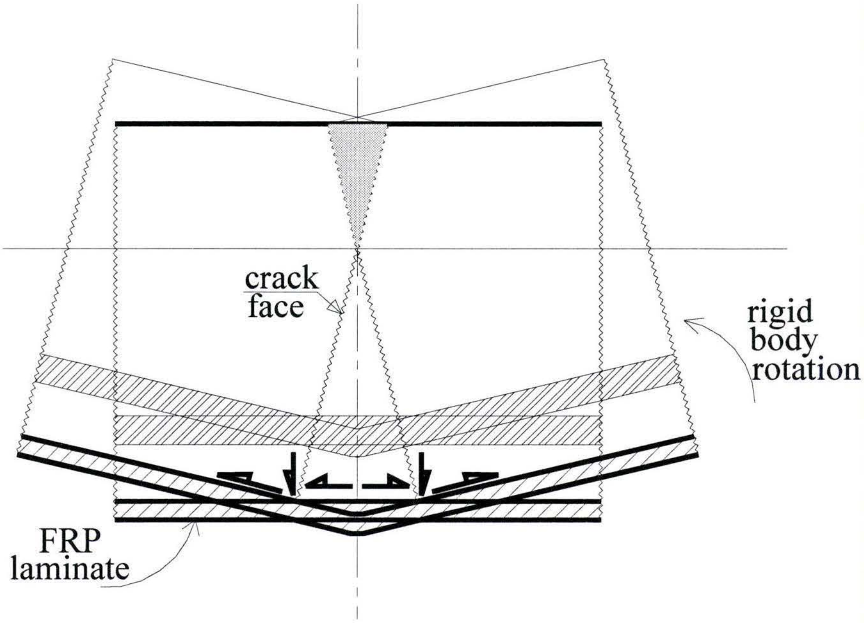

Fig.1-3: Flexural rigid body deformation

Curvature variation along a cracked reinforced concrete beam is another issue to consider and since the stress in the FRP is a function of the curvature of the beam at any section, sudden changes in curvature can cause rapid changes in the FRP stress and rapid increase in shear stresses at the interface. This is illustrated in Fig.1-4(a), where we can see that due to the change in curvature, the force T in the FRP laminate changes and as a consequence normal stress σ_n is needed to equilibrate the vertical component of the tensile force T. Similarly, the horizontal component of the increase in T is equilibrated by the shear stress τ along the interface. These interface stresses are responsible for the FRP laminate delamination.

When the laminate is anchored as in Fig.1-4(b), normal stress σ_a and shear stress τ_a are developed in the anchor legs. The laminate transfers some of the shear to the anchor head at the contact surface between the two and this shear partially to the concrete at its contact surface with the concrete as illustrated in Fig.1-4 (c). Hence, the anchor reduces the shear stress intensity at the laminate-concrete interface. It also assists in resisting peeling stresses.

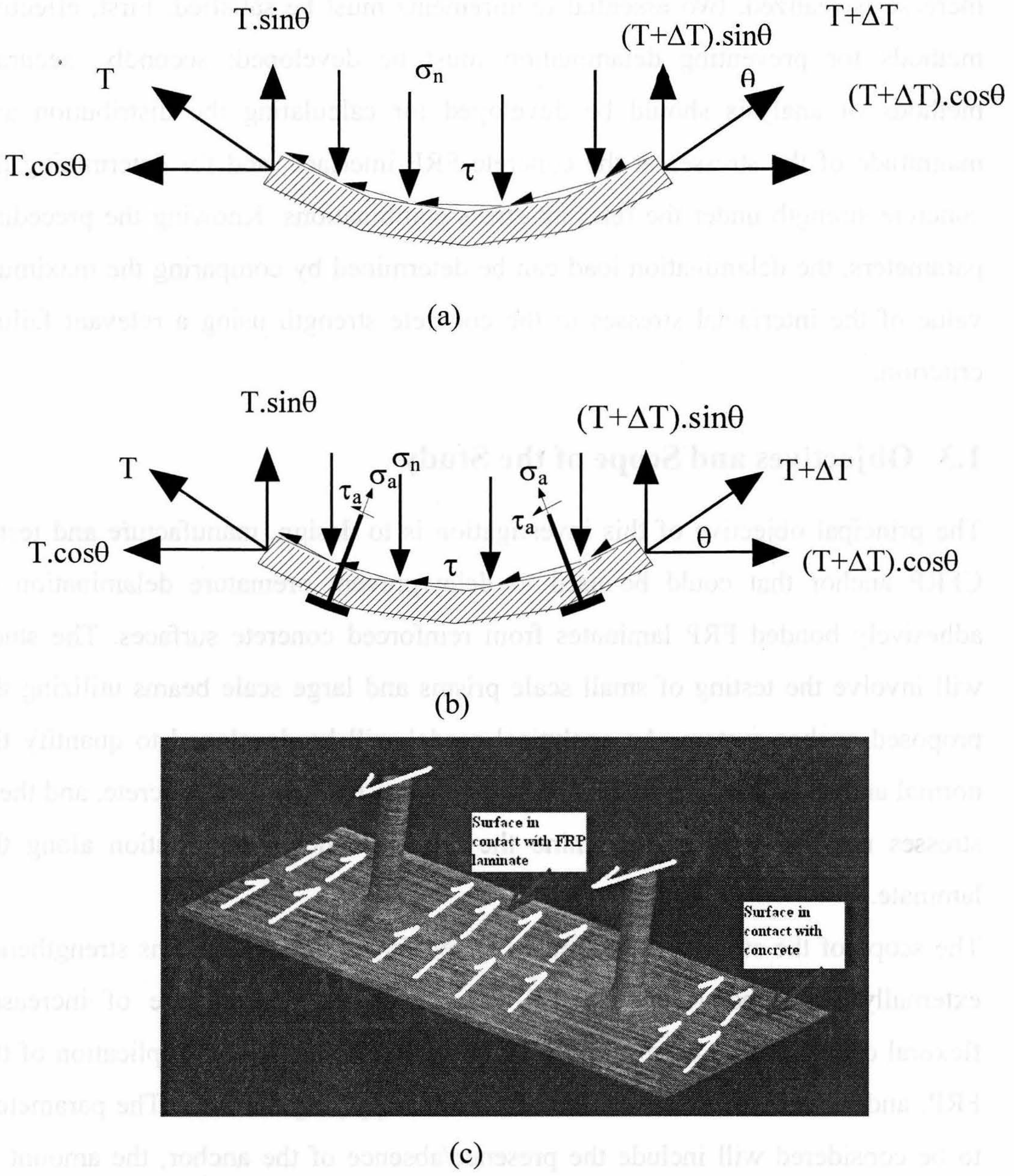

Fig.1-4: FRP segment subjected to axial force in the zone of maximum moment (a) segment without FRP anchor, (b) segment with FRP anchor (c) stress transfer across the anchor

Premature failure due to delamination makes the task of ascertaining the increase in a RC beam flexure capacity via externally bonded FRP plates rather difficult. To render this system of repair reliable and to ensure that the expected capacity increase is realized, two essential requirements must be satisfied. First, effective methods for preventing delamination must be developed; secondly, accurate methods of analysis should be developed for calculating the distribution and magnitude of the stresses at the concrete-FRP interface, and for determining the concrete strength under the relevant stress combinations. Knowing the preceding parameters, the delamination load can be determined by comparing the maximum value of the interfacial stresses to the concrete strength using a relevant failure criterion.

1.3 Objectives and Scope of the Study

The principal objective of this investigation is to design, manufacture and test a CFRP anchor that could be used to delay/prevent premature delamination of adhesively bonded FRP laminates from reinforced concrete surfaces. The study will involve the testing of small scale prisms and large scale beams utilizing the proposed anchor system. An analytical model will be developed to quantify the normal and shear stresses at the interface between the FRP and concrete, and these stresses may be used to determine the required anchor distribution along the laminate.

The scope of the study will be limited to reinforced concrete beams strengthened externally with epoxy-bonded CFRP laminates for the purpose of increased flexural capacity. The beams would be under-reinforced before application of the FRP, and would remain under-reinforced after applying the FRP. The parameters to be considered will include the presence/absence of the anchor, the amount of FRP laminate, the laminate width, the anchor spacing and location. End anchors, mid-span anchors or both will be investigated to find the best arrangement for preventing delamination.

1.4 Methodology

The following methodology will be followed to achieve the proposed objectives:

(1) A comprehensive literature survey will be carried out to review existing strengthening methods involving FRP as external reinforcement for RC beams. A review of available guidelines and code provisions to design against intermediate crack debonding will be carried out. The review will include available anchoring methods and systems for FRP retrofitted concrete members.

(2) A new anchor will be manufactured and tested. The salient feature of the anchor would be its wide head to resist high interfacial shear stress and its shanks that are inserted inside the concrete to provide mechanical anchorage and to resist pullout. Figs.1-5 illustrates the proposed anchor system with a wide head and two shanks or legs.

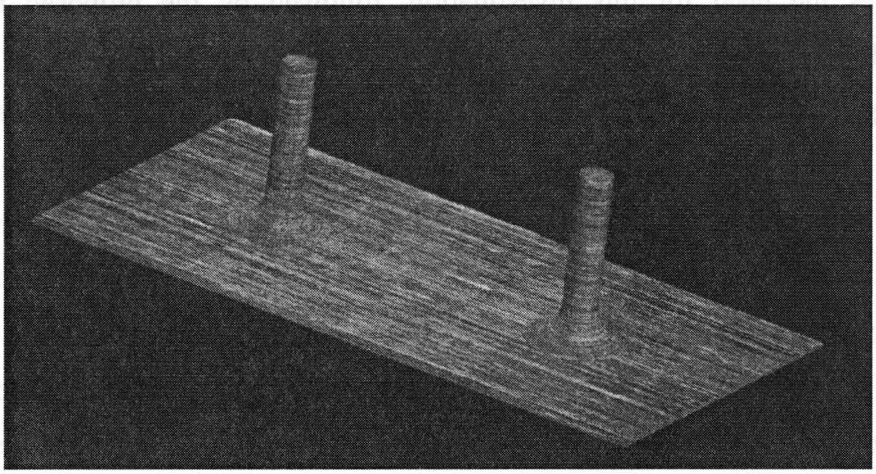

Fig.1-5: Two anchors with wider head

(3) To check the effectiveness of the anchors, they will be applied to the ends of laminate strips that will be bonded to small size concrete prisms and the prisms will be tested in tension.

(4) To investigate the effectiveness of the new anchor system in applications very similar to those in the field, the proposed system will be applied to full scale beams externally retrofitted with adhesively bonded laminates for increased

flexural capacity. The test will include parameters such as, the presence/absence of the anchor, number and spacing of anchors, location of the anchors and thickness and width of the laminate.

(5) An analytical model will be used to predict the magnitude and the distribution of the shear and normal stresses at the concrete-adhesive interface. The analytical model results will be compared with the results of nonlinear finite element analysis and the corresponding experimental data.

(6) Simple design recommendations will be made based on the current experimental data and analytical results.

1.5 Thesis Arrangement

The content of this thesis is divided into the following chapters. Chapter 1 is an introduction to the subject. It gives an overview of the objectives of this study and identifies the need for this investigation, followed by the proposed research methodology.

In Chapter 2, a comprehensive review of available strengthening techniques and a critical review of up-to-date anchoring methods and systems is carried out for RC beams externally strengthened with FRP. Furthermore, available methods and models used to predict the delamination load and the limiting strain in the laminate at debonding are examined. A detailed discussion and comparison between the available methods is curried out. Chapter 3 gives a detailed description of the different phases of the current experimental investigation. Specimens geometry, dimensions, reinforcement, material properties, instrumentations and test setup are presented.

Chapter 4 presents the test results from the different phases while a detailed discussion and analysis of the results are presented in Chapter 5. The analysis includes the application of some available methods of predicting delamination to the current test results.

Finally, a relatively simple analytical model is used to predict the normal and shear stresses along the interface between the concrete and the FRP laminate. The results of this analysis are compared with the experimental data and with the results of non-linear finite element analysis. The results are also used to propose a simple design method for finding the ultimate strength of CFRP strengthened beams retrofitted with the proposed anchor. Based on the above work, conclusions and recommendations for future work are presented in Chapter 6.

CHAPTER 2

Literature Review

General

In recent years the use of Fiber Reinforced Polymers (FRP) for strengthening and rehabilitation of RC structures has been rapidly growing. One of its major applications in RC structures is as external reinforcement, bonded to the surface of structural elements such as beams and slabs, or wrapped around columns for confinement. Different factors must be considered when strengthening structural elements with FRP, such as interfacial bond strength, relative increase in flexural/shear strengths and ductility requirements. In addition, the ability of the FRP-concrete interface to resist the induced interfacial stresses, without premature failure, is the key to the successful performance of this strengthening technique.

One of the key requirements for the effectiveness of FRP in flexural and shear strengthening is the maintenance of bond between the FRP laminate and the concrete surface. Since the FRP is bonded to the concrete surface by a high strength adhesive, the governing parameter for maintaining full bond is the strength of the interface between the concrete and the adhesive. Failure at the interface normally leads to delamination and renders the FRP ineffective. The problem of delamination, its causes, and procedures for delaying/preventing it have been studied by a number of researchers over the past two decades. The following literature review will briefly describe the nature of these investigations and their results and conclusions. The available anchorage techniques will be discussed in addition to the developed methods, guidelines and codes for design against delamination. The objective of the review is mainly to demonstrate the need for a new anchorage system to delay/prevent delamination of FRP in structures externally strengthened with FRP laminate.

Extensive research has been performed by a large number of investigators on the performance and behaviour of reinforced concrete beams strengthened with FRP laminates (e.g. Ritchie et al.1991, Triantafillou and Plevris 1992, Chajes et al.

1994, Sharif et al.1994, Meier 1995, Heffernan and Erki 1996, Takeda et al. 1996, Arduini and Nanni 1997, Taljsten 1997, Varastehpour and Hamelin 1997, Saadatmansesh and Malek 1998, Juvandes et al. 1998, Gardent and Hollaway 1998, Ross et al. 1999, Taljsten 1999, Bonfiglioli et al. 2003, Buyukozturk et al. 2004, Li et al.2006, Pham and Al-Mahaidi 2006, Xiong et al.2007, Teng and Yao 2007, Smith and Kim 2008, Rashid et al.2008, Smith 2009). In all of these investigations carbon or glass sheets /laminates were adhesively bonded to the soffit of simply supported beams loaded either in three point or four point bending until the beam failed.

Various failure modes in structures externally strengthened with FRP laminates have been observed and reported by Teng et al. (2002) and Oehlers and Seracino (2004) such as (a) normal flexural failure due to the crushing of concrete in the compression zone, (b) flexural tension failure due to rupture of the FRP , (c) failure initiated by separation of the concrete cover at the tension steel reinforcement level, (d) delamination of the FRP at the concrete-adhesive interface near the section of maximum moment, and (e) delamination of the FRP at the plate ends due to high interfacial shear and normal stresses. The failure can be generally classified as sectional failure or premature failure due to delamination. Sectional failure occurs under retention of full bond between the internal steel reinforcement and the concrete and between the external reinforcement and the concrete. It can be predicted using conventional beam theory and strain compatibility. On the other hand, delamination failure is difficult to predict due to the complexity of the failure mechanisms, which can be divided into two major types: intermediate span debonding and plate end debonding, where the term plate refers to the FRP laminate or plate. The former is caused by flexural or flexural-shear cracks which cause high local stresses at the FRP plate-concrete interface while the latter is initiated by high normal and shear stresses at the plate end. In order to fully utilize the tensile capacity of the FRP laminate, delamination needs to be delayed or prevented and this often requires the use of an anchorage system.

Although the interfacial normal and shear stresses are considered the main cause of the debonding failure, there are other factors which might affect the failure mechanism such as the un-sheeted length. This length is defined as the distance between the support and the end of the FRP laminate which is considered a principal factor influencing the increase of the interfacial stresses (Li et al.2006). Not only the length of the FRP laminates but also the thickness of the laminate has an effect on the overall performance, cracking pattern and failure type. In that regard, Li et al (2006) tested six strengthened RC beams in four point bending to examine the effect of the length and thickness of the FRP laminate. All the beams had the same cross sectional area, 120 mm wide x 200 mm deep x 2000 mm long. Two types of strengthening were used. In the first group, a single layer of CFRP laminate was used with three different un-sheeted lengths while in the second group, two layers of the CFRP laminate were used. The first layer had the same un-sheeted length in the three beams but the second layer had three different un-sheeted lengths. Test results showed that the stiffness of the strengthened beam was increased with the increase of the thickness and length of the CFRP after cracking. Furthermore, longer CFRP laminates can effectively restrain the crack development than shorter ones. There were no recommendations on how to take the debonding failure into account in the design. Toutanji et al. (2006) tested eight RC beams each 158 mm deep x 108 mm wide x 1800 mm long under four point bending. Three to six layers of CFRP laminate were used to strengthen the beams using an inorganic matrix. Test results showed that the load carrying capacity increased up to 170 % compared to the control beam as the number of laminate layers increased. Rupture of the CFRP laminate was reported in the case of three and four layers, while delamination was reported in the case of five and six layers. The authors also reported that the ductility of the strengthened beams was reduced compared to the control beam. An average ultimate tensile strain of 0.65% in the laminate was suggested when using an inorganic adhesive.

Numerous researchers have investigated the problem of delamination, but their work is not discussed here because the main focus of this study is the development of an anchorage system for ideally preventing delamination. Therefore, this topic is reviewed in greater detail in the following section.

2.2 Available Anchorage Techniques to Prevent Delamination

Researchers have investigated different mechanical techniques to delay/ prevent delamination in RC beams externally strengthened with FRP laminates. A very popular method of anchorage is FRP U-jackets. The U-jackets are made of FRP sheets and bonded to the bottom and sides of the beam in the anchorage zone. It has been reported by Takahashi et al. (1997) that the presence of U-jackets can increase the longitudinal FRP laminates resistance to peeling, and by appropriate selection of the anchor system, it can change the failure mode from delamination to rupture of the FRP. Takahashi et al. (1997), however, reported that the U-jacket did not increase the ultimate moment capacity of the beams compared to similarly strengthened beams without U-jacket, but it enabled the beam to undergo up to 50% more deformation before failure, which confirms the findings of Swamy et al.(1987) with respect to the benefit of steel plate anchorage. Oller et al. (2001) tested beams with equally spaced U-jackets throughout the length of the beam. It was reported that in the case of the beams with U-jacket, despite delamination and some slippage, they failed at 34.6% higher load than the unstrengthened control beam and at a modest 9% higher load than similarly strengthened beams without anchors.

Xiong et al. (2007) tested ten beams with 125x200 mm cross section and 2300 mm length rectangular RC beams externally strengthened with CFRP laminate. They used bi-directional GFRP sheets as a U-jacket to prevent the delamination of concrete cover at midspan. Five strengthening configurations were investigated: (i) beams longitudinally reinforced with two layers of CFRP laminate without any anchorage, (ii) beams with the same type of longitudinal reinforcement as (i) but reinforced with FRP U-jackets near the laminate ends, (iii) beams similar to (i) but with continuous U-Jacket covering the entire length of the laminate, (iv) beams strengthened with one layer of laminate along the length and two layers of GFRP U-jacket near the ends, and finally, (v) beams with one layer of CFRP along the length and two layers of continuous GFRP jacket along the length. It was reported that the strain in the compression portion of the concrete never reached the crushing strain, yet all the internal longitudinal tension reinforcement yielded. The authors reported that the hybrid CFRP/GFRP strengthening system could not only prevent the delamination of the bottom concrete cover, but also led to a 51.5% increase in the deflection. However, they did not present any specific design method. It is important to note that the test beams were rather small and applying one layer of laminate to a full size beam would rarely result in any significant increase in strength unless the laminate is sufficiently thick.

Ceroni et al. (2008) reviewed the available anchorage systems including fan anchor, an anchor system also referenced in Fib Bulletin 14, (2001), spike anchor, and U jackets as illustrate in Fig.2-1. It was reported that distributing the U-jackets evenly along the span will increase the strength and the ductility of a strengthened member. Local slippage, rupture or debonding, accompanied by loss of effectiveness before reaching the laminate tensile strength at mid-span, might be observed if the U jackets are concentrated at the ends only. They also discussed steel U- shaped strips and they reported that this method increases ductility.

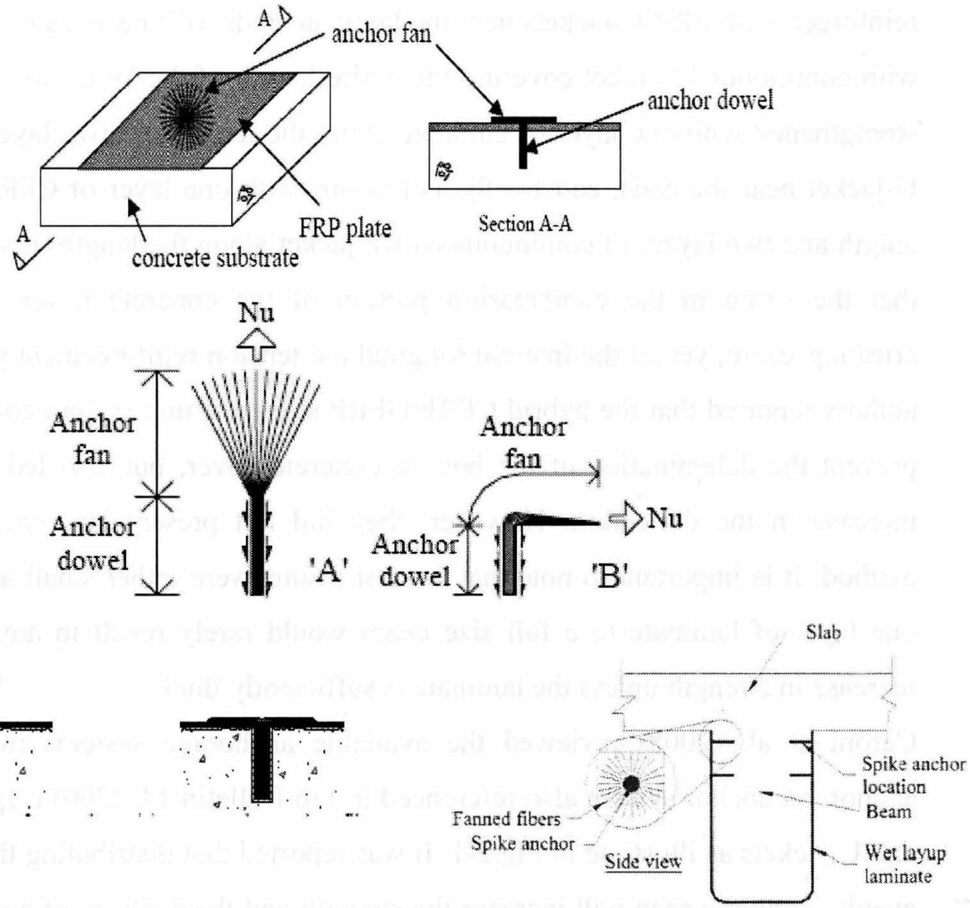

Fig.2-1: Different proposed anchorage systems (Smith 2009)

Fan and spike anchors have been used in a number of investigations (Smith and Kim 2008 and Smith 2009). This anchor is made of CFRP tow and acts similar to a nail with a thin round head and a shank formed by the bundled tow that is inserted inside epoxy-filled predrilled holes in the concrete. Smith and Kim (2008) tested seventeen concrete prisms each, 200 wide, 300 mm long and 150 mm deep in a standard single shear set-up, with the two main variables being (1) method of anchor and plate installation, and (2) anchor fibre content. Test results showed that the control specimens without anchors failed by debonding of the FRP plate while the anchored specimens failed by one of following four distinct modes:

Mode 1: Simultaneous plate debonding and anchor shear failure

Mode 2: Plate debonding followed by anchor shear failure

Mode 3: Plate debonding followed by anchor fan debonding

Mode 4: Plate debonding followed by anchor pull-out

Mode 1: Specimens failing in this mode experienced the greatest enhancement over the control specimen with 32.5% increase in strength before the anchors sheared off without warning.

Mode 2: The plate delaminated but the anchor continued to resist more load while experiencing considerable slippage. The failure was due to the anchor rupture at the bend section. The increase in the strength was a marginal 10% over the control beam. The only advantage of this failure mode was noticeable deformation and adequate warning before failure.

Mode 3: This mode is similar to Mode 2 in which the FRP plate delaminated followed by debonding of the anchor head but the anchor leg remained bonded to concrete. In this case a practically negligible 4.7% increase in ultimate load over the control beam was observed.

Mode 4: A complete debonding of the FRP plate followed by full pull out of the anchor from the concrete. In this case, considerable slippage and only 4.9% increase in ultimate load were reported. They attribute the poor performance of this system to improper workmanship and installation. However, this is somewhat based on speculation because they did not make any attempt to improve the performance by better workmanship. These investigators did not report the rupture of the FRP laminate using their anchor nor did they test their proposed anchor on large size beams.

Lamanna et al. (2001) used mechanical fasteners to attach CFRP strips to the bottom of concrete beams. They discovered that due to the presence of the fasteners, cracks developed in concrete; consequently, the strengthened beams did not achieve their expected ultimate moment capacity. Martin and Lamanna (2008) used steel fasteners to improve the performance of FRP strengthened concrete beams. In this study, the spacing and the pattern of the screws were investigated.

Test results showed that using this method can increase the flexural capacity and stiffness of reinforced concrete beams 10-39%.

Elsayed et al. (2009) conducted an investigation similar to Martin and Lamanna (2008) by performing a series of direct shear tests to investigate the parameters which govern the interfacial stresses in special GFRP/CFRP strips mechanically fastened to concrete. They considered two types of fasteners: namely; the shot and screwed fasteners, with different arrangements and spacings. Pullout of the shot fastener was reported due to the cracks developed at the location of the fastener which weakened the surrounding concrete and the governing mode of failure was reported as bearing failure associated with pullout. On the other hand, the screwed fasteners were more efficient as they did not damage the concrete or the FRP strip to the same extent. The failure mode was bearing in the FRP strip which switched to rupture of FRP as the number of anchors increased. It is important to mention that these investigations were performed using small concrete prisms subjected to tension force and that results of such tests cannot be applied directly to RC beams subjected to bending and cracking of concrete in the zone of maximum moment.

Chahrour and Soudki (2005) tested six beams, each 2400 mm long, 150 mm wide, and 250 mm deep with a tension reinforcement ratio of 1.18%. This investigation was carried out to study the flexural behaviour of RC beams externally strengthened involving end-anchorage and partially bonded CFRP strips. The CFRP strips were bonded to the tension face of the beam at their ends only and the ends were also mechanically anchored. Different unbonded lengths were used. Test results showed that all the strengthened beams with CFRP laminate, with and without end anchorage, failed due to interfacial debonding of the CFRP strip. The highest ultimate load was 45% larger than that of the control beam and was reached in the beam which had an unbonded length of 250 mm in the central region of the beam. It was reported that reduction of the flexural resistance occurred with increase in the CFRP strip unbonded length with the exception of the one beam. No anchorage design equation was provided, and the only recommendation made was to use a smaller unbonded lengths.

Orton et al. (2008) reviewed different anchorage systems and performed an experimental investigation to obtain the initial design parameters for anchors. They recommended using an anchor with a cross sectional areas at least double the longitudinal FRP laminate cross section and distributing the anchor evenly along the span length. Furthermore, they recommended that the anchor should be inserted inside the concrete at least to a depth of 130-150 mm to prevent its pull-out. They, however, did not recommend a design procedure for such an anchorage system.

Galal and Mofidi (2009) tested 4 half-scale RC T-beams under four point bending to investigate the effectiveness of a new hybrid fiber-reinforced polymer sheet /ductile anchor system. One beam was tested as a control beam without any strengthened systems. The second beam was retrofitted with one layer of CFRP sheet as a conventional FRP bonding method while the last two beams were retrofitted with one layer of CFRP using the new anchor system where the CFRP sheet was unbonded and in the last beam, the CFRP layer was bonded to the concrete. The new anchor system mainly consisted of FRP sheets wrapped around two steel plates at their ends and then epoxy bonded to the original FRP sheet. The steel plates have rounded corners to prevent stress concentration or rupture of the FRP sheet. They introduced an overlap of 150 mm to prevent the debonding between the FRP sheets. The steel plate is attached to two steel link members then attached to a steel angle which is anchored to the concrete by means of a high threaded steel rod. The anchor system was designed to yield before rupture or debonding of the FRP sheet. As reported by the authors, the advantage of this new anchor system is that the work done is needed at the end of the beam and therefore, that will not interrupt traffic in the case of applying it to a bridge and not many temporary supports are required. Test results showed that the beam strengthened with the conventional epoxy bonded FRP sheet reached 7% higher load capacity compared to the control beam and the failure mode was governed by debonding of the CFRP sheet. The beam strengthened with the unbonded hybrid FRP/ductile anchorage system achieved 21% increase in the load capacity to that of the control beam and 4.75 % increase in the ductility. The increase achieved over the beam strengthened using conventional externally bonded CFRP sheet was 13%. On the other hand, the beam with the hybrid bonded CFRP anchorage system achieved 27% increase compared to the control beam. The failure mode in this case was rupture of the FRP at a lower ductility compared to the beam with the unbonded CFRP sheet.

Some design guidelines and standards, such as CSA standard S806-02, deal with the problem of premature delamination by limiting the ultimate strain to 0.007 in the FRP. Generally, longitudinal strain limits of 0.6-0.8% are recommended, however, test results by Oller et al. (2001) have shown that these values are too high and that none of their tested beams could exceed 0.5% strain before failure. Therefore, they recommended the use of externally applied anchors to delay the debonding of FRP plates. Other guidelines such as ACI Committee 440 (2002) also recommend FRP strain limitations. Fib 14 (2001) has three design criteria which will be discussed in detail in the next section and it includes FRP strain and interfacial shear stress limitations. The Japanese Society of Civil Engineers recommendations (JSCE 2001) specify limits on the stress in the FRP laminate to avoid delamination.

Poulsen et al. (2001) discussed other methods of anchorage applied by Meier (1995), including transverse strips bonded to the beam soffit and to the FRP plate, as well as anchoring of FRP at its ends but no guideline was provided.

Another anchorage system was developed by Mostafa (2005), Fig.2-2. The π shaped anchor was made by cutting the ribs of a carbon fibre grid known as NEFMAC. The NEFMAC grids have square openings, with ribs of equal dimensions running in two orthogonal directions. The grids have been extensively tested by both its manufacturer and by another investigator (Zaghloul 2002). The guaranteed tensile strength of CFRP NEFMAC is 1200 MPa and its elastic modulus is 100 GPa. Due to the rough finish of its surface, it bonds very well with both concrete and the epoxy adhesive. Mostafa (2005) tested nine simply supported reinforced concrete beams to investigate the effectiveness of this anchor. Eight beams were strengthened with externally bonded CFRP sheet or laminate while one beam was not strengthened and used as a control beam. Four of the strengthened beams were retrofitted with the preceding anchor system. The strengthened beams were tested to failure in three point bending over a 3.0 m span. Different parameters were used in that investigation such as, the number of anchors, the anchor spacing, and the amount of the FRP. Due to the preliminary nature of the study and due to lack of any design guidelines for such anchors, the number and spacing of the anchors were based on practical considerations.

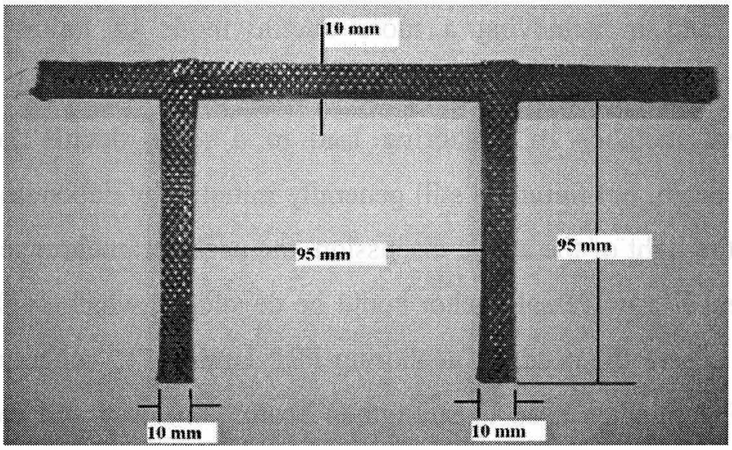

Fig.2-2: NEFMAC CFRP anchor

Test results showed that delamination started in the mid-span region and then it propagated towards the supports. The advent of delamination was always heralded by a loud noise and by a noticeable drop in the applied load. It was observed that beams with anchors had generally 5-10% higher delamination load than their companion beams without anchors, but the true significance of the observed increase can be only measured by proper statistical analysis. Higher deformation at failure was experienced in beams with anchors compared to their companion beams without anchors. Although complete separation of the external reinforcement from the concrete was not observed in any of the beams with anchors, there was substantial slip at one end of the FRP reinforcement and it is believed that the partial debonding and end slip contributed to the observed ductile response of the beams. It is important to mention that the anchors were effective in limiting the extent of delamination along the interface, thus indirectly contributing to the flexural stiffness of the beam by limiting the extent of cracking along the span. All the beams externally reinforced with FRP had failure loads that exceeded their theoretical failure loads based on the CSA Standard S806-02 method (CSA2002), but the control beam failed at a lower load due to excessive shear combined with high moment. One beam with a large number of anchors achieved higher load and exhibited remarkable ductility compared to a similar beam with fewer anchors. This anchor system was found to be effective in delaying delamination and in achieving a more ductile mode of failure, but further investigation is needed to further refine and improve its performance.

All the above methods of anchoring lead to a more ductile failure of the strengthened beam, but failure is still generally initiated by debonding of the FRP laminate. In the light of the above discussion, the need for anchorage exists, but it would be ideal if a universal anchor could be developed which could be used in any situation where the need for anchoring FRP laminate to concrete exists. This includes FRP laminates used to strengthen beams, one-way and two way slabs against flexure and/or shear.

2.3 Available Proposed Methods to Predict the Interfacial Normal and Shear Stresses

As mentioned earlier, Teng et al. (2002,2004) classified the different types of failure modes of RC beams externally strengthened with FRP in two major groups, sectional failure and debonding failure. Debonding may initiate at a flexural or flexural-shear crack in the high moment zone and propagates towards the plate ends. This debonding failure mode has been referred to as intermediate crack (IC) induced interfacial debonding or simply IC debonding (Yao and Teng 2007, Teng and Yao 2007). Debonding may also occur near the plate ends. Plate end debonding occurs in three distinctly different modes: (a) critical diagonal crack (CDC) debonding, (b) concrete cover separation and (c) plate end interfacial debonding. A number of studies in the literature have been carried out to predict the plate end debonding failure mode, and methods have been developed to relatively accurately predict the debonding stresses (Malek et al.,1998; Smith and Teng, 2001, 2002; Rasheed and Pervaiz, 2002; Abdelouahed 2006; Qiao and Chen, 2008; Tounsi et al. 2009). However, the principal focus of this study is IC debonding and its delay by means of a new anchor system. Consequentially, issues related to plate end debonding will not be discussed in any detail.

One of the keys to the development of an effective anchor system and practical anchor design method is to achieve greater understanding of the factors that affect delamination in externally strengthened concrete beams. This means that the distribution and magnitude of the stresses at the FRP plate-concrete interface must be relatively accurately known at various load levels. In this section, delamination caused by intermediate crack debonding will be discussed in more detail and the available design methods and guidelines will be reviewed. Chen and Qiao (2009) discussed a so-called cohesive model for beams externally strengthened with FRP. The model takes into account the moment and transverse shear forces in the FRP and concrete substrates into account. They also proposed a closed form solution and analysis of the local bond slip versus applied load along the interface, thus enabling them to obtain the axial force in the FRP at different stages. They reported that if the size of the softening zone increased, the capacity of the FRP-concrete interface would increase with an increased thickness of the adhesive layer. The model can predict the delamination process at different load levels. The governing equation proposed was similar to the one introduced by Teng et al. (2006), except that there were additional terms which reflect the effect of the shearing force and the moment in the plated concrete beam on the FRP-concrete cohesive interface. These investigators classified the IC debonding into two types: (1) single crack induced debonding (first type of IC debonding), in which one crack exists in the concrete and there is no other crack between the free end and the crack where debonding initiates, and (2) multi-crack induced debonding (second type of IC debonding), in which more than one crack are distributed along the bond length. The latter is considered more practical since debonding will initiate after the concrete cracks and the main steel reinforcement yields. IC debonding usually occurs in the zone of maximum moment where the strain in the FRP plate is the highest (Oehlers et al. 2004). Since concrete has a lower tensile strength compared to the adhesive, then the debonding crack occurs in the concrete adjacent to the adhesive-concrete interface, and subsequently the horizontal cracks propagate gradually towards the plate end as shown in Fig.2-3.

In the IC debonding induced by flexural cracks, crack widening causes debonding propagation, but the relative vertical displacement prior to a critical diagonal crack forming between the two faces of the crack produces peeling stresses at the interface. However, this effect is less significant, hence it is considered that the propagation of debonding is predominately caused by widening of the crack (Chen and Teng 2001)

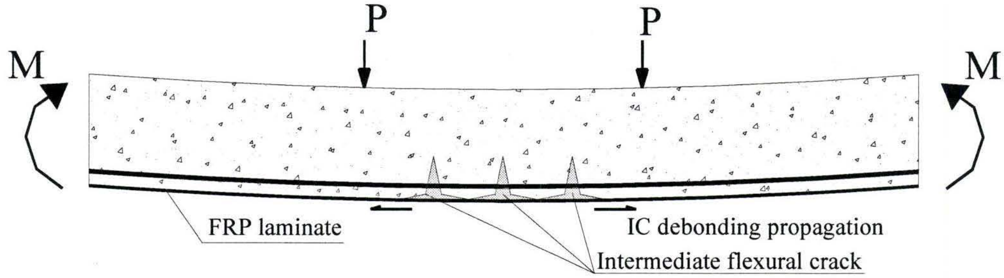

Fig.2-3: Intermediate crack debonding mechanism Liu et al.(2007)

Liu et al. (2007) proposed the partial interaction model to describe the IC debonding of plated RC beams. They reported that three main factors may significantly affect the local behaviour and the resultant strains in the plated beams. These factors are: (1) the crack spacing, (2) the rate of moment change and (3) number of cracks in the beam. Before flexural cracking of concrete, there is no slip at the concrete/plate interface and so the strain is linearly distributed along the cross section of the plated beam. Therefore, the assumption of plane sections remaining plane holds and there is full interaction between the plate and the concrete, i.e., the plate strain at the interface is equal to the strain in the concrete adjacent to it. However, when cracking occurs, this causes high bond stresses to develop near the crack, and as a result, slip occurs between the concrete and the plate. The slip at the interface given by

$$s = u_p - u_c \qquad \text{Eq.2-1}$$

where u_p and u_c represent the displacements of the plate and the concrete, respectively. Therefore, the strain in the plate ε_p is no longer equal to the strain in the adjacent concrete ε_c and full interaction no longer applies. The difference between the plate and adjacent concrete strain is defined as slip strain ds/dx, and this is now a partial interaction problem

$$\frac{ds}{dx} = \frac{du_p}{dx} - \frac{du_c}{dx} = \varepsilon_p - \varepsilon_c \qquad \text{Eq.2-2}$$

As discussed by Liu et al. (2007), performing partial interaction analyses on plated beams requires performing segmental analyses along the member at fixed increments x to a point where known boundary conditions must be satisfied. Iterative procedures should be carried out by changing the guessed slip at a crack. The location of the first crack needs to be chosen. For a beam subjected to a concentrated load, the first flexural crack is assumed to occur immediately under the applied load. Generally, in beams under flexure, the flexural cracks will occur in regions of high moment and due to these cracks, there will be slip between the plate and the adjacent concrete. This cracked region is known as the partial interaction hinge, as illustrated in Fig. 2-4, where the partial interaction model applies.

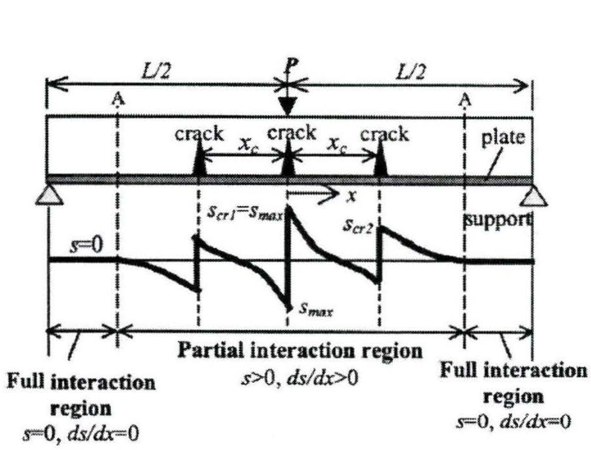

Fig.2-4: Partial interaction model and interfacial shear variation for plated beams, Liu et al.(2007)

To be able to analyse the partial interaction hinge, the boundary conditions should be evaluated. The following boundary condition was used by Liu et al. (2007) in the undisturbed zone which they defined to be a zone without any cracks.

(1) For each layer of reinforcement, there is a position along the beam beyond which there is no slip at the concrete/ reinforcement interface, and full-interaction at the extremities of the partial-interaction region can be assumed. In cases where there is no full interaction along the beam, i.e., slip has propagated towards the beam end, the boundary condition is zero strain at the beam end.

(2) At each crack, the applied moment M and crack height h are known from an analysis of the boundary moment.

(3) For cases with multiple reinforcing layers, i.e., beams with external FRP plate and internal steel reinforcing bars, the crack faces act as rigid bodies so that there is a linear variation in crack width from the crack tip. When the crack widens and slip occurs at the plate/ concrete interface, the crack width adjacent to the plate, w_p, is equal to the algebraic sum of the slip of the left crack face s_l and that of the right crack face s_r . The same applies to the bar layer. The variation in crack width is assumed to be linear from the crack tip. Therefore at each layer of reinforcement/plate the crack width is given by

$$w_b = w_p(\frac{h_b}{h_p}) \ , \quad w = s_r - s_l \qquad \text{Eq.2-3}$$

where h_b and h_p = distance of the bar and the plate from the crack tip, respectively. They concluded that a lower bound to the debonding strain is a beam with a single flexural crack (which is equivalent to a pull test) and that the debonding strain can be significantly increased when there are increasing number of flexural cracks. Substantial increase in debonding strain can also occur as the crack spacing reduces, i.e., as secondary cracks form between existing flexural cracks, which shows the importance of locating cracks. Furthermore, the rate of change of moment, that is the vertical shear force, can significantly affect the debonding strain. Note that neither the crack width nor the magnitude of slip can be easily and quantitatively determined.

Lu et al. (2007) used the finite element analysis to study the IC debonding based on the smeared crack approach for concrete. They captured the effect of the local slip concentration near a flexural crack using a dual local debonding criterion and the interfacial behaviour within the major flexural crack zone. They compared their finite element results with the results of 42 beams and proposed a new model that can be used for design. In this finite element model the concrete was modeled using plane stress elements, while the reinforcement and the FRP plate were modeled using beam elements. They divided the interfacial shear stress in a FRP-strengthened RC beam in two components, referred to as τ_s and τ_c. τ_s is due to the shear force in the beam and it is zero in the zone of maximum moment. On the other hand, τ_c is due to the opening of the flexural crack in the RC beam and the constraint provided by the FRP plate bridging the crack. The total shear interfacial stress can be defined as:

$$\tau_{\max} = \tau_{s,\max} + \tau_{c,\max} \qquad \text{Eq.2-4}$$

The interfacial shear stress τ_s is distributed over a large part of the shear span. Although these interfacial shear stresses are due to the transverse shear force in the beam, their distribution is different from that of the shear force as the section material properties after cracking and yielding vary over the length of the beam. The interfacial shear stress τ_c due to the opening of the major crack was found to be distributed over a small length L_{ee}, which equals the effective bond length corresponding to the bond-slip mode II for the major flexural crack zone and can be approximated by (Yuan et al. 2004):

$$L_{ee} = \sqrt{\frac{4E_f t_f}{\frac{\tau_{\max}}{s_o}}} = 0.228\sqrt{E_f t_f} \qquad \text{Eq.2-5}$$

where E_f and t_f are the elastic modules in MPa and thickness of the FRP laminate in mm respectively, and s_o is the slip at maximum shear. The total axial force in the FRP plate at the loaded section was calculated using:

$$T = \left(\frac{\tau_{s,\max} L_d}{2} + \frac{\tau_{c,\max} L_{ee}}{2} \right) b_f \qquad \text{Eq.2-6}$$

where b_f is the laminate width and L_d is the distance from the loaded section to the end of the cracked region or to the plate end if the plate is terminated within the cracked region. Lu et al. (2007) suggested taking the distance L_d to be the distance from the loaded section to the end of the FRP plate which will lead to an acceptable error in the force calculated in the FRP. Since the maximum interfacial stress will be induced at the loaded section, the factor α was introduced to represent the ratio between the interfacial stress $\tau_{s,\max}$ and the total interfacial stress at the critical section

$$\begin{aligned} \tau_{s,\max} &= \alpha \tau_{\max} \\ \tau_{c,\max} &= (1-\alpha)\tau_{\max} \end{aligned} \qquad \text{Eq.2-7}$$

The strain in the FRP at the critical section ε_f^{IC} can be obtained as:

$$\varepsilon_f^{IC} = \frac{T}{E_f t_f b_f} = \frac{(1-\alpha)\tau_{\max} L_{ee} + \alpha \tau_{\max} L_d}{2E_f t_f} \qquad \text{Eq.2-8}$$

The value of α was calibrated using the experimental results and the finite element analysis and was found to vary mainly with $\frac{L_{ee}}{L_d}$. The value of α was found to be

$$\alpha = 3.41 \frac{L_{ee}}{L_d} \qquad \text{Eq.2-9}$$

Therefore, the strain in the FRP plate at delamination can be rewritten as

$$\varepsilon_f^{IC} = 0.114(4.41-\alpha)\frac{\tau_{\max}}{\sqrt{E_f t_f}} \qquad \text{Eq.2-10}$$

Ascione (2009) proposed a mathematical model for studying the equilibrium problem of adhesive joints between FRP adherents in double and single -lap joints, both in the case of normal and shear stresses acting on the joint. The adhesive layer was modeled by means of two independent interfacial cohesive bilinear laws, for fracture mode I and mode II, respectively. This model is rather complicated to be used in practical design.

Aram et al. (2008), summarized all the available codes and guidelines debonding criteria for preventing midspan debonding as shown in Table 2-1. They reported that most of the guidelines and codes are based on two approaches. Generally, a limit is placed on either the interfacial shear stress or on the FRP tensile strain (or stress). Fib 14 (2001) specifics three different approaches based on the FRP tensile stress that can lead to maximum interfacial bond stress. The strain (stress) limits of Fib14-2 (2001), JSCE (2001) and Teng et al. (2003) depend on the axial rigidity of the FRP ($E_f t_f$) and on the concrete properties. On the other hand, the American Concrete Institute guidelines (ACI Committee 440, 2002) uses the FRP rigidity and rupture strain, ε_{fu} , for determining the delamination load. The bond shear stress limits specified by Fib14-3 (2001) and the Swiss Standard SIA 166 (2003) are based on the tensile and shear strength of concrete, respectively. A summary of the available codes, guidelines, models and recommendations for determining the delamination load is presented in Table 2-1. Note that all symbols are defined in the text.

Table 2-1: Design guidelines and code limitations to prevent midspan debonding

Codes and guidelines	Debonding Criteria
ACI 440 [Strain Limitation]	$\varepsilon_f = \frac{1}{60\varepsilon_{fu}}\left(1-\frac{nE_f t_f}{360000}\right) \leq 0.9$ if $nE_f t_f \leq 180000$ ACI 440-02 $\varepsilon_f = \frac{1}{60\varepsilon_{fu}}\left(\frac{90000}{nE_f t_f}\right) \leq 0.9$ if $nE_f t_f > 180000$ Eq.2-11 $\varepsilon_f = 0.41\left(\frac{f_c'}{m}\right)^{0.5} \leq 0.9\varepsilon_{fu}$ ACI 440-08 $m = nE_f t_f$ Eq.2-12 n=No. of FRP layers, ε_{fu} =ultimate strain capacity of FRP
Fib14-1 (2001) Strain Limitation	The strain limitation has a range of 0.65% to 0.85%

Fib14-2 (2001) Shear Stress Limitation	$\sigma_{\min} \leq \frac{0.185E_f}{S_{cr}} - 0.285\sqrt{f_c f_{ctm}}\frac{S_{cr}}{4t_f}$ $\Delta\sigma_{f,\max,fib} = \Delta\sigma^{(A)}_{f,\max,fib} - \frac{(\Delta\sigma^{(A)}_{f,\max,fib} - \Delta\sigma^{(B)}_{f,\max,fib})}{\sigma^{(B)}_f}\sigma_{\min}$ $\Delta\sigma^{(A)}_{f,\max,fib} = \frac{1}{\gamma_c}\sqrt{\frac{0.053E_f\sqrt{f_c f_{ctm}}}{t_f}}$ $\Delta\sigma^{(B)}_{f,\max,fib} = \frac{1}{\gamma_c}\left[\sqrt{\frac{0.053E_f\sqrt{f_c f_{ctm}}}{t_f} + (\sigma^{(B)}_f)^2} - \sigma^{(B)}_f\right]$ (MPa) $\sigma_{\min} > \frac{0.185E_f}{S_{cr}} - 0.285\sqrt{f_c f_{ctm}}\frac{S_{cr}}{4t_f}$ $\Delta\sigma_{f,\max,fib} = \min\left(\frac{1}{\gamma_c}\left[\sqrt{\frac{0.053E_f\sqrt{f_c f_{ctm}}}{t_f} + (\sigma_{\min})^2} - \sigma_{\min}\right], (\sigma_{fd} - \sigma_{\min})\right)$	Eq.2-13
Fib14-3 (2001) Shear Stress Limitation	$\tau_b = \frac{\Delta T_f}{b_f \Delta x} \leq 1.8 f_{ctk}$	Eq.2-14
ISIS (2001)	Debonding can be solved by using sufficient anchorage	
JSCE (2001) Stress Limitation	$\sigma_f \leq \sqrt{\frac{2G_f E_f}{n_f t_f}}, \mathrm{G_f} \approx 0.5\frac{\mathrm{N}}{\mathrm{mm}}$	Eq.2-15
SIA166 (2003) Strain and Shear Stress	$\varepsilon_f \leq 0.8\%$, $\tau_b \leq 2.5\tau_{cd}$, $\tau_{cd} = 0.3\sqrt{f_c}$	Eq.2-16

TR55 (2004) Strain and Shear Stress Limitations	$\tau_b \leq 0.8\text{N/mm}^2$, $\varepsilon_f = 0.8\%$	Eq.2-17
Teng et al. (2003)	$\sigma_{db} = 0.48\beta_w\beta_L\sqrt{\dfrac{E_f\sqrt{f_c'}}{t_f}}$ $\beta_w = \sqrt{\dfrac{2-\dfrac{b_p}{b_c}}{1+\dfrac{b_p}{b_c}}}$	Eq.2-18
Werner et al. (2003) Strain Limitation	$\varepsilon_f \leq 0.65\%$, $\tau_{b,ave} = 1.6\text{MPa}$, $l_A = \dfrac{T_f}{b_f\tau_{b,ave}}$	Eq.2-19
Neubauer and Rostasy (2001) shear Stress Limitation	$\tau_{b,B} = \dfrac{V}{b_c z_m} \leq \tau_{B,DB}$	Eq.2-20

Lu (2004)	$$\varepsilon_{db} = \left(\frac{0.492}{\sqrt{E_f t_f}} - \frac{0.086}{L_d}\right) 1.5\beta_w f_t$$ $$\beta_w = \sqrt{\frac{\left(2.25 - \frac{b_f}{b_c}\right)}{\left(1.25 + \frac{b_f}{b_c}\right)}}$$	Eq.2-21
Said and Wu (2008)	$$\varepsilon_{db} = \frac{0.23 f_c'^{0.2}}{\left(E_f t_f\right)^{0.35}}$$	Eq.2-22
Neale et al. (2009)	$$\varepsilon_{db} = 0.75\varepsilon_u + 70.9 f_c' + 106.81l - 225.7\rho - 113.1(EA)_{FRP} - 283.4d$$	Eq.2-23
CNR-DT 200/2004	$$\varepsilon_{fd} = \min\left\{\eta_a \frac{\varepsilon_{fk}}{\gamma_f}, \varepsilon_{fdd}\right\}$$	Eq.2-24

All the notations in Table 2-1 are defined as follow:

E_f modulus of elasticity of FRP

A_f cross section area of the FRP

G_a shear modulus of adhesive

G_f fracture energy of concrete

M_{cr} cracking moment

M_{end} bending moment at plate end

M_u bending moment capacity of strengthened cross section

S_{f0} ultimate slip where debonding occurs

$T_{f, max}$ maximum FRP force which can be anchored

V shear force

V_c concrete shear strength

V_{end} shear force at plate end

b_c width of concrete cross section

b_f width of FRP plate

f_{ctk} characteristic value of concrete tensile strength

f_{ctH} surface tensile strength of concrete

f_{ctm} mean value of concrete tensile strength

f_{cu} cube concrete strength

f_c' concrete cylinder compressive strength

f_{fu} tensile strength of FRP

f_u ultimate tensile strength of reinforcement

f_y yielding stress of steel reinforcement

I_c moment of inertia of concrete cross section

I_{cs} second moment of area of strengthened concrete equivalent cracked section

I_f moment of inertia of FRP cross section

l_b available bond length

$l_{b,\,max}$ maximum anchorage length

n number of plate layers

t_f thickness of FRP plate

t_a thickness of adhesive

y_c distance from the bottom of concrete to its centroid

y_f distance from the FRP plate to its centroid

z_m average internal lever arm

z_f lever arm of plate

z_s lever arm of steel

β_p width coefficient

β_L bond length coefficient

ε_c' ultimate concrete strain in compression

ε_f FRP strain

ε_{fu} rupture strain of FRP

σ_{db} ultimate plate stress

σ_f FRP stress at the location of flexural crack

$\sigma_{x,\,max}$ maximum axial stress

$\sigma_{y,\,max}$ maximum normal stress

$max\Delta\sigma_f$ maximum anchorable FRP tensile stress

τ_b bond shear stress

τ_{bu} mean bond strength of the FRP to concrete

$\tau_{B,DB}$ shear stress at initiation of debonding

τ_{cd} design shear strength of concrete

γ_c material safety factor

A similar comparison was made by Said and Wu (2008) who investigated five models and code provisions and carried out a comprehensive comparison among these models in order to evaluate their performance and accuracy. In the following sections, a detailed discussion of these provisions and models will be carried out.

As reported by Aram et al. (2009) when comparing the experimental results with the available guidelines, the ACI Committee 440-02 recommendations give more accurate results. Furthermore, the JSCE (2001) and Teng et al. (2003) models show a large discrepancy with other guidelines. The maximum bond shear stress reported by a number of investigators varies from 0.9 to 5 MPa, therefore, they concluded that the bond shear stress limitations proposed by Fib 14-3 and SIA (2003) are on the unsafe side while those of TR55 (2004) are very conservative. They also reported that the FRP strain limitation given by the different codes and guidelines are not sufficient to predict the mid-span debonding since the maximum load transferred from the FRP to the concrete depends mainly on the strength of the concrete at the interface. They recommended that a combined strain and shear stress limitation is necessary although such a criterion is not developed yet. The use of a strain limit of 0.008 and a shear stress limit of $\tau_b = f_{ct}$ was recommended, where f_{ct} is the tensile strength of concrete . Finally they reported that the bond model by Neubauer and Rostasy (2001) has the best agreement with the experimental results, however, it is very complex and not feasible in practical design.

2.3.1 JSCE (2001)- Wu and Niu Model (2007)

The JSCE (2001) model is based on fracture mechanics and its application is mainly governed by two parameters: the fracture energy G_f and the distance L along which $\Delta\sigma_f$ is calculated, where, $\Delta\sigma_f$ is the difference of the FRP tensile stress between two cracks. Due to insufficient experimental data, a value of G_f =0.5 N/mm, and L in the range of 150-250 mm was recommended. JSCE (2001) specifies that no debonding of the continuous fiber sheet occurs when the stress σ_f of the continuous fiber sheet at the location of flexural crack caused by the maximum bending moment in the member satisfies Eq.2-15.

The JSCE (2001) recommendations also suggest that the flexural capacity and axial load-carrying capacity of members failing due to debonding of the continuous fiber sheets may be calculated in such a way that the maximum value, $\Delta\sigma_f$, satisfies Eq.2-25

$$\Delta\sigma_f \le \sqrt{\frac{2G_f E_f}{t_f}} \qquad \text{Eq.2-25}$$

In order to calculate G_f and L, Wu and Niu (2007) developed the following equations:

$$\begin{aligned} G_f &= 0.644 f_c'^{0.19} \\ L &= Max.(L_e', L_y) \\ L_e' &= 1.3\sqrt{\frac{E_f t_f}{f_c'^{0.095}}} \end{aligned} \qquad \text{Eq.2-26}$$

where L_y = distance between the critical section and the end of the yield region at the debonding load as shown in Fig.2-5. Since the debonding load is not known, the value of L_y may be calculated by trial and error.

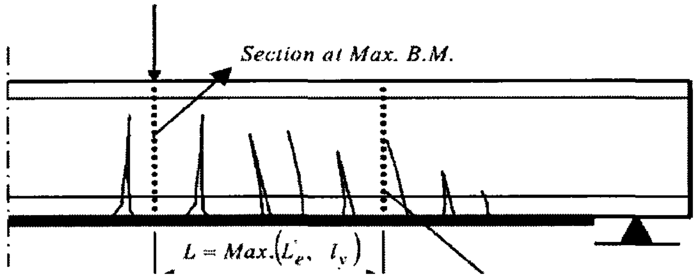

Section at the end of the equivalent transfer length or the end of the yielded region whichever is larger

Fig.2-5: Definition of the distance in which the variation of the FRP stress is calculated based on Wu and Nie model (2007)

2.3.2 Fib 14 (2001)

As can be seen in Table 2-1, the Fib Bulletin 14 (2001) has three different approaches for design against IC debonding. Fib14-1 (2001) limits the FRP strain between 0.65% and 0.85 %, but this limit is not suitable in all applications. On the other hand, Fib 14-3 (2001), which is based on shear stress limit criterion contains two steps: the verification of the end anchorage and limiting the interfacial shear stress resulting from the change of tensile force along the FRP composite. The accuracy of the prediction of this method is highly variable, in some cases it has been found to overestimate the actual failure load by more than 400%, while in other cases, it has severely underestimated the actual load. Despite the inherent complexity of Fib14-2 (2001) approach, which is based on fracture mechanics, it seems to be rather unreliable. It has similarity to the JSCE (2001) recommendations, and states that the stress check against delamination between two adjacent cracks can be carried out by applying the following equation:

$$\Delta\sigma_f \leq \Delta\sigma_{f,\max,fib} \qquad \text{Eq.2-27}$$

where, $\Delta\sigma_f$ is the difference in the FRP stress between two specific sections; $\Delta\sigma_{f,\max,\,fib}$ is the maximum possible increase in the FRP tensile stress according to the Fib bulletin.

The application of Fib can be summarized in the following three steps:

1- The average spacing between two consecutive flexural cracks equals 1 to 2 times the transmission length, and may be calculated assuming constant mean bond stresses for both the internal and external reinforcements as follows:

$$s_{rm} = \frac{2M_{cr}}{z_m}\left(\sum \tau_{fm} b_f + \sum \tau_{sm} d_s \pi\right) \qquad \text{Eq.2-28}$$

$$\begin{aligned} M_{cr} &= k f_{ctk,0.95}\, b_c \frac{h^2}{6}, \; k = 2 \\ \tau_{sm} &= 2.25 f_{ctk,0.95} = 1.85 f_{ctm} \\ \tau_{fm} &= 0.44 f_{ctm} \\ z_m &= 0.3\left(f_{ck}\right)^{\frac{2}{3}} = 0.3\left(f_c' - 8\right)^{\frac{2}{3}} \end{aligned} \qquad \text{Eq.2-29}$$

where, s_{rm} is the mean crack spacing, M_{cr} is the cracking moment, z_m is the mean lever arm of internal forces; τ_{fm} is the mean bond stress of the FRP; τ_{sm} is the mean bond stress of steel reinforcement; b_f is the width of the FRP plate, d_s is the diameter of the reinforcement bar; f_{ctm} is the mean value of the concrete tensile strength; $f_{ctk,0.95}$ is the upper bound characteristic tensile strength of concrete; f_{ck} is the characteristic value of the concrete compressive strength; h is the concrete depth, b_c is the concrete width, and f'_c is the compressive strength of concrete.

2- Determine the difference in the FRP tensile stresses between two consecutive cracks, $\Delta\sigma_f$, which can be easily calculated based on strain compatibility and internal forces equilibrium of each section.

3- Determine the maximum increase in the tensile stress in the FRP $\Delta\sigma_{f,max,fib}$ which depends mainly on the average crack spacing s_{rm}, the minimum stress between the two cracks σ_{min}, and the interfacial fracture energy G_f according to Eq. 2-30.

$$\sigma_{\min} \leq \left(c_3 \frac{E_f}{s_{rm}} - c_4 \left(\frac{s_{rm}}{4t_f} \right) \sqrt{f_{ck} f_{ctm}} \right) MPa \qquad \text{Eq.2-30}$$

$$c_3 = 0.185, \; c_4 = 0.285$$

For more details, refer to Table 2-1

2.3.3 Teng et al. Model (2003)

Similar to the ACI, Teng et al. (2003) suggested a limit on the allowable strain in the FRP in order to avoid premature debonding failure. Their proposed stress limit is given by Eq.2-18, which is based on a simple modification of the empirical model of Chen and Teng (2001). In this model the effects of concrete compressive strength and the ratio of the FRP laminate width to the concrete width are taken into consideration. The model can be expressed as follows:

$$\varepsilon_{deb} = \begin{cases} 0.48\beta_w \sqrt{\dfrac{\sqrt{f_c'}}{E_f t_f}} & if\ \mathrm{L}_f \geq \sqrt{\dfrac{E_f t_f}{\sqrt{f_c'}}} \\ 0.48 \sin\left(\dfrac{\pi L_f}{2\sqrt{\dfrac{E_f t_f}{\sqrt{f_c'}}}} \right) \beta_w \sqrt{\dfrac{\sqrt{f_c'}}{E_f t_f}} & if\ \mathrm{L}_f > \sqrt{\dfrac{E_f t_f}{\sqrt{f_c'}}} \end{cases}$$

where Eq.2-31

$$\beta_w = \sqrt{\frac{\left(2 - \dfrac{b_f}{b_c}\right)}{\left(1 + \dfrac{b_f}{b_c}\right)}}$$

where, L_f is the distance from the FRP cutoff to the nearest applied load.

2.3.4 ACI Committee 440 (ACI 2002)

ACI Committee 440 (2002) recommends a limit on the strain of the FRP plate, ε_f, to prevent premature failure due to debonding. The limit is calculated according to the procedure shown in Table 2-1. Note that the ACI equations as shown are based on SI units.

2.3.5 Lu (2004) Model

This model is similar to the Teng et al. (2003) model and is based on the strain limit. Based on numerical simulations and regression of test data, Lu (2004) proposed the effective FRP strain at debonding, εdb, as expressed in Table 2-1, Eq.2-21.

where L_d is the distance from the FRP plate end to the section where the plate is fully used, f_t is the concrete tensile strength and is equal to f_{ctm}.

According to the database collected by Said and Wu (2008), the Wu and Niu (2007) model exhibited the lowest level of dispersion with a coefficient of variation of 10.7% when comparing the predicted delamination loads to the corresponding experimental values. It had the narrowest range of prediction ratios of 59%. They reported that the good performance of the model may be due to the theoretical basis of the model. On the other hand, the Fib model was found to be the most conservative, but it had the highest level of dispersion. Except for one specimen, all predictions underestimated the actual load, with an average predicted-to-experimental load ratio of 67%, and a coefficient of variation of 21%. They reported that the inaccurate prediction may be due to the low value of fracture energy, G_f ,used by Fib, which is calculated based on Eq.2-32

$$G_f = \frac{0.026\sqrt{f_{ck} f_{ctm}}}{\gamma_c} \qquad \text{Eq.2-32}$$

where, γ_c is the material safety factor of the concrete and is equal to 1.5. According to Fib bulletin 14, Eq.2.32 gives values ranging between 0.08 N/mm and 0.26

N/mm. These values are considered much lower than the values calculated based on the Wu and Niu (2007) model. The model also requires calculation of the distance along which the FRP stress varies, s_{rm}. The equation given to calculate s_{rm} may not be adequate since it is greatly affected by the longitudinal steel reinforcement ratio ρ_s. The less the reinforcement ratio, the higher the distance, s_{rm} consequently, the smaller the predicted debonding load. The inherent complexity of the model makes it hard to be applicable in normal engineering practice. The ACI Committee 440 (2002) model was found to be the least conservative among all the investigated models, with an average predicted-to-experimental load ratio of 102%. However, the general performance of the model seemed good, with a reasonable level of dispersion and a relatively narrow range of predictions ratios. The coefficient of variation and the range of the prediction ratios of the ACI model were 11.5% and 63%, respectively. Even this model has several problems. It is entirely dependent on the axial rigidity of the FRP laminate, $E_f t_f$, as a unique parameter for estimating the debonding FRP strain. As indicated before, other parameters may also affect the debonding failure load, such as the concrete fracture energy, as represented by the concrete compressive strength. The new ACI 440-08 took into account the effect of the concrete compressive strength as shown in Table 2-1, Eq.2-12. Furthermore, the total debonding moment, M_{DEB} , is the sum of the internal reinforcement moment contribution M_s and the contribution of the FRP composite M_f. This can be expressed as

$$M_{DEB}=M_S+M_F \qquad \text{Eq.2-33}$$

Since the delamination always occurs after yielding of the steel and assuming elasto-plastic behaviour, then M_s can be expressed as

$$M_s = A_s \sigma_y y_t \qquad \text{Eq.2-34}$$

where A_s is the tension reinforcement area, y_t is the internal lever arm of the reinforcement and σ_y is the reinforcement yield stress.

The moment from the FRP composite can be expressed as:

$$M_f = A_f E_f \varepsilon_f y_f \qquad \text{Eq.2-35}$$

where y_f is the internal lever arm of the FRP. Using the ACI strain limitations, the contribution of the FRP laminate moment can be expressed as

$$M_f = A_f E_f \frac{1}{60\varepsilon_{fu}}\left(1 - \frac{nE_f t_f}{360000}\right) y_f \quad \le 0.9 \quad for\ nE_f t_f \le 180000$$
$$M_f = A_f E_f \frac{1}{60\varepsilon_{fu}}\left(\frac{90000}{nE_f t_f}\right) y_f \quad \le 0.9 \quad for\ nE_f t_f > 180000 \qquad \text{Eq.2-36}$$

This shows that the bending capacity of the strengthened section will not be enhanced by increasing the FRP axial stiffness $E_f t_f$ above 180000 N/mm, which may be the reason for the less accurate predictions of the ACI model. In general this model underestimates the actual debonding load of members strengthened with high stiffness FRP laminates.

The Teng et al. (2003) model has a similar overall performance to the Fib model in terms of its conservatism and a high level of dispersion. The mean and the coefficient of variation of the ratio of the predicted over experimental debonding load by the Teng et al.(2003) model were 69% and 21%, respectively.

Lu's model (2004) has the widest range of prediction ratios of 82%. Although this model has the highest predicted-to-experimental load ratio of 138%, some of the predicted loads are lower than the corresponding yielding loads, especially for beams with high-stiffness FRP composites. The lack of conservatism for a considerable number of specimens accompanied by a wide range of prediction ratios is a problem in this model. It needs a high factor of safety if used in design since it tends to overestimate the debonding loads, but using a higher factor in each case may lead to uneconomic design. It is not clear why the value of L_d should affect the effectiveness of FRP strain at debonding if a sufficient bonding length is provided; therefore, the physical meaning of this parameter is not clear.

Said and Wu (2008) proposed an empirical model based on the previous discussion and the above comparisons. They proposed that the debonding strain can be expressed as

$$\varepsilon_{deb} = \frac{0.23(f_c^{'})^{0.2}}{\left(E_f t_f\right)^{0.35}} \qquad \text{Eq.2-37}$$

Accordingly, the debonding moment capacity of FRP strengthened flexural member may be expressed:

$$M_{deb} = A_s \sigma_y y_s + 0.23 b_f (f_c^{'})^{0.2} (E_f t_f)^{0.65} y_f \qquad \text{Eq.2-38}$$

where y_s and y_f are the internal lever arms for the steel and FRP reinforcement which can be calculated by applying the strain compatibility and static equilibrium requirement. The proposed empirical model was calibrated against a relatively large database and it was found that the coefficient of variation is 9.5% which is considered better than any other proposed method.

Saxena et al. (2008) , did a similar study and investigated the applicability of the existing models to the prediction of debonding. They concluded that the available methods are not sufficiently robust. They reported that none of the models can predict debonding load correctly in every case and the level of inaccuracy is similar in midspan and plate end debonding.

Rosenboom and Rizkalla (2008) tested six 9.14 m long prestresed concrete bridge girders to failure to evaluate the bond characteristics of carbon FRP strengthening systems. They used CFRP U-jacket placed throughout the girder length and they found that it increased the tensile strain in pre-cured CFRP laminates at IC debonding by 20%. They used the ACI Committee 440 (2002) model to predict the failure load and they found it to be unconservative. Their proposed model provided a more accurate prediction of the IC debonding load and is applicable to both reinforced and prestressed concrete structures.

Assessment of the available models was performed by the same authors in a different study. Only those models with clear failure criteria were examined. The empirical model by Maeda et al. (1997) was compared with the database collected for double lap-shear specimens and it was found that the model tends to overestimate the debonding strain as the axial stiffness of the FRP decreases. Matthys (2000) defined a failure criterion called "transfer of forces," where the derivative of the tensile envelope due to applied loading is determined and compared to the shear strength of the concrete. Two simple design equations were presented to determine the maximum shear force that could cause debonding before or after steel yielding. Although the predicted shear at debonding showed good correlation to the experimental shear force, this is mainly due to the large disparity between the sizes of the beams in the database. The correlation could be deceiving since a significant increase in debonding strain does not lead to a proportional increase in applied shear force.

Leung and Tung (2001) proposed an analytical model to assess IC debonding. One of the benefits of the model is its ability to predict the debonding strain at the main flexural crack and at various unbonded distances from the crack due to interfacial cracking. The value of acceptable localized debonding around the main flexural crack is assumed to be in the range of 25% of the height of the cross section of the beams. When compared to experimental data, the model was found to underestimate the strain at debonding. The model of Harmon et al. (2003) was also assessed and was found to take into account the flexural crack spacing, and calculates the maximum force that can be developed in the FRP through an iterative procedure. One of the important variables in the estimation of the force in the FRP at the critical crack location is the effective bond length, L_{eff}, which is equal to

$$L_{eff} = \sqrt{\frac{E_f t_f t_b}{G_a}} \qquad \text{Eq.2-39}$$

where E_f and t_f = elastic modulus and thickness of the FRP material, t_b = thickness of the bond or adhesive layer; and G_a = shear modulus of the adhesive. The effective bond length calculated using Eq.2-39 is much less than the calculated value using other models (e.g., Chen and Teng 2001; Oehlers and Seracino 2004).

Teng et al. (2004) developed a set of equations to predict the IC debonding resistance based on mechanics and fracture-based behaviour. The one parameter in the model, the distance from the loaded end to the end of the cracked region, L_{ee}, was calculated using the following equation:

$$L_{ee} = a - \frac{M_{cr}}{M_{db}} a + s \qquad \text{Eq.2-40}$$

where a=shear span; s=distance from the center of the support to the FRP termination point; and M_{cr} and M_{db} = cracking moment and nominal moment at the predicted debonding strain of the FRP-strengthened section. Since M_{db} can only be calculated once a debonding strain is assumed, the model becomes iterative. This model also generally overestimates the debonding strain and its predictions do not agree with experimental data.

The fracture-based model of Ulaga et al. (2003) was derived from an experimental program on double lap-shear specimens and assuming a linearly descending interface shear stress versus slip relationship. Similar to the other fracture based models, which are derived from test results on lap-shear specimens, the mean value of the model is conservative when applied to the IC debonding in beams. This model is an extension of the Chen et al. (2005) model and it uses a linearly descending shear stress versus slip relationship and multiple flexural cracks. The model derived based on the behaviour of a single lap-shear specimen with the force applied to the FRP laminate from two directions, which simulates the behaviour of the bonded joint between two flexural cracks. Two sets of equations are presented, one that ignores the deformation in the concrete and the other equation that includes it. The equations that include the deformation in the concrete layer do not give results which match well available experimental data and are more conservative than the equations ignoring the concrete deformation. The ratio of the loads applied to the two ends of the FRP segment was assumed to be 0.8. It should be noticed that even thought this model was derived on the basis of data from small-scale specimens, still its results compare well to data from large scale specimens and are not overly conservative like earlier models (e.g., Chen and Teng 2001). This is most likely due to the more realistic boundary and loading conditions assumed in the derivation of the latter model.

The latter model ascribes the interface shear stress to two distinct sources: (1) the change in the applied moments along the length of the member and (2) stress concentrations at intermediate cracks. The calculation of the yielding moment M_y , is required and the corresponding strain in the FRP, $\varepsilon_{FRP\ @y}$. The debonding moment M_{db} can be calculated by assuming a debonding strain ε_{db}. The maximum shear stress τ_{cmax} can be calculated as

$$\tau_{c\max} = nE_f t_f \left(\frac{\varepsilon_{db} - \varepsilon_{f@y}}{S - X_y} \right) + 3\left(1.1 - \frac{M_y}{M_{db}} \right)\sqrt{f_c'} \qquad \text{Eq.2-41}$$

where, S is the shear span and the X_y is the distance from the support to the location of the first yielding of the internal tensile steel. The value of ε_{db} is iterated until τ_{cmax} is equal to1.8 f'_c. The total strain in the CFRP (ε_{db}) is the summation of the debonding strain and the strain due to stress concentration (ε_{sc}) which can be calculated as:

$$\varepsilon_{sc} = 0.342\left(1.1 - \frac{M_y}{M_{db}} \right)\sqrt{\frac{f_c'}{nE_f t_f}} \qquad \text{Eq.2-42}$$

If the total strain (ε_{db}+ ε_{sc}) exceeds the rupture strain of the CFRP sheet, then rupture will occur before debonding.

Neale et al. (2009) proposed a design equation for debonding strains in RC structures externally strengthen with FRP. They used the numerical results obtained from finite element model and integrated these results into statistical analyses. They used the response surface methodology (RSM) to define the FRP debonding strain. This strain was expressed as a function of the type of application. Monte Carlo simulations were conducted to generate a large combination of various variables. A nonlinear regression analysis was employed to establish relatively simple design equation that best fits the data. Eq. 2-43 shows their proposed equation for maximum FRP strain at delamination, ε_{FRPd}

$$\varepsilon_{FRPd} = 0.75\varepsilon_{FRP} + 70.9f_c^{'} + 106.81L - 225.7\rho - 113.1(EA)_{frp} - 283.4d \qquad \text{Eq.2-43}$$

where ε_{FRP} is the FRP rupture strain, f'_c is the concrete compressive strength, L is the beam span, ρ is the internal steel reinforcement ratio, E and A are the Young's modules and cross sectional area of the FRP, respectively, and d is the effective depth of the beam. This equation is considered easy to use in practice and it accounts for the effect of different variable on the predicted FRP debonding strain.
The Italian code (CNR-DT 200/2004) limits the strain in the FRP as shown in Eq.2-45

$$\varepsilon_{fd} = \min\left\{\eta_a \frac{\varepsilon_{fk}}{\gamma_f}, \varepsilon_{fdd}\right\} \qquad \text{Eq.2-44}$$

where ε_{fk} is the characteristic strain at failure of the strengthened system; γ_f and η_a are coefficients that depend on the material and the environmental conditions respectively, and ε_{fdd} is the maximum strain due to intermediate debonding.

2.4 Summary

In the light of the above discussion, a need exits for a reliable design method for structures strengthened with FRP. Most of the design equations underestimate the actual strain of the FRP which leads to under-utilization of the full capacity of the FRP material.
Another important factor that must be considered in the design of FRP-retrofitted members is the mode of failure. Failure initiated by delamination can be very brittle, which is quite undesirable. Therefore, to be able to take advantage of the full strength of the FRP and to prevent sudden delamination, there is need for a robust and effective anchor system. To date none of the available anchors systems

have proven effective in every situation and very few have ever been tested in large size beams with multiple layers of FRP. Consequently, the need exists for both proper analytical models to predict delamination and for a universal and reliable anchor system.

CHAPTER 3
Experimental Program

3.1 General

The main objective of the current experimental work is to investigate the proposed new anchorage system for delaying/preventing delamination and to find the most appropriate anchor arrangement which can be used to achieve this objective. This investigation was done in three phases. In phase I, six CFRP strengthened concrete prisms were tested in tension to failure. Phase II included sixteen concrete prisms to confirm the findings in phase I. Finally, twenty one large scale RC beams were constructed to examine the anchor effectiveness in beams under four point bending. In this chapter, the details of the experimental program will be presented; results will be discussed in the following chapter.

3.2 Phase I

The specimens tested in this phase are schematically shown in Figs. 3-1, 3-2 and 3-3. Six nominally identical prisms with 200x250 mm cross-section and length of 1000 mm were built. All the specimens were reinforced with 4 No.15 ($\varnothing \approx 16$ mm) bars as longitudinal reinforcement and No.10 ($\varnothing \approx 11.3$ mm) stirrups as transverse reinforcement. Two No.25 ($\varnothing \approx 25$ mm) steel bars, each bolted to a steel plate (80x80 mm) at one end for anchorage, were placed inside the prisms as shown in Fig. 3-1. The FRP laminate used to strengthen the prisms consisted of a CFRP laminate impregnated with epoxy resin. The concrete surface to which the FRP was bonded was roughened by grinding it and then cleaning it with air pressure. A layer of epoxy paste was used as primer to fill surface voids and uneveness before the application of the CFRP laminate.

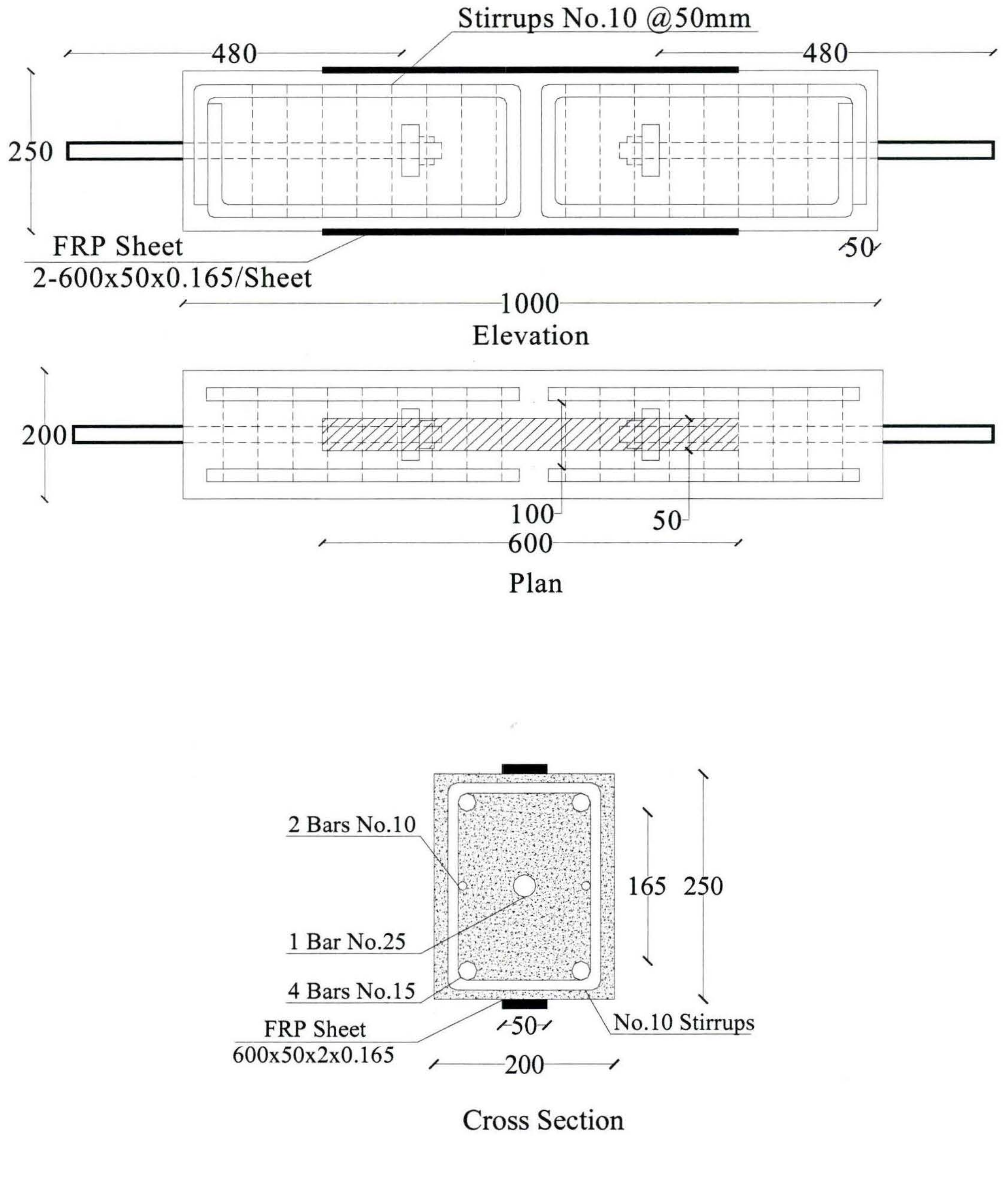

Fig.3-1: Typical concrete prism externally strengthened with CFRP laminate

Note: All dimensions are in mm.

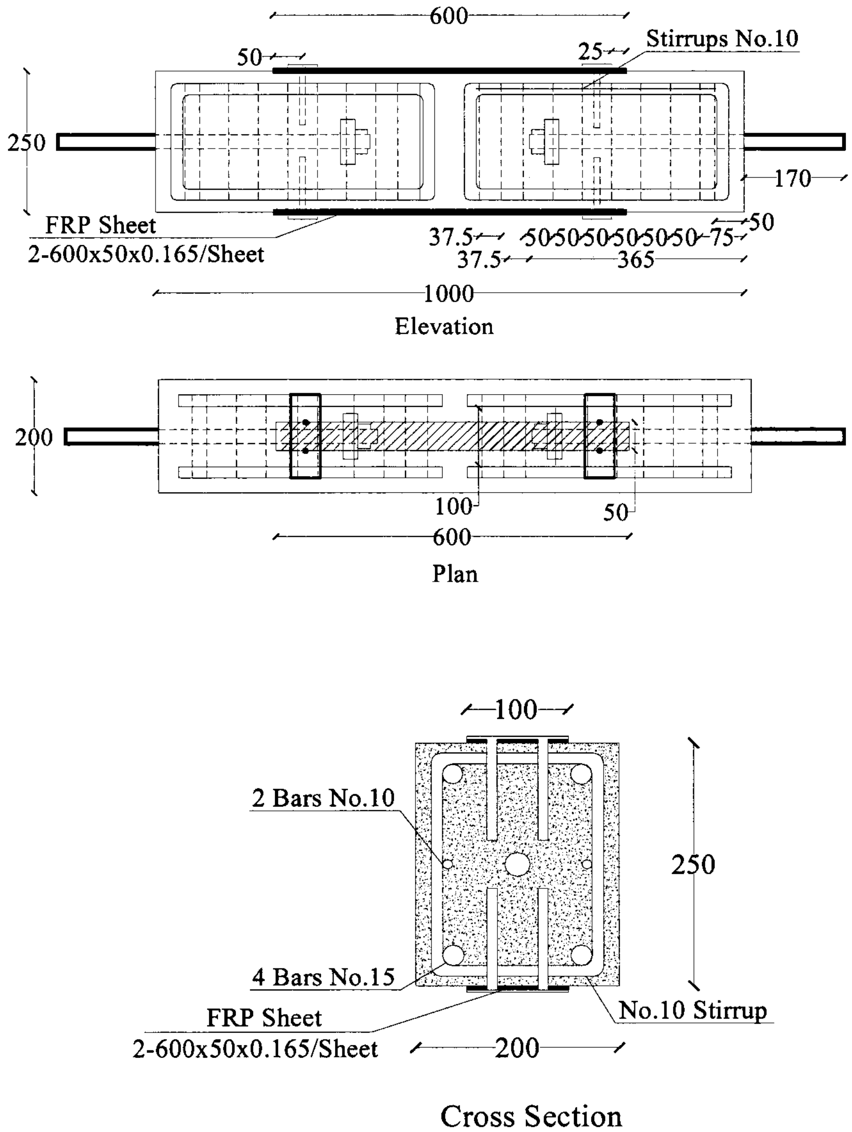

Fig.3-2: Typical concrete prism externally strengthened with anchored CFRP laminate

Note: All dimensions are in mm.

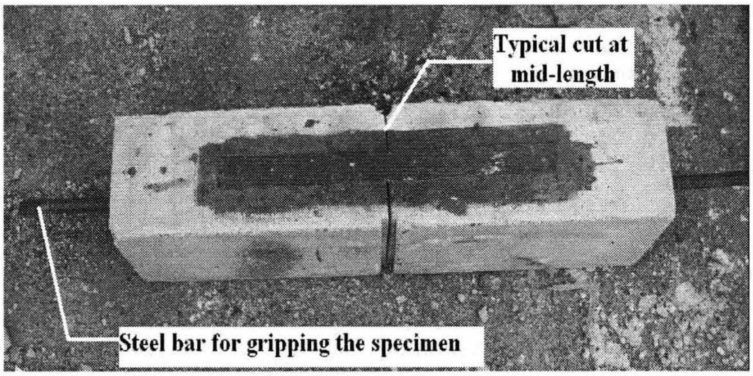

Fig.3-3: Prism strengthened with CFRP laminate

CFRP laminates were bonded on two opposite faces of the specimens as illustrated in Figs.3-1 and 3-2. Each face had two layers of laminate, each laminate being 50 x 0.165 x 600 mm. Strain gauges were placed on the laminate surface to measure its strain along its bonded length. Two prisms were used as control specimens and were not strengthened. The six prisms are classified as follows:

- Two control prisms, without CFRP reinforcement. [C1 and C2]
- Two prisms strengthened with two layers of CFRP laminate on two opposite faces, (each single laminate being 8.25mm^2 in cross section). [C3 and C4], Fig.3-1.
- Two prisms strengthened with two layers of CFRP laminate on two opposite faces and the laminates being anchored by one anchor at 25 mm from the laminate end. [C5 and C6], Fig.3-2.

3.2.1 Material Properties

Concrete

Ready mixed concrete was ordered from a local plant and was delivered to the laboratory. During casting, a total of 8 standard concrete cylinders (150x150x300mm) were cast and cured under the same conditions as the test prisms. Curing consisted of moist curing for seven days and air-curing subsequently. Eight cylinders were tested 28-days after casting, five under compression and three in tension (splitting test); the results are summarized in Table 3-1. The table shows compression strength f'_c and splitting tensile strength f'_t

of each specimen. Notice that both the compression and tensile strength values are reasonably consistent.

Table 3-1: 28-day compressive and tensile strength of concrete for test prisms

Age (days)	Specimen	Compression test	Splitting test
		f'_c (MPa)	f'_t (MPa)
28	1	26.5	2.5
	2	28.0	2.4
	3	26.5	2.5
	4	27.9	-
	5	27.5	-
	Average	27.3	2.5

Steel Reinforcement

Since the steel reinforcement is not the focus of this study nor it is expected to influence the results of the current tests, it was not tested to determine its properties. All the steel rebars used to reinforce the prisms had normal yield strength of 400 MPa.

CFRP Laminate

The laminate used in this investigation was a unidirectional high strength carbon fiber fabric, known as Wabo Mbrace CF 130 (Mbrace CF130, 1998). A summary of the CFRP material properties, as provided by the manufacturer, is given in Table 3-2.

Table 3-2: CFRP composite material properties provided by the manufacturer

Properties	Wabo MBrace CF130
Tensile strength	3800 MPa
Modulus of elasticity	227GPa
Ultimate rupture strain	1.67%
Thickness	0.165 mm/ply
Width	610 mm

Note that the MBrace CF 130 is available in 82 m (270 ft) length and 610 mm (24 in) width. It should be stated that the focus of this study is on delamination, which is governed primarily by epoxy-concrete interfacial strength and the axial rigidity of the FRP laminate. Although it is desirable to obtain the CFRP properties from coupon tests, the current testing facilities at ADL, especially the lack of hydraulic grips for the Universal Testing Machine, makes it quite difficult to obtain reasonably accurate and consistent results. Therefore, in this study the manufactuer recommended values will be used.

Epoxy

Part A and Part B of the epoxy were mixed together with a mix ratio A: B = 3:1 by volume. For the Wabo MBrace CF130 CFRP sheet, Wabo MBrace Primer and Wabo MBrace Saturant were used. Each has Part A and Part B. Table 3-3 includes the relevant material properties for both Wabo MBrace Primer and Wabo MBrace Saturant.

Table 3-3: Wabo MBrace primer and saturant properties used

<table>
<tr><th colspan="2">Properties</th><th>Wabo MBrace Primer</th><th>Wabo MBrace Saturant</th></tr>
<tr><td rowspan="6">Tensile properties</td><td>Yield strength</td><td>14.5 MPa</td><td>54 MPa</td></tr>
<tr><td>Strain at yield</td><td>2.00%</td><td>2.50%</td></tr>
<tr><td>Elastic modulus</td><td>717 MPa</td><td>3034 MPa</td></tr>
<tr><td>Ultimate strength</td><td>17.2 MPa</td><td>55.2 MPa</td></tr>
<tr><td>Rupture strain</td><td>40%</td><td>3.50%</td></tr>
<tr><td>Poisson's ratio</td><td>0.48</td><td>0.4</td></tr>
<tr><td rowspan="5">Compressive properties</td><td>Yield strength</td><td>26.2 MPa</td><td>85.2 MPa</td></tr>
<tr><td>Strain at yield</td><td>4.00%</td><td>5%</td></tr>
<tr><td>Elastic modulus</td><td>670 MPa</td><td>2620 MPa</td></tr>
<tr><td>Ultimate strength</td><td>28.3 MPa</td><td>86.2 MPa</td></tr>
<tr><td>Rupture strain</td><td>10%</td><td>5%</td></tr>
<tr><td rowspan="5">Flexural properties</td><td>Yield strength</td><td>24.1 MPa</td><td>138 MPa</td></tr>
<tr><td>Strain at yield</td><td>4.00%</td><td>3.80%</td></tr>
<tr><td>Elastic modulus</td><td>595 MPa</td><td>3724 MPa</td></tr>
<tr><td>Ultimate strength</td><td>24.1 MPa</td><td>138 MPa</td></tr>
<tr><td>Rupture strain</td><td>Large deformation-no rupture</td><td>5%</td></tr>
<tr><td rowspan="3">Color</td><td>Part A</td><td>Amber</td><td>Blue</td></tr>
<tr><td>Part B</td><td>Clear</td><td>Clear</td></tr>
<tr><td>Mixed</td><td>Amber</td><td>Blue</td></tr>
<tr><td rowspan="4">Mix</td><td>Mixed weight</td><td>1103 g/L</td><td>984 g/L</td></tr>
<tr><td>Density</td><td>1102 kg/m^3</td><td>983 kg/m^3</td></tr>
<tr><td rowspan="2">Mixed ratio</td><td>3:1 (part A :part B) by volume</td><td>3:1 (part A: part B) by volume</td></tr>
<tr><td>100:30(part A: part B) by weight</td><td>100:34(part A: part B) by weight</td></tr>
</table>

CFRP Anchor

In this study, CFRP anchors were fabricated and used to anchor the externally bonded laminates to the concrete. Figure 3-4 shows two typical anchors that were manufactured. Each anchor is made from a carbon fibre tow and CFRP fabric immersed in the Wabo Mbrace epoxy, and then placed in a specially fabricated aluminum mould as shown in Fig.3-5, which illustrates the geometry and dimension of the mould. The fibres were continuous and laid in two longitudinal grooves that were machined in both the male and female halves of the mould. The fibres were left in the mould undisturbed for 24 hours. Note that the moulds allow one to manufacture anchors with different leg spacing. The leg spacing of the anchors used in the current prisms was 50 mm.

Each anchor is made from a carbon fibre tow and CFRP fabric immersed in the Wabo Mbrace epoxy, and then placed in a specially fabricated aluminum mould as shown in Fig.3-5, which illustrates the geometry and dimension of the mould. The fibres were continuous and laid in two longitudinal grooves that were machined in both the male and female halves of the mould. The fibres were left in the mould undisturbed for 24 hours. Note that the moulds allow one to manufacture anchors with different leg spacing. The leg spacing of the anchors used in the current prisms was 50 mm .

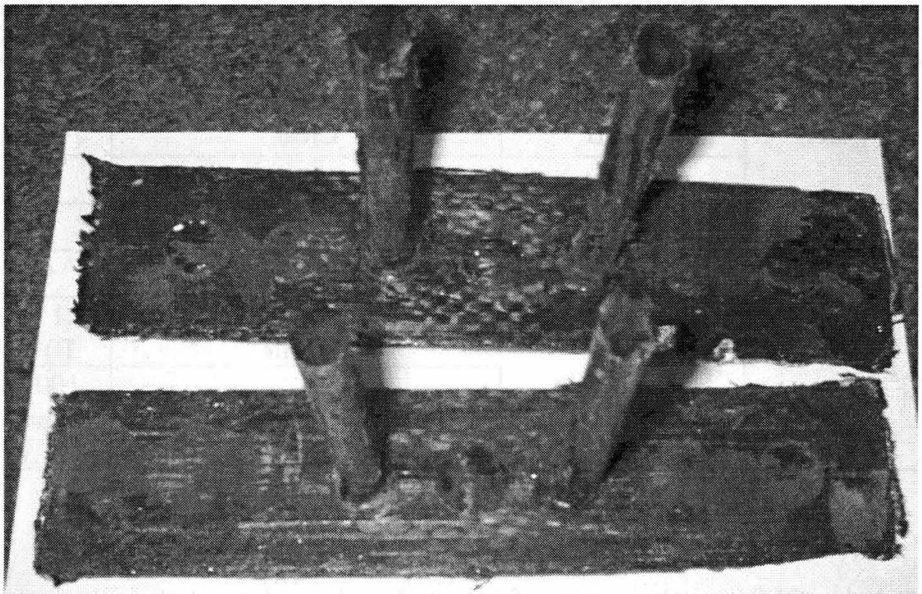

Fig.3-4:Typical anchors manufactured and tested to prevent delamination

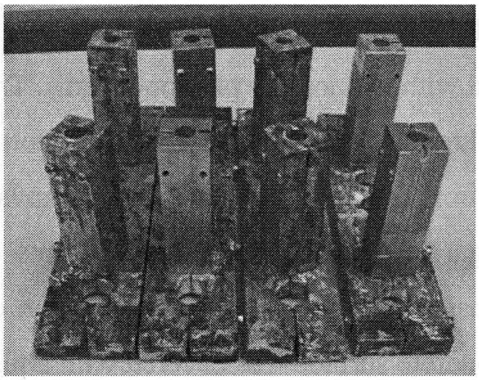

(a): Aluminum moulds for anchor fabrication

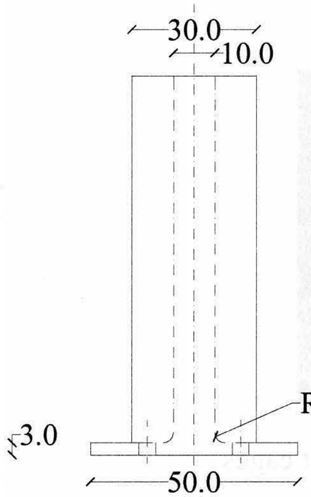

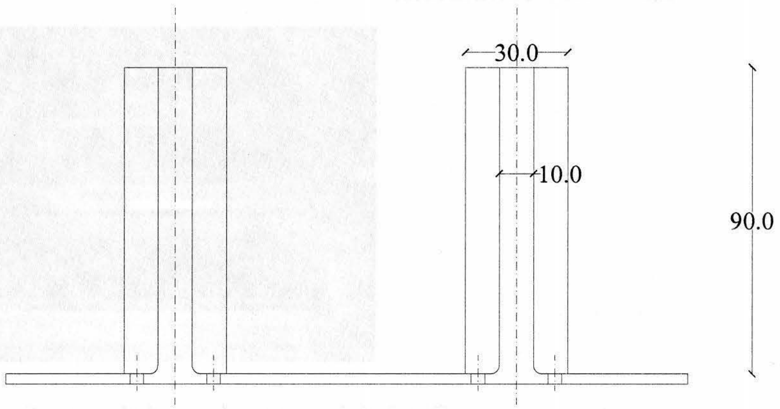

(b): Side view (c): Cross sectional elevation

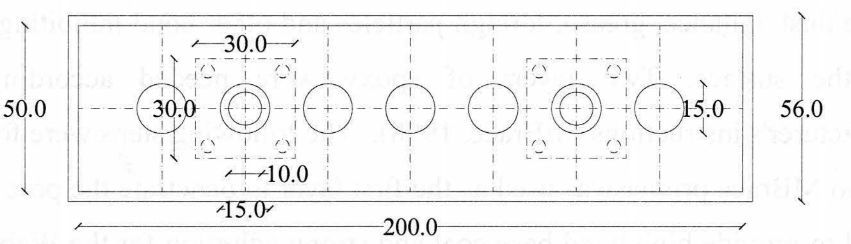

(d): Plan view

Note: All dimensions are in mm.

Fig.3-5: (a) Anchor moulds, (b) Side view, (c) Cross sectional elevation, (d) Plan view

3.2.2 Fabrication of Phase I

The construction started with making the plywood forms. The reinforcement cages were constructed with high accuracy and placed in the formworks. All the forms were brushed with oil from inside to facilitate their removal after the casting and curing of concrete. Figure 3-6 shows the concrete forms and the reinforcement cages. All of the prisms were vibrated properly using an electric vibrator. After casting, the exposed concrete surface was covered with a plastic sheet. The curing was at room temperature and the surface was kept moist for at least 10 days. The forms were removed after 3 weeks and the specimens were cured under the normal laboratory conditions.

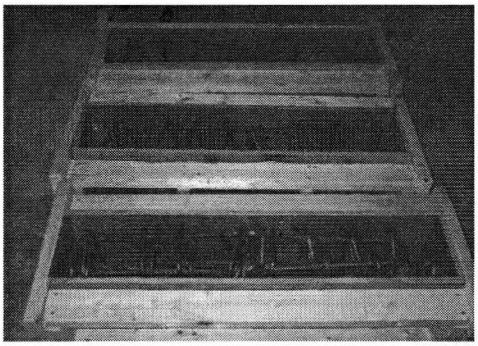

Fig.3-6:Formworks and the reinforcement cages

After the removal of the formworks, the processes of applying the CFRP laminate and placing the anchors started using air pressure to clean and dry the surface, remove dust, laitance, grease, foreign particles and other bond inhibiting materials from the surface. Two layers of epoxy were needed according to the manufacturer's instructions (MBrace, 1998). The following steps were followed:

1. Wabo MBrace primer was used as the first layer to penetrate the pore structures and to provide high bond base coat and strong adhesion for the Wabo MBrace epoxy.
2. The MBrace saturant was applied using a normal painting roller.

3. The first ply of the CFRP laminate was placed onto the first layer of wet saturant using the roller. The laminate was pressed down until the adhesive exuded from under the sheet.
4. The second layer of the saturant was applied using a roller, and then steps 2 and 3 were repeated to install the next two plies of the laminate. After the installation of the last ply, the epoxy was allowed to cure undisturbed for at least 24 hours.

3.2.3 Test Equipment and Instrumentation

The following equipment and instrumentation were used in the testing program:

1. Tinius Olson Universal Testing machine to apply the axial load.
2. MTS data acquisition system attached to a microcomputer.
3. Three dial gauges installed on opposite sides to measure displacement along the prism [Phase I].
4. Three potentiometers installed on three faces to measure displacement along the prism [Phase II].

Figure 3-7 shows the strain gauges arrangement for the tested prisms with and without anchors and Fig.3-8 shows a typical prism during the tests.

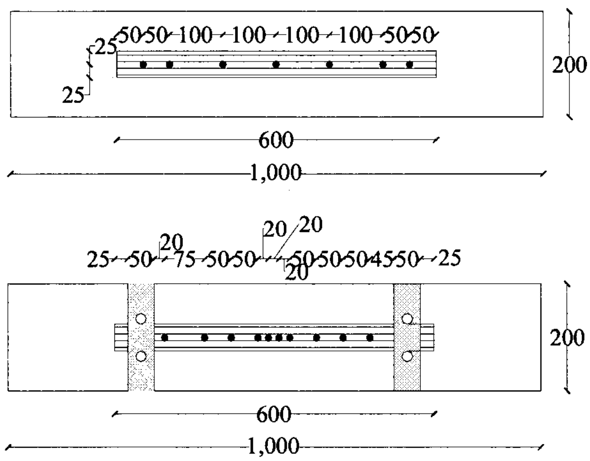

Fig.3-7: Arrangement of the anchors and the strain gauges in the test prisms in Phase I

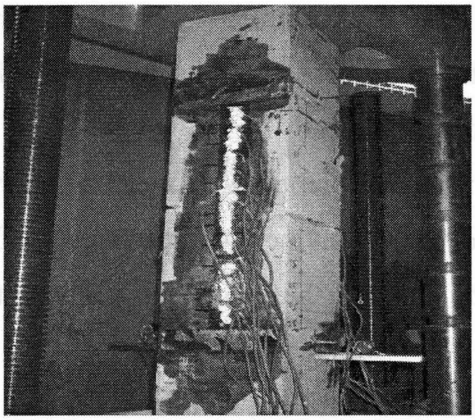

Fig.3-8: Typical concrete prism during the test

Measurement of strains in CFRP laminate was taken using electrical resistance strain gauges with gauge length of 5 mm. The strain gauges were sensitive to 0.01 micro strain with a standard deviation of 2%. After the adhesive cured, strain gauges were installed on the CFRP surface along its length. A thin layer of silicone coating was applied on each strain gauge to ensure protection against impact, moisture and possible damage during handling.

3.2.4 Test Setup

The tests were conducted in the Applied Dynamics Laboratory of the Department of Civil Engineering at McMaster. The load was applied using the Tinius Olson Universal Testing Machine as shown in Fig.3-8. The loading rate was relatively slow at 0.1 inch/minute to simulate static loading condition.

3.3 Phase II

Based on the results found from the first phase, it was clear that the results obtained were not as expected. The two No.10 reinforcing bars dominated the strength of the prisms and the anchor behaviour was not clear. Therefore, it was decided that another set of concrete prisms be constructed and tested to overcome and eliminate the problem encountered during the first phase. The new set consisted of 16 identical concrete prisms, and the following parameters were investigated:

1- Number of anchors

2- Location of the anchors

3- Presence/absence of mechanical CFRP anchors

4- CFRP laminate with pre-delaminated segment

Sixteen 250 mm deep, 200 mm wide, and 1000 mm long concrete prisms were tested in tension. The cross section was reduced at mid-length to ensure failure at this location. Two No.25 steel bars were placed inside the concrete, as shown in Fig.3-9. Each bar was bolted to a steel plate (80x80 mm) at one end to prevent it from being pulled out of the prism when subjected to tension. The CFRP laminate and anchors were applied as in phase I. Figures 3-9, 3-10 and 3-11 show the geometry, dimension and anchors arrangement for all the tested prisms. Notice the anchor locations in Figs.3-10 and 3-11.

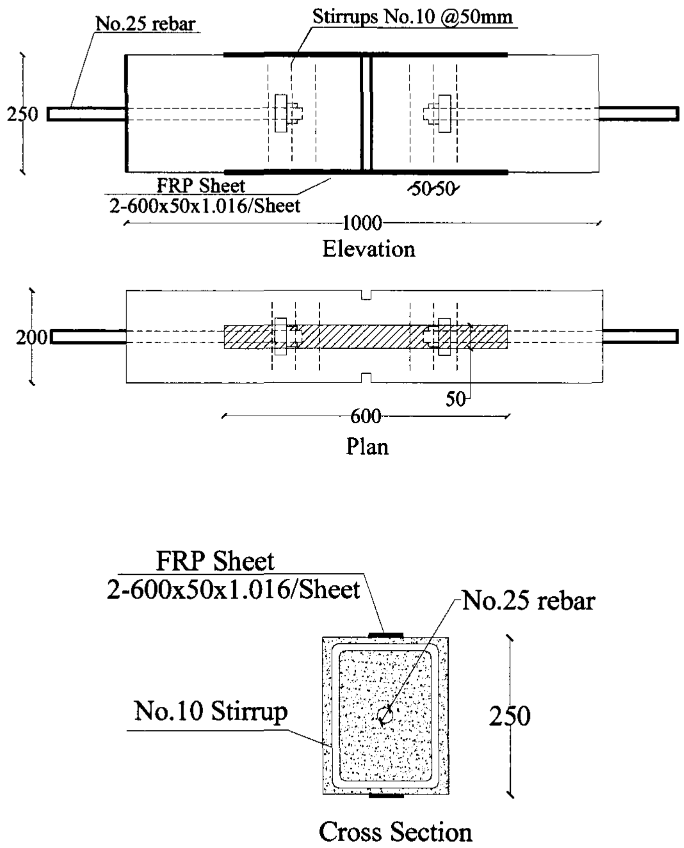

Fig.3-9: Geometry and dimension for typical concrete prisms strengthened with CFRP laminate

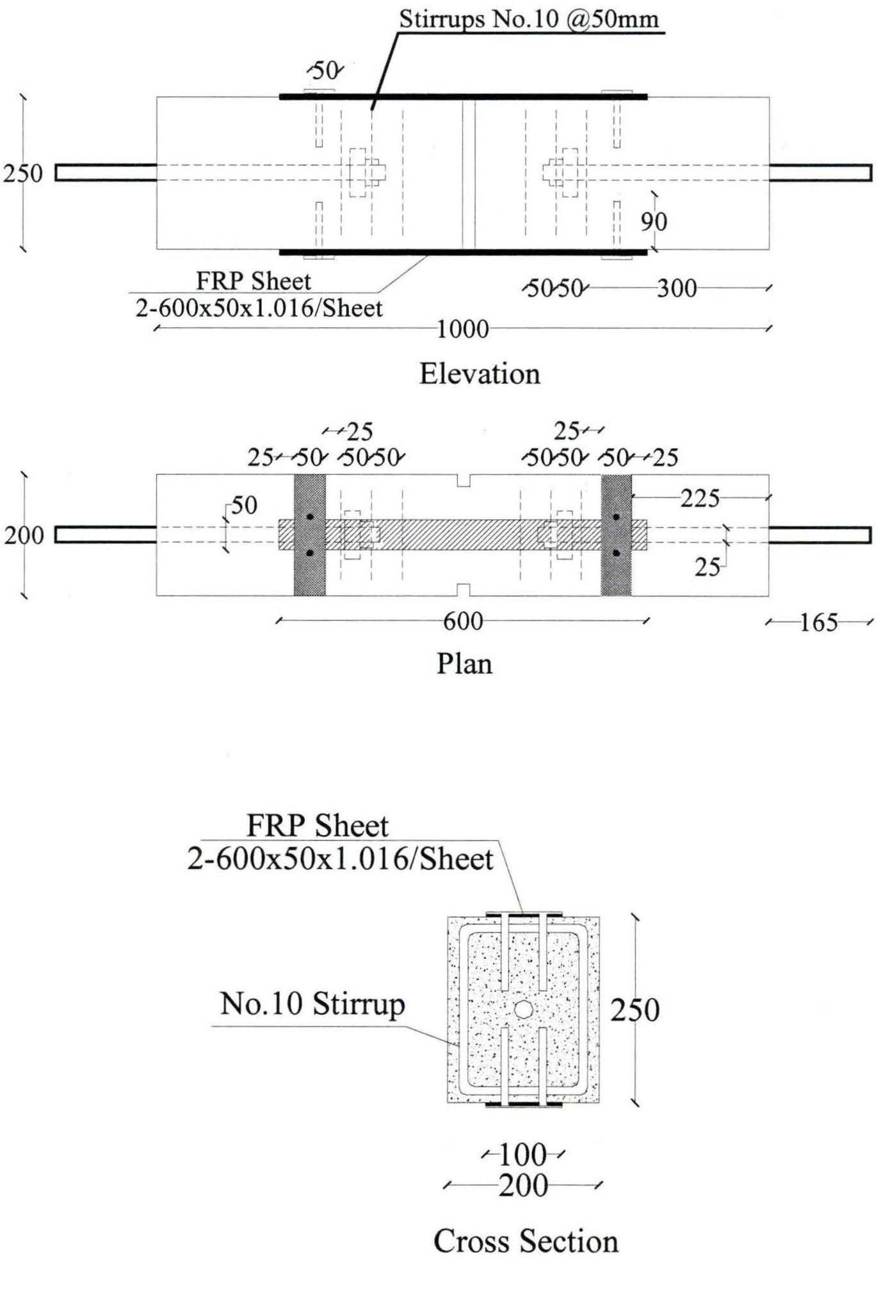

Fig.3-10: Geometry and dimension for typical concrete prisms strengthened with CFRP laminate and anchored with 2 anchors/side

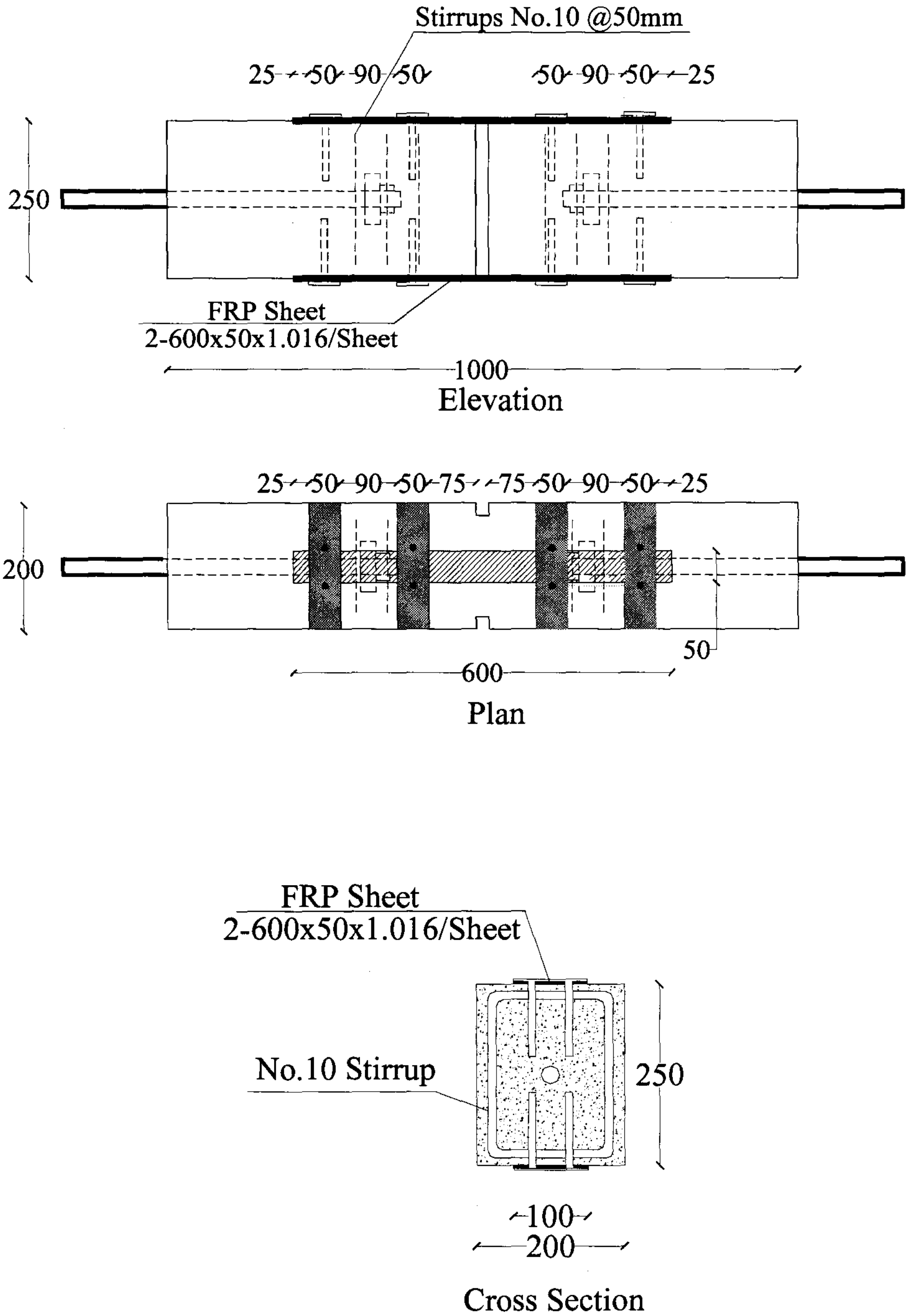

Note: All dimensions are in mm.

Fig.3-11: Geometry and dimension for typical concrete prisms strengthened with CFRP laminate and 4 anchors/face

3.3.1 Material Properties

Concrete

Ready mixed concrete was ordered from the plant and was delivered to the laboratory. During casting, a total of 8 standard concrete cylinders (150x150x300mm) were cast and cured under the same conditions as the test prisms. The curing consisted of moist curing for seven days and air-curing subsequently. Eight cylinders were tested after 60-days; five cylinders were tested under compression and three cylinders in tension (splitting test). Table 3-4 summarizes the results for the tested specimens after 60-days, with average compressive and tensile strength of 27.5 MPa and 2.4 MPa, respectively.

Table 3-4: Concrete cylinder test results at the age of 60-days

Age (days)	Specimen	Compression test	Splitting test
		f_c' (MPa)	f_t (MPa)
60	1	28.2	2.6
	2	27.3	2.1
	3	27.7	2.6
	4	26.8	-
	5	28.5	-
	Average	27.5	2.4

Transverse Steel Reinforcement

To prevent concrete splitting in the vicinity of the plates attached to the ends of the No.25 steel bars, three No.6 stirrups were placed in the concrete near each of these plates and were spaced at 50 mm (see Fig.3-9).

CFRP Laminate and Anchors

The CFRP laminate used in this investigation was unidirectional high strength carbon fiber fabric, known as SikaWRAP HEX 103C. As reported by the manufacturer of the material, its nominal thickness, modulus of elasticity, tensile strength, and ultimate rupture strain are 1.016 mm/ply, 70.55 GPa, 849 MPa and 1.13%, respectively.

The adhesive in this phase was the same as in Phase I, which was described in section 3.2.1. Similarly, the anchors were manufactured as explained in section 3.2.1.

3.3.2 Concrete Prism Configurations

To be able to investigate the effectiveness of the proposed anchor, the following modifications were introduced in phase II:

1- The mid-section of the prisms was without steel reinforcement.

2- Only three stirrups were used in the vicinity of the steel plates used to provide anchorage for the loading rod and to prevent splitting of concrete.

3- The mid-length cross section of the prisms was reduced by cutting the concrete using a concrete saw. The reason for this was to make sure that the prism cracked at its mid-length and allowed the CFRP to take the full tension force.

The CFRP laminates were bonded on the two opposite faces of each prism. Each face had two layers of CFRP laminate with each laminate being 50 mm wide x 1.016 mm thick x 600 mm long. Strain gauges were installed on the CFRP laminate to measure the strains along its bonded length. The test prisms included the following:

- Six control prisms without CFRP laminate. [P1 to P6]
- Two prisms strengthened with two layers of CFRP laminate on each of the two opposite faces, (each single laminate was 50.8 mm^2 in cross section). [P7 and P8]
- Three prisms strengthened with CFRP laminate similar to the previous two prisms but with four anchors, two on each face. [P9, P10 and P11]

- Two prisms strengthened with CFRP laminate similar to prisms [P7 and P8], but with eight anchors, four on each face. [P12 and P13]
- One prism strengthened with CFRP laminate, with four anchors, two on each face placed at 25 mm from the laminate end. One face had a pre-delaminated segment of 150 mm at the mid-section of the prism. [P14]
- Two prisms strengthened with CFRP laminate and anchored with eight anchors, four on each face. Both prisms had a pre-delaminated segment of 100 mm at mid-section of the prism on both faces. [P15 and P16]

The π- shape anchors were inserted into holes made by hollow tubes going thought the formwork. The tubes were removed after casting the concrete, and to permit the insertion of the anchors they were enlarged using a drill. Note that the holes were drilled into the concrete adjacent to the CFRP laminate but not into it because holes through CFRP would damage the fibres and reduce its cross-sectional area. Due to the preliminary nature of the current investigation and the fact that concrete cracking and nonlinearity can lead to more complex stress distribution than that predicted by elastic theory, it is not feasible to arrive at precise spacing for the anchors. The first anchor was always placed at 25 mm from the laminate end and the anchors were spaced at 140 mm C-C. Furthermore, in practice, the anchor spacing is dictated by the presence of the internal steel reinforcement because an anchor cannot be placed where a stirrup exists or where a longitudinal steel bar lies. In this case, arrangements were made to place the anchors away from the stirrups.

3.3.3 Fabrication of Phase II

The construction started with making the plywood forms. The reinforcement cages were constructed and placed in the formworks. All the forms were brushed with oil from inside to facilitate their removal after the casting and curing of concrete. Figure 3-12 shows the concrete formworks and the reinforcement cages.

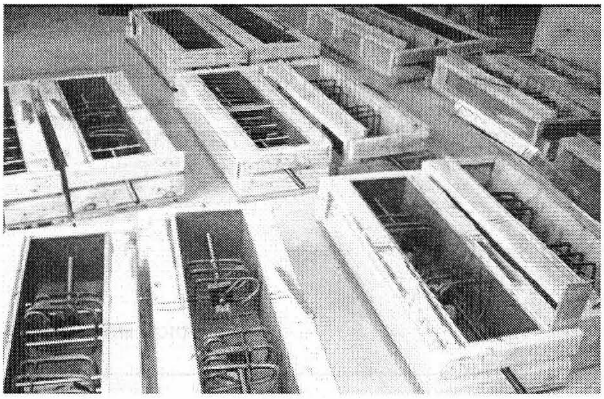

Fig.3-12: Formworks for phase II

The concrete was supplied by a local concrete plant. All of the prisms were vibrated using an electric vibrator. After casting, the exposed concrete surface was trawled smooth and covered with a plastic sheet. The concrete was cured at room temperature and the surface was kept moist for a minimum of 10 days. The forms were removed after 3 weeks and the specimens were cured under the normal laboratory conditions. Two layers of epoxy were used according to the manufacturing instructions (MBrace, 1998) and the whole process followed the same procedures as described in section 3.2.2.

3.3.4 Test Equipment and Instrumentation

The same test equipment and instrumentation were used in this phase as in the previous phase and as discussed in section 3.2.3, and shown in Fig.3-13.

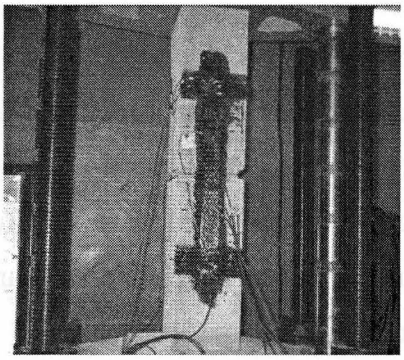

Fig.3-13:Typical concrete prism after the installation of the CFRP laminate and anchors

Figure 3-14 shows the location of the strain gauges along the CFRP laminate for each of the tested prisms. Note that strain gauges were symmetrically disposed on each of the two faces strengthened with CFRP laminate.

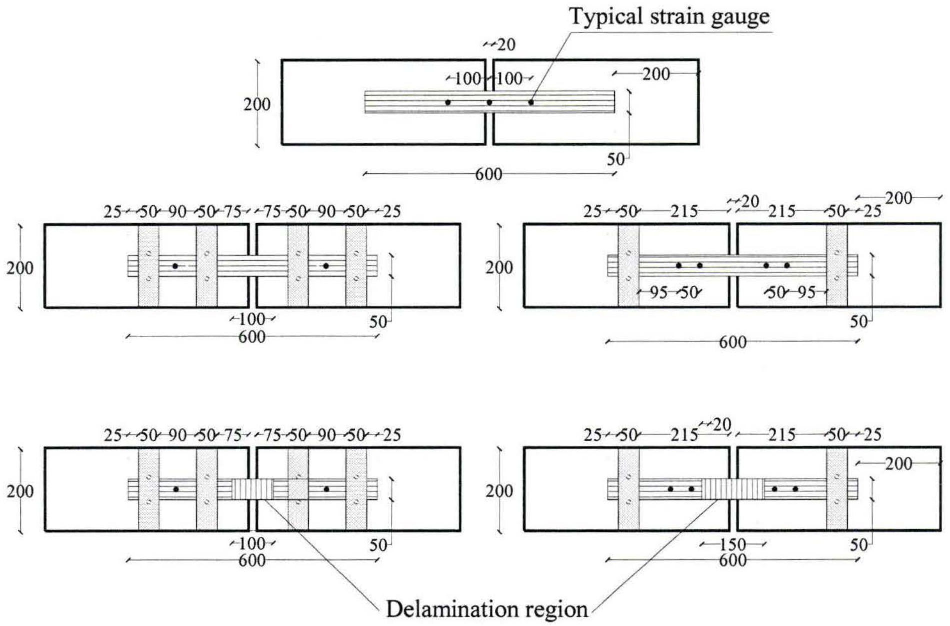

Fig.3-14: Arrangement of the anchor, strain gauges and the debonded segment in the tested prisms

3.4 Large Scale RC beams- Phase III

It was decided after the analysis of the experimental data obtained from phases I and II involving concrete prisms to extend the study to full scale RC beams. The purpose of phase III is to apply the proposed anchors to full scale RC beams and to confirm the findings obtained from the concrete prisms and to test the performance and effectiveness of this anchorage system in delaying/preventing the delamination. The arrangement and number of anchors are key factors which will be investigated during this phase.

3.4.1 Test Specimens

A total of twenty one nominally identical simply supported beams were designed according to the CSA Standard A 23.3-04 (CSA 2004). Three No.15 (Ø=16 mm) deformed bars (f_y = 400 MPa) were used in the tension zone and two No.10 (Ø=11.3 mm) deformed bars (f_y = 400 MPa) in the compression zone. The beams were designed to prevent shear failure before flexural failure and the shear reinforcement consisted of No.10 U-stirrups (f_y = 400 MPa) spaced at 150 mm centre to centre. Due to space and other limitations and given the large size of these beams, it became necessary to cast the beams in two stages.

3.4.2 Parameters Investigated

All the beams have the same dimensions and internal steel reinforcement, with the main test parameters being:

1. Amount of CFRP reinforcement, using three FRP reinforcement ratios.
2. Presence / absence of mechanical CFRP anchors.
3. Number/spacing of anchors.
4. Anchor locations along the beam length

It is important to recall that delamination in such beams occurs either near the ends of the laminate close to the beam supports or in the midspan region. Whereas end delamination can be explained by the presence of high interfacial shear stresses near the beam ends, intermediate span delamination, which in laboratory tests occurs in the region of constant moment, are more difficult to explain. The delamination in the latter case is instigated by local stresses and deformations in the neighbourhood of flexural cracks in the constant moment region. The size and distribution of these cracks, which are affected by a large number of parameters, strongly influence the initiation and the propagation of delamination. Unfortunately, until now, no theory exists that can satisfactorily predict either the actual location of cracks or the local stresses at the FRP-concrete interface in the vicinity of these cracks. For this reason, in this study, similar to all previous studies on this subject, the anchor locations and number could not be rationally determined prior to testing; therefore, these variables constitute the test parameters in this investigation. It is also important to mention that given the unique behaviour of each anchor type, results of tests from other types of anchors cannot be used to arrive at the disposition of the anchors in the current study.

For easy identification of the beams with different characteristics, the following notation will be used: CB designates the control beam, B refers to the beam, the first number after the letter B represents the order of the beam tested in that specific series and F represents the CFRP and the number after F refers to the number of CFRP layers. N indicates lack of anchor; E refers to the use of anchors in the plate end zone and M to the use of the anchors in mid-span zone. The numbers following the letters E and M represent the number of anchors used at the particular location. Beams with smaller FRP laminate width were designated by b90 where the number 90 represents the width of the FRP laminate in mm. For example, B1-F4-E3-M9 refers to the first beam tested in this specific configuration and externally strengthened with four layers of CFRP laminate. This beam has 3 anchors at each end and 9 anchors in the midspan zone.

3.4.3 Beams Geometry and Reinforcement

Due to the fact that different FRP reinforcement ratios will be used during this investigation, the increase in the beam tensile reinforcement will require a huge compression force in concrete to achieve equilibrium, therefore, it was decided to test T beams. Furthermore, often in practice beams are of T-shape rather than rectangular. All the beams have the same size and internal steel reinforcement as shown in Fig.3-15, which shows typical beam elevation, cross section, dimensions and reinforcement arrangement. Each beam is 4880 mm long, with span length of 4500 mm. The beam cross-section consists of 500 mm wide and 100 mm thick flange, 250 mm wide web and total height of 400 mm. The reinforcement consists of 3No.15 bars as tension steel and 2No.10 bars as hanger bars in the compression zone. The stirrups are No.10 bars at 150 mm centre to centre throughout the length of the beam.

Table 3-5 shows the amount and disposition of the external CFRP reinforcement and the anchors used in each beam. Notice that the beams are divided into 14 groups. Due to the high cost of manufacturing and the time required to test these full scale beams, it is not feasible to test duplicate specimens in each case or to gather sufficient data for studying random variation caused by the various parameters affecting the response of these beams. The writer is aware of this problem, but these details can be investigated in future studies.

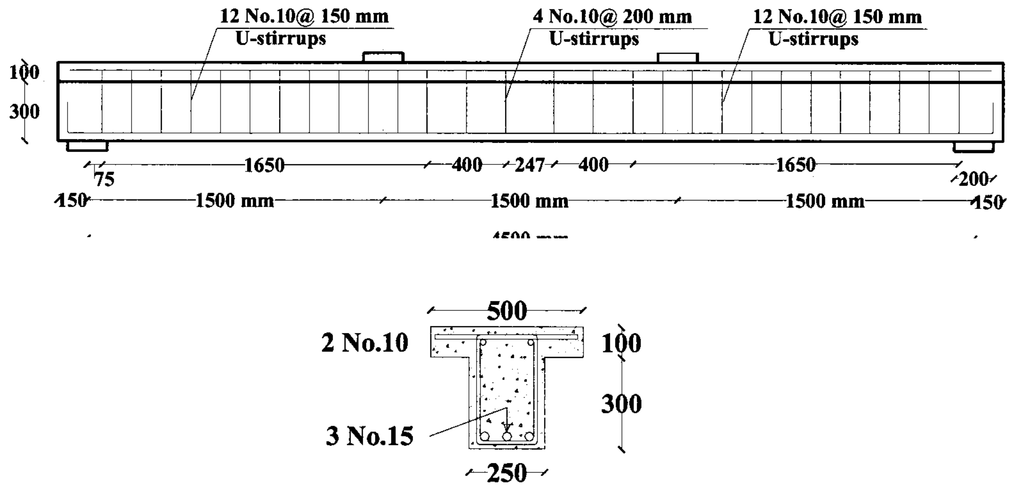

Fig.3-15: Beam elevation, cross section and dimension

Note: All dimensions are in mm.

Table 3-5: Test matrix

Group	Beam designation	FRP width (mm)	FRP Area (mm^2)	Beam description
1	CB1	-	-	Control beam-No anchor
	CB2	-	-	
	CB3	-	-	
2	B1-F1-N	220	36.3	Beam with 1 layer of CFRP- No anchor
	B2-F1-N	220	36.3	
3	B1-F2-N	220	72.6	Beam with 2 layers of CFRP- no anchor
	B2-F2-N	220	72.6	
4	B1-F4-N	220	145.2	Beam with 4 layers of CFRP- no anchor
	B2-F4-N	220	145.2	
5	B1-F1-E3	200	33.0	Beam with 1 layer of CFRP+ 3 anchors at each end
	B2-F1-E3	200	33.0	
6	B1-F2-E3	200	66.0	Beam with 2 layers of CFRP+ 3 anchors at each end
	B2-F2-E3	200	66.0	
7	B1-F4-E3	200	132.0	Beam with 4 layers of CFRP+ 3 anchors at each end
8	B1-F4-E3-M9	200	132.0	Beam with 4 layers of CFRP+ 3 anchors at each end+9 anchors at region of max. moment
9	B1-F2-E3-M9	200	66.0	Beam with 2 layers of CFRP+ 4 anchors at the end and 9 anchors at region of max. moment

Table 3-5: Test Matrix Cont.

Group	Beam designation	FRP width (mm)	FRP Area (mm^2)	Beam description
10	B1-F2-E4-M11	200	66.0	Beam with 2 layers of CFRP+ 4 anchors at each end+11 evenly distributed anchors at region of max. moment
113	B-F4-N-b90	90	59.4	Beam with 4 layers of CFRP equivalent to a full 2 layers-no anchor
12	B1-F4-E2-M15-b90	90	59.4	Beam with 4 layers of CFRP+ 4 anchors at each end+15 evenly distributed anchors at region of max. moment
13	B-F8-N-b90	90	118.8	Beam with 8 layers of CFRP equivalent to a full 4 layers-no anchor
14	B1-F8-E3-M17-b90	90	118.8	Beam with 8 layers of CFRP+ 3 anchors at each end+17 evenly distributed anchors at region of max. moment

3.4.4 Material Properties

Concrete

Ready mixed concrete was ordered from the plant and was delivered to the laboratory. For the first group of beams, concrete with a specified compressive strength f'_c = 40 MPa, slump of 100 mm and maximum aggregate size of 12.5 mm (1/2") was ordered. The concrete was made with super-plasticizer, but no other supplementary cementations materials. During casting, it was discovered that the amount of concrete delivered was not enough to finish the last beam and to cast many cylinders, therefore, only 4 standard concrete cylinders (150x150x300mm) were cast and cured under the same conditions as the test beams. The curing consisted of moist curing for seven days and air-curing subsequently. Due to the limited number of cylinders, all of them were tested in compression to obtain the concrete average compressive strength. Table 3-6 summarizes the results for the tested specimens after 48-days. Notice that the actual average-strength of 54 MPa much higher than the specified strength of 40 MPa.

Table 3-6: Concrete cylinder test results at 48-days for the first group of beams

Age (days)	Specimen	Compression test f'_c (MPa)
48	1	51.3
	2	54.7
	3	53.6
	4	56.6
	Average	54.0

Table 3-7 gives the compressive and splitting tensile strength of each concrete batch at 46 days after casting. Notice that the strength values marked with asterisks in this table are quite different from the other values given by their companion cylinders. Clearly, these are outliers due to either improper preparation or testing.

Therefore, they will be discarded and not used for evaluating the relevant concrete strength.

Table 3-7: Concrete cylinder test results at 46-days

Specimen	First batch		Second batch	
	Compressive test f_c' (MPa)	Splitting test f_t' (MPa)	Compressive test f_c' (MPa)	Splitting test f_t' (MPa)
1	59.9	3.0	61.9	4.6
2	58.8	1.7*	56.8	3.6*
3	58.6	3.4	61.0	4.4
4	57.3	3.4	59.1	4.7
5	62.1	-	58.3	-
6	60.1	-	52.2*	-
Average	59.5	3.3	59.4	4.6

Longitudinal Steel Reinforcement

Longitudinal steel bars were used as tension and compression reinforcement in all the 21 beams. Three straight No.15 deformed bars were used as tension reinforcement in each beam while 2 No.10 bars were used in the flange as hanger bars. Four samples from each reinforcement bars were tested to obtain the reinforcement properties in the form of stress-strain relationship. The tensile test results for the four bars are presented in Table 3-8. Shown in the table are f_y = yield stress (MPa), ε_y = strain at yield, E_s = modulus of elasticity of steel (MPa), f_u = ultimate strength (MPa), ε_u= ultimate strain and ε_{sh}= strain corresponding to beginning of strain hardening. Figure 3-16 shows a typical stress strain curve obtained from one of the test coupons.

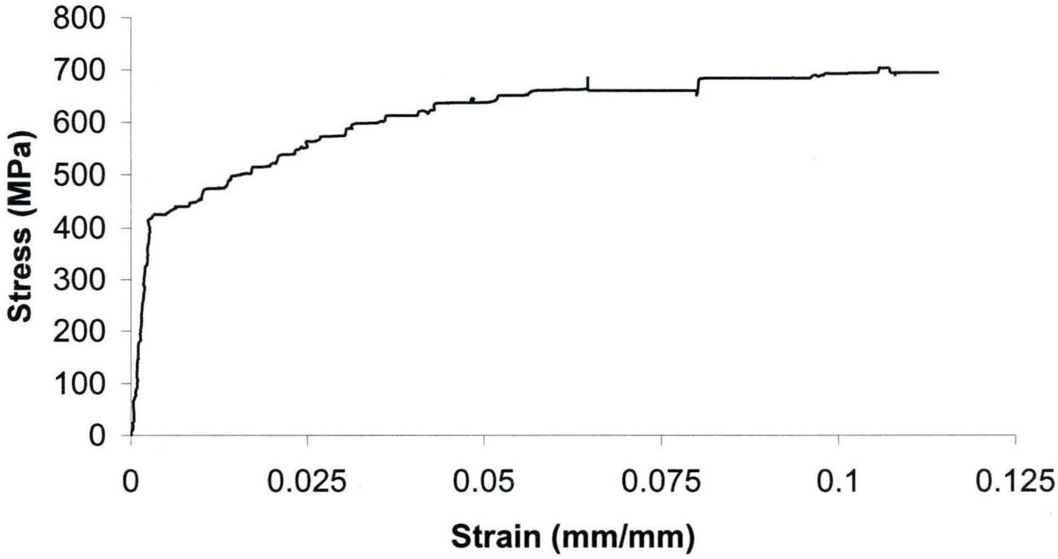

Fig.3-16: Typical stress strain for the steel

Table 3-8: Summary of longitudinal tension steel reinforcement properties

Sample	F_y (MPa)	ε_y	ε_{sh}	ε_u	E_s (GPa)	f_u(MPa)
1	505.0	0.0025	0.0078	0.03	202.0	637.0
2	464.6	0.0023	0.0050	0.114	202.0	660.0
3	407.7	0.0020	0.0071	0.100	203.9	656.0
4	428.2	0.0028	0.0066	0.097	152.9	690.5
Average	451.4	0.0024	0.0066	0.009	190.2	660.9

Transverse Steel Reinforcement

Deformed No.10 bars were used as U- stirrups in all of the twenty one beams. As the focus of the current investigation is the flexural behaviour of beams externally strengthened with CFRP laminates, the stirrups were not tested to find their yield strength, but the specified yield stress of 400 MPa and E_s = 200 GPa were used in design calculations.

CFRP laminate, Epoxy and CFRP Anchors

The CFRP laminate used in this investigation was unidirectional high strength carbon fiber fabric, known as Wabo Mbrace CF 130 (Mbrace CF130, 1998). A summary of the CFRP material properties is given in Table 3-2. The epoxy used in this phase is the same as the one used before and is described in section 3.2.1. Table 3-3 includes all the material properties for both Wabo MBrace Primer and Wabo MBrace Saturant.

The CFRP anchors used were manufactured the same way described in section 3.2.1 The spacing between the anchor rod was kept constant at 100 mm for this phase.

3.4.5 Design of the Strengthened Beams

The ultimate capacity of the tested beams was calculated according to the CSA Standard A23.3-04 (CSA 2004), assuming full bond between the concrete and the FRP laminate until failure using the following concrete, reinforcement and CFRP properties:

Concrete

Concrete strength f'_c = 54 MPa for all the beams and ultimate concrete strain ε_{cu} = 0.0035

Longitudinal steel reinforcement

1- Tension steel:

f_y =400 MPa , E_s= 200 GPa

Effective depth d =360 mm

2- Compression steel:

f_y =400 MPa , E_s= 200 GPa

Effective depth d'= 40 mm

Transverse steel reinforcement (Stirrups)

f_y =400 MPa , E_s= 200 GPa

CFRP Laminate

f_{fu}= 3800 MPa , E_f = 227 GPa , ε_u = 1.67%, FRP thickness = 0.165mm

Strain compatibility was used in the analysis, but strain hardening was ignored and the steel was assumed to be elasto-plastic. The shear strength of the beams was calculated using the simplified shear design method in the CSA Standard A23.3-

04. Table 3-9 shows a summary of the beam designs, the maximum ultimate moment and the maximum corresponding load that each beam can sustain.

Table 3-9: Summary of the designed beams

Beam	c (mm)	Bottom steel strain	Top steel strain	FRP strain	M (kN.m)	P (kN)	$\frac{P}{P_{CB}}$
CB	9.22	0.133	0.01100	-	82.58	110.1	-
B-F1-N	17.16	0.070	0.00465	0.078	141.50	183.3	1.71
B-F2-N	25.11	0.046	0.00210	0.050	193.70	252.8	2.35
B-F2-M9-E3	23.69	0.050	0.00240	0.006	184.27	240.2	2.23
B-F4-N-b90	59.40	0.053	0.00280	0.059	174.82	227.6	2.12
B-F4-N	46.77	0.023	0.00051	0.026	291.20	390.1	3.53
B-F4-M9-E3	43.34	0.026	0.00027	0.029	273.40	365.4	3.31
B-F8-N-b90	39.78	0.028	0.000019	0.032	255.51	340.5	3.09

In this table c designates the depth of the neutral axis at ultimate, P denotes the ultimate flexural load ad P_{CB} is the control beam failure load.

3.4.6 Fabrication of the Tested Beams

Fabrication of the First RC Beams

All the beams were constructed in two phases, the construction started with making the plywood forms and attaching the strain gauges to the longitudinal steel. A thin layer of silicon was applied to each strain gauge to protect it against impact, moisture and possible damage during the casting processes. The reinforcement cages were constructed with high accuracy and placed in the formworks. All the forms were brushed with oil from inside to facilitate their removal after the casting and curing of concrete. Plastic chairs were placed under the reinforcement cages to maintain a clear cover of 40 mm at the bottom of the beam. Figure 3-17 shows the concrete forms and the reinforcement cages for the first group of RC beams

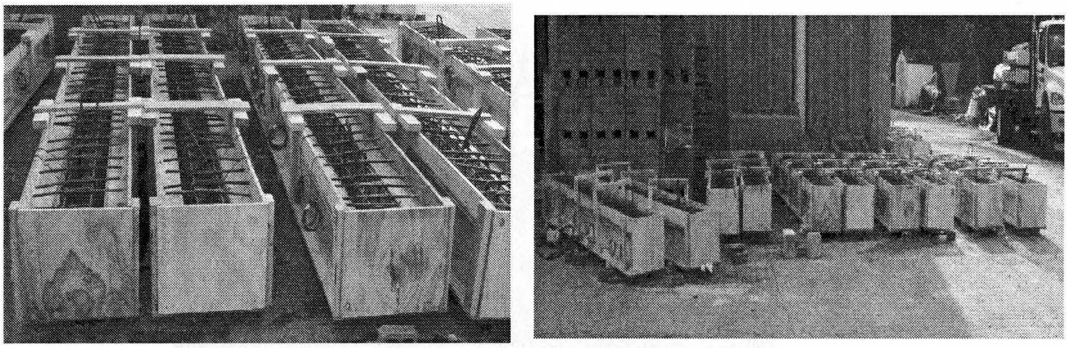

Fig.3-17: Formwork and the reinforcement cages inside them

The concrete was supplied by a local concrete plant. The specified maximum aggregate size and slump were 12.5 mm (1/2") and 100 mm, respectively. All of the beams were vibrated properly using an electric vibrator. After casting, the exposed concrete surface was smoothly finished and covered with a plastic tarp. During casting the slump was measured and was determined to be 95 mm. The forms were removed after one week as shown in Fig. 3-18. Although the specified concrete strength was 40 MPa, the actual strength from standard cylinders was found to be 54 MPa at 48 days.

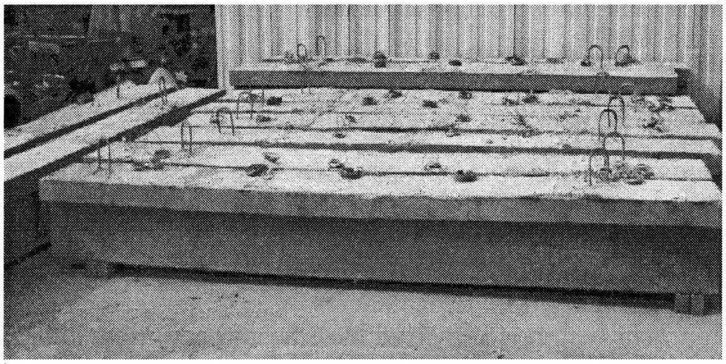

Fig.3-18: Beams after stripping the formwork

For beams strengthened with CFRP, two layers of epoxy were used according to the manufacturer's specifications. (MBrace, 1998) as discussed in Section 3.2.2. The second set of 12 beams was constructed similarly to the first set as shown in Fig.3-19.

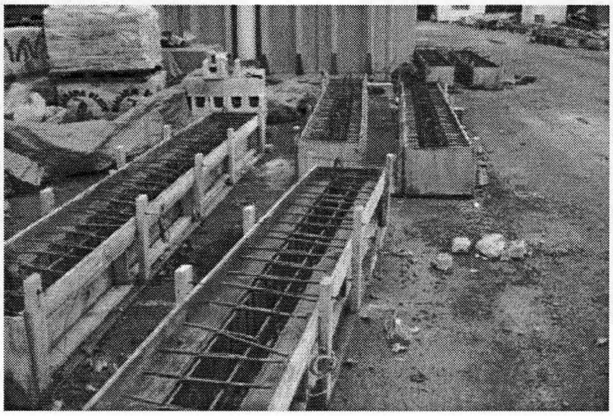

Fig.3-19: Formwork and the reinforcement cages inside them

3.4.7 Details of FRP Reinforcement

Table 3.5 shows the test matrix of the tested specimens. A total of twenty one beams were tested in flexure to investigate the effectiveness of the proposed anchorage system. Different test parameters were investigated, but only one type of CFRP laminate was used; namely, CFRP CF-130. The un-sheeted length was kept constant for all the tested beams.

Figure 3-20 shows the details of the external FRP reinforcement and anchors. The CFRP laminate used in this study is available as 600 mm wide sheet. It may be noticed in the latter figures that the external reinforcement is not extended to the ends of the beams, which is common practice. The reason is that extension to the ends may retard delamination, but this can not be done in the field because the beams are normally supported on columns or other types of supports. Also, only a nominal development length is provided in order to encourage delamination and to check the effectiveness of the proposed anchor.

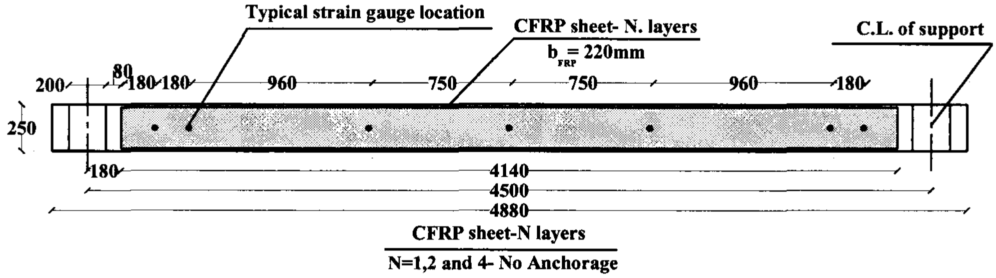

(a)

Typical B-F-N group of beams (Number of beams within this configuration equals 6 beams)

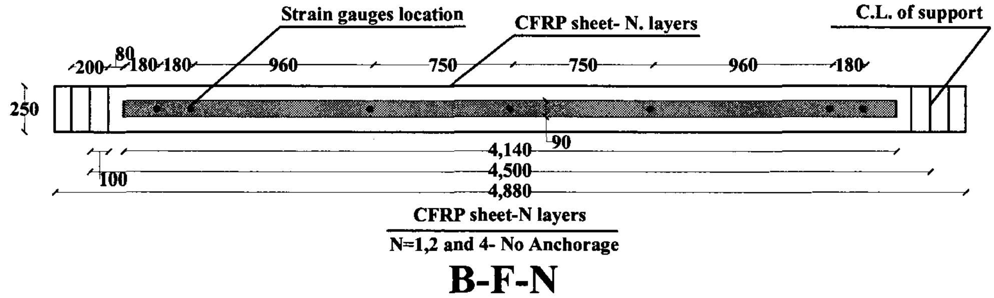

(b) Typical B-F-N group of beams (Number of beams within that configuration equals 2 beams)

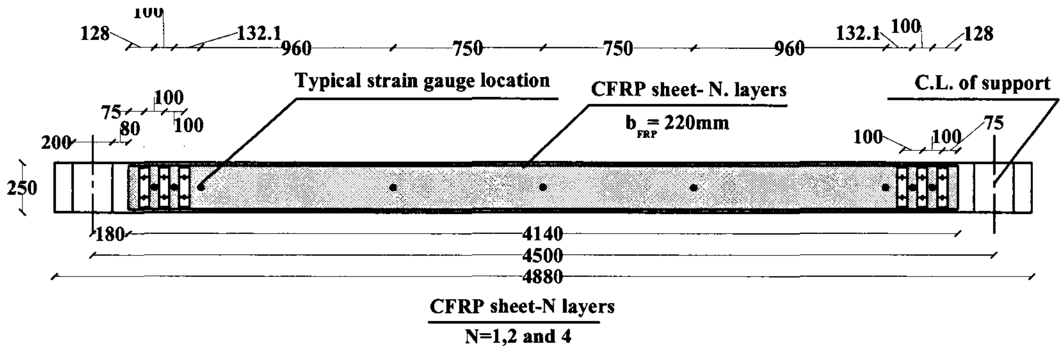

(c) Typical B-F-E3 group of beams (Number of beams within this configuration equals 5 beams)

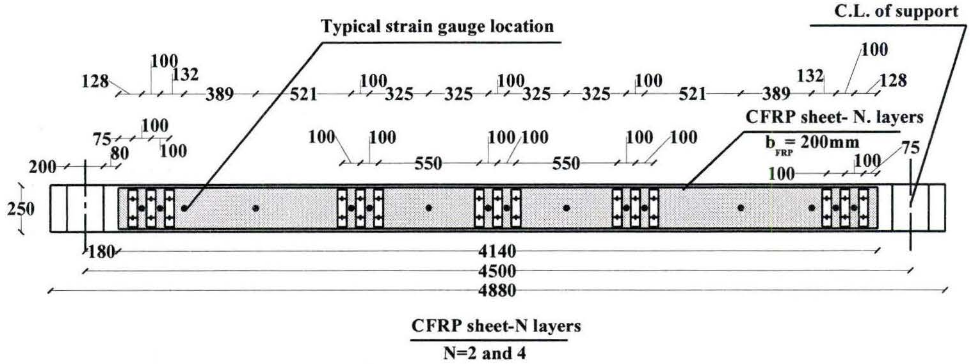

(d) Typical B-F-E3-M9 group of beams (Number of beams within this configuration equals 2 beams)

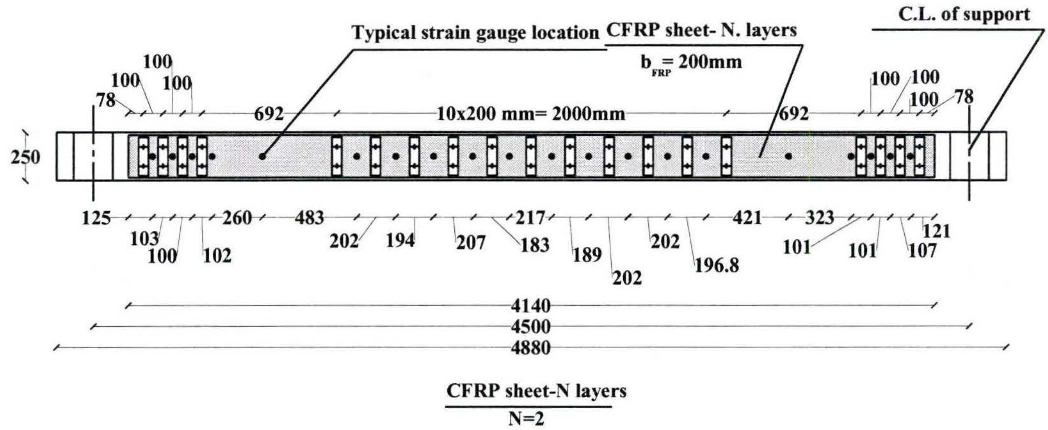

(e) Typical B-F-E4-M11 group of beams (Number of beams within this configuration equals 1 beam)

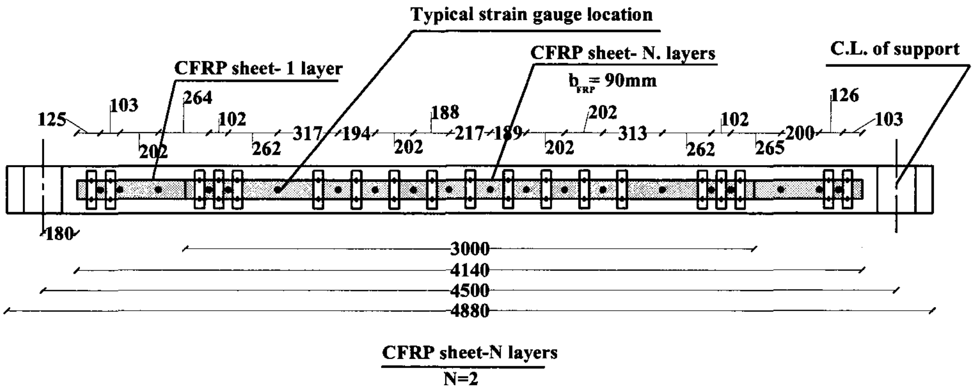

(f) Typical B-F-E2-M15 group of beams (Number of beams in this configuration equals 1 beam)

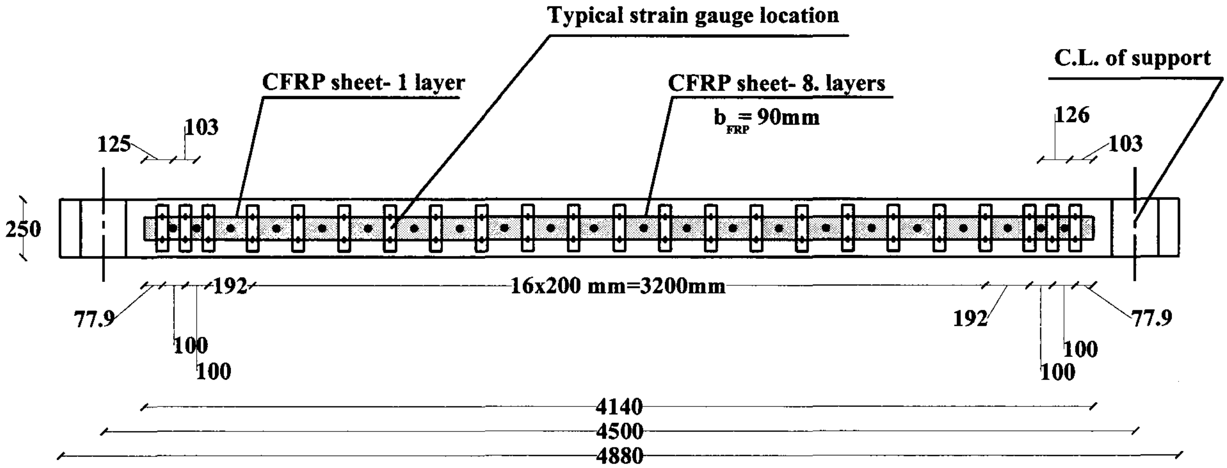

(g) Typical B-F4-E3-M17 group of beams (Number of beams with this configuration equals 1 beam)

Fig.3-20: Bottom view of the beam web showing the arrangement and spacing of the anchors and strain gauges locations

3.4.8 Test Equipment and Instrumentation

The following equipment and instrumentation were used in the testing program:

1. One closed-loop servo-controlled electro-hydraulic jack as actuator, a commercially available load cell (Type: CM1C), with the capacity of 200,000 lbs

(890 KN) and stroke length of 20 inch (500 mm). The actuator-load cell assembly was attached to a horizontal cross beam, which was connected to two vertical reaction columns.

2. Knife-edge bearing plates with roller supports.
3. MTS data acquisition system attached to a microcomputer. Displacement control was used in this investigation.
4. Five String pots to measure deflection.
5. Electrical strain gauges to measure the strain along the CFRP laminate longitudinal steel and the concrete surface.

Figure 3-21 shows two typical beams externally strengthened with CFRP laminates. Five string pots were used along each beam length to measure its deflections. Seven strain gauges were used on the middle rebar in the tension zone as shown in Fig. 3-22 (a). Three strain gauges on the top concrete surface were used to measure the compression strain as shown in Fig.3-22(b). Figure 3-23 shows the arrangements of the strain gauges on the longitudinal steel in the plan view.

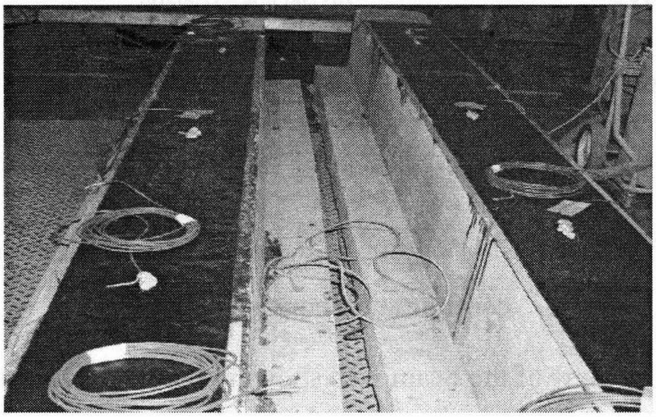

Fig.3-21:Typical T-beam with CFRP laminate and strain gauges

Measurement of strains in the longitudinal reinforcing steel, concrete and CFRP laminate was taken using electrical resistance strain gauges with gauge length of 5 mm for longitudinal steel and CFRP laminate and 30 mm for concrete. The strain gauges were sensitive to 0.01 micro strains with a standard deviation of 2%.

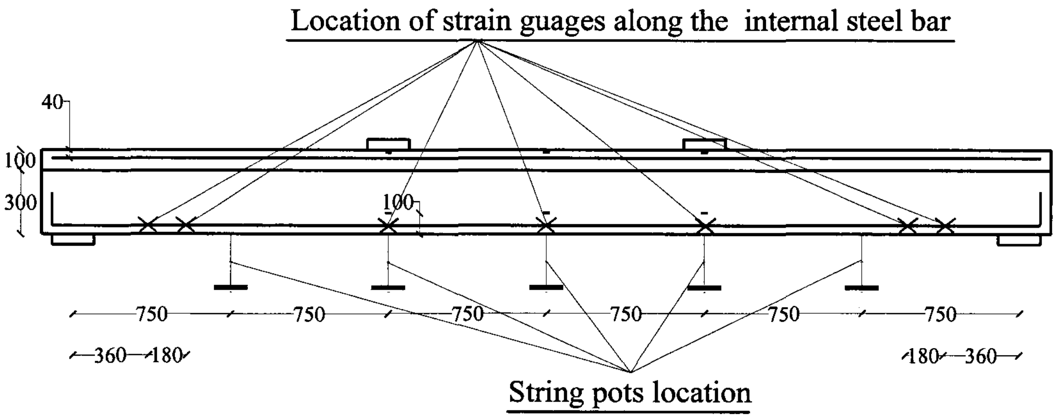

(a): Strain gauges along the internal steel bar

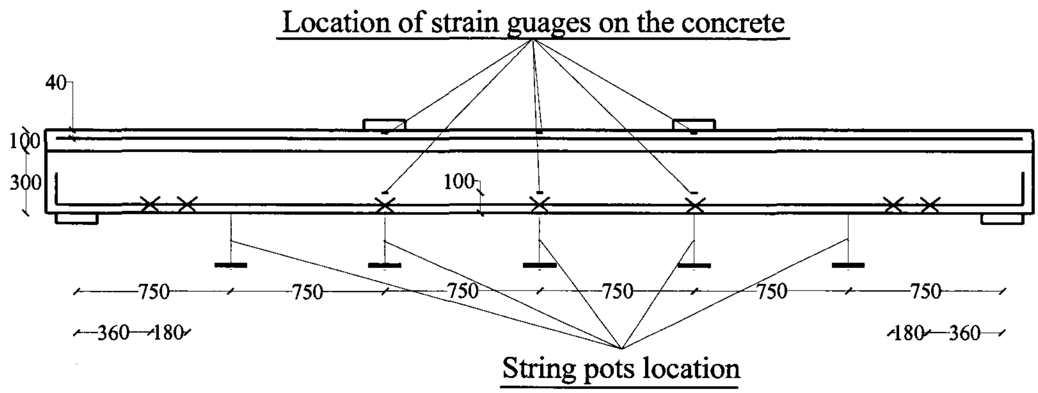

(b): Strain gauges on the concrete surface

Fig.3-22: Location of strain gauges and string pots a) Strain gauges along the internal steel bar, b) Strain gauges on the concrete surface

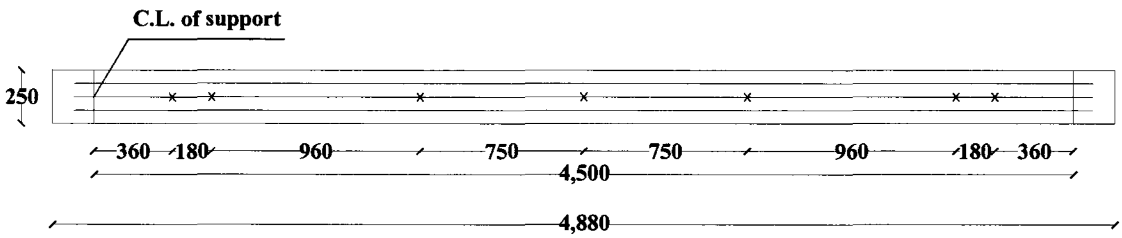

Fig.3-23: Typical strain gauge positions on the longitudinal tension steel

3.4.9 Test Setup

The tests were conducted at the Applied Dynamics Laboratory of the Civil Engineering Department. The steel frame supporting the actuator was fixed to the 1.0 m thick laboratory floor. The roller and the hinge supports were sitting directly on reinforced concrete blocks resting on the strong floor. All the beams were simply supported and were loaded in four point bending with a shear span of 1500 mm. The load was applied using a hydraulic jack and displacement control. The loading and support plates were levelled using hydrostone compound. Figure 3.24 shows a typical beam and the corresponding loading jack and supports. The loading rate was relatively slow to simulate static loading condition. The load was applied via displacement control with a rate of 2 mm/minute. As cracks appeared and propagated, the load was stopped and the cracks were traced. Generally after the formation of a large number of vertical cracks along each beam and the yielding of the main longitudinal steel reinforcement, the CFRP laminate started to delaminate.

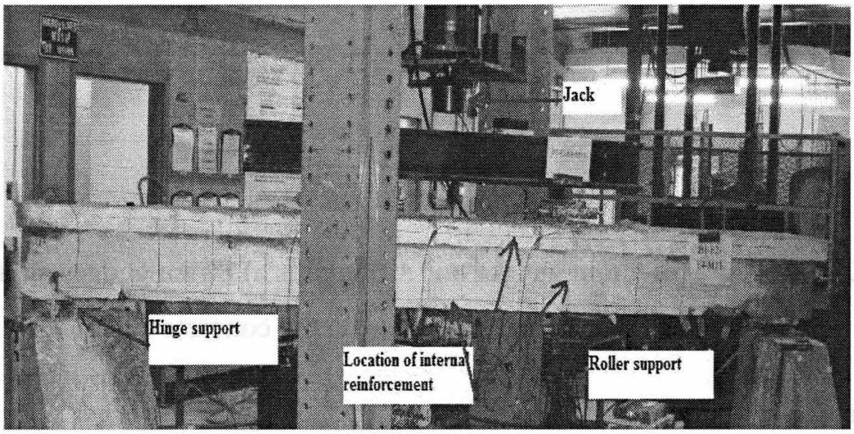

Fig.3-24: Typical test set up for the tested beams

CHAPTER 4
Experimental Results

4.1 General

In this chapter, the full behaviour of all the tested specimens will be presented and discussed for all the three test phases. During the test, the behaviour of each specimen was monitored, including its displacements and the strain in the CFRP laminate and the steel reinforcement. Therefore, for each specimen its load deflection curve and the strain variation along the internal reinforcement and the CFRP laminate will be presented.

4.2 Behaviour and Observations for Concrete Prisms in Phase I

The testing of the prisms was an exploratory exercise designed to test the preliminary performance of the proposed anchor; therefore, it is not the focus of this study. They will be briefly discussed, without extensive observations.

4.2.1 Control Prisms

Two identical externally unstrengthened concrete prisms were tested in direct tension as control prisms, P1 and P2. It was observed that the first crack occurred near mid-length at 95 kN and subsequently the prism experienced bending. The concrete split at the mid-length and the prism failed at 102.5 kN as shown in Fig.4.1. The bending was unintended and was likely due to the eccentricity of the applied axial load. As can be observed in Fig.4.1, the crack is for the most part nearly perpendicular to the axis of the prism which indicates that the axial effect dominated the prism response.

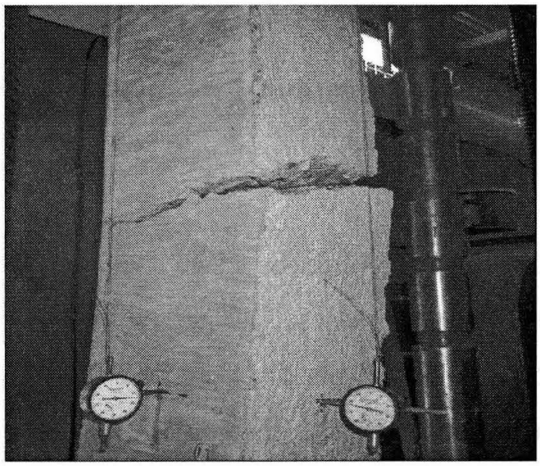

Fig.4-1: Cracks at mid-length of control prism P1

The second prism, P2, reached 70 kN when the first crack appeared at mid-length and it failed at 102.5 kN. Although this prism reached the same maximum load as the companion prism P1, the cracks indicated some torsion. It is believed that the torsion was caused by the misalignment of the steel rods at the two ends of the prism. Figure 4-2 shows the crack pattern for prism P2 at failure.

The load mid-length elongation curves for the two prisms are presented in Figs.4-3 and 4-4. The plotted curves are for the three dial gauges placed at mid-length on three faces of each prism. Note that strain gauges were not used in this case. The average elongation is plotted for both prisms as shown in Fig. 4-5 where one can observe that their overall responses do not agree but both reached practically the same ultimate load. The disagreement is due to the secondary bending and torsion that was experienced by the prisms. Also, given the relatively small displacements involved, the dial gauges were not sufficiently precise to measure all the displacements accurately. Therefore, in the remaining prisms, string pots were used to measure prism deformations.

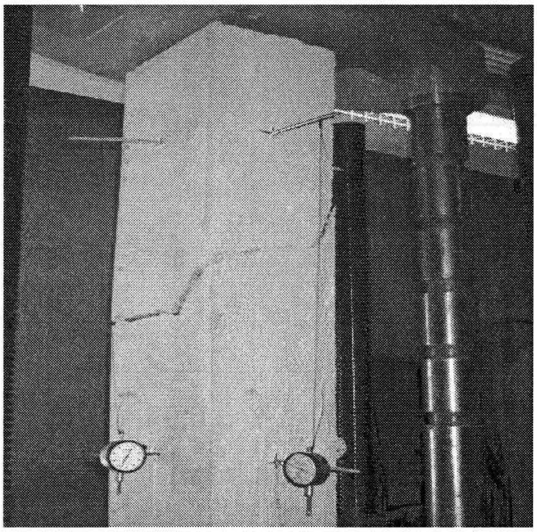

Fig.4-2: Cracks at mid-length for control prism P2

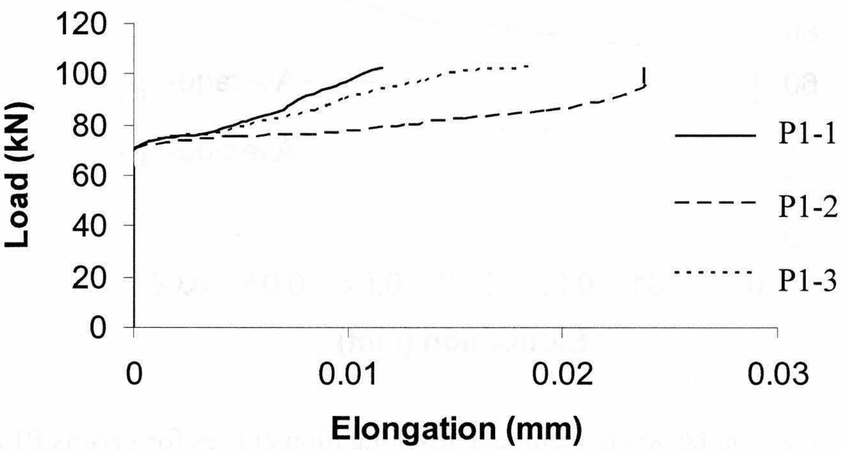

Fig.4-3: Load- elongation curve for P1

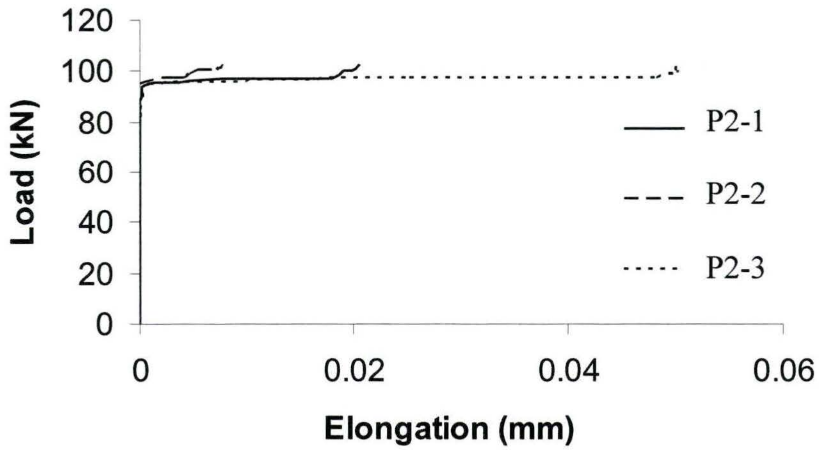

Fig.4-4: Load-elongation curve for P2

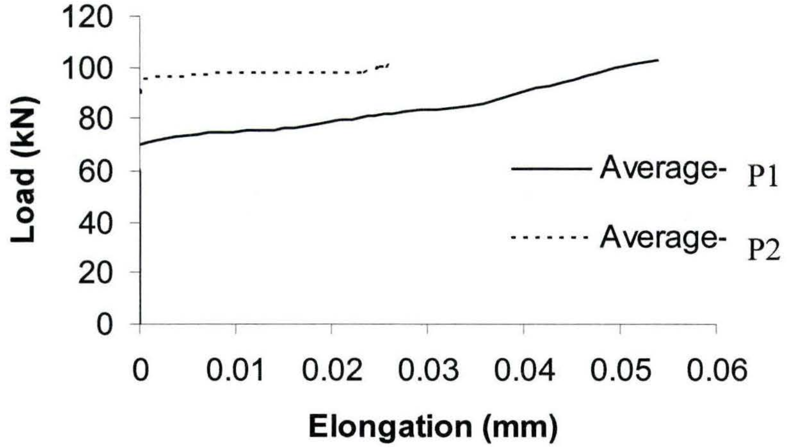

Fig.4-5: Comparison between average load-elongation curves for prisms P1 and P2

4.2.2 Concrete Prisms Strengthened with CFRP Laminates

Two identical concrete prisms, P3 and P4, were strengthened with four layers of CFRP laminate, two layers on each opposite face, each layer being 50 mm wide, 0.165 mm thick and 600 mm long. Both prisms were tested in tension similar to the control prisms. One string pot with a gauge length of 40 mm was placed on each of the two opposite faces of the prism to measure its axial deformations. Fourteen strain gauges were installed on the CFRP laminate, 7 on each face, to measure the strain and obtain the strain variation along the laminate length. Figure 4-6 shows the concrete prism with one of the string pots near its left face.

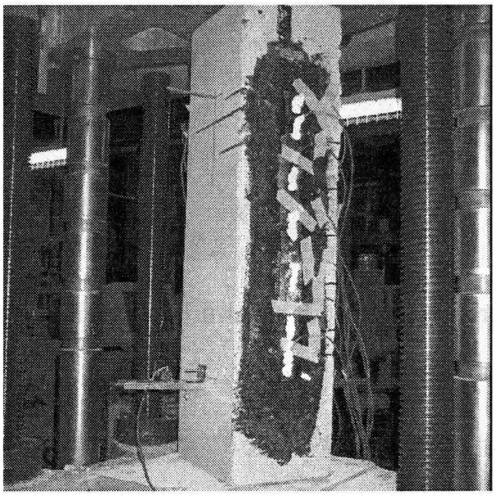

Fig.4-6: Typical concrete prism strengthened with CFRP laminate, location of strain gauges and string pots

The first crack occurred at 95 kN at mid-length. The prism continued to carry load and reached 147.5 kN before the first major delamination initiated on one face; thereafter, the load dropped to 90 kN. The prism regained its strength and reached 140 kN before full delamination occurred on the second face. Subsequently, the load dropped to 117.5 kN, but it once again increased and reached 126 kN before a loud sound was heard and the load dropped to 19 kN. The load increased again and reached 65 kN and a yielding plateau was formed before the prism failed completely. It was unusual for a concrete prism to carry load in tension given that the concrete was already cracked and the CFRP laminates on both faces were delaminated. From visual inspection during the test, it was noticed that one of the internal bars was ruptured before failure and the second bar ruptured at failure. It is believed that the ductile behaviour of the prism was due to the yielding of the internal bars. Also due to bending, the prism was no longer under pure axial load. Figure 4-7 shows the delaminated part of the CFRP laminate from one face. The average load elongation curve of this prism can be seen in Fig.4-8.

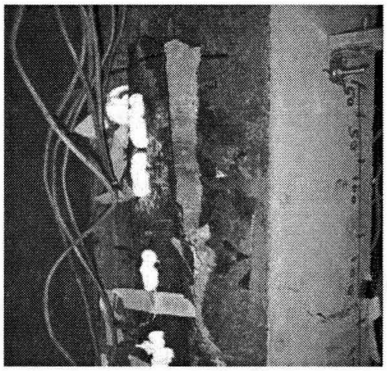

Fig.4-7: Concrete prism with delaminated CFRP laminate from one face

The load-elongation curve shows a ductile response for this reinforced concrete prism strengthened with a CFRP laminate. As mentioned earlier and based on visual inspection, the internal bars reached rupture and the ductility was due to the internal steel bars. Since the post-delamination response of these prisms was dominated by the steel reinforcement, it was decided to cut the internal bars at mid-length in the companion prism, P4. Figure 4-9 shows prism P4 with the mid-length cut. This prism reached 63.7 kN at first crack and the load dropped to 42.5 kN immediately after, but it subsequently regained its strength and reached 55 kN. Local delamination was observed at this load level, but the prism continued to carry more load and the CFRP laminate delaminated at 71.8 kN.

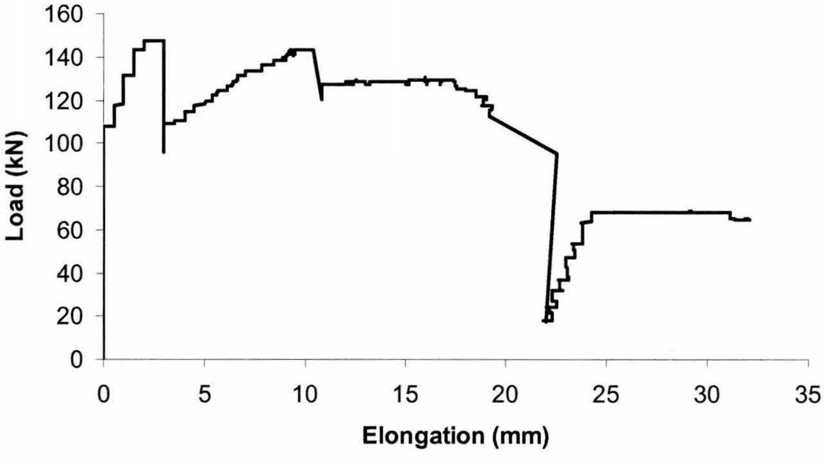

Fig.4-8: Average load- elongation curve for P3

Subsequently, the load dropped to 57.5 kN, but upon further extension of the prism, the load once again climbed to 72.5 kN. This specimen experienced large ductility, followed by a drop in the load and eventually failure of the prism. From visual inspection, it was noticed that in fact only one of the two internal rebars had been initially cut and therefore the intact bar was the reason for ductility observed in Fig.4-10.

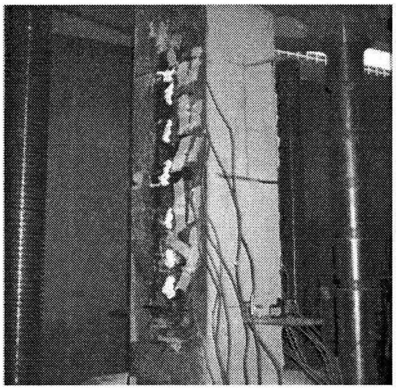

Fig.4-9: Mid-length cut made for prism P4

As stated earlier, these tests were exploratory and were performed to refine the test method rather than obtain detailed test data. The principal finding was that the middle section of the prisms should not be internally reinforced if the FRP contribution to their strength were to be accurately measured. It is difficult to separate the contribution of the internal reinforcement from that of the FRP and the prism behaviour appears to be dominated by the internal steel reinforcement.

4.2.3 Concrete Prisms with CFRP Laminates and Anchors

Two identical concrete prisms, P5 and P6, were strengthened with a total of four layers of CFRP laminate, two layers on each opposite face. To measure the prisms axial deformation and the strain in the CFRP, two string pots were placed near two opposite faces of each prism and 14 strain gauges were installed on the CFRP laminate, 7 on each face, to obtain the strain variation along the laminate length. One anchor near each end was installed in predrilled holes to fasten the laminate. The CFRP anchor was placed at a distance of 50 mm measured from the centerline of the anchor to the end of the laminate. The average load elongation curve of P5 is presented in Fig.4-11. This prism was tested without cutting the internal bars. It is clear that the load- elongation curve shows a yielding plateau. Since it is well known that the CFRP laminate is a brittle material, the plateau must be due to the yielding of the internal steel bars.

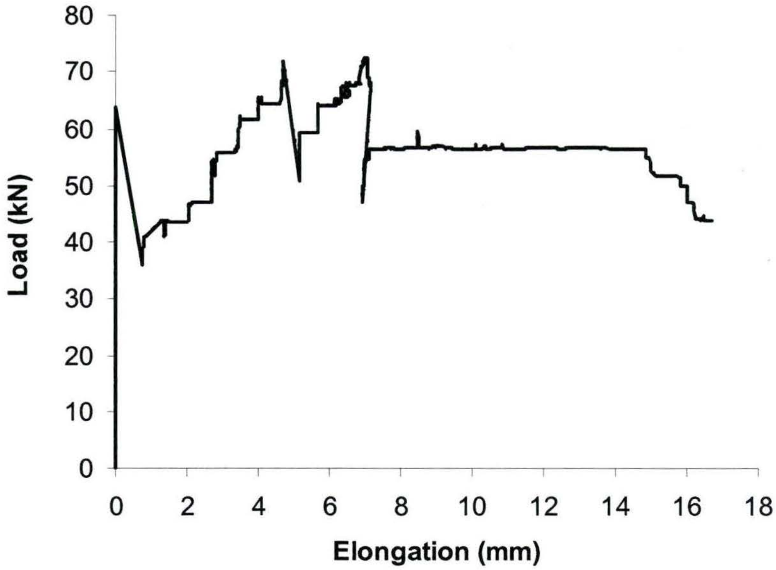

Fig.4-10: Average load-elongation curve for P4

The maximum load reached was approximately 173 kN and then it dropped due to delamination to 116 kN. The prism regained its strength and the load slightly increased with the corresponding load elongation response exhibiting a yield plateau. The anchor prevented the laminate from full delamination but slippage occurred from one end and the prism experienced bending, with the internal bars on one side visibly exposed. It is believed that the two plateaus and the drops were due to the yielding and rupture of internal bars, respectively. Figure 4-12 shows the rupture of CFRP laminate, bending of the prism and the FRP end slippage.

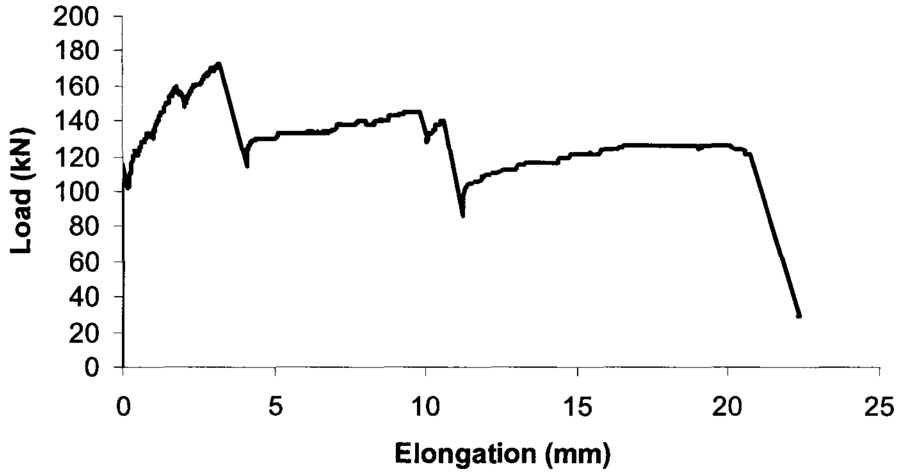

Fig.4-11: Average load elongation curve for prism P5

The companion prism, P6, was identical to prism P5. As indicated in Fig.4-13, the internal bars were cut using a concrete saw to eliminate the contribution of the these bars to the strength of the prism. The first crack occurred at 47.5 kN. As Fig.4-14 shows, the prism reached a maximum load of 110 kN when a loud sound was heard, which signalled delamination of the CFRP laminate on one face, and the load dropped to 54.2 kN. Based on visual inspection, the CFRP laminate had slipped but full delamination had not occurred. The load subsequently increased to 90.9 kN and then further delamination occurred with the laminate experiencing slippage and the anchor being pulled out. The load dropped to 39.8 kN, but increased again to 54 kN, producing a small plateau, followed by complete failure.

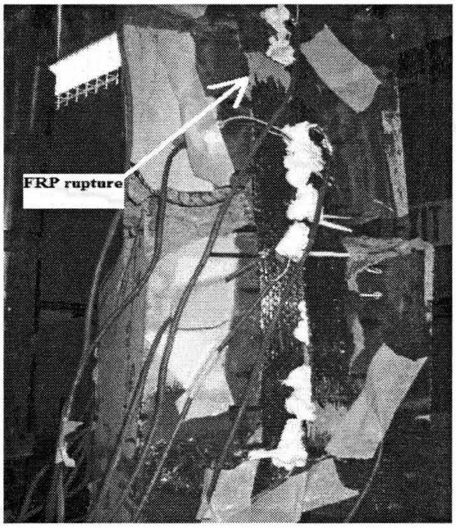

Fig.4-12: Rupture of CFRP laminate, prism bending and slippage of CFRP laminate from one face in prism P5

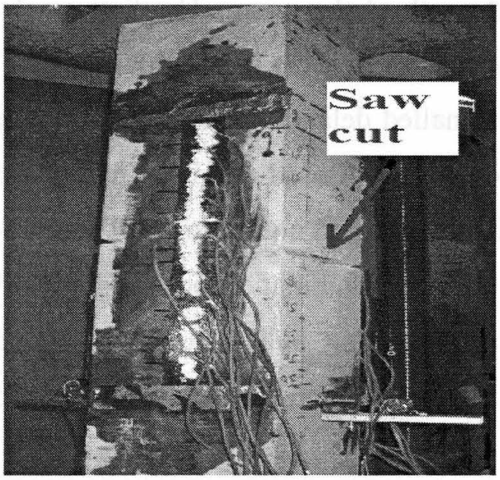

Fig.4-13: Concrete prism P6

Figure 4-15 shows the slippage that occurred in this case. The maximum slippage was measured to be 15 mm. Note that the prisms in which the steel reinforcement was cut prior to testing are expected to have lower strength than their companion prisms in which the steel was not cut.

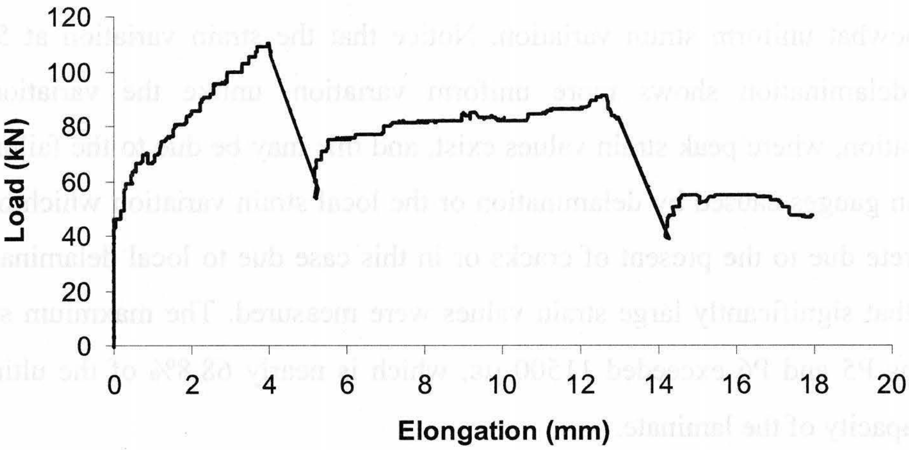

Fig.4-14: Average load elongation curve for prism P6

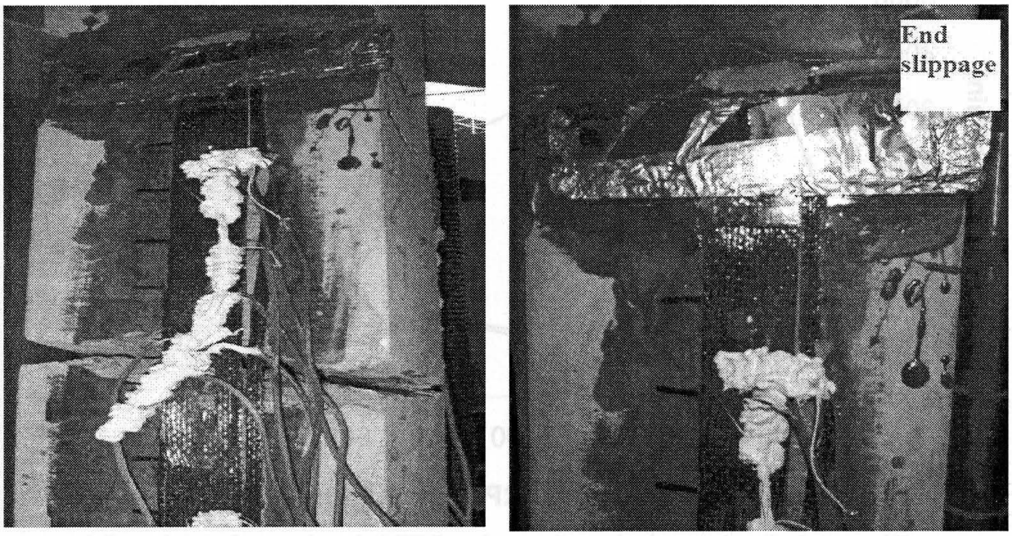

Fig.4-15: Longitudinal ruptures of CFRP laminate

4.2.4 Strain Variation in the Laminate

Figures 4-16, 4-17 and 4-18 show the variation of the strain along the FRP laminate on both faces of the prism and at two load levels, at 5 kN before delamination and at delamination. Before the delamination, the strain variation indicates a more uniform distribution, with the exception of prism P6. The anomalous behaviour of P6 may be due to the failure of the strain gauges. Since delamination occurred in the mid-length section, the laminate would have been attached to the concrete at the ends by the anchors and this may be the reason for the somewhat uniform strain variation. Notice that the strain variation at 5 kN before delamination shows more uniform variation, unlike the variation at delamination, where peak strain values exist, and this may be due to the failure of the strain gauges caused by delamination or the local strain variation which occur in concrete due to the present of cracks or in this case due to local delamination. Notice that significantly large strain values were measured. The maxmium strain in prisms P5 and P6 exceeded 11500 με, which is nearly 68.8% of the ultimate strain capacity of the laminate.

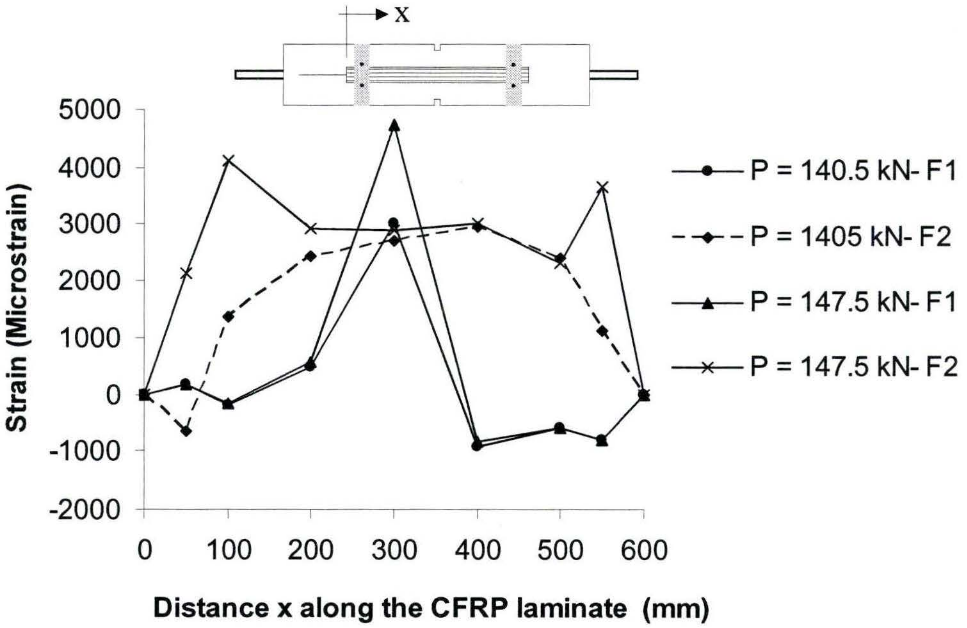

Fig.4-16: Strain variation along the CFRP laminate for prism P4

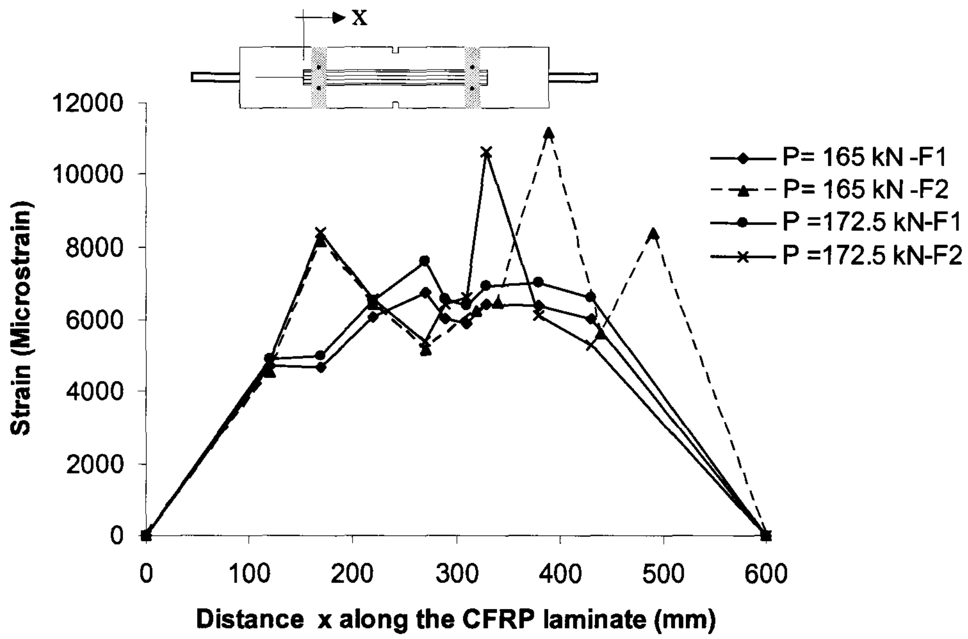

Fig.4-17: Strain variation along the CFRP laminate for prism P5

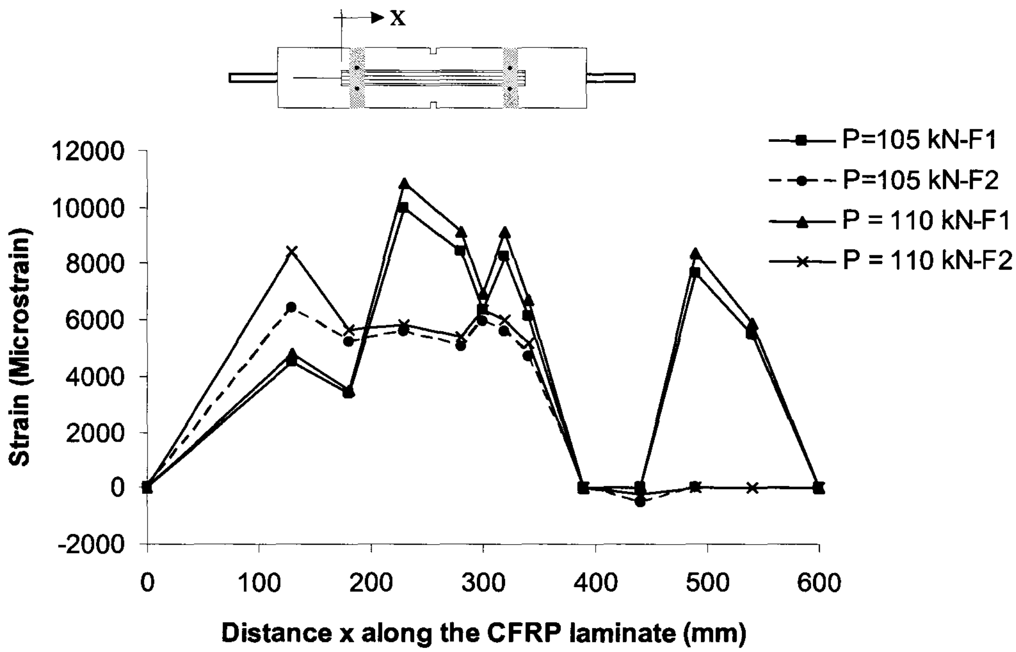

Fig.4-18: Strain variation along the CFRP laminate for prism P6

4.3 Discussion of the Results of Phase I

4.3.1 Prisms with CFRP Laminate

The comparison between the load elongation curves for the two externally strengthened prisms with or without anchors is presented in Fig. 4-19. As mentioned earlier, one prism had 2 No.10 bars going through its mid-length section, while the other had only one bar because the other bar was intentionally cut.

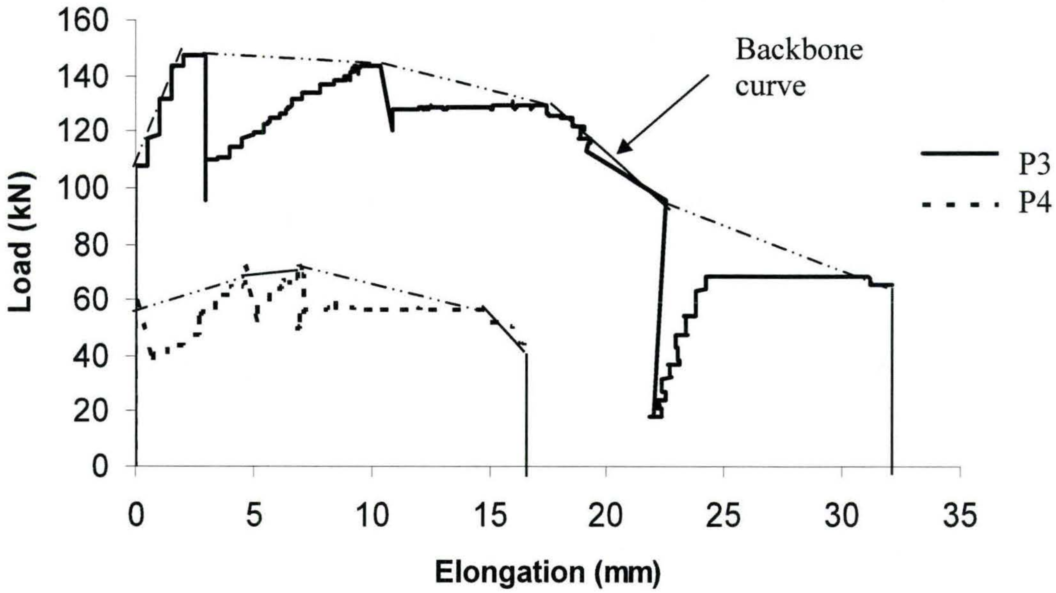

Fig.4-19: Comparison between the load elongation curves for prisms P3 and P4

The prism with two intact bars reached 147.5 kN before delamination and then it experienced a sudden drop in load. There appears to be a yield plateau in the curve of prism P3 which can be attributed to the yielding of the 2 No.10 bars. The first plateau and the drop in loading occurred due to the rupture of one of the two bars and the second plateau and drop was caused by the rupture of the second bar. On the other hand, prism P4 showed only one plateau due to the presence of one uncut rebar and the drop in this case was due to the rupture of that bar. This prism reached 71.8 kN at first delamination and the load dropped immediately after. A close comparison of the load-elongation curves of the two prisms reveals that the curve of prism P3 can be obtained by shifting upward the curve of P4 by a constant load of almost 80 kN. Considering that the No.10 bar has a cross sectional area of 100 mm^2 and considering the fact that the two bars reached their yield strength, each bar must have reached an axial load of 40 kN, assuming the bars yield strength to be 400 MPa. The fact that both bars were ruptured during the test means that they must have experienced strain hardening and, therefore, the bar force just before rupture must have been greater than the yield force based on the assumed yield stress of 400 MPa. However, at delamination the strain hardening effect would have been relatively small, therefore, the difference between the delamination load and the sum of the yield forces of the two bars, would have been resisted by the laminate. This would result in the FRP force being approximately 67 kN at delamination. Since four layers of 50 mm wide and 0.165 mm thick laminate was used to strengthen these prisms, the stress in the laminate at delamination can be approximated as $\frac{67x10^3}{4x0.165x50} = 2030$ MPa, which is approximately 53% of the laminate ultimate capacity.

4.3.2 Prisms with CFRP Laminate and Anchors

The load elongation curves for the two prisms with anchors are shown in Fig.4-20. Two anchors were installed close to the laminate end on each opposite face. The prism with both internal rebars initially intact reached 172.5 kN before the first delamination compared to 110 kN for the prism with the two internal rebars initially cut. It is clear from Fig.4-20 that the two curves seem shifted by almost 60 kN. Two yielding plateaus can be seen in the case of the prism with the two rebars initially not cut, i.e. prism P5. Based on visual inspection, it was found that in the companion prism with the two internal bars supposedly initially cut, there is a yielding plateau. Since the CFRP material has no yielding point and it fails in a brittle manner, therefore, it is believed that the internal bar might not have been fully cut.

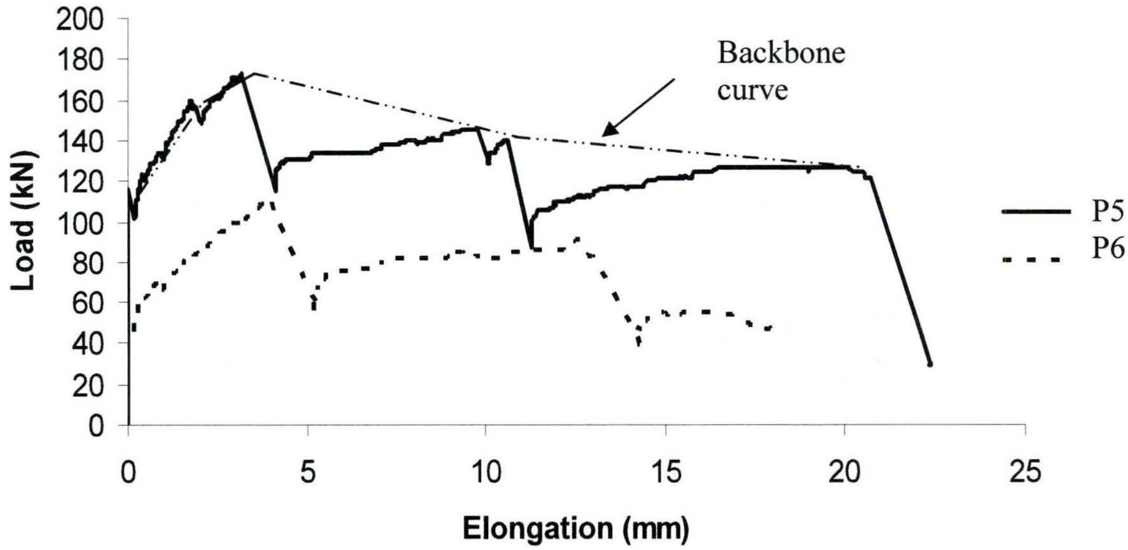

Fig.4-20: Comparison between the load elongation curves for P5 and P6

4.3.3 Prisms with CFRP Laminate and no Anchors and Prism with CFRP Laminate and Anchors

Figure 4.21 shows the comparison between the load-elongation curves for these prisms with and without anchors. In both cases the internal steel was not cut. The advantage of anchors seems to be that they allowed the prism to achieve 16.9% higher delamination load (172.5 kN) compared to the companion prism with anchors, which delaminated at 147.5 kN. Also in P4 the load dropped to 100 kN versus 125.6 kN in P5.

4.3.4 Prism with CFRP Laminate only (P3) and Prism with CFRP Laminate and Anchors (P6)

Figure 4-22 shows the load-elongation curves of prisms P3 and P6. In this case one of the internal steel bars was cut in prism P3 while in prism P6 both bars were cut. In Fig.4-22, it is clear that the prism with an anchor achieved 53.2% higher delamination load compared to the prism with CFRP only. The delamination load was 110 kN in prism P3 compared to 71.8 kN in prism P6.

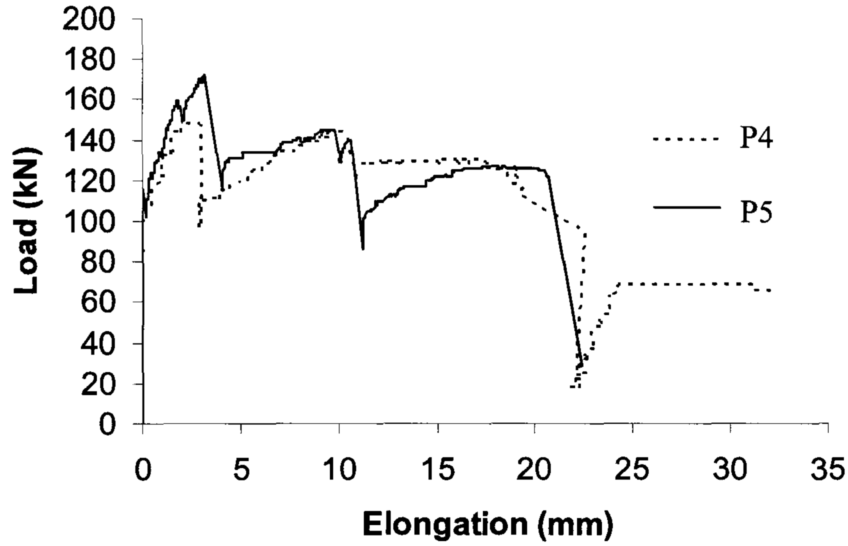

Fig.4-21: Comparison between the load elongation curves for P4 and P5

The plateaus in the load-elongation curves are due to the yielding of the internal bars which were not apparently fully severed as intended. The initial drop in load in the prism with anchor was 54.3 kN, but the load subsequently increased and reached 87.7 kN, which is almost 27 % higher than the maximum load reached in the prism with CFRP laminate only. Thereafter, the load dropped again due to delamination of the FRP on the other face of the prism. This difference in the maximum load capacities of the two strengthened prisms with and without anchors demonstrate the potential benefits of the proposed anchor.

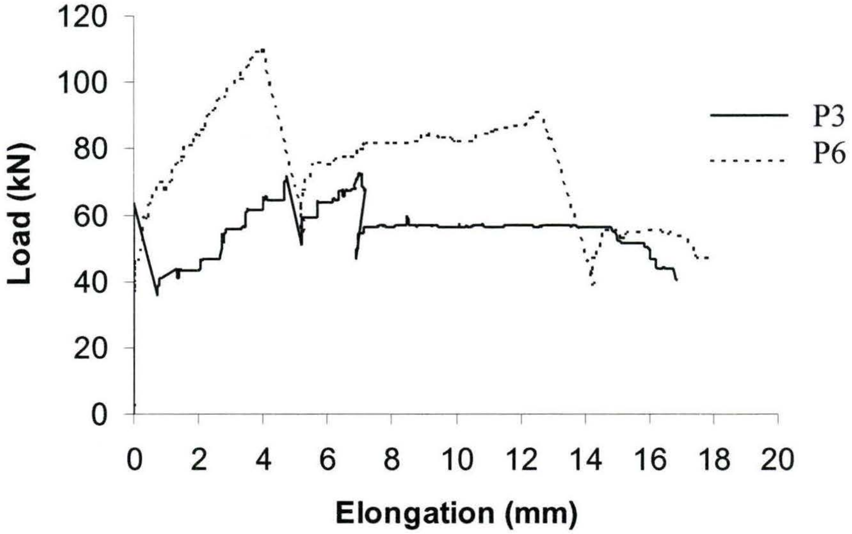

Fig.4-22: Comparison between the load elongation curves for P3 and P6

Table 4-1 summarizes the delamination and failure loads reached in each of the prisms tested in this phase. Although the beneficial effect of the anchor was obvious in these tests, assuming the degree of its effectiveness is somewhat difficult due to the presence of internal steel reinforcement and the extent to which they contributed to the total load resisted by each prism at delamination. As a consequence of this problem, the next phase of the testing program was initiated.

It is not easy to assess the effectiveness of the anchors based on the results obtained in this phase. In fact the present of the 2 No.10 steel bars dominate the strength of the prisms and therefore, the effectiveness of the anchors was not observed.

Table 4-1: Delamination and failure load for all the tested prisms

Beam	Delamination load kN	Failure load kN	Deflection at failure mm	Note
P1	-	102.5	0.018	2 steel bars
P2	-	102.5	0.026	2 steel bars
P3	63.7	72.5	14.8	One steel bar was cut
P4	147.5	65.0	32.1	2 steel bars effective [no cut]
P5	172.5	121.5	20.7	2 steel bars effective [no cut]
P6	110.0	50.2	17.2	Two bars cut

4.4 Behaviour and Observations for Concrete Prisms in Phase II

Sixteen prisms were tested under tension in Phase II. These prisms had no internal reinforcement crossing the middle section along the prism, thus the problem of steel rebars contributing to the prisms tensile strength was eliminated. The reader may refer to section 3.3 for the test details. The following parameters were considered:

1- Absence/presence of anchors.

2- Number of anchors.

3- Location of anchors.

4- Presence of pre-delaminated segment in the CFRP laminate.

4.4.1 Control Prisms

The control prism was an un-reinforced concrete tension element and it failed at 81.6 kN, but failure occurred at the location of one of the internal steel plates bolted to the end of the steel rods though which the axial load was being applied. A second prism tested similarly failed at 68.5 kN and at same location as the first prism. Consequently, to ensure failure at mid-section of the prism, it was decided to reduce the cross section at mid-length by notching it. The new cross section was

90 mm x 250 mm. The notched prism was tested and it failed at 71.6 kN at the mid-section as expected. To ensure repeatability, a prism with notched mid-section was tested, but it failed at 65 kN and the failure was still at the internal steel plate section. Consequently, it was decided to reduce the mid-length cross section further using a concrete saw. The new cross section was 50 mm x 250mm. Two more prisms were tested to make sure that the failure would occur at the mid-length section. Both prisms failed at 32.5 kN and 41.8 kN, respectively, and the failure was in both cases at the mid-length section.

4.4.2 Prisms with CFRP Laminates

Two identical prisms with two layers of CFRP laminate bonded to two opposite faces without anchors were tested in tension. The first prism reached 38.2 kN when delamination occurred on one face and the concrete failed at the mid-length. The load initially dropped but the prism regained its strength and reached 47.4 kN before the laminate on the other face delaminated. Immediately after, the prism failed in a brittle manner, as can be inferred from its load-elongation curve plotted in Fig.4-23.

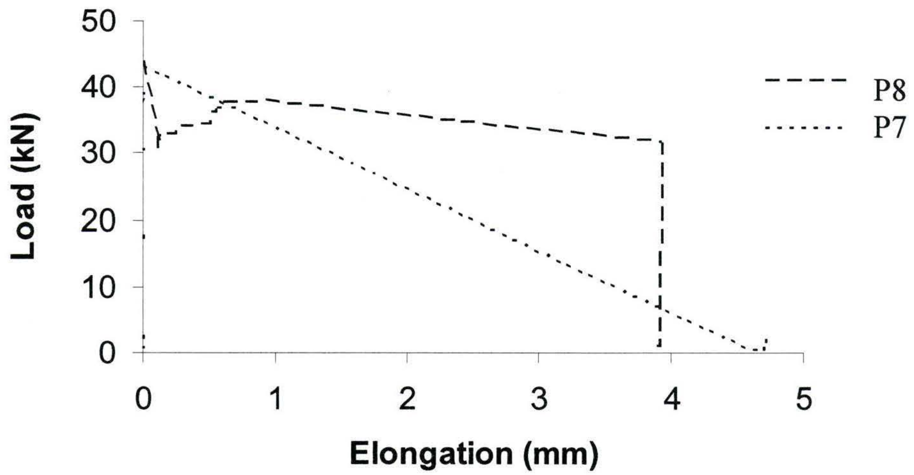

Fig.4-23: Load-elongation curves for prisms P7 and P8

Only three strain gauges were installed on each face. The maximum strain recorded was 0.0023 just before delamination after which the prism failed and no readings were recorded. Figure 4-24 shows the strain variation along the laminate length at different load levels for the two opposite faces of prism P7. It is clear that the strain gauge data on two faces are in relatively good agreement and they show reasonably uniform distribution in the vicinity of the middle section before failure. This uniformity is indicative of delamination. It should be pointed out that the zero strain values at the two ends of the laminate as plotted in Fig.4-24 were not measured but were assumed to be zero. Therefore, the linear variation of strain from the ends to the adjacent strain gauge location is not necessary reflective of the true behaviour of the laminate.

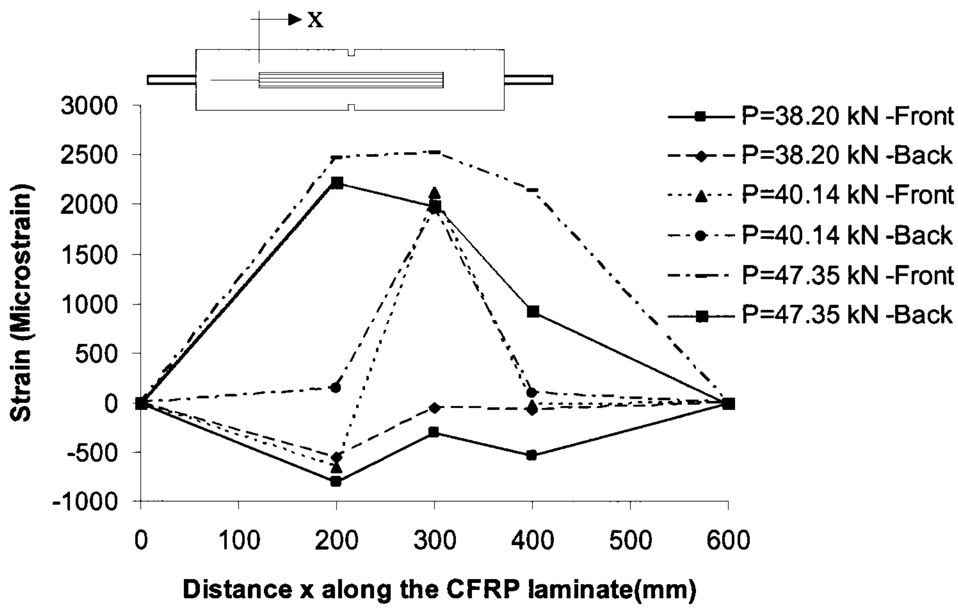

Fig.4-24: Strain variation along the laminate length in prism P7

Prism P8 was the companion to prism P7 and was tested similarly to it. It reached a maximum load of 44.1 kN when the FRP on one face delaminated and the load afterwards dropped to 31.6 kN. Thereafter, the prism continued to carry more load until delamination occurred on the other face at 37.8 kN, and eventually it failed in a brittle manner. Figures 4-25 (a) to (c) show the prism before and after delamination. The load-elongation curve of P8 is presented in Fig.4-23, while its laminate strain variation is plotted in Fig.4-26. The displacement graphs are not as informative as the strain graphs because the displacement before delamination is small, but the sudden drop in load indicates the advent of delamination which is associated with a loss of stiffness. It appears that the initial delamination is limited to a small segment of the FRP, but as the load is increased therefore delamination spreads along the laminate until the bonded length becomes insufficient for transferring the required interfacial shear and the laminate completely separates from the concrete at one end as in Fig.4-25 (b) and (c). As can be observed in Fig.4-25 (c), the failure occurred in the concrete because one can clearly observe the concrete mortar particles that have separated from the prism surface.

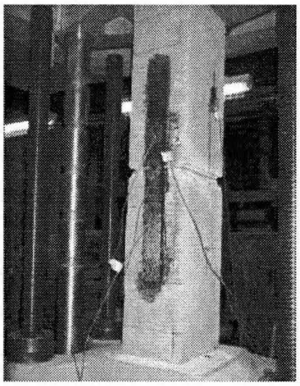

a- Prism P8 during the test

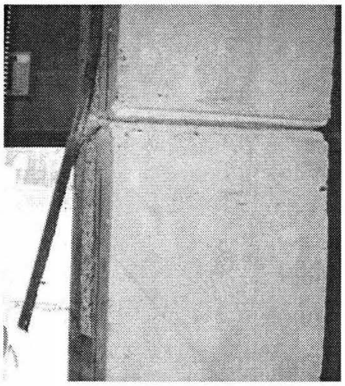

b- Delamination of CFRP

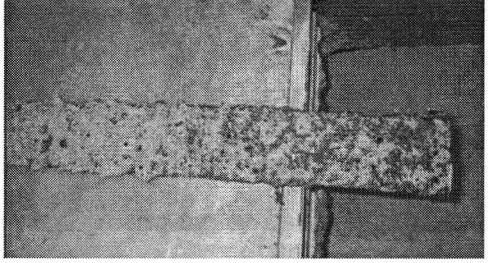

c- Thin layer of concrete attached to the CFRP laminate after delamination

Fig.4-25: Prism P8 during the test and after delamination

The strain variation in Fig.4-26 again shows that at delamination the measured strain in the CFRP strip on one face is nearly uniform, which is only possible if the laminate loses bond with the concrete over the length with uniform strain. It should be pointed out that the smaller strain values at mid-length before delamination may be due to some bending caused by the lack of co-axiality of the applied tension forces at the ends of the prism. Of course, once delamination occurs on one face, the prism begins to bend and the strain in the bonded FRP is due to combined bending and tension.

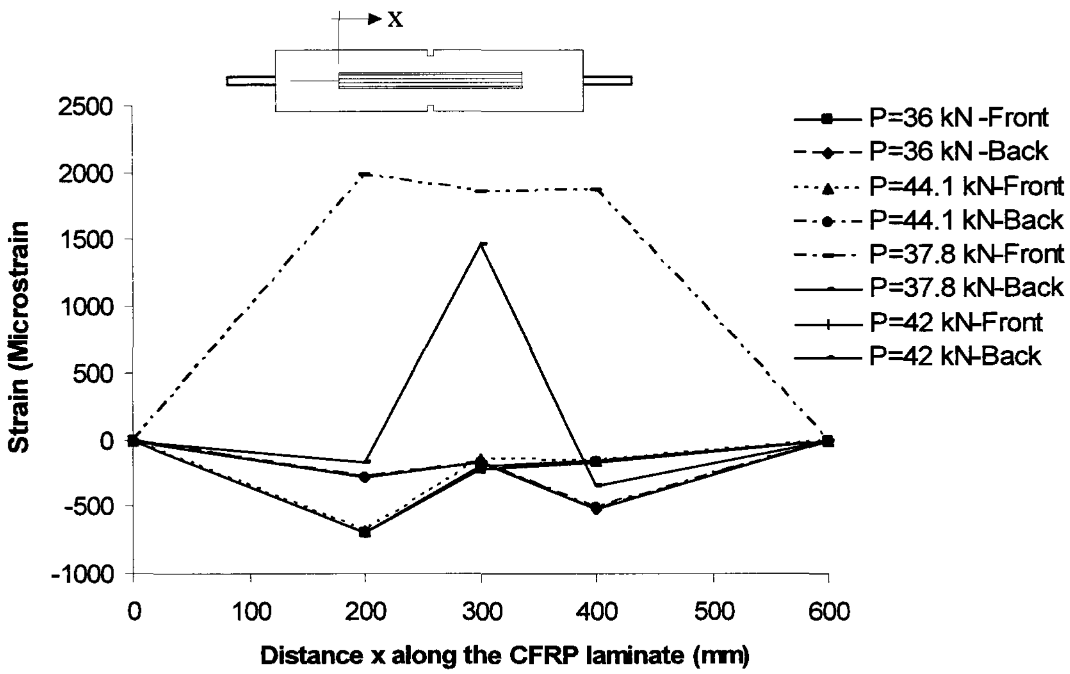

Fig.4-26: Strain variation along the CFRP laminate for P8

4.4.3 Prisms with CFRP Laminate and one Anchor at Each End

Three identical concrete prisms (P9 to P11) were externally strengthened with two layers of CFRP laminate on two opposite faces, and on each face one anchor was installed at 50 mm from the laminate ends. Only four strain gauges were installed on one face to record the CFRP strain. The strain in prism P11 was also monitored by using an experimental non-contact high speed imaging system that will be discussed more in the following section.

Prism P9 reached 22.9 kN before the concrete cracked at mid-length and the load dropped to 19.2 kN. The prism subsequently regained its strength and reached 66.3 kN before major delamination occurred on one face. The load thereafter gradually dropped and reached 55.6 kN before failure, and the laminate slippage was measured to be 15 mm at one end. From visual inspection, it was observed that the CFRP laminate was fully delaminated on face, but the anchor prevented it from complete separation from the concrete surface. After delamination on one face, as expected the prism experienced bending, the laminate on the intact face did not delaminate. Figures.4-27 and 4-28, respectively, show the load-elongation curve and the strain variation along the laminate length at different load levels for this prism.

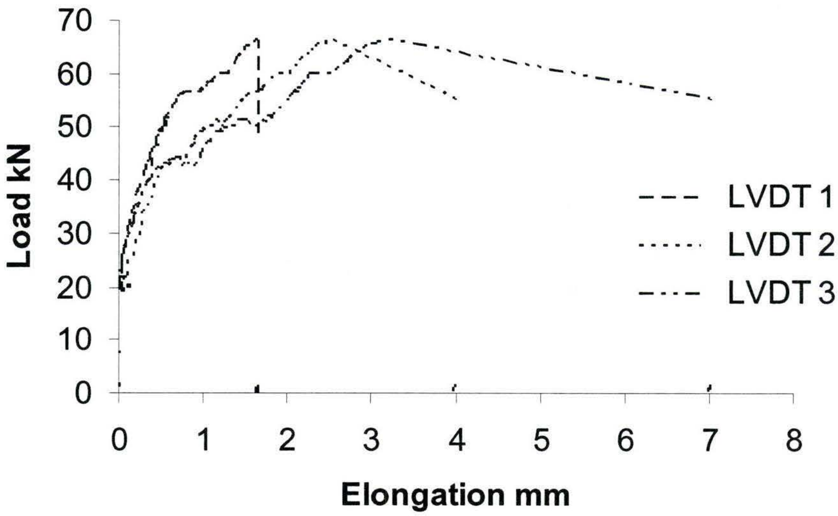

Fig.4-27: Load elongation curve for prism P9

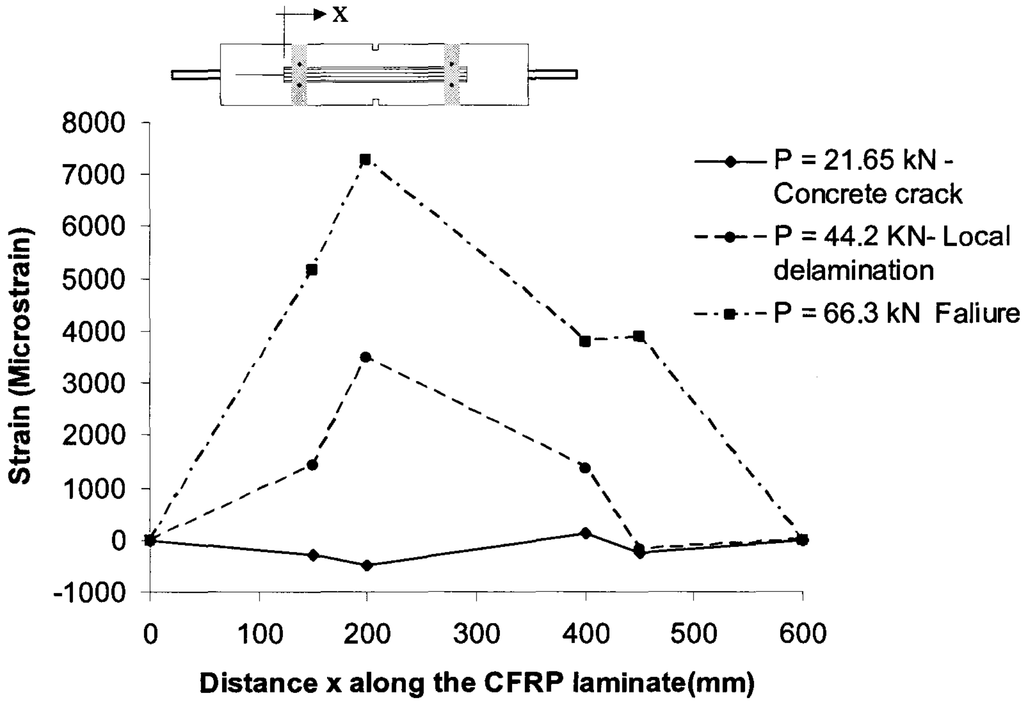

Fig.4-28: Strain variation along the laminate length for P9

If we compare the load-elongation curve of prism P9 with that of prism P8 in Fig.4-23, we observe that the two prisms exhibit completely different type of response. Prism P9 does not exhibit a sudden drop in load, undergoes significantly higher deformation before failure and reaches an ultimate load of 66.3 kN, which is 50% higher than that of prism P8. Furthermore, the response of P9 is relatively ductile compared to that of P8. The maximum strain in P9 reached 0.0073, which is 65% of the rupture strain of the laminate. This strain is significantly greater than the approximately 0.002 maximum strain reached in prism P8. It is important to remark that the anchor is not able to prevent the initiation of delamination because delamination initiated at approximately the same load in the two prisms; however, the anchor prevented the delamination from spreading to the end of the laminate and thus enabled it to resist the additional load as an unbonded but anchored reinforcement. Figures 4-29 to 4-32 show one of these prisms, its mode of failure and the FRP slippage at the end of the laminate.

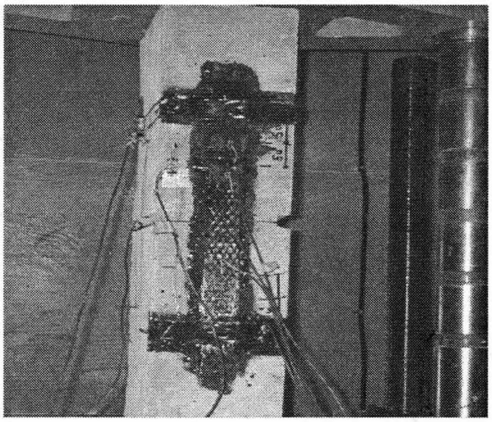

Fig.4-29: Typical prism with one end anchors during the test

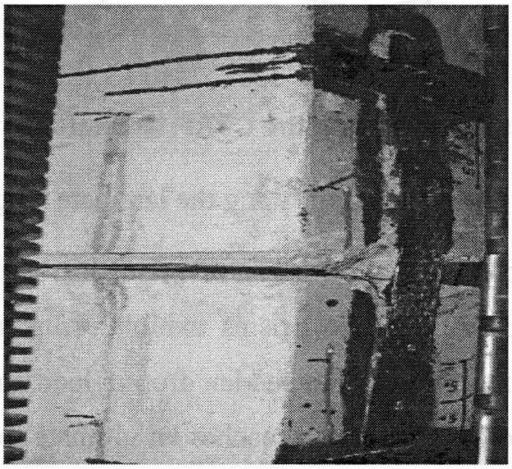

Fig.4-30: CFRP held by anchors in prism P9

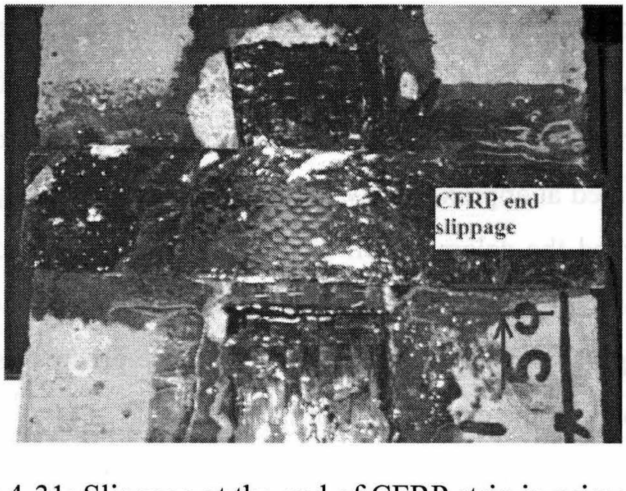

Fig.4-31: Slippage at the end of CFRP strip in prism P9

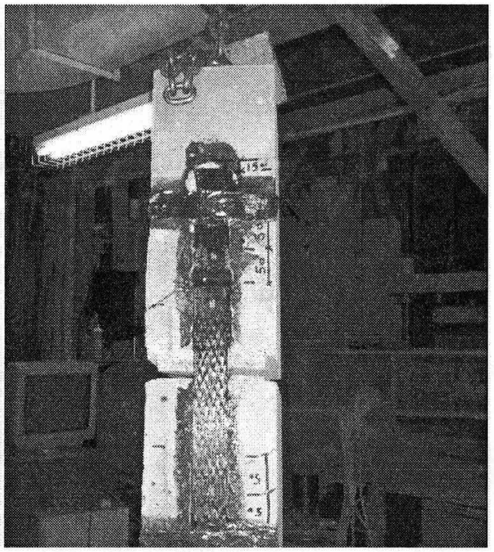

Fig.4-32: Anchors holding the CFRP laminates after full delamination and large separation of the two halves of the prism P9

Prism, P10, was nominally identical to prism P9. Four strain gauges were used to measure the strain along the surface along one face as shown in Fig.4-33. The prism reached 36.9 kN before the concrete cracked at its mid-length and the load subsequently dropped to 27.6 kN. The prism regained its strength and reached 45.7 kN before local delamination occurred on one face and the load dropped to 42.2 kN. It is important to mention that during the test, local delamination was occurring but the major drop in load happened once the prism reached 54.2 kN, at which point a loud sound with a was heard and the load abruptly dropped to 28.9 kN. In this case, the slip at the laminate end was measured to be 15 mm. notwithstanding the delamination; the anchor prevented the laminate from full delamination and full separation from the concrete surface. After the major delamination, the prism experienced bending, the load continued to increase until it reached 42.9 kN, thereafter it gradually decreased. The prism again experienced a dramatic reduction in load once the FRP on the other face delaminated, a phenomenon which again accompanied by a loud sound. The string pots reached their maximum stroke and no measurement could be thereafter taken. However, the prism regained its strength and reached 24.76 kN before complete failure. The opening in the concrete at mid-length was measured to be 70 mm and the anchor practically ruptured, but it still prevented the laminate from full separation. Final slippage was measured to be 55 mm on the tension face and 50 mm on the compression face where the anchor was fully ruptured. Figures 4-33 to 4-37 show the test setup, failure mode and load elongation curve of this prism.

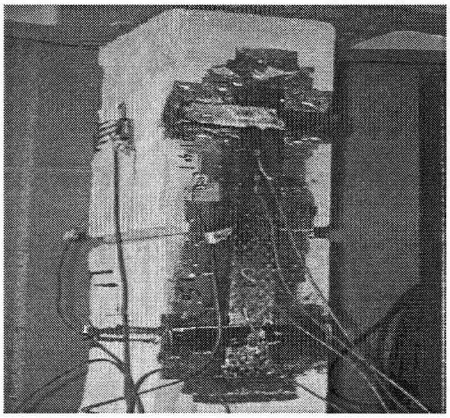

Fig.4-33: Test setup

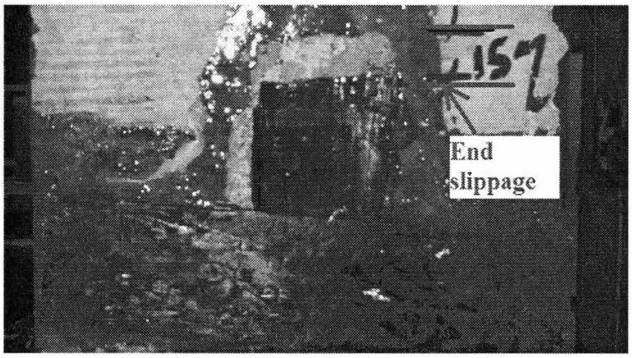

Fig.4-34:CFRP laminate end slippage

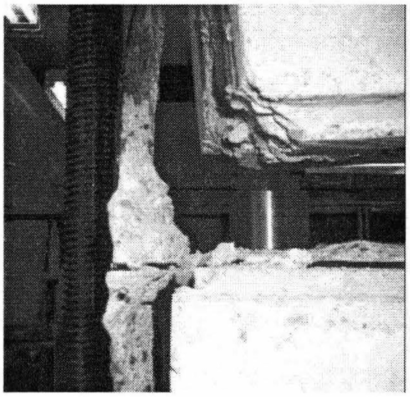

Fig.4-35: Concrete layer attached to the laminate

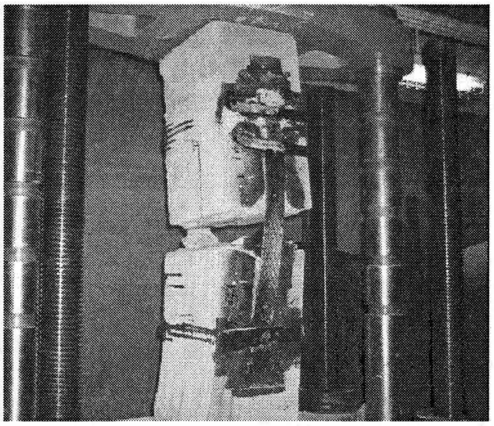

Fig.4-36: Separation of the concrete held together by the anchored CFRP laminate

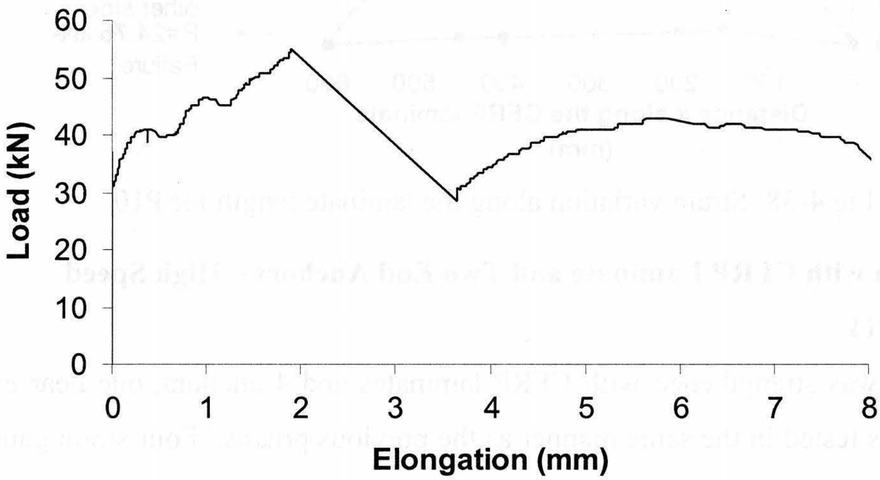

Fig.4-37: Load elongation curve for prism P10

Figure 4-38 shows the strain profile along the laminate length at different load levels. The maximum measured strain was 0.0062, which is 55% of the laminate ultimate strain capacity. Comparing the results with those of the companion prisms without anchors indicate that the anchors allowed the laminate to reach significantly higher strains compared to the two prisms without anchors. Also, due to the anchors the failure was more ductile compared to that observed in the two prisms without anchors. Furthermore, the maximum load reached in the case of the prisms with anchors was 66.3 and 55 kN with an average value of 60.1 kN compared to 47.4 and 44.2 kN with an average value of 45.8 kN for the prisms without anchors.

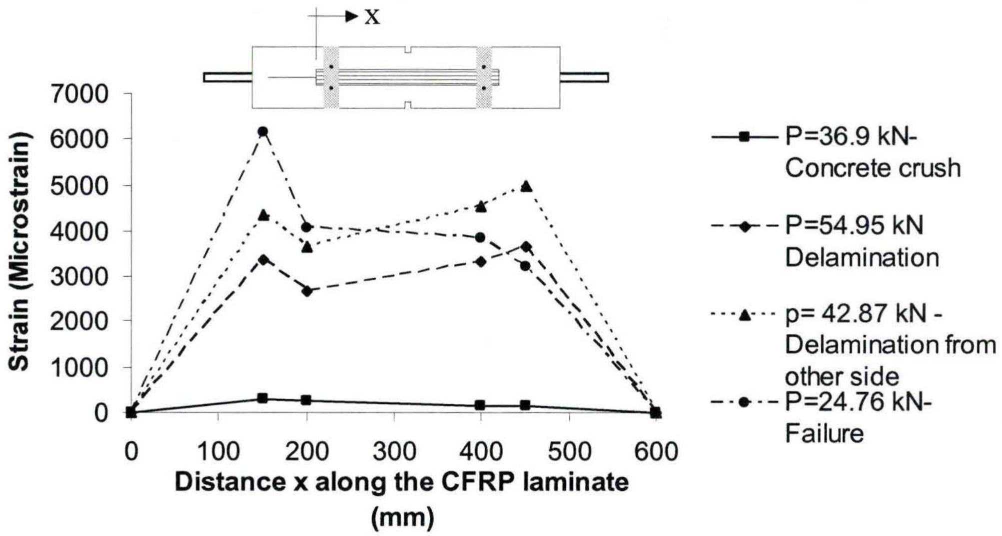

Fig.4-38: Strain variation along the laminate length for P10

4.4.4 Prism with CFRP Laminate and Two End Anchors – High Speed Camera- P11

One prism was strengthened with CFRP laminates and 4 anchors, one near each end and was tested in the same manner as the previous prisms. Four strain gauges were installed on one face. In this case, an experimental data image correlation system was used to monitor the strains and displacements along the laminate length. The high speed camera used had 1.25 MPI/sec and could take up to 7.8 frames /sec. The process started by spraying the monitored face with white speckled paint. Fig.4-39. The camera tracked the dark speckles before and after deformation and the associate software determined their planar displacements during the test. Using these displacements, the system software calculated the strain at selected locations. Figure 4-39 shows the test setup and the prism preparation. As shown, only the painted parts (CFRP laminate and the anchors) were tracked by the camera.

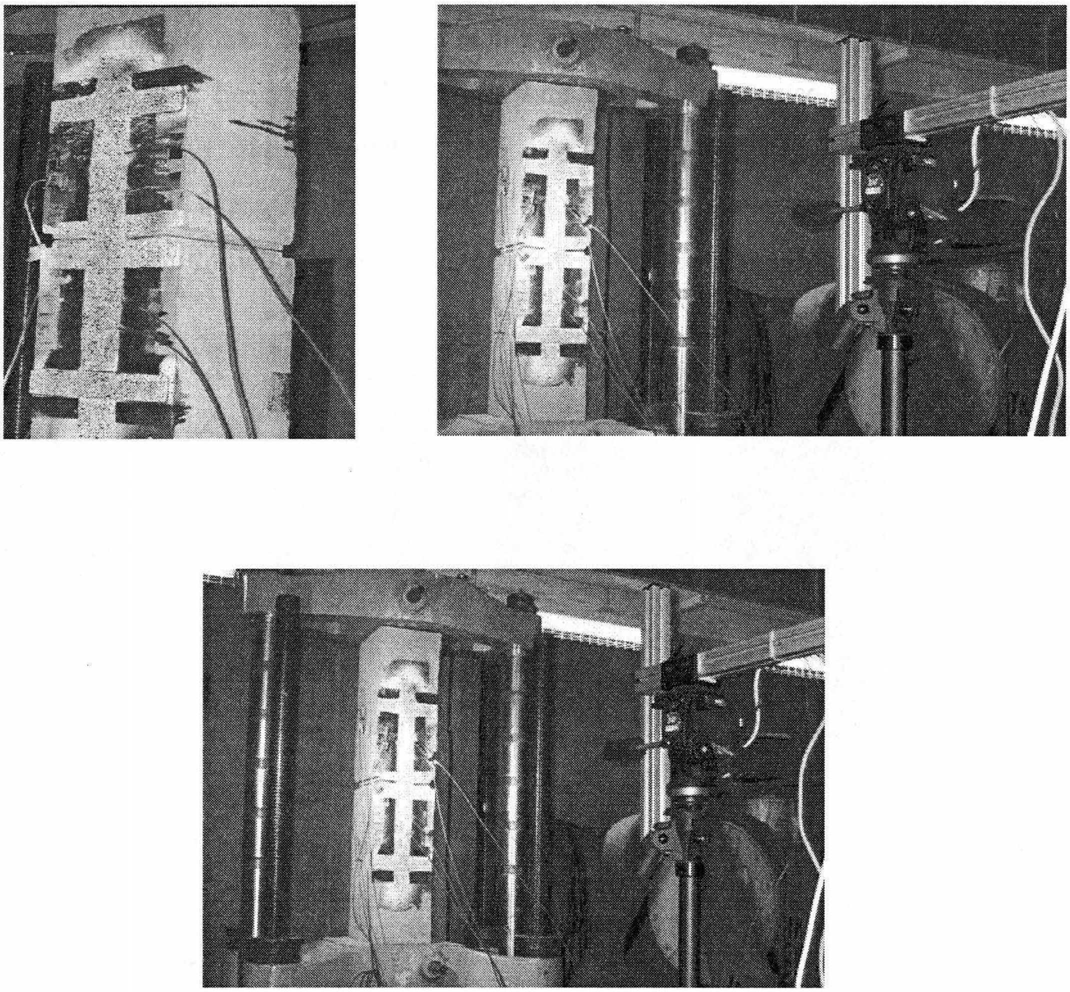

Fig.4-39: Test setup and prism preparation for P11

This prism reached 32.4 kN and then the concrete cracked at the location of the mid-length and the load dropped. The prism regained its strength and reached a value of 42.9 kN before local delamination occurred with a major drop in the load accompanied by a loud sound at 48.4 kN. This event was triggered by the delamination on one face, which caused the load to drop to 22 kN, but the anchor prevented the CFRP from full delamination; however, based on visual inspection it was found that the laminate was practically fully delaminated on one face but it was still attached to the concrete by the anchor. After the initial drop in load, the load increased again and reached 39 kN and then another drop in the load occurred to 13 kN. The latter was caused by delamination on the other face. The load increased again and reached 27.2 kN but at this point the laminate on the front face completely separated at its top end and the load dropped to 4 kN. The load increased slightly thereafter and reached 10.9 kN at failure. Figures 4-40 to 4-42 show the delamination and slippage for this prism. Note that the opening in the mid-length and the slippage were measured after the test and found to be 70 mm.

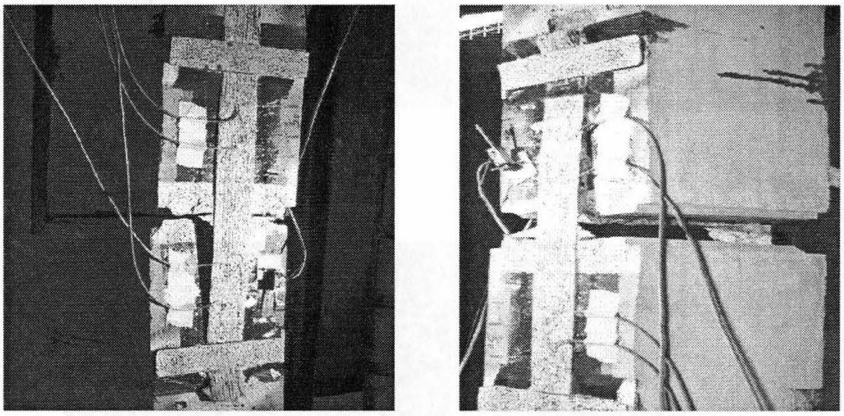

Fig.4-40: Delamination occurred

Figure 4-43 shows the load mid-length deflection obtained from the three LVDT's on three faces. Due to bending after initial delamination the prism is no longer in pure tension; therefore, the displacements of its three faces are not equal.

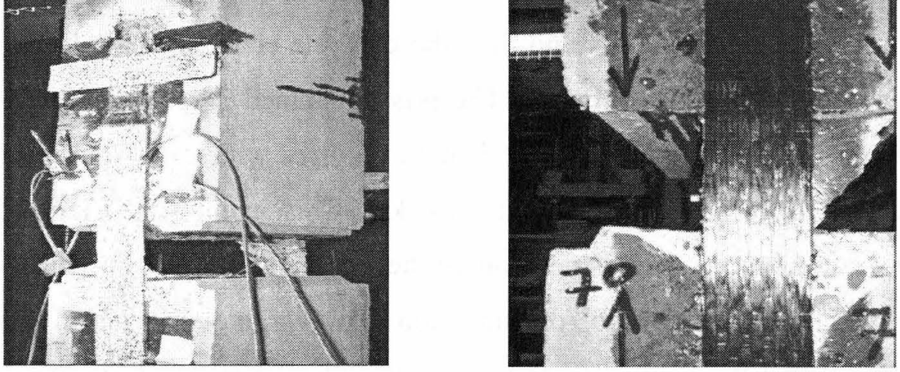

Fig.4-41: Opening at the mid-length

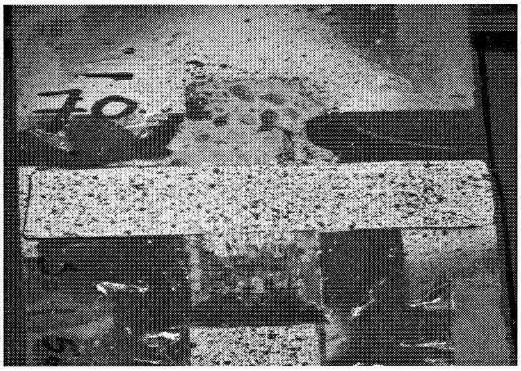

Fig.4-42: Slippage at the laminated end

The recorded values for strains are presented in Fig.4-44 for different load levels along the laminate length. The maximum strain reached was 0.0058. The data image coloration results were analyzed by the engineer who was responsible for operating the camera. It was a demo to illustrate the capability of the camera for to measuring strain and deformations; therefore, all the information about how to handle and work on the software was not available to the auther. Also, the data from the camera was a function of the time, but the camera does not track the load. On the other hand, the results from the strains gauges, LVDTs, and load jack were not stored as a function of time.

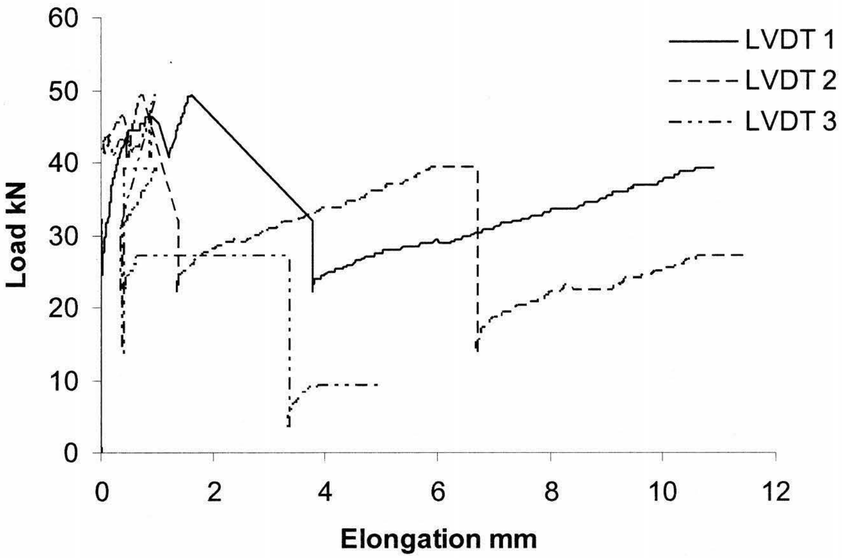

Fig.4-43: Load elongation curves for P11

This creates some difficulty in relating the camera based displacements and strains to the applied load. Figures 4-45 and 4-46 show a comparison between the strain profile along the laminate length obtained from the camera and the strain gauges at the same location and at different load levels.

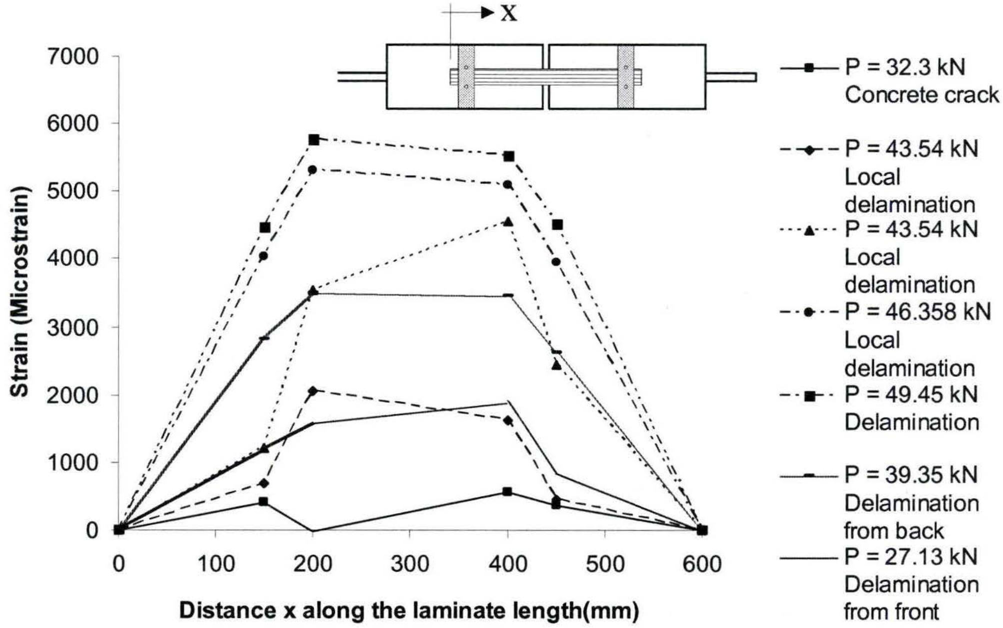

Fig.4-44: Strain variation along the laminate length at different load levels for P11

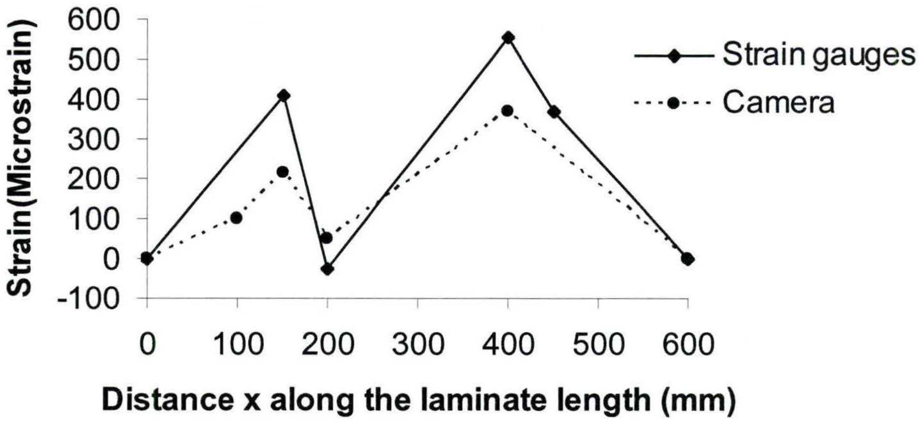

Fig.4-45: Laminate strain values using strain gauges versus the camera

(P = 32.3 kN)

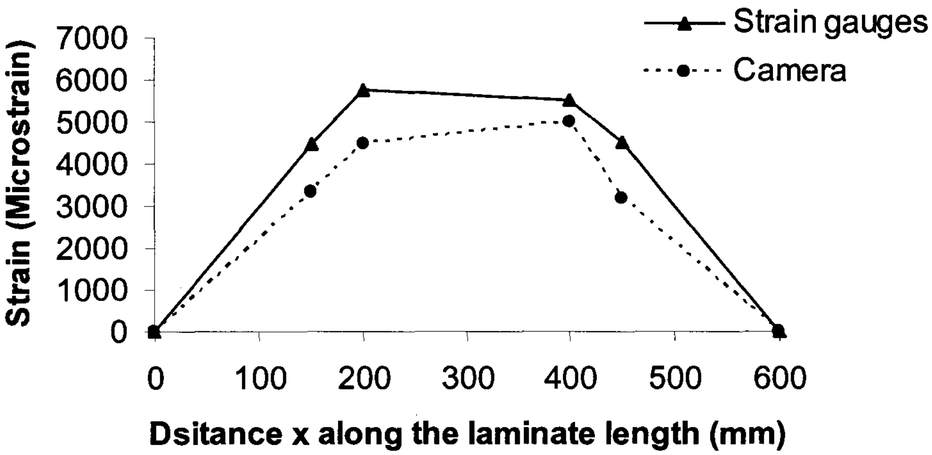

Fig.4-46: Strain variation along the CFRP laminate length measured by the strain gauges versus the camera (P = 49.5 kN)

It is clear that the readings from the strain gauges installed on the CFRP laminate and the readings from the high speed camera are in good agreement and this new vision-based system has great potential for measuring surface strains.

4.4.5 Prisms with CFRP Laminate and Two Anchors at Each End

Two identical concrete prisms (P12 and P13) were strengthened with two layers of CFRP laminate on two opposite faces and four anchors on each face. i.e. two anchors near each end of the laminate. The concrete in prism P12 cracked at mid-length and the two concrete blocks were totally separated at 28.1 kN, the load thereafter dropped to 17.5 kN. The prism regained its strength and reached 80.4 kN before a local delamination and a small drop in the load occurred. The prism afterwards reached 94.1 kN before major delamination occurred on the top end of the laminate on one face and the load dropped to 13 kN. The prism experienced bending at this stage causing more tension on the delaminated side and compression to the intact side. As the load started to increase again, the compression face picked up the load and the net force become in tension. The opening was measured and found to be 40 mm from the tension side at failure.

After a visual inspection it was found that the CFRP laminate was fully delaminated from one face but the anchors prevented it from full separation and there was no sign of end slippage. Therefore, it increased again and reached 30.9 kN at which point at which point local delamination, accompanied by a small drop in the load occurred. The prism load continued to increase until it reached 60 kN and thereafter another major delamination occurred. The load dropped to 43.5 kN and then gradually decreased and the test was stopped at 19 kN because there was major concrete damage and clear slippage of the loading rod. It is important to mention that cracks appeared at the level of the internal steel plate and propagated towards the outer top anchors. These cracks expanded very rapidly causing the concrete to split at the level of the loading rod. Furthermore, the load did not drop suddenly even though the concrete was severely damaged. The CFRP anchors were not pulled out and they did not allow the laminate to fully delaminate. Figures 4-47 and 4-48, respectively, show the load elongation curve and the strain profile along the laminate length at different load levels.

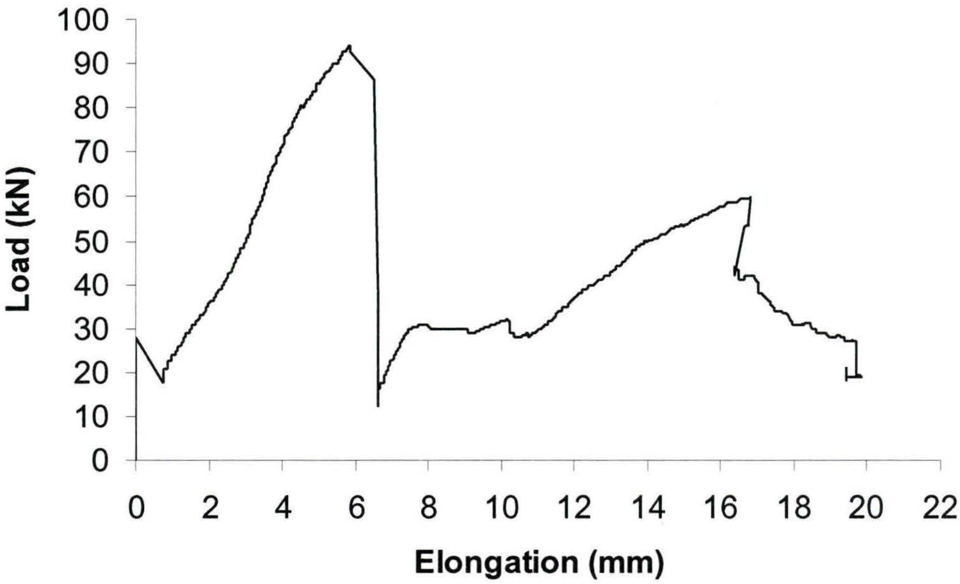

Fig.4-47: Load elongation curve for prism P12

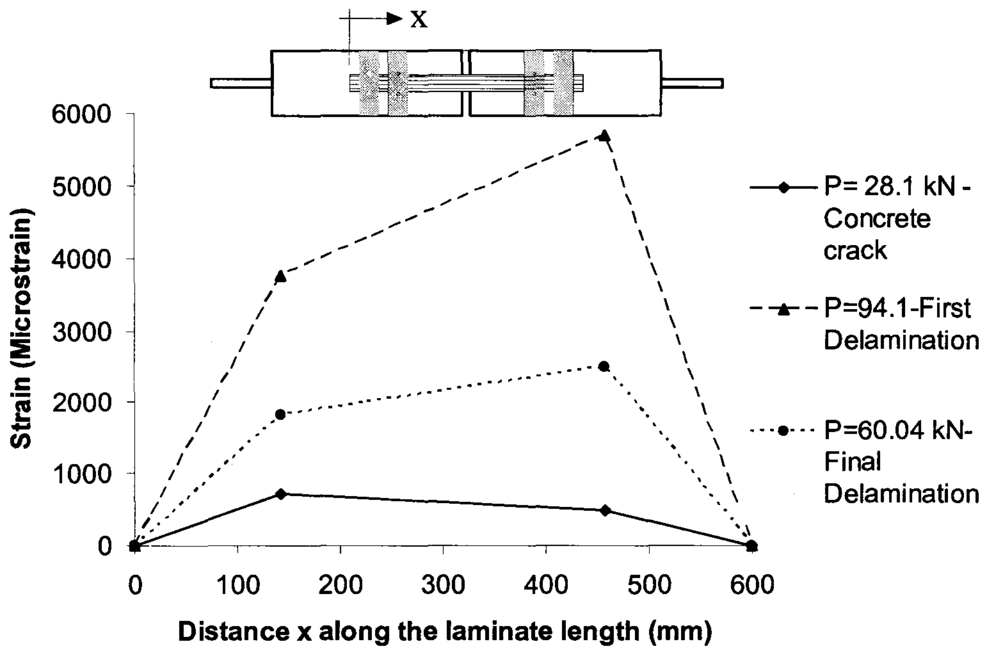

Fig.4-48: Strain variation along the laminate length for P12

The maximum strain reached was 0.0057 which is less than the maximum strain reached in the two prisms with only two anchors on one face. Note that in this case the failure was due to the crushing of concrete, and not due to full separation of the CFRP laminate, pull out of the anchor, or rupture of the CFRP laminate. The CFRP strain was far from its ultimate value but the anchors could prevent the laminate from full delamination until the failure in the concrete occurred at the level of the internal steel plate as shown in Figs.4-49 and 4-50.

The second identical prism, P13, had 4 anchors on each face and the same configuration as P12. This prism reached 38.3 kN before the concrete cracked at the mid-length. The load dropped to 27 kN but the prism regained strength accompanied by local delamination. This prism reached 81.4 kN before full delamination occurred at one face and the load dropped to 60 kN. Even though one side was delaminated, the prism regained its strength and reached 61.6 kN before another sudden drop with a big bang occurred. The prism at this stage could hold the load at 44 kN. Local delamination was observed and the prism reached 56.1

kN before another delamination from the back face occurred. The prism at this stage started to lose stiffness and the load dropped gradually. It is important to mention that the anchor prevented the laminate from pulling out or full delamination. Also it was observed that the concrete at the level of the steel plate was cracked and heavily damaged. Visual inspection was performed and none of the anchors were pulled out until full concrete failure. Figures 4-51 and 4-52 show the load elongation curve and the strain profile along the laminate length with different load levels, respectively. It is important to mention that in case also a ductile behaviour was observed Figures 4-53 to 4-55 show the prism setup and failure mode.

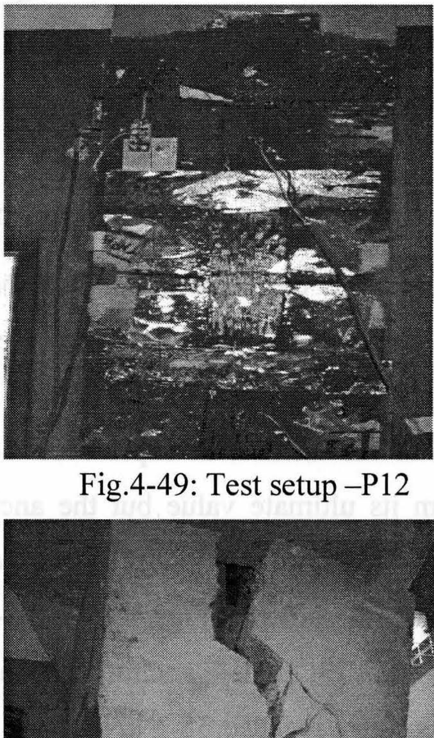

Fig.4-49: Test setup –P12

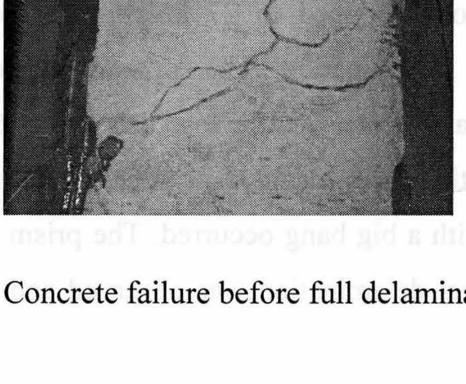

Fig.4-50: Concrete failure before full delamination-P12

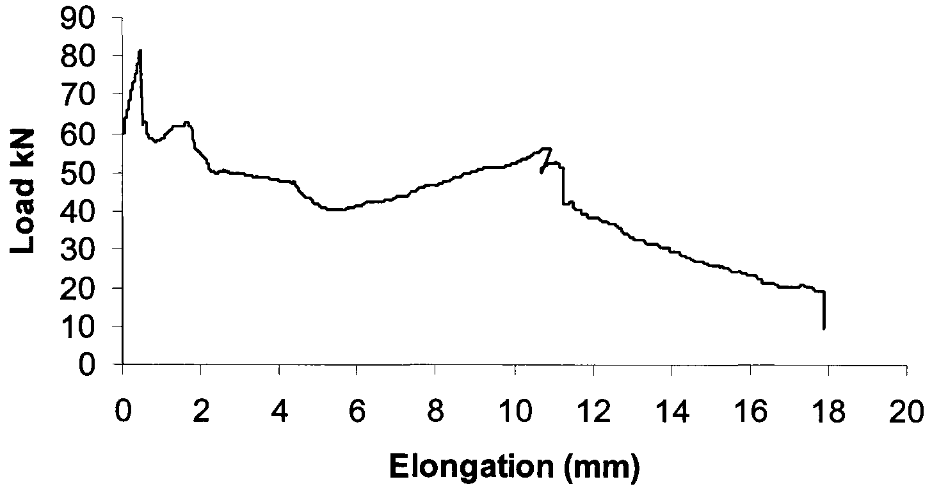

Fig.4-51: Load elongation curve P13

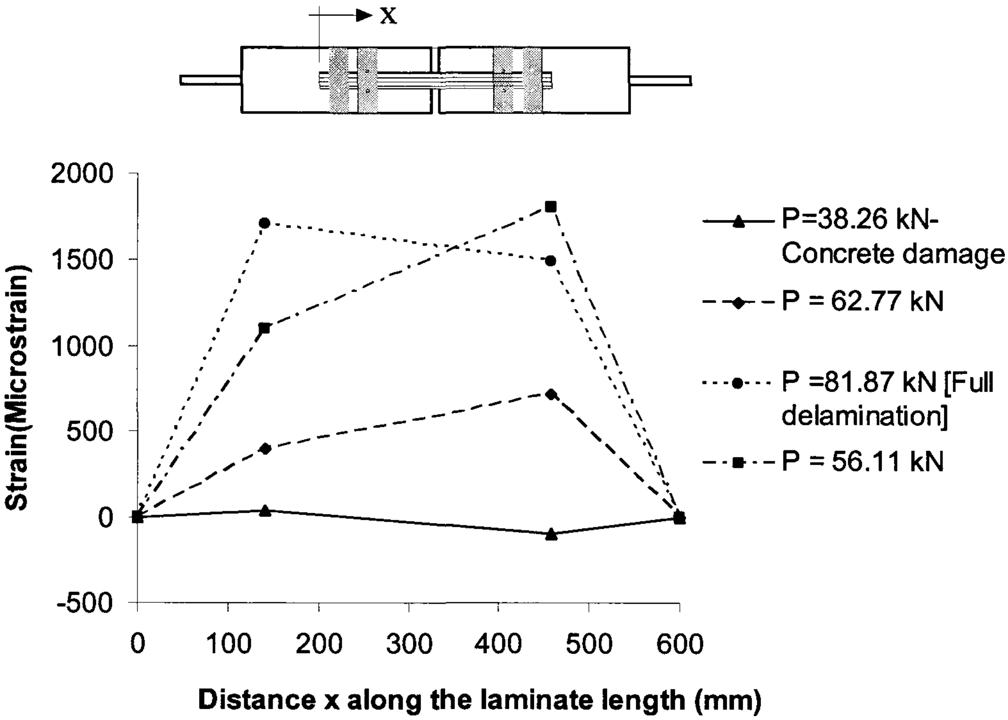

Fig.4-52: Strain variation along the laminate length for the P13

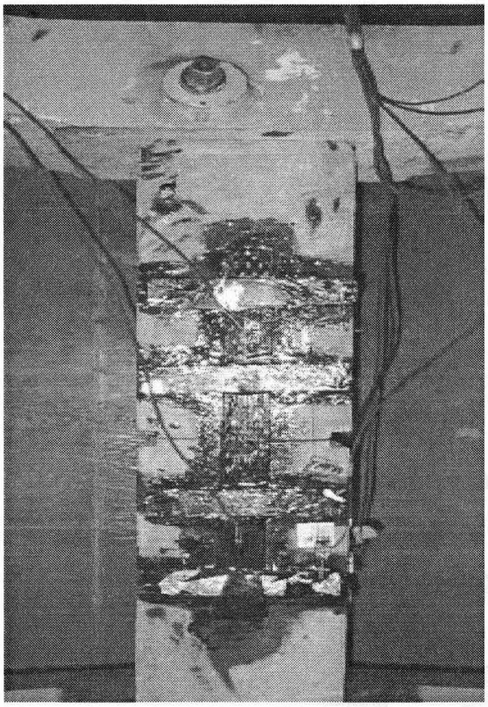

Fig.4-53: Test Setup-P13

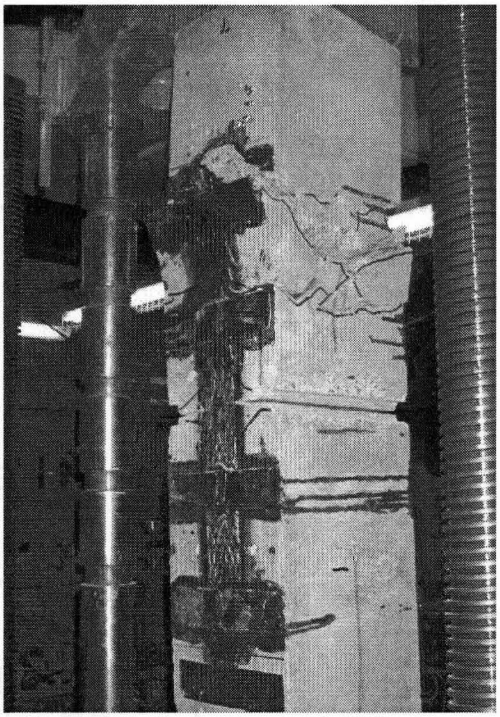

Fig.4-54: Concrete crush-P13

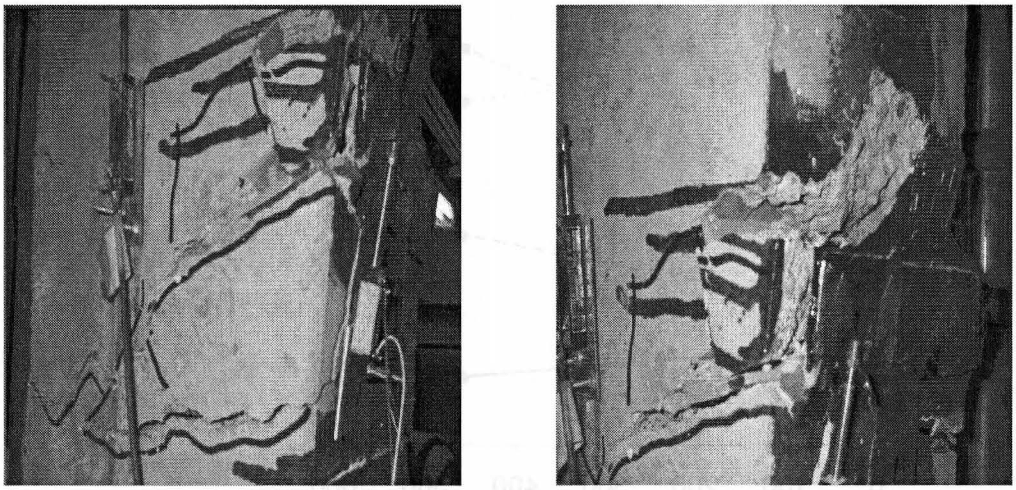

Fig.4-55: Concrete crush at the level of the internal steel plate-P13

4.4.6 Prism with Unbonded Segment and with One Anchor at Each End

Prism P14 was built with a 150 mm segment of the CFRP laminate not bonded to one concrete surface in the mid-length region. One prism was tested in this configuration and only one anchor was used near each end. Four strain gauges were installed on the un-bonded face of the prism. This prism experienced local delamination at 44.5 kN and then the load dropped to 41.5 kN. The concrete completely separated at mid-length as expected at load level 51.5 kN, with a sudden drop to 22.5 kN. The prism regained its strength and reached 36.7 kN before another local delamination from the back face occurred with a small drop of the load to 36 kN. Although the prism regained strength, local delamination, accompanied by an audible sound, was observed, but at 51.2 kN another sudden big bang was heard and delamination on the back face occurred.

The anchor could prevent the laminate from full slippage and full delamination. It is important to mention that once delamination occurred from the back face, and due to the fact that the concrete was already cracked at mid-length, the prism experienced bending, causing tension on the back side and compression to the front face. Eventually, the whole back face was delaminated, but the anchors prevented the laminate from full slippage and full delamination and the prism was able to reach 37.1 kN before the front face delaminated. Again the anchor from the front face prevented the laminate from slippage and delamination but a sudden drop occurred at 34 kN. Ultimately, the prism reached 37.8kN before complete failure. The mid-length gap was measured to be 25 mm at failure.

As shown in Figure 4-56, the prism experienced a relatively ductile behaviour compared to the prisms without anchors. In this case, as shown in Fig.4-57 the maximum strain was measured to be 0.011, which is almost 94 % of the CFRP laminate rupture strain. As mentioned earlier, the behaviour of the prisms was governed by the anchors, and the ductility exhibited by the prisms with anchor could prevent brittle failure of FRP retrofitted members and give adequate warning of failure. Such enhancement was also previously reported a in the literature through usage of fan anchors (Smith and Kim 2008). However, they only reported 32% increase in the failure load using the fan anchor versus the 244% maximum increase achieved thought the usage of the proposed anchor.

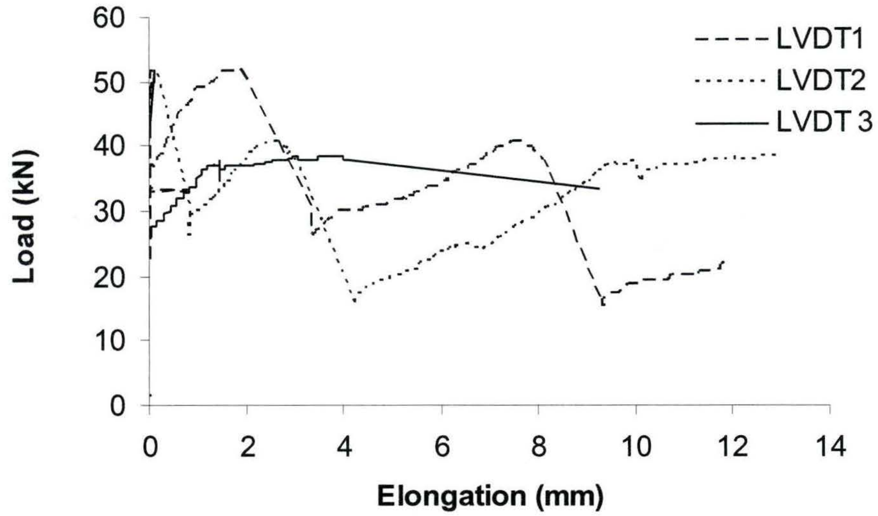

Fig.4-56: Load elongation curve for prism P14

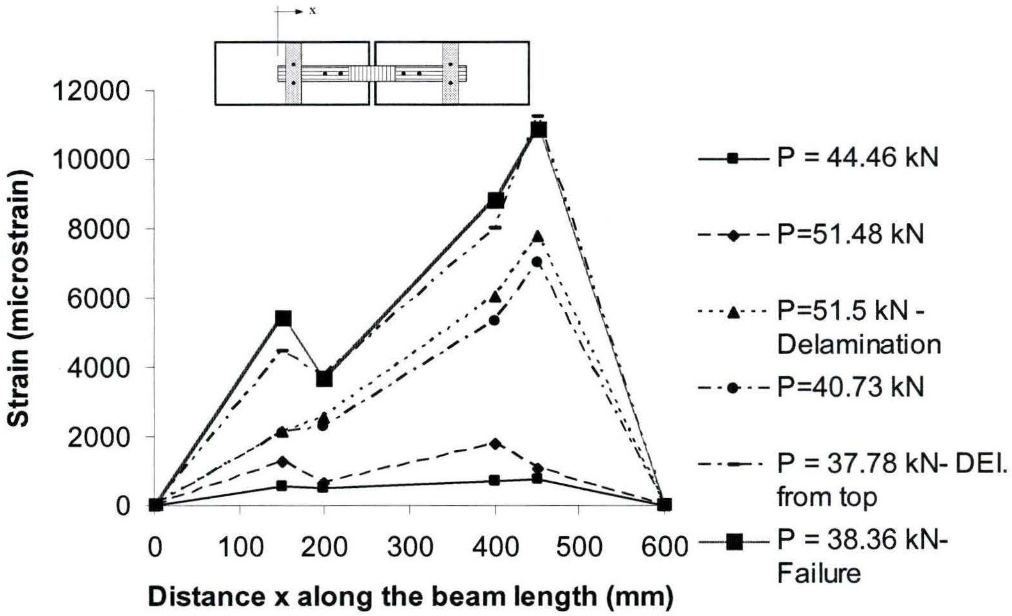

Fig.4-57: Strain variation along the laminate length for P14

4.4.7 Prisms with Unbonded Laminate Segment and 2 Anchors at Each End

Two identical prisms with 2 anchors at each end and with a 100 mm long segment of the CFRP laminate unbonded to the concrete surface in the mid-length region were tested. The first prism reached 51 kN and then the concrete cracked at the mid-length, which caused the load to drop to 24.1 kN. Thereafter, the load increased again and reached a maximum value of 74.1 kN. After the maximum load, cracks appeared at the level of the internal steel plate and propagated towards the outer anchors, which caused the load to drop to 70 kN. Upon inspection, it was found that the laminate had not delaminated, but a block of concrete to which the laminate and the anchor were still fully bonded had broken away from the prism. After this event, the load oscillated by first increasing to 72 kN, then dropping to 47.6 kN and again increasing to 57.9 kN. Thereafter, the load kept dropping, the cracks propagated between the two anchors on both faces, causing the concrete to fail but with no sign of delamination as can be seen in Fig.4-58.

The load elongation curve of the specimen is presented in Fig.4-59, while the strain profile along the laminate length is plotted in Fig.4-60. The maximum strain was found to be 0.0024, which is only 20% of its ultimate strain, but given the measured load level, this value does not seem to be correct and this may be due the failure of the strain gauges.

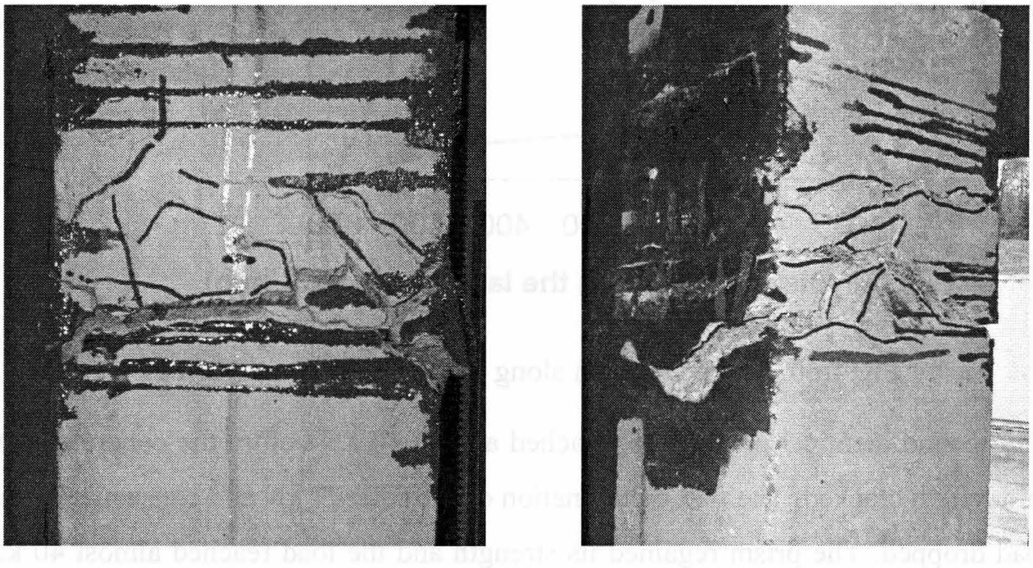

Fig.4-58: Failure in the concrete at the level of the internal reinforcement P14

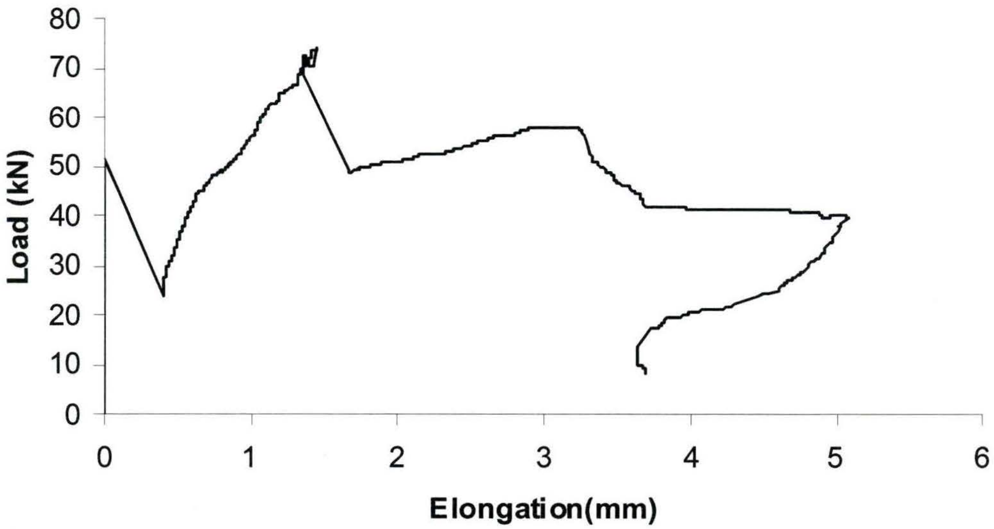

Fig.4-59: Load elongation curve for P15

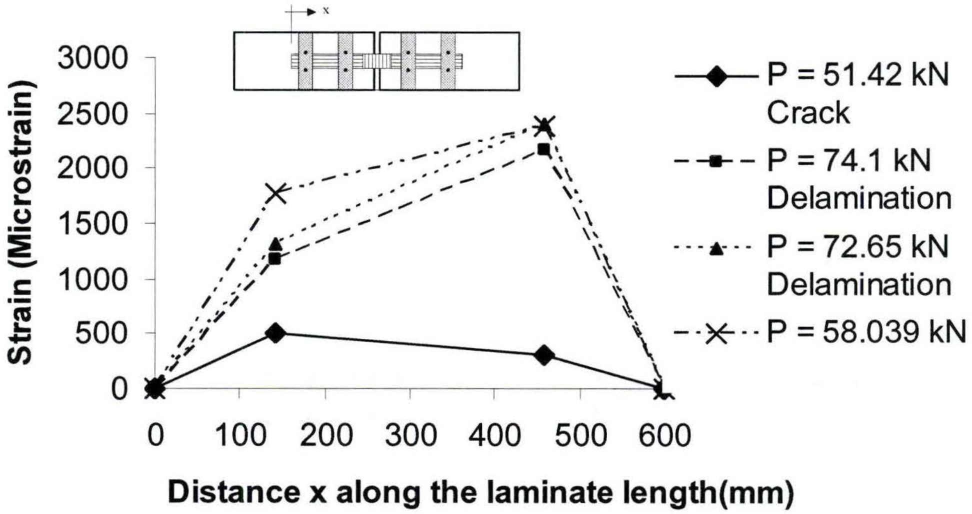

Fig.4-60: Strain variation along the laminate length for P15

The second identical prism, P16, reached almost 40 kN before the concrete at its mid-length cracked. The first delamination occurred at 77 kN and consequently the load dropped. The prism regained its strength and the load reached almost 40 kN before it started to gradually decrease until failure. The maximum strain reached in this case was 0.0039 which is 60% over than the maximum strain reached in prism P15. The load mid-length elongation and the strain profile for this prism are presented in Figs.4-61 and 4-62, respectively. Note that after the maximum load, the elongation readings are no longer useful as all the LVDTs reached their maximum stroke. The behaviour of this prism was almost the same as the companion prism where failure occurred in the concrete at the level of the internal steel plate as shown in Fig.4-63.

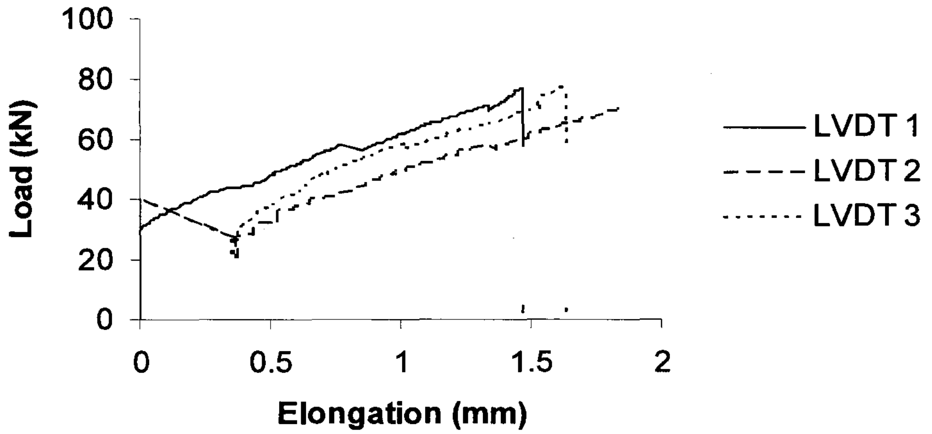

Fig.4-61: Load elongation curve for P16

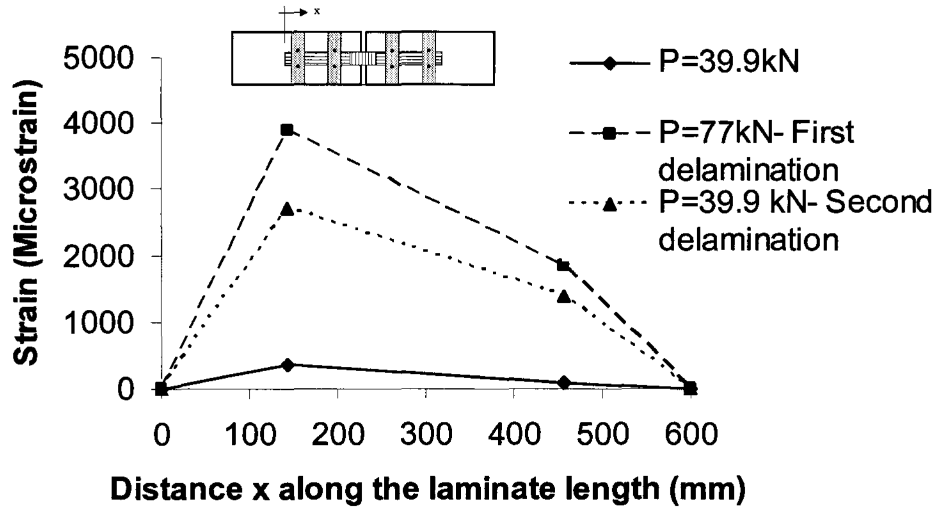

Fig.4-62: Strain variation along the laminate length for P16

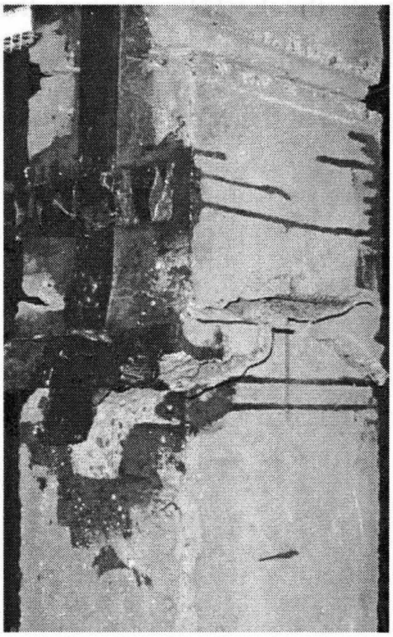
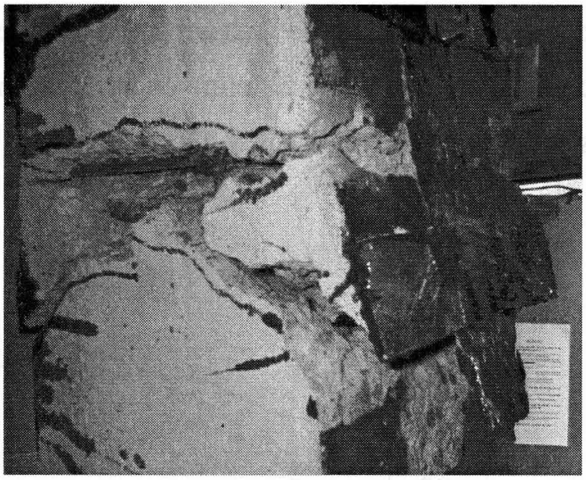

Fig.4-63: Failure occurred in P16

4.5 Discussion of Results

Table 4-2 summarize the axial strength values obtained for the prisms in Phase II. The control prisms theoretical strength is not calculated because it depends on the concrete tensile strength which can be highly variable, especially in direct tension tests similar to the tests performed here. Furthermore, it is not germane to the current discussion. The theoretical tensile capacity of the prisms strengthened with CFRP laminates is calculated based on the tensile capacity of two 50 mm wide and 1.016 mm thick strips of the laminate because the concrete contribution to the tensile resistance would be zero once the concrete cracks. Since the laminate has a tensile strength of 849 MPa, the tensile capacity of the four strips (two on each face) is 172.5 kN. Note that the theoretical strength is based on the assumption of full bond and is independent of the presence of anchors.

Table 4-2: Summary of test results

Prism	Prism description	Average ultimate load P_u (kN)	$\frac{P_u}{0.5(P5_u + P6_u)}$	$\frac{P_u}{0.5(P7_u + P8_u)}$	$\frac{P_u}{0.33(P9_u + P10_u + P11_u)}$
P5 & P6	Control	37.2	1.0	0.81	0.66
P7 &P8	CFRP, no anchor	45.8	1.22	1.0	0.81
P9, P10 & P11	CFRP+ 1 anchor at each end	56.3	1.51	1.23	1.0
P12 &P13	CFRP+ 2 anchors at each end	90.8	2.44	1.98	1.61
P14	CFRP+ 1 anchor at each end, one face partially pre-delaminated	51.5	1.38	1.12	0.92
P15 &P16	CFRP+ 2 anchors at each end, one face partially pre-delaminated	75.5	2.03	1.65	1.34

Column 3 of Table 4-2 gives the measured tensile strength of the prisms. To gauge the effectiveness of the two anchors versus the control prisms and the prisms with one anchor, we normalize the measured strength of the prisms with respect to the average strength of the control prisms and prisms with one anchor as shown in columns 4 and 5 of the same table. The effectiveness of the anchors can be assessed by considering the ratios in column 4 of Table 4-2. We notice that for the fully bonded CFRP laminates, one anchor at each end increased the strength by 51 % while two anchors at each end increased it by 244% compared to the strength of the control specimens. We can see in column 5, that the two anchors increased the strength by 98% compared to prisms without anchors and the one anchor increased the strength by 23% compared to the strengthened prism without any anchor.

On the other hand, the presence of a pre-delaminated segment reduced the strength of the prism compared to the companion prisms with fully bonded CFRP strips. It may be recalled that the pre-delamination was introduced to diminish the effect of the dynamic stresses caused by the advent of the delamination process. The release of the strain energy due to delamination is rather abrupt and it is akin to an impulsive action; consequently, the process leads to stress amplification at the concrete-CFRP interface. One of the advantages of an anchor is that it disrupts the propagation of the dynamic stresses to the end of the CFRP laminate strip. Further delamination, following the initial delamination process, appears to be less gradual in the presence of anchors.

It is obvious from this discussion that the proposed anchor is effective in allowing the CFRP laminate strip to achieve its capacity. The issue that needs to be further investigated is whether it would perform as effectively if used with multiple layers of FRP in large scale beams that are strengthened with externally bonded CFRP laminate to increase their bending strength.

4.6 Behaviour of the T-section RC beams

A total of 21 RC beams externally strengthened with CFRP laminates were tested to investigate the effect of a number of parameters on their behaviour and strength. The parameters included:

1. Amount of CFRP reinforcement.
2. Number/spacing of anchors.
3. Anchors distribution along the beam length.
4. The width of the CFRP laminate.

5. The number of layers of the laminate.

In this section, load deflection curves, strain profiles along the internal reinforcement and the CFRP laminate will be presented for each of the tested beams. Shear stress distributions along the CFRP laminate will be also presented and discussed.

4.6.1 Procedure for Calculation for the Interfacial Shear Stress Based on Experimental Data

To relate the shear stresses to the measured strains, consider the free-body diagram of an infinitesimal element dx of the FRP as shown in Fig.4-64. Let us assume the FRP to have a unit width and thickness t_f. If we consider the equilibrium of the longitudinal forces acting on this element, we obtain

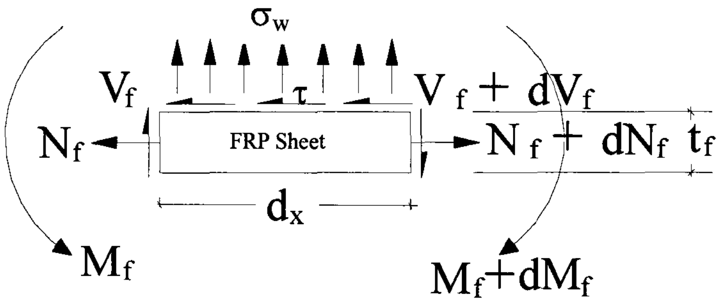

Fig.4-64: Free body diagram of an infinitesimal element of FRP

$$(N_f + dN_f) - N_f - \tau_{xz} dx = 0 \qquad \text{Eq.4-1}$$

where $N_f = \sigma t_f$ and where σ is the longitudinal stress in the laminate. Therefore,

$$\tau = t_f \frac{d\sigma}{dx} \qquad \text{Eq.4-2}$$

Since FRP is a linear elastic material

$$\sigma = E_f \varepsilon_f \qquad \text{Eq.4-3}$$

where ε_f is the longitudinal strain and E_f = the elastic modulus of the laminate. Substituting for σ from Eq.4-3 into Eq.4-2, we obtain

$$\tau = E_f t_f \frac{d\varepsilon_f}{dx} \qquad \text{Eq.4-4}$$

Notice in Eq.4-4 that the derivative term is the slope of the longitudinal strain diagram. For the purposes of the current study, the slope will be estimated by assuming a linear variation between any two consecutive measured strains on the FRP, and Eq.4-4 will be used to estimate the interfacial shear stress. Clearly, in the case of delamination, the slope of the longitudinal strain diagram would be theoretically zero because the FRP strain along any delaminated segment would be constant as long as the laminate remains attached to the concrete at the ends of the delaminated segments.

4.6.2 Control Beams

Three control beams were tested to determine the ultimate load capacity of these unstrengthened beams. Control beams CB1 and CB3 were made of the same concrete batch with a compressive strength of 54 MPa while beam CB2 was made of another batch with compressive strength of 59 MPa.

The load- midspan deflection curves of these beams are shown in Fig.4-65. The behaviours of the replicate beams CB1 and CB3 are quite similar but CB3 appear to be slightly stronger than CB1. On the other hand CB2 had the highest failure load among the three beams. The maximum load carried by CB1, CB2 and CB3 were 163.7 kN, 180.2 kN and 192.7 kN, respectively. Theoretically, the slightly higher concrete strength in CB2 is not expected to make a large difference in the ultimate capacity, but this will be explained later.

The first beam tested was the control beam CB1. The first crack occurred at a total load of 44 kN and yielding of the longitudinal reinforcement was observed at 113.6 kN. The maximum strain recorded for the steel at 126.8 kN was 0.003. One of the strain gauges showed a strain of 0.046 at failure. It is not clear why this strain gauge did not show any reading at the beginning of the load process, but later it started to show readings. The beam reached 163.7 kN when the top of the compression flange crushed and the maximum deflection reached 200 mm. After the maximum load, the load dropped suddenly to 108 kN and then it increased again until it reached 142 kN at which point the test was stopped because the stroke of the loading jack was exhausted. The maximum strain on the concrete surface was recorded to be 0.0048 at 154.5 kN. The drop in the load at 163.2 kN in Fig.4-65 is due to the crushing of the concrete in the flange of the beam.

Figure 4-66 shows this beam at failure where one can clearly see the crushed concrete flange. It is important to mention that longitudinal cracks spacing was practically coincident with the spacing of the internal stirrups.

Figure 4-67 shows typical longitudinal steel strain variation along the beam length. Notice that some of the strain values do not follow theory. The strains under the load seem much higher than at midspan even though theoretically they are supposed to be equal. The reason may be the significant local variations in strain that occur in cracked concrete structures. The measured strain over small gauge lengths is affected by the proximity of the gauge to the crack.

The second control beam tested was CB2. During the test, it was observed that the jack transducer was jammed and therefore the recorded deflection showed unusual values. Later the problem was fixed and as can be observed in Fig.4-65, it has a similar load-deflection curve as the other two beams. The beam reached a maximum load of 180.2 kN with a corresponding maximum deflection of 280 mm at which time the flange crushed. The steel strain values showed yielding at mid-span under 127 kN of load. This agrees with the load at which a noticeable change in stiffness occurred in the load-deflection curve.

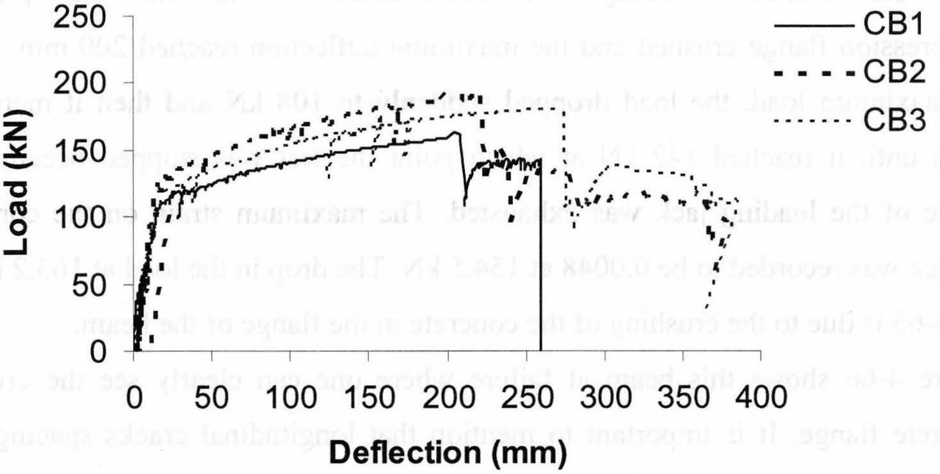

Fig.4-65: Load midspan deflection curve for the control beams

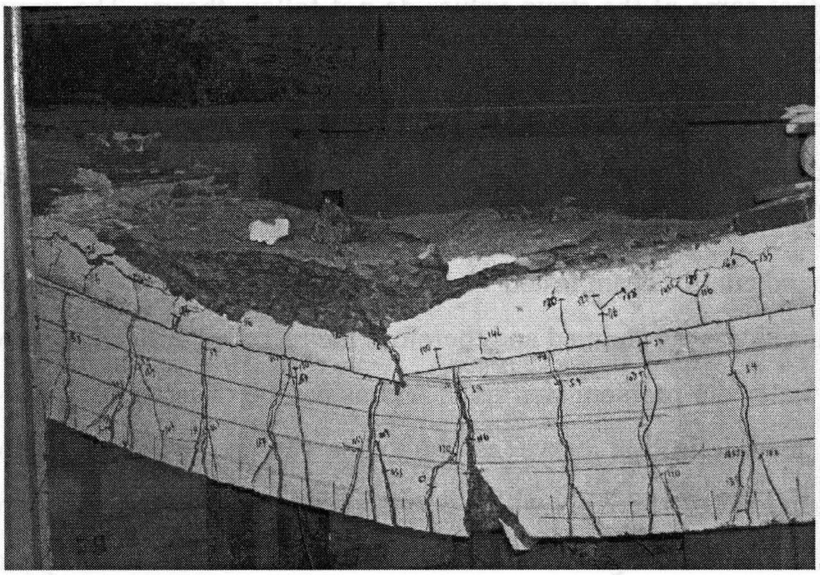

Fig.4-66: Control beam CB1 at failure

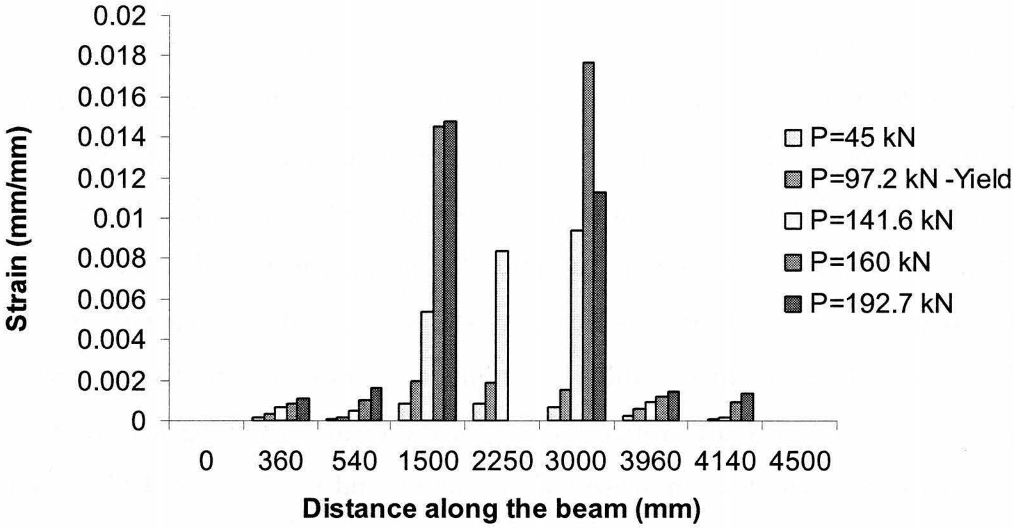

Fig.4-67: Tension steel strain variation along the beam length of the control beam CB2

Control beam CB3 was tested similarly to the previous two beams. In this case, the beam was unloaded and reloaded because the loading rate was deemed too fast. The process of loading-unloading are reflected by the load-deflection curves in Fig.4-65

This beam reached 190.6 kN at a maximum deflection of 221.72 mm. It reached a higher load compared to the companion control beam CB1. The difference in strength could be due to the higher strength of the compression flange, which may have resulted from better concrete compaction and curing. The beam reached 97.2 kN when the strain gauge attached to the internal reinforcement showed a maximum strain of 0.002. The maximum strain recorded underneath the position of the load was 0.02 at a load of 177.4 kN.

The main purpose of testing these beams was to obtain their ultimate load capacity, which can be used to gauge the effectiveness of the FRP strengthening method, with and without anchors.

4.6.3 Beams B1-F1-N and B2-F1-N

Two beams were externally strengthened with one layer of the CFRP laminate without anchors and tested. Seven strain gauges were installed on the CFRP laminate at the same longitudinal locations as the strain gauges attached to the internal reinforcement. Beam B1-F1-N was the first to be tested. In the early stages of loading, the beam was unloaded and then reloaded because the loading rate was deemed still too fast. Fig.4-68 shows the load-midspan deflection curve of this beam. The first crack appeared at 35 kN and this beam reached 130 kN when the internal reinforcement began to yield. As the load was further increased, the first sound of delamination was heard at 182 kN. This beam reached 203.5 kN when the CFRP laminate fully delaminated from the mid-span and the delamination propagated towards one end of the beam, which caused the load to drop to 140 kN. The load increased subsequently and reached 176.4 kN at which point the concrete top flange crashed. It is important to mention that the delamination observed was accompanied by the rupture of the CFRP laminate, and it appeared that both phenomena occurred concurrently.

The companion beam B2-F1-N was tested in the same manner as the previous beam. Figure 4-68 shows the load deflection curves for both beams. In the companion beam, the load reached 209 kN with a corresponding 91 mm deflection when full delamination occurred. Based on visual inspection it was noticed that the CFRP laminate partially ruptured at the same time as delamination occurred. The load thereafter dropped to 148 kN, but increased again and reached 175 kN at 210.6 mm deflection. The steel yielded when the load reached 112 kN and that the CFRP strain at this load level was 0.00255 at mid-span, which is about 15% of its ultimate rupture strain. The maximum strain recorded in the CFRP laminate at midspan was 0.0167, which is its ultimate rupture strain and that this strain supports the observed rupture of the CFRP laminate at the same time as the advent of delamination. After delamination, all the strain gauges stopped functioning and no more readings could be taken. The maximum strain recorded in the internal reinforcement was 0.01 and was measured when the CFRP delaminated. Note, the dramatic increase in deflection after full delamination. It is important to mention that in conventional reinforced concrete members, the beam experiences a noticeable increase in deflection and the difference between the yield moment and ultimate moment is 15-20%. In the case of this CFRP strengthened beam, the difference between the latter two moments is nearly 90% and a dramatic loss of stiffness occurred after delamination rather than after yielding. Thus, the FRP contributed to both the stiffness and strength of the beam. The delamination started from mid-span and propagated to the roller side. The moment curvature curves for the mid-span and the section underneath the loading was determined using the strain gauges installed on the concrete, the internal reinforcement and the CFRP laminate at these locations.

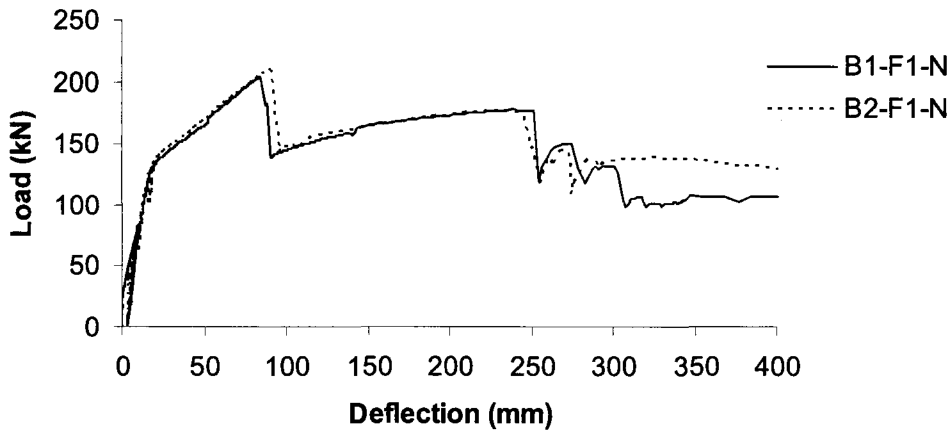

Fig.4-68: Load midspan deflection for beams strengthened with one CFRP laminate

The strain variations along the CFRP laminate length are shown in Figs.4-69 and 4-70 for beams B1-F1-N and B2-F1-N, respectively. As can be seen from those figures, the strain in the CFRP laminate reached the rupture strain of 1.67% and the strain in the steel at the same time was almost 1.2%. The strain in the steel is smaller than in the CFRP because it is located closer to the neutral axis. The strain measurements along the beam height were used to calculate the curvature of the cross section at 2250 mm from the left support, and the moment curvature diagram for a typical beam is plotted in Fig.4-71. Observe that the moment curvature relations are approximately trilinear. This response is quite interesting because theoretically the last segment of this trilinear relationship is unexpected.

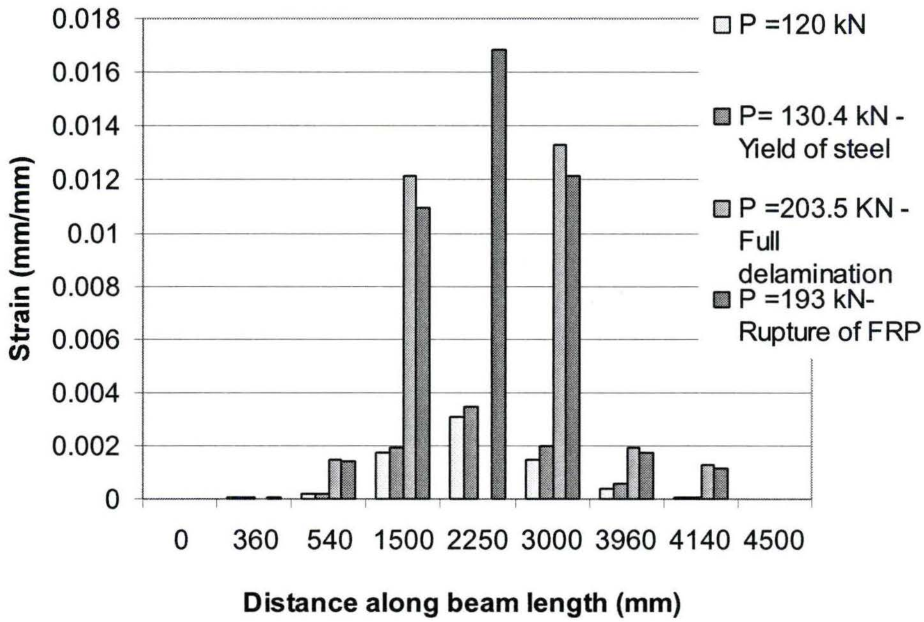

Fig.4-69: CFRP strain variation along the length of beam B1-F1-N

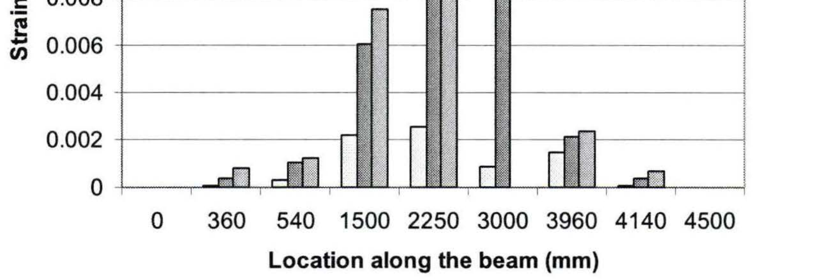

Fig.4-70: CFRP strain variation along the length of beam B2-F1-N

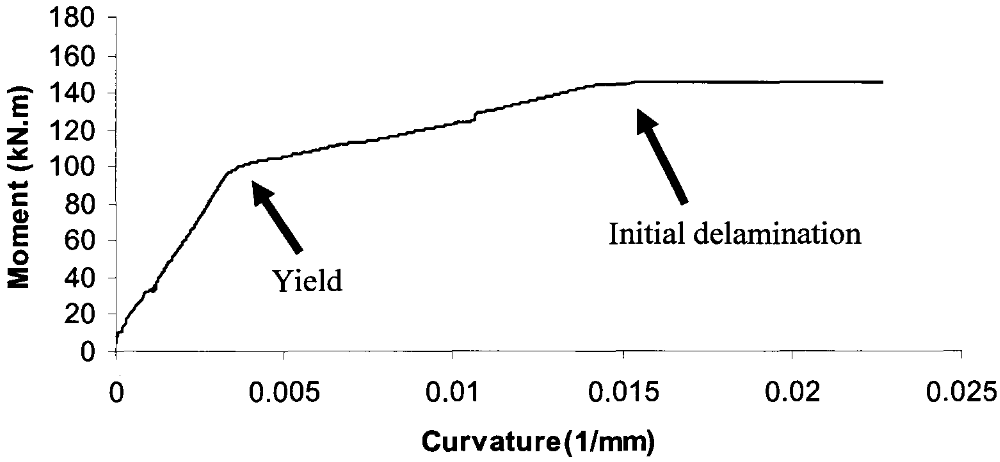

Fig.4-71: Moment curvature of beam B1-F1-N

The shear stress variation along the CFRP laminate for beam B1-F1-N is shown in Fig.4-72 where the maximum shear stress reached was 0.44 MPa. The plotted shear stresses do not follow the shear force diagram, but they drop to zero at mid-span as expected. The shear stress distribution seems more uniform near the failure load since the delamination gradually spread, from the mid-span towards the ends.

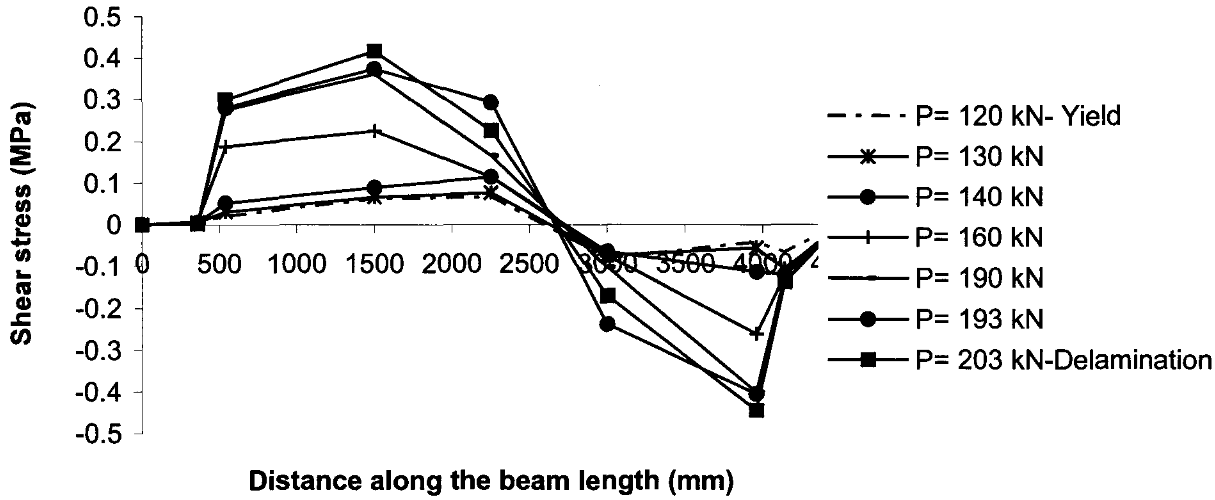

Fig.4-72: Shear stress distribution along the CFRP laminates in beam B1-F1-N

The shear stress profile along the CFRP laminate for beam B2-F1-N is shown in Fig.4-73, where the maximum shear stress is 0.86 MPa. The plotted shear stress shows peaks at the location of the loading points. In this case, the shear stress distribution is even further from the shear force distribution along the span based on simple theory. The reason is that the shear stress distribution at the FRP-concrete interface is dependent on the level of the load and the size and spacing of the flexural cracks, which is difficult to predict. To a large extent the variability of crack spacing, leads to different delamination loads in nominally identical beams. Figure 4-74 shows the failure mode of beam B2-F1-N.

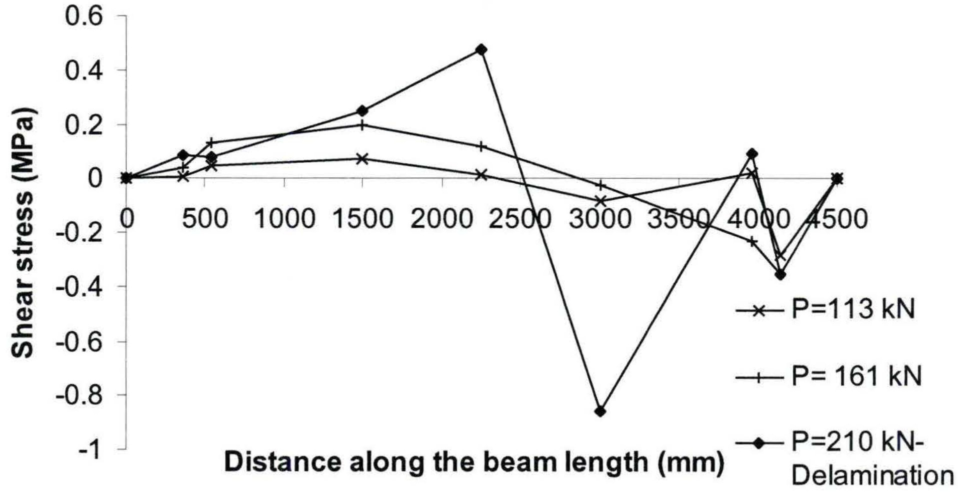

Fig.4-73: Shear stress distributions along the CFRP laminate for beam B2-F1-N

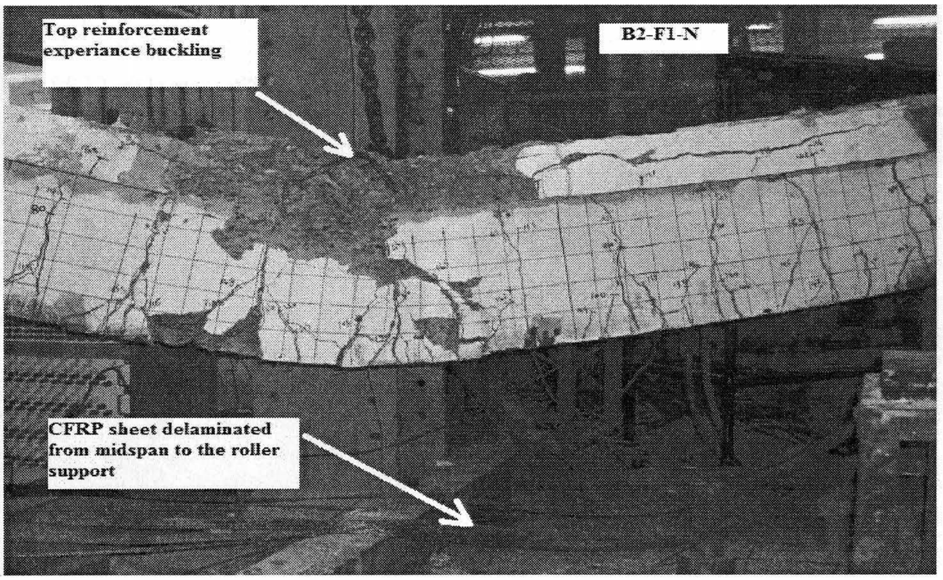

Fig.4-74: Beam B2-F1-N after delamination

4.6.4 Beams B1-F1-E3 and B2-F1-E3

Beam B1-F1-E3 is the first beam containing the developed anchors that was tested. It was strengthened with one layer of a 220 mm wide CFRP strip. Only three anchors were used at each end, with the anchor spacing being 100 mm and with a 75 mm distance from the end of the CFRP laminate to the center line of the first anchor. This beam was tested in 4 point bending similar to the previous beams. This beam reached almost 200 kN when the laminate ruptured. The strain recorded at the time of delamination / rupture was 1.67%, which is the rupture strain reported by the manufacture. The corresponding maximum steel strain was 0.011. Figure 4-75 shows the ruptured CFRP laminate.

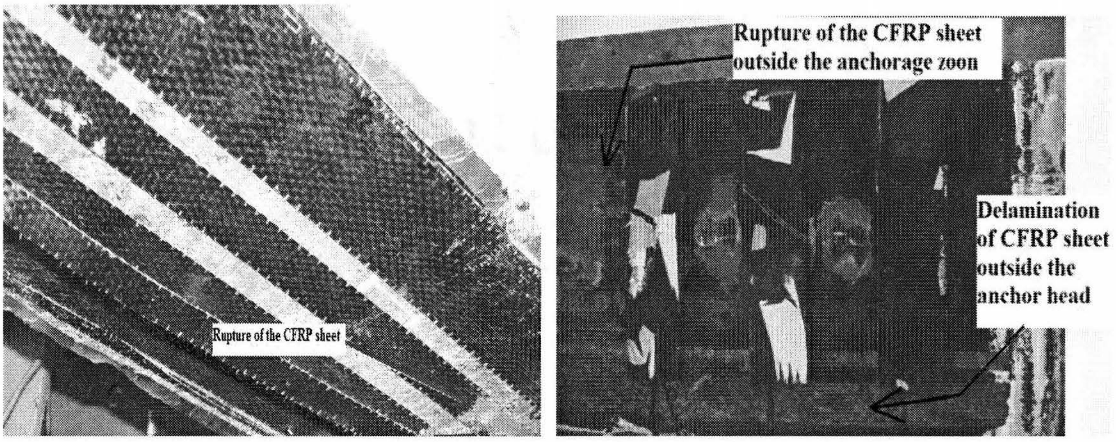

Fig.4-75: Rupture of CFRP laminate in beam B1-F1-E3

It is important to mention that the CFRP laminate outside the anchor head delaminated earlier and was not effective, thus only the part covered by the anchor was effective until rupture. Beam B2-F1-E3 is the companion to beam B1-F1-E3 and was tested similarly. This beam reached 198.2 kN when the CFRP laminate ruptured, and the strain recorded was the rupture strain of the laminate as reported by the manufacturer. The internal reinforcement strain under the same load reached a maximum value of 0.013, which is very close to the strain under the maximum load recorded in the previous beam. This beam reached a maximum deflection of 92 mm under the maximum load compared to 114 mm observed in beam B1-F1-E3. The drop in the load after the rupture of the CFRP laminate was 37 kN, Fig.4-76, compared to the 62 kN observed in the companion beam.

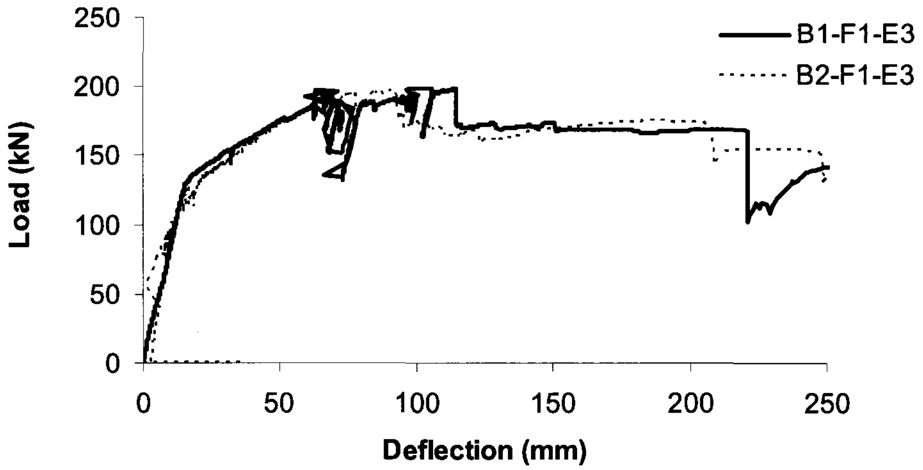

Fig.4-76: Load midspan deflection curves of beams B1-F1-E3 and B2-F1-E3

The strain profiles at different load levels along the CFRP laminate for the two beams are plotted in Figs.4-77 and 4-78. It can be observed that the anchors did not affect the behaviour of these beams since they both reached the rupture of the CFRP laminate. The strain profile along the CFRP laminate for beam B2-F1-E3 is practically symmetric, with the highest strain at midspan equal to 0.0153, which is 91.6% of its specified rupture strain. Since the strain gauges generally peel-off when rupture strain is approached, it is likely that the actual strain at rupture was at least equal to the manufacturer's specified rupture strain. Using the recorded concrete and steel strains for the beam in Fig.4-79, its moment-curvature diagram is plotted for the section underneath the load located at 1500 mm from the left support. The diagram exhibits the typical features of reinforced concrete flexural members with the slope of the various segments being coincident with the uncracked, cracked- unyielded, yielded, ultimate (FRP rupture) and post-ultimate states. These segments can be idealized by straight lines for practical purposes.

The shear stress variation along the CFRP laminate for beam B1-F1-E3 is shown in Fig.4-80, which indicates a maximum shear stress of 1.90 MPa. The shear stress distribution along the CFRP laminate for the companion beam B2-F1-E3 is shown in Fig.4-81. The maximum shear stress in this case was calculated to be only 0.40

MPa. This is a rather small shear stress but it is only based on the recorded strain values. The maximum shear could have occurred elsewhere along the laminate where there were no strain gauges present. Consequently, it can not be assumed that the shear stress variation in Fig.4-81 captures the actual variation of stresses.

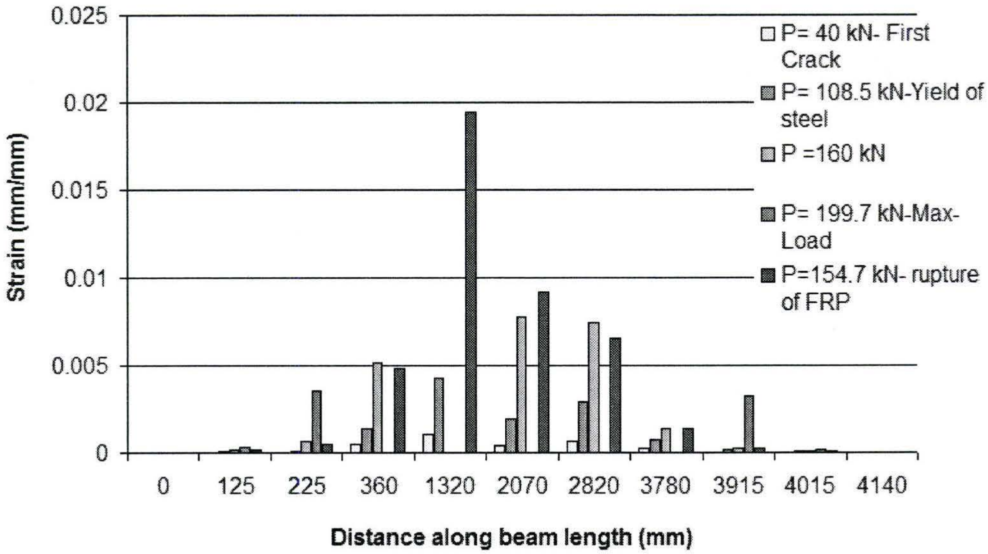

Fig.4-77: CFRP strain profile along the beam length for beam B1-F1-E3

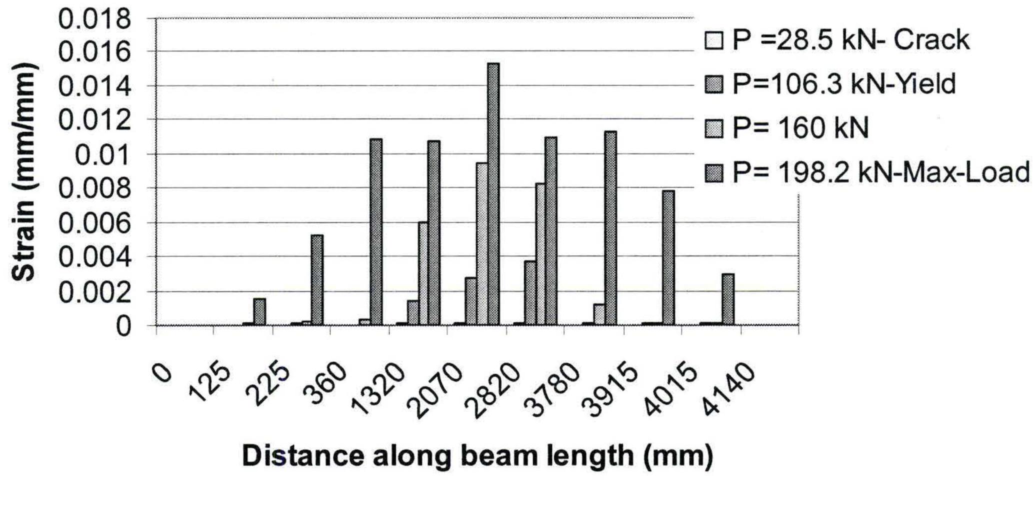

Fig.4-78: CFRP strain variation along the length of beam B2-F1-E3

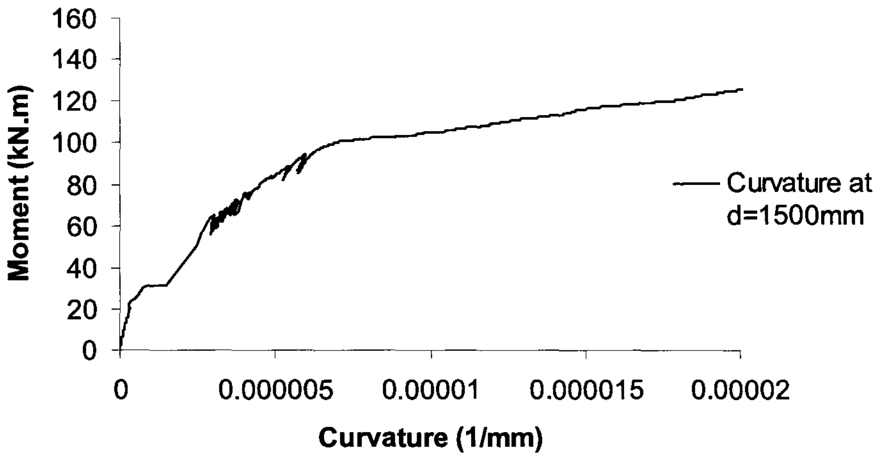

Fig.4-79: Moment curvature of beam B2-F1-E3

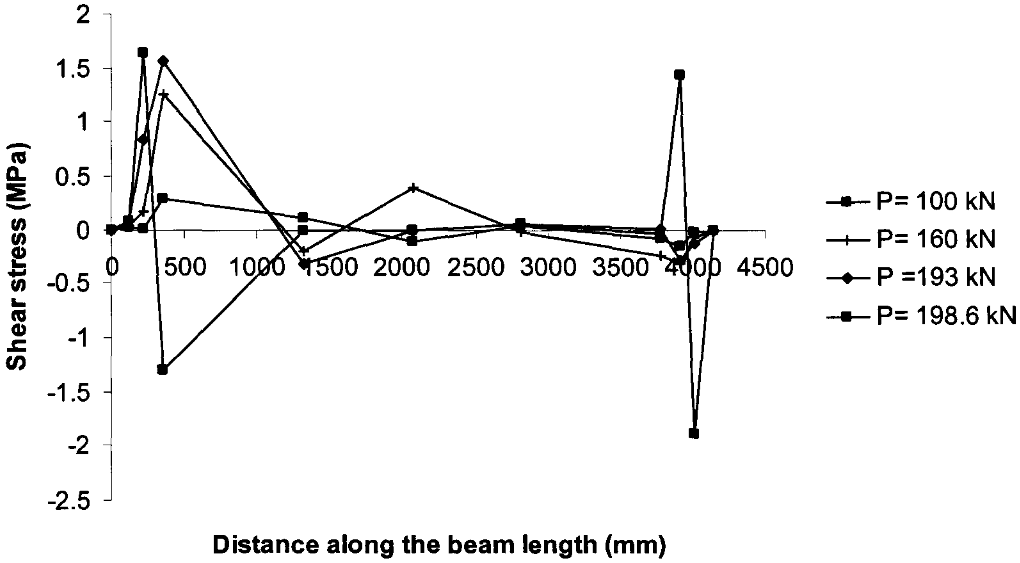

Fig.4-80: Shear stress distribution along the CFRP laminate for beam B1-F1-E3

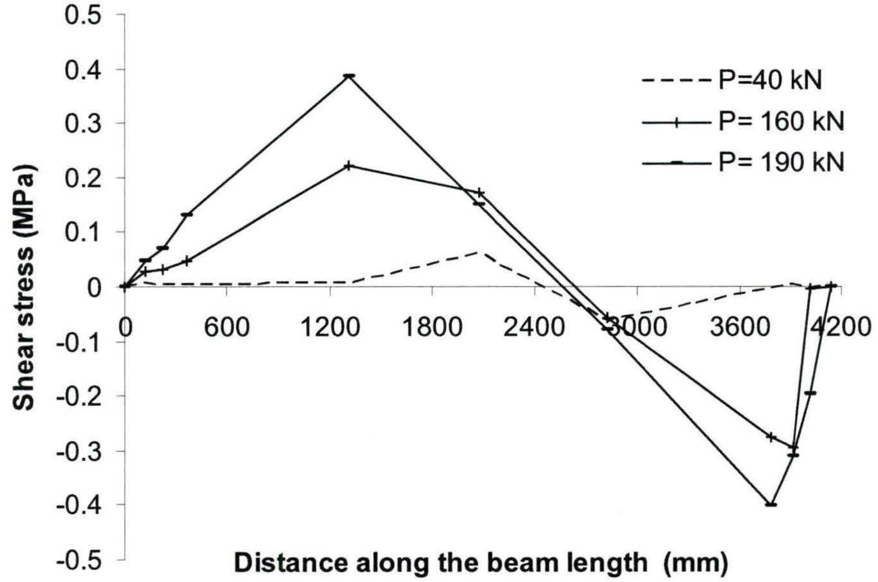

Fig.4-81: Shear stress distribution along the CFRP laminate of beam B2-F1-E3

4.6.5 Beams B1-F2-N and B2-F2-N

B1-F2-N is the first beam to be tested with two layers of CFRP laminate. Each layer was 220 mm wide and 0.165 mm thick. The beam reached 230.1 kN just before delamination as can be observed in its load-midspan deflection curve in Fig.4-82. The maximum strain in the CFRP laminate was recorded to be 0.014, which is 84% of its specified rupture strain, with the corresponding internal reinforcement maximum strain being 0.0069. As can be seen in Fig.4-82, after the delamination the load dropped significantly from 230.1 kN to 121 kN and thereafter the behaviour followed that of the unretrofitted RC beam. The post-delamination load increased due to the shift in the neutral axis and possible strain hardening in the steel rebars. It is interesting to observe that the maximum load reached after delamination nearly equals the load before delamination.

Beam B2-F2-N is the companion beam to beam B1-F2-N. This beam reached only 205.4 kN when the laminate delaminated as shown in Fig.4-83. The load dropped after delamination to 124 kN, but subsequently increased and reached 170.1 kN when the top concrete crushed similar to the previous beam. The maximum recorded steel strain was 0.0065 at delamination, which is in agreement with that in the companion beam. However, in this beam the maximum strain in the CFRP laminate was recorded to be only 0.01, which is 60% of its rupture strain. This strain is significantly less than the maximum CFRP strain of 0.014 recorded in its companion beam. The reason may be due to the difference in the quality of the interface between the FRP and concrete in the two beams. Although efforts were made to maintain uniform quality among the tested beams, it is not possible to check the actual quality using non-destructive techniques. This is one of the dilemnas of this technology, both in the laboratory and in the field. Such variations can be used to justify the need for anchoring the laminates, which is expected to reduce the degree of variability among the strength of nominally identical beams.

Figures 4-83 and 4-84 show the strain variations along the CFRP laminate for the two beams. The strain profile for both beams exhibit practically the same behaviour, the strain is maximum at midspan; accordingly, one expects delamination to initiate at midspan.

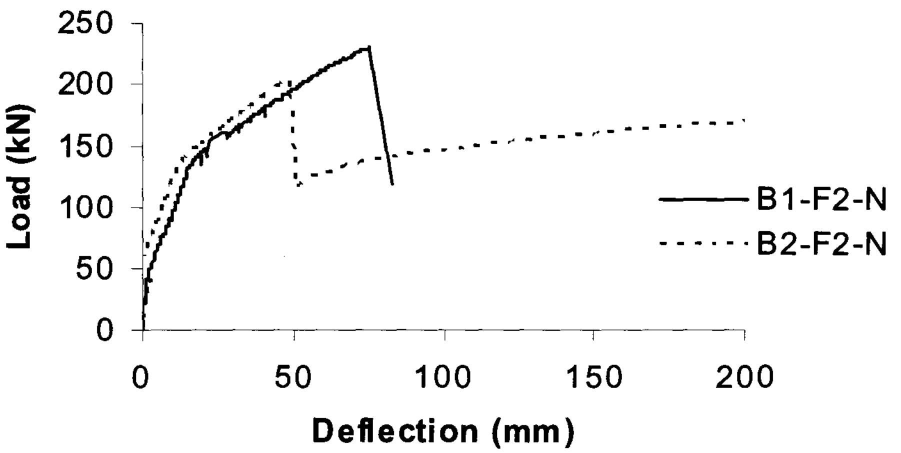

Fig.4-82: Load midspan deflection curves of beams B1-F1-E3 and B2-F1-E3

It is important to mention that the steel strain values in the vicinity of the applied point loads are much higher than at midspan, despite the fact that the moments in the two regions are practically equal. A possible explanation for this behaviour can be the manner in which so-called tension-stiffening (tension carried by concrete between two cracked sections) affects the external CFRP reinforcement versus the internal steel reinforcement. It appears that the CFRP does not benefit from tension stiffening while the steel reinforcement does. This raises the possibility that the tensile stresses in the concrete between two cracked sections follows a more complex distribution along the beam height than the commonly accepted linear distribution. A plausible explanation may be the change in stress caused by presence of the epoxy layer between the FRP and the concrete surface. Assuming continuity of strain at the interface, due to the lower elastic modules of the epoxy than the concrete, the tensile stress contribution of the epoxy may be less than that of the concrete, consequently, the FRP does not benefit from tension-stiffening.

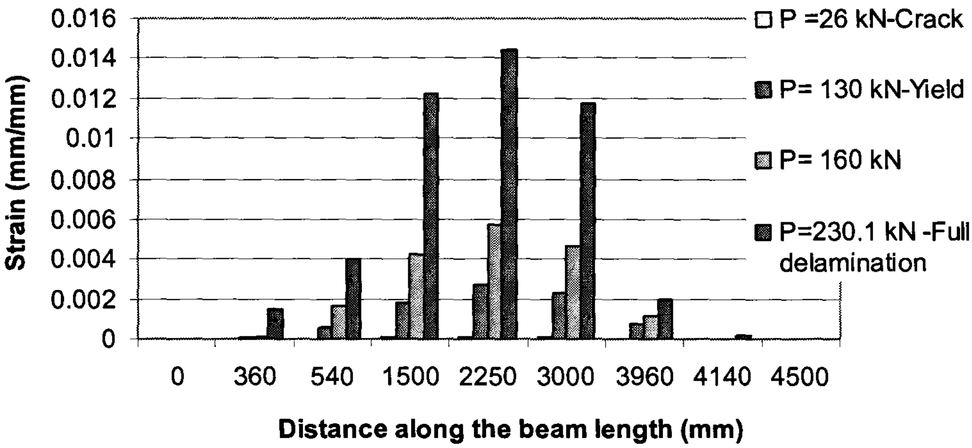

Fig.4-8623: CFRP strain variation along the length of beam B1-F2-N

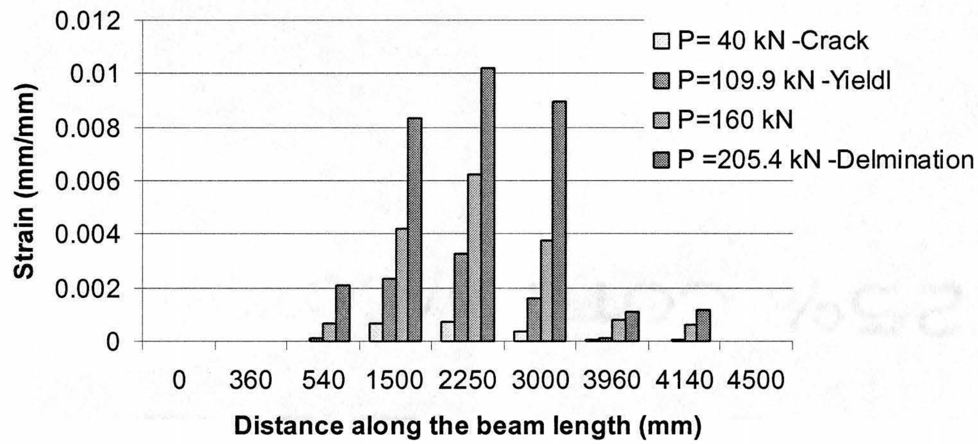

Fig.4-84: CFRP strain variation along the length of beam B2-F2-N

In the test it was obvious that delamination initiated at midspan and then propagated towards one of the supports in beam B1-F2-N (see Fig. 4-85), whereas in the companion beam B2-F2-N, the concrete cover was pulled out in the midspan zone as shown in Fig.4-86.

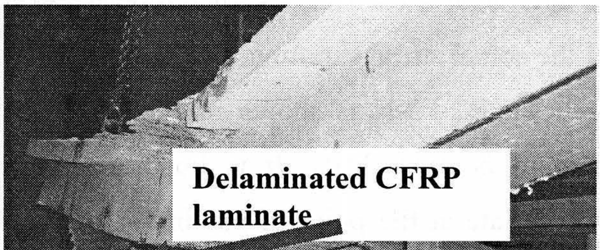

Fig.4-85: Beam B1-F2-N after delamination

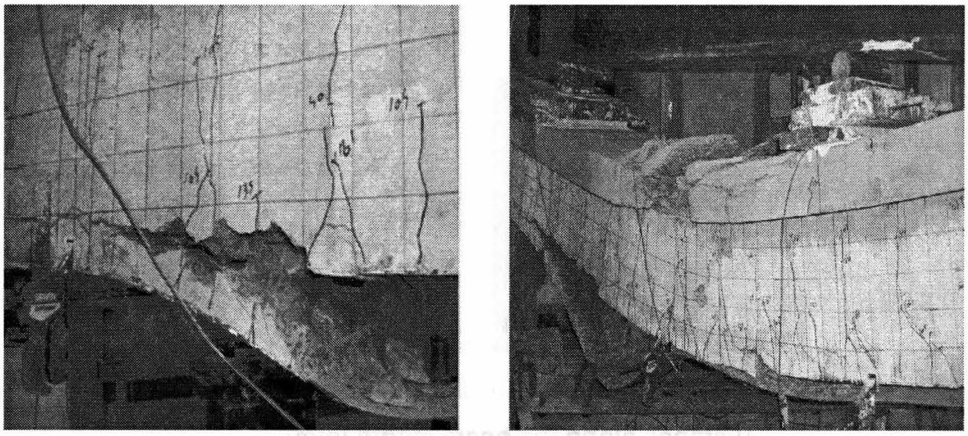

Fig.4-86: Beam B2-F2-N after delamination

The shear stress variation along the CFRP laminate for beam B1-F2-N is shown in Fig.4-87. The maximum shear stress reached was calculated to be 1.1 MPa. The plotted shear stress follows the shear force diagram from the roller side, however the hinge side shows the peak shear stress near the laminate end. It must be emphasized that the preceding diagram cannot provide the many local perturbations of the interfacial shear stresses; therefore, it can only be used as an average indicator of the actual stress variation. The shear stress variation along the CFRP laminate for beam B2-F2-N is shown in Fig.4-88. The maximum shear stress was calculated to be 0.88 MPa. It is important to point out that the delamination did not initiate at the point of maximum interfacial shear stress in Fig.4-89. This is also true in the case of the previous beams. The a reason may be the presence of the peeling stresses at the interface, which have rather complex distribution and which vary from tension to compression along the interface.

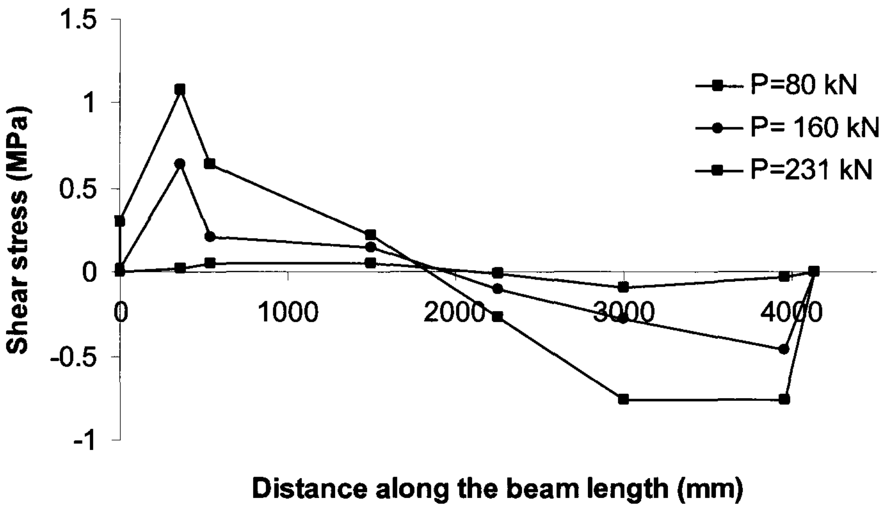

Fig.4-87: Shear stress distribution along beam B1-F2-N

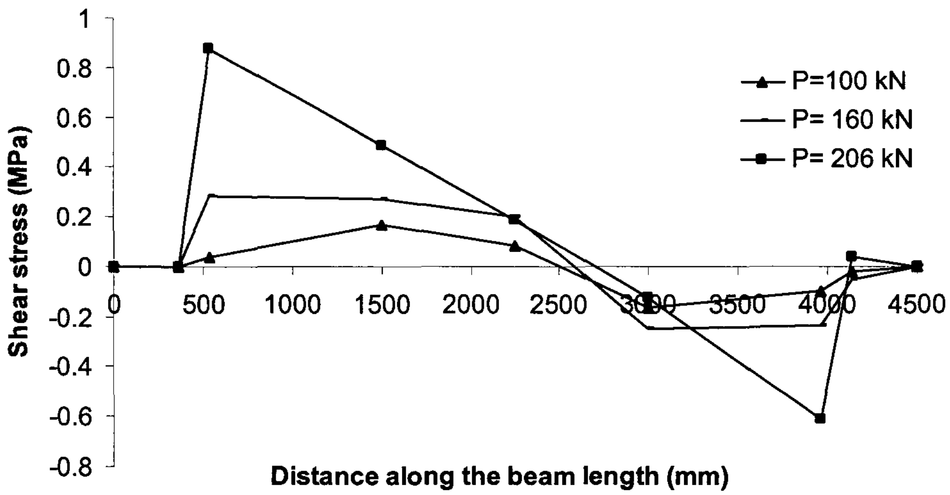

Fig.4-88: Shear stress distribution along beam B2-F2-N

4.6.6 Beams B1-F2-E3 and B2-F2-E3

Beam B1-F2-E3 is the first beam to be tested with three anchors at each end, with the anchors spaced at 100 mm evenly. The beam had two layers of the CFRP laminate similar to the previous two beams. Delamination occurred at 224.5 kN, which is less than the maximum load reached in one of the two beams with the same number of CFRP layers but without anchors. Clearly, the end anchors were not able to prevent delamination. However, theoretically the anchors should be able to hold the laminate strips at their ends and to allow them to reach their rupture strain as unbonded external reinforcement. While this occurred to a small extent, as manifested by the first small increase in the load after delamination, the anchors were not able to provide the necessary anchorage for achieving the full strength of the laminate. Another reason for the failure to achieve a higher load may be the fact that the holes made in the laminate to allow the anchor legs to pass through reduced the effective area of the FRP by at least 10% and since after delamination the tension in the FRP is expected to be uniform along its length, the smaller FRP section at the anchor location would not have the strength to resist the required tension force for a higher load. Another phenomenon that may have contributed to the inability of the laminate to carry higher load after delamination is the fact that the portion of the laminate cross-section that lied outside the anchor plate completely separated from the concrete upon delamination. Hence, only the part of the laminate cross-section that was under the laminate plate, with its reduced area due to the presence of the holes, resisted tension. These two effects represent a significant reduction in the laminate cross-section; therefore, the maximum recorded strain in the laminate may not represent the actual maximum strain experienced by the laminate.

Beam B2-F2-E3 is a replicate of beam B1-F2-E3, and is nominally identical to it and it failed at 216.7 kN. The load midspan deflections for both beams are plotted in Fig.4-89. It is important to mention that in this beam the anchor plates (heads) also delaminated and the laminate was able to slip. In fact, the laminate was bearing against the anchor legs. But due to the small thickness of the laminate, its bearing strength is not expected to be high. However, if we carefully examine the load deflection curve, we observe that after initial delamination, despite the laminate slip, it continued to make some contribution to the moment resistance of the beam because the maximum load reached 183 kN before the second drop in the load, which is 89% higher than that in its companion beam without end anchors.

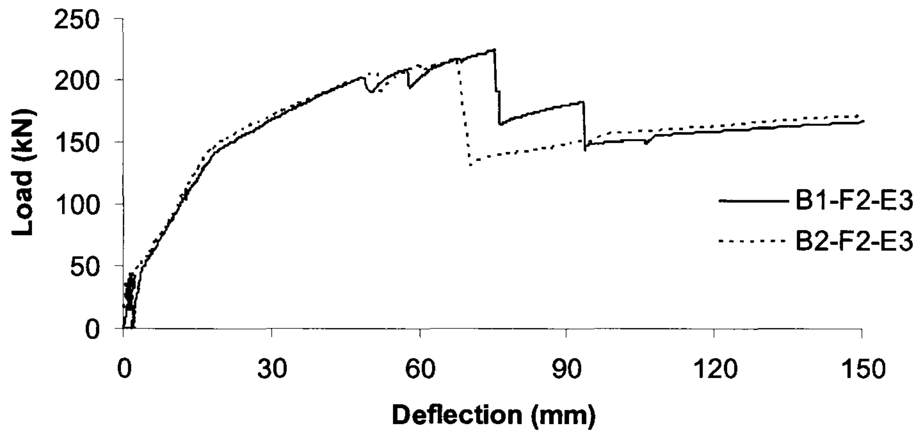

Fig.4-89: Load midspan deflection curves of beams B1-F2-E3 and B2-F2-E3

The CFRP strain variations along the beam length for the two beams are shown in Fig.4-90 and 4-91, respectively. Notice the nearly equal values of strain over a large part of the middle portion of the beam. This clearly indicates the strain distribution in an unbonded reinforcement anchored at the ends. The maximum strain at one end reached approximately 0.012, which imposes very high shear demand on the anchorage zone. This shear must rapidly build up from a value of zero at the free end of the inner most anchors, causing a peak shear stress significantly higher than the average shear stress which may not allow the three anchors to equally resist the tension in the CFRP.

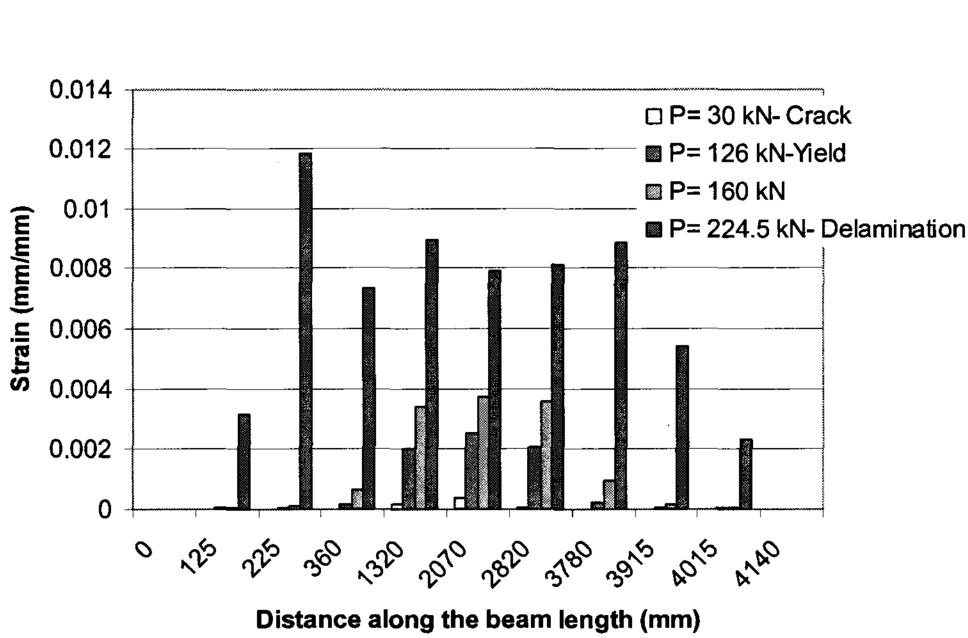

Fig.4-90: CFRP strain variation along the length of beam B1-F2-E3

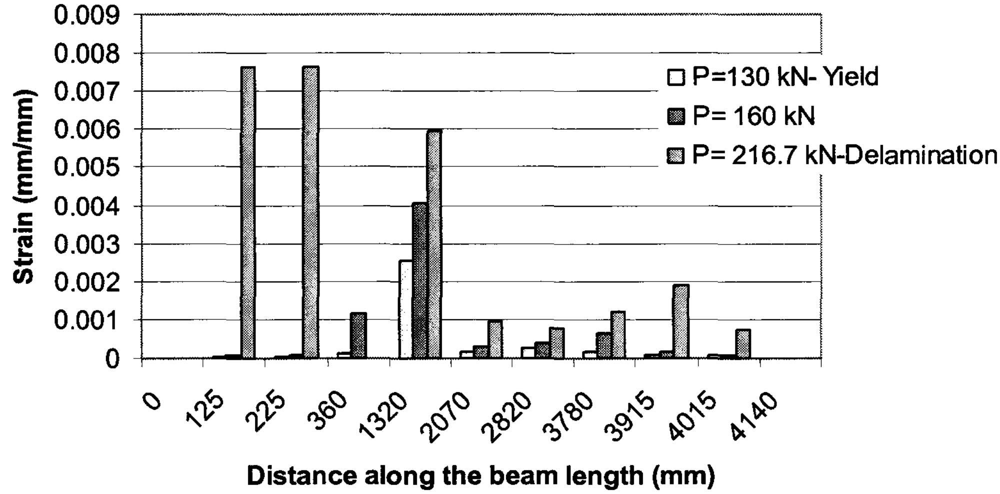

Fig.4-91: CFRP strain variation along the length of beam B2-F2-E3

Most of the strain gauges malfunctioned for beam B2-F2-E3 and the one underneath the load. Due to the failure of the strain gauges, it is difficult to draw definite conclusions from the strain data. Accordingly, the shear stresses will not be plotted for this beam. Figure 4-92 shows the failure of beam B1-F2-E3.

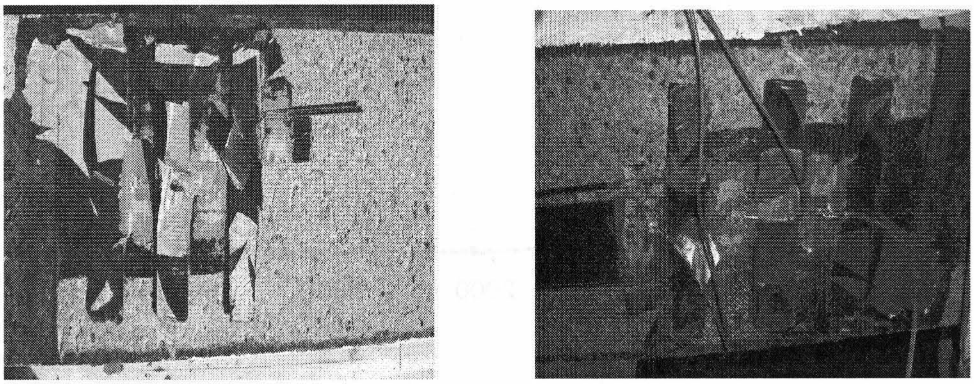

Fig.4-92: Rupture of the CFRP laminate at the anchorage zone for beam B1-F2-E3

In beam B2-F2-E3, one of the anchors ruptured at the junction of the anchor plate and the anchor rod, causing the laminate to slip and the shear stress to increase in the other two anchors and leading to their rupture as shown in Figure 4-93 (a), (b) and (c).

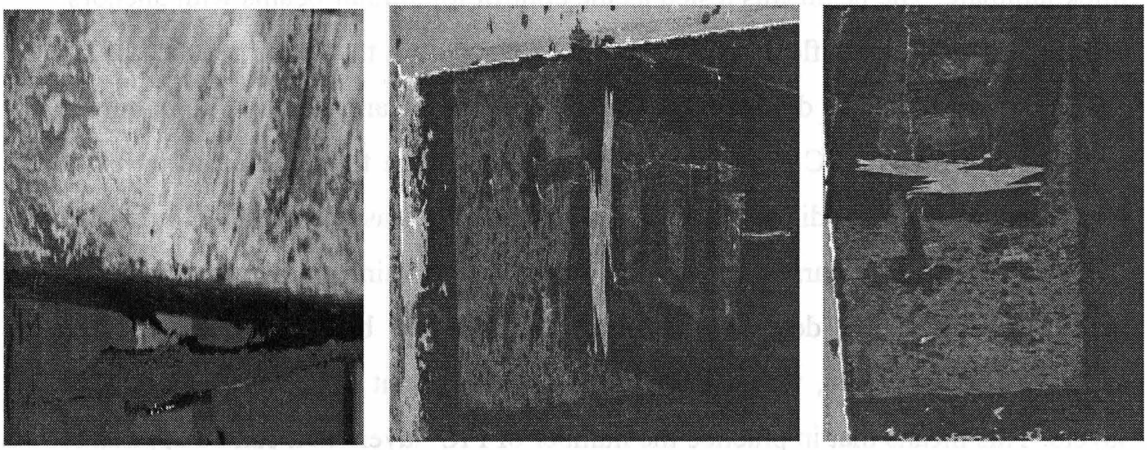

(a) (b) (c)

Fig.4-93: Failure of the anchor in beam B2-F2-E3

The calculated shear stress variation along the CFRP laminate for beam B1-F2-E3 is shown in Fig.4-94. The maximum shear stress was 6.9 MPa. This is a rather high shear stress, which corroborates the earlier statement made regarding the high shear demand in the anchorage zone and the fact that the peak shear occurs in the vicinity of the middle anchor and the laminate end.

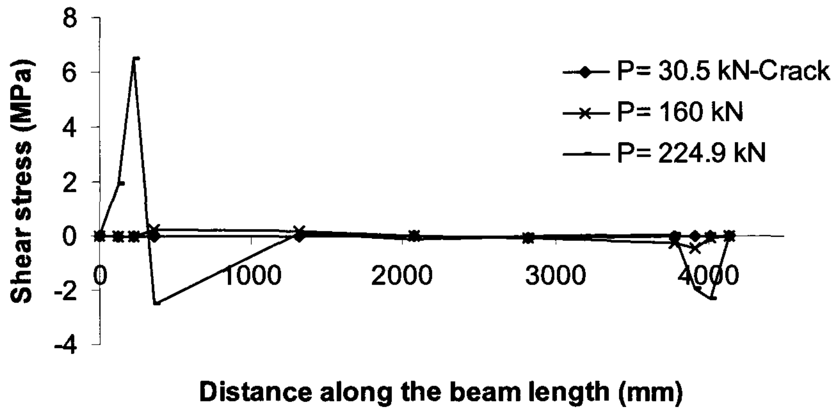

Fig.4-94: Shear stress distribution along the CFRP laminate of beam B1-F2-E3

4.6.7 Beams B1-F4-N and B2-F4-N

This beam is the first to be tested with 4 layers of 220 mm wide and 0.165 mm thick laminate. The beam was tested as the control for similar beams with anchors. As the load midspan deflection curve on Fig.4-95 shows, this beam reached 252.7 kN and then the load dropped to 116 kN due to delamination. Thereafter, it reverted to a regular RC beam until failure. Notice that the addition of an extra two layers of laminate did not lead to a significant increase in the maximum load that this beam could carry compared to the beam containing only two layers of laminate because the delamination load is controlled by the strength of the laminate-FRP interface, which is practically independent of the number of FRP layers. This means that in practice the number of FRP layers that can be applied to a beam is limited by the strength of the concrete-FRP interface, and unless special measures are taken to enhance the interface resistance, the degree to which one can increase the strength of an RC beam via external bonding of FRP laminates is limited. Beam B2-F4-N is a replicate of the previous beam and was similarly tested. The load-midspan deflection curve of the beam is shown in Fig.4-95, which indicates that it reached 213 kN just before delamination. As observed earlier, due to the lack of anchors, the laminate completely separated from the concrete and the beam reverted to a regular RC beam.

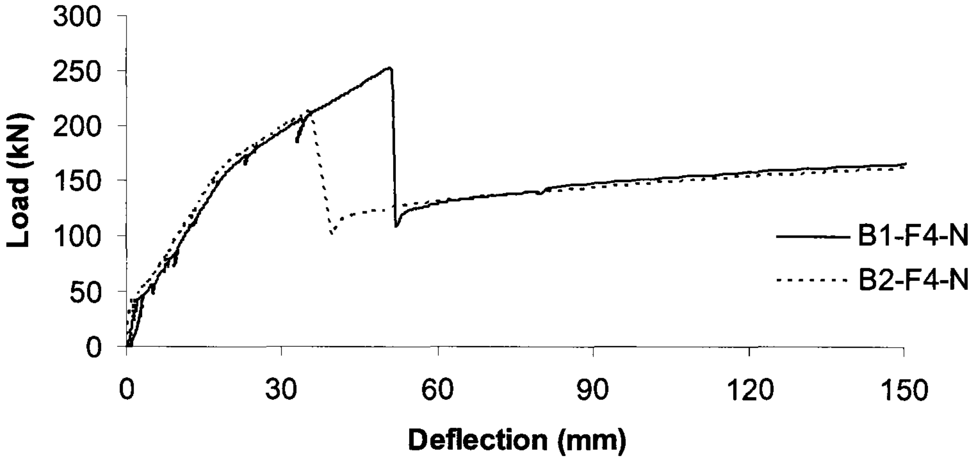

Fig.4-95: Load midspan deflection curves of beams B1-F4-N and B2-F4-N

Strain variations along the CFRP laminate for both beams are shown in Figs.4-96 and 4-97. The maximum strain recorded in the steel for beam B1-F4-N was 0.005 at the maximum load and it reached 0.0083 at failure. On the other hand, at delamination the strain in the CFRP laminate was 0.009, which is only 54% of its rupture strain. Once delamination occurred, the strain gauges no longer functioned and therefore no reading could be recorded. Notice that the strain distribution in Fig.4-97 is typical of that of a bonded reinforcement and follows essentially the moment diagram. The higher strain values at midspan may be due to the proximity of the strain gauges to a crack. Many of the strain gauges malfunctioned in beam B2-F4-N so the strain could be captured only at certain locations. The maximum strain reached before delamination was 0.005, which is only 30% of the expected rupture strain of the laminate. This level of strain may seem rather low but is not unexpected because it is approximately equal to half of the maximum strain in beam B2-F2-N at delamination. Since the latter beam had only two layers of laminate versus the four layers in the current beam and since FRP is a linear elastic material, the total force in the laminate layers at delamination in the two beams are nearly equal. Thus, it is quite obvious that the strength of the FRP-concrete interface limits the level of increase in the moment capacity of a beam that can be achieved through external bonding of FRP laminate.

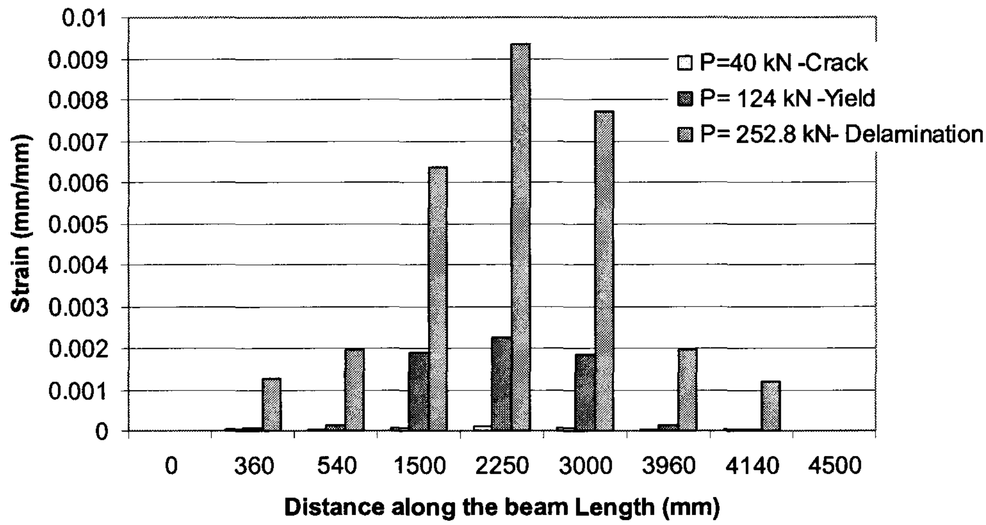

Fig.4-96: CFRP strain variation along beam B1-F4-N

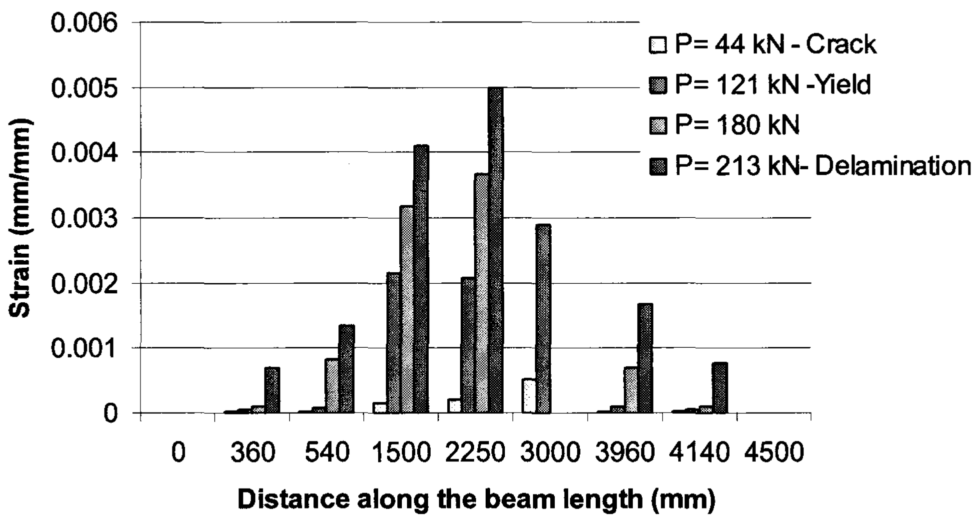

Fig.4-97: CFRP strain variation along the length of beam B2-F4-N

The failure of this beam can be seen in Figure 4-98 which shows the delaminated CFRP laminate. Notice that the concrete cover at mid-span separated in this case.

This is one of the failure modes often observed in beams retrofitted with many layers of FRP. The ultimate failure of beam B2-F4-N is shown in Fig.4-99, where one can clearly observe the delaminated CFRP strip.

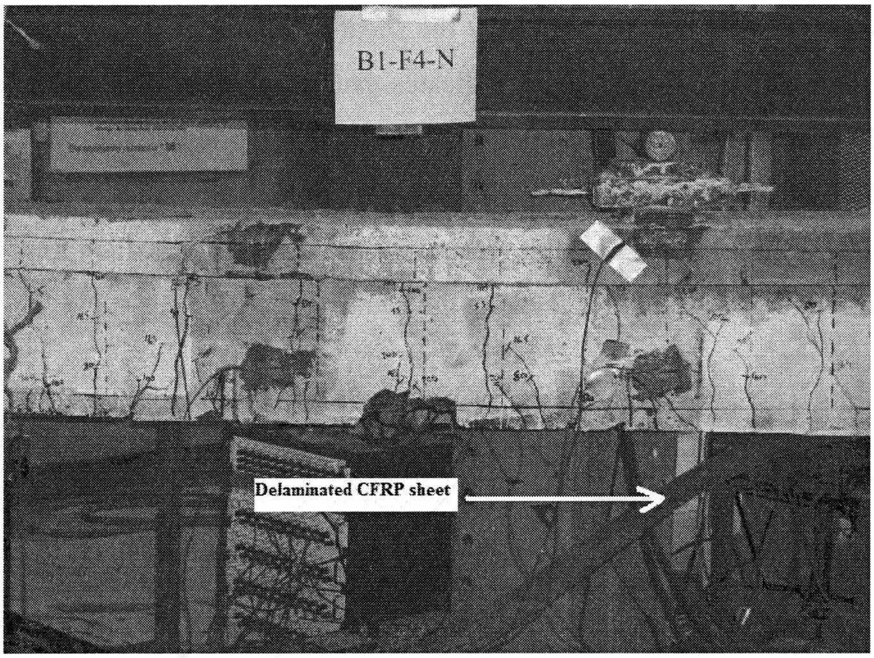

Fig.4-98: Failure of the anchor in beam B1-F4-N

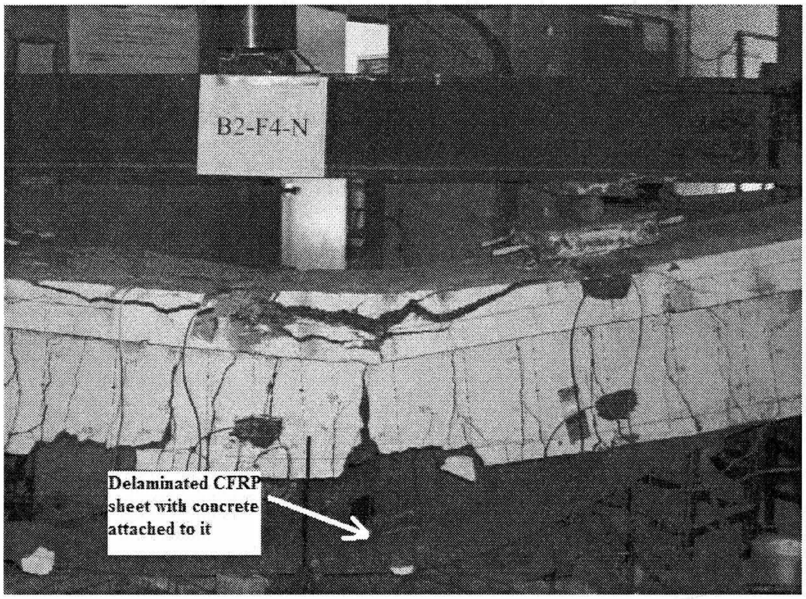

Fig.4-99: Failure of the anchor in beam B2-F4-N

The shear stress variation along the CFRP interface is shown in Fig.4-100. The maximum shear stress was calculated to be 0.89 MPa before delamination. The plotted shear stresses follow essentially the shear force diagram. The shear stress shows a more uniform stress, which indicates that before delamination, it acted as a typical composite beam. The computed shear stresses along the interface for beam B2-F4-N are plotted in Fig.4-101, where the maximum stress is shown to be 1.1 MPa. The shear stresses exhibit rather unusual distribution which may be due to the formation of flexural cracks along the beam.

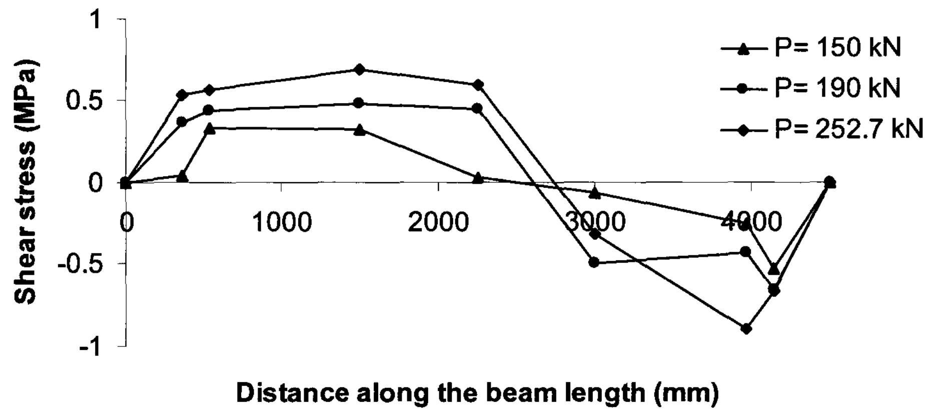

Fig.4-100: Shear stress distribution along beam B1-F4-N

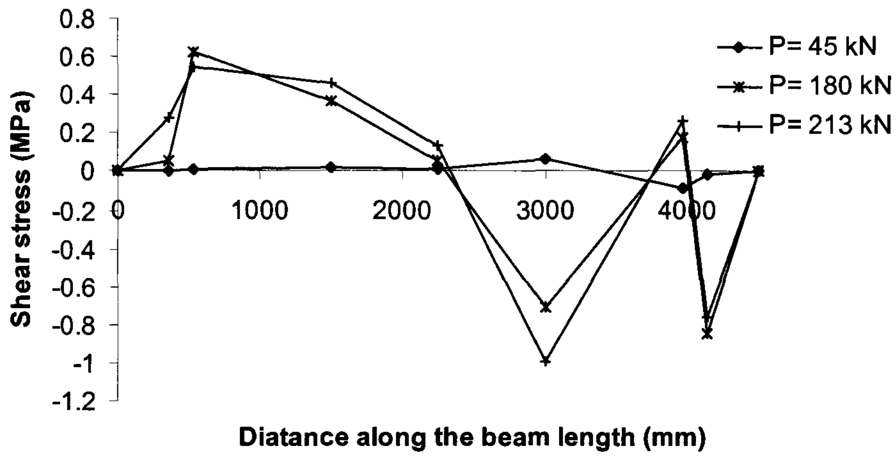

Fig.4-101: Shear stress distribution along beam B2-F4-N

4.6.8 Beam B1-F4-E3

This beam had 4 layers of CFRP laminate and 3 anchors at each end with 100 mm spacing. The load reached 256.5 kN when delamination occurred as can be seen in the load-midspan deflection curve in Fig.4-102. After delamination, the load immediately dropped to 116.5 kN and it appears that the beam reverted to a regular RC beam. In this case the delamination initiated at mid-span with a large piece of concrete being pulled off the bottom of the beam while still attached to the laminate. The recorded strains in the CFRP laminate are plotted in Fig.4-103. It can be observed that the maximum in the CFRP reached almost 0.01, which is slightly higher than the maximum strain in the companion beam without end anchors. The maximum strain in the internal steel reinforcement was 0.006 at delamination. It is obvious that three end anchors were insufficient for providing the laminate with adequate anchorage to continue resisting the applied loads after delamination.

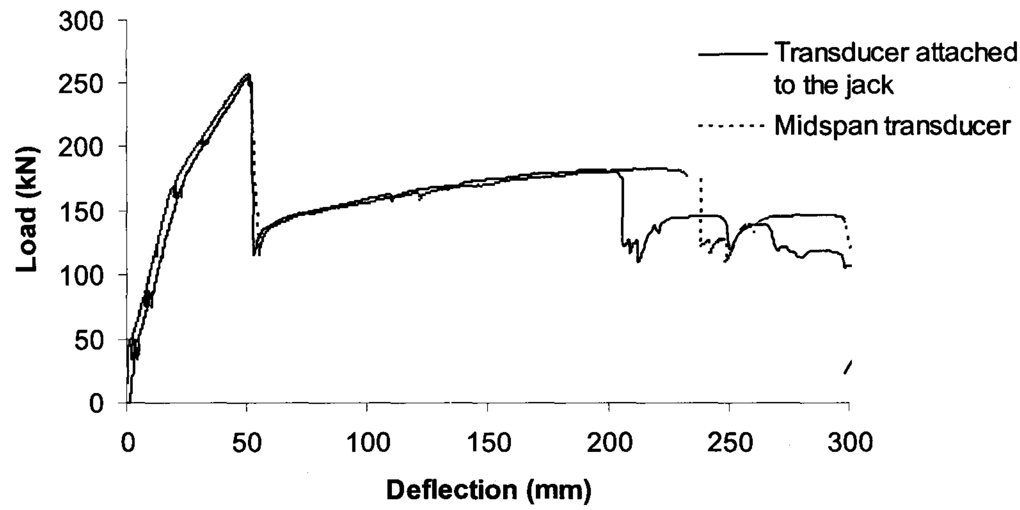

Fig.4-102: Load deflection curve of beam B1-F4-E3

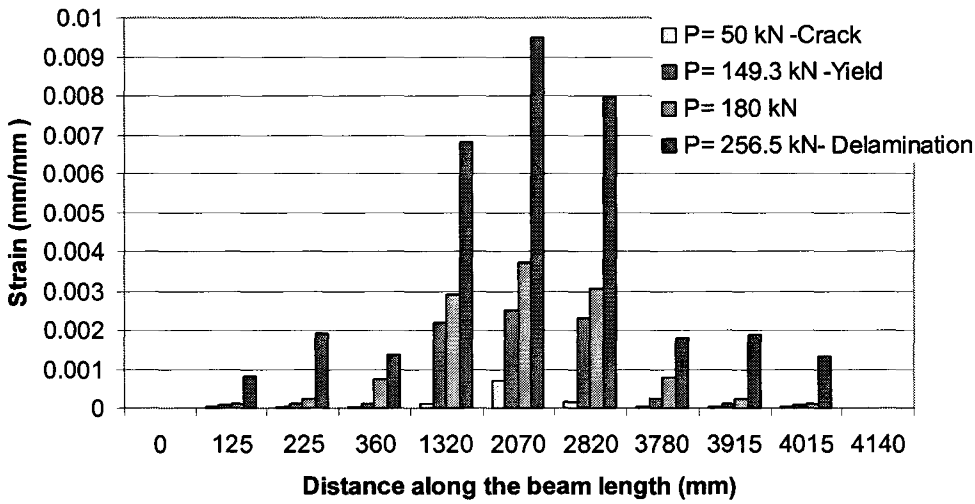

Fig.4-103: CFRP strain variation along the length of beam B1-F4-E3

As stated earlier, it was observed that upon delamination the concrete cover had separated at mid-span as can be seen in Fig.4-104; thereafter, the mode of failure of this beam was different from those of the companion beams without end anchors. Note that the laminate did not separate right away as the anchors at the end were still holding it. However, slippage occurred and the laminate started fraying in the longitudinal direction as shown in Figure 4-105.

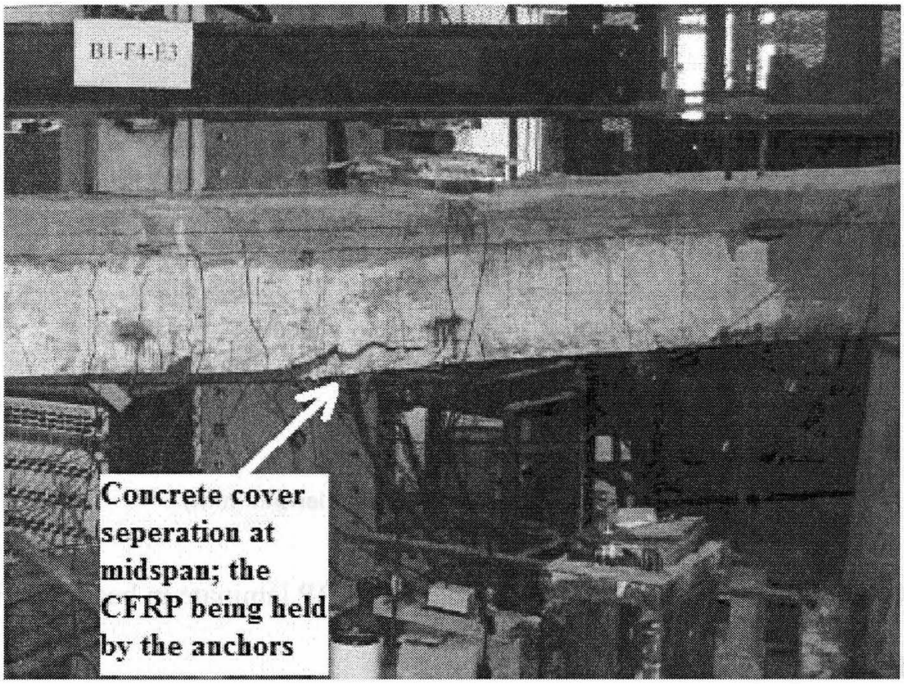

Fig.4-104: Failure of the anchor and concrete cover separation in beam B1-F4-E3

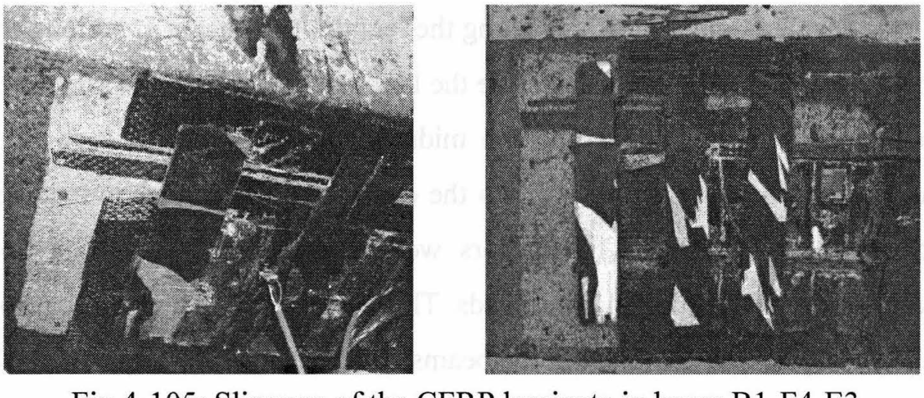

Fig.4-105: Slippage of the CFRP laminate in beam B1-F4-E3

The calculated shear stress variation along the CFRP laminate in beam B1-F4-E3 is shown in Fig.4-106, where the maximum shear stress is 1.86 MPa. However, these stresses show a highly unusual distribution as failure is approached. The shear reversals near the beam ends are indicative of a complex state of stress in the anchor zone.

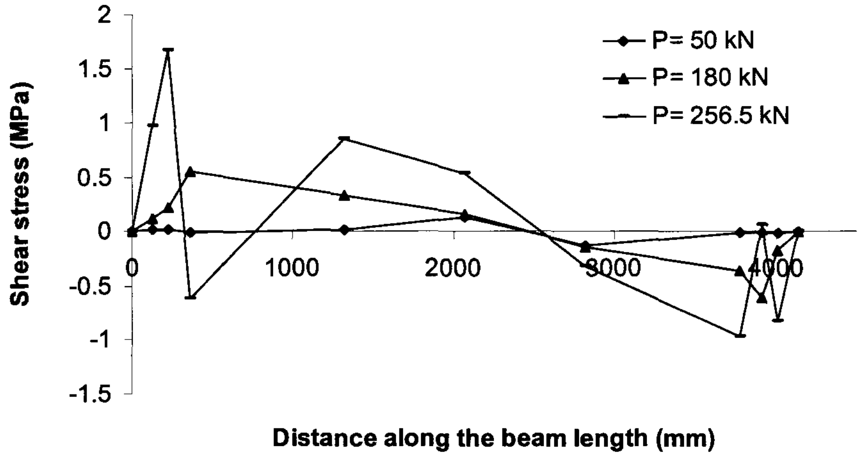

Fig.4-106: Shear stress distribution along the CFRP laminate in beam B1-F4-E3

4.6.9 Beam B1-F4-E3-M9

Since the last two beams with 4 layers and anchors at the two ends did not achieve their theoretical capacity and the CFRP laminate delaminated and/or slipped at one end, it was decided to place anchors along the length of the beam at various critical locations. The critical regions are, beside the laminate end zones, the regions under the applied concentrated loads and the midspan. Accordingly, at each of these regions three anchors were inserted into the concrete and the anchor spacing was kept constant at 100 mm. The anchors were symmetrically disposed both at midspan and under the applied point loads. This beam reached a maximum load of 279.5 kN, compared to 256.5 kN in the beams with end anchors only, which shows an approximately 10% increase. As can be seen in Fig.4-107, which shows the load-midspan deflection curves of this beam, the load dropped to 154 kN after delamination and then it did not increase much until the concrete crushed. If we assume the 154 kN to be the load carrying capacity of the un-retrofitted beam, then the addition of the CFRP laminate increased its capacity by 81%. This increase was achieved with at least a 10 % smaller CFRP cross-section than the section in the companion beams without anchors. Consequently, the midspan region anchors clearly mobilized a greater fraction of the theoretical strength of the laminate.

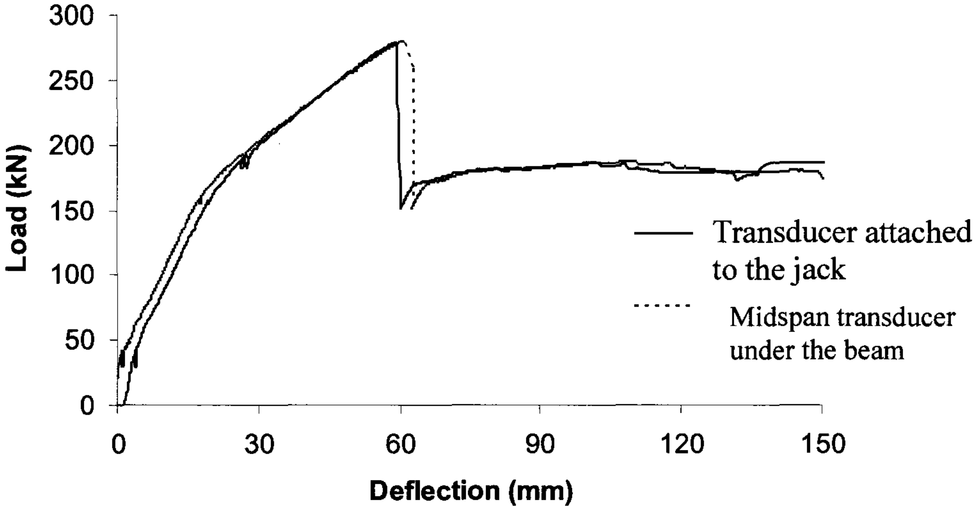

Fig.4-107: Load deflection curve of beam B1-F4-E3-M9

The strain variation along the internal steel and the CFRP laminate are shown in Figs.4-108 and 4-109. The maximum strain in the steel was 0.012 under one of the point loads while it was somewhat smaller in the midspan region. It should be pointed out that the higher strain in the reinforcement in the vicinity of the point loads can be explained by the contribution of both the bending moment and the shear to the total strain while at midspan only the bending moment causes the strain. This is a well-established principle in conventional reinforced concrete design. One other factor that contributes to the local strain variations in the reinforcement is the presence of discrete cracks, which cause higher strain at the crack location.

The strain variation along the CFRP laminate length shows a more symmetric and uniform distribution. The maximum strain recorded was 0.01, which is almost 60 % of its rupture strain. This indicates that the laminate has basically lost its bond with the concrete and is held by the anchors, but is still able to resist the applied loads.

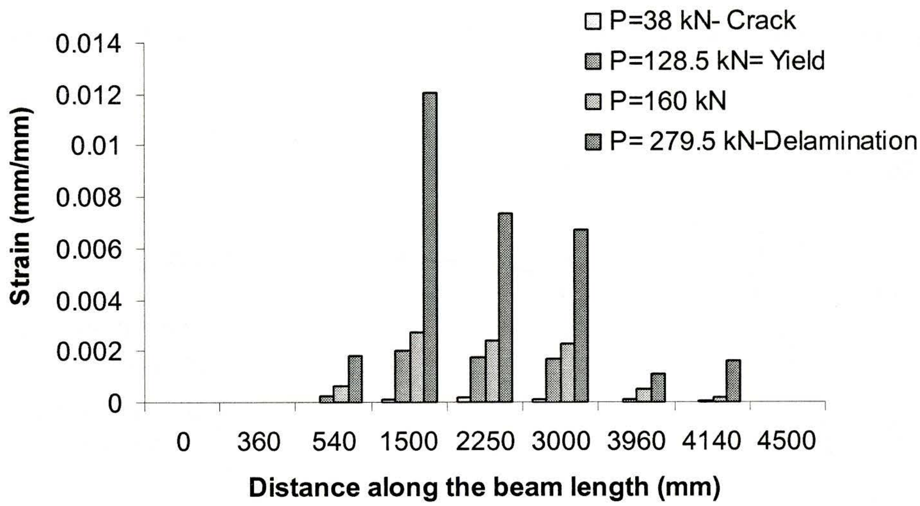

Fig.4-108: Steel reinforcement strain variation beam B1-F4-M9-E3

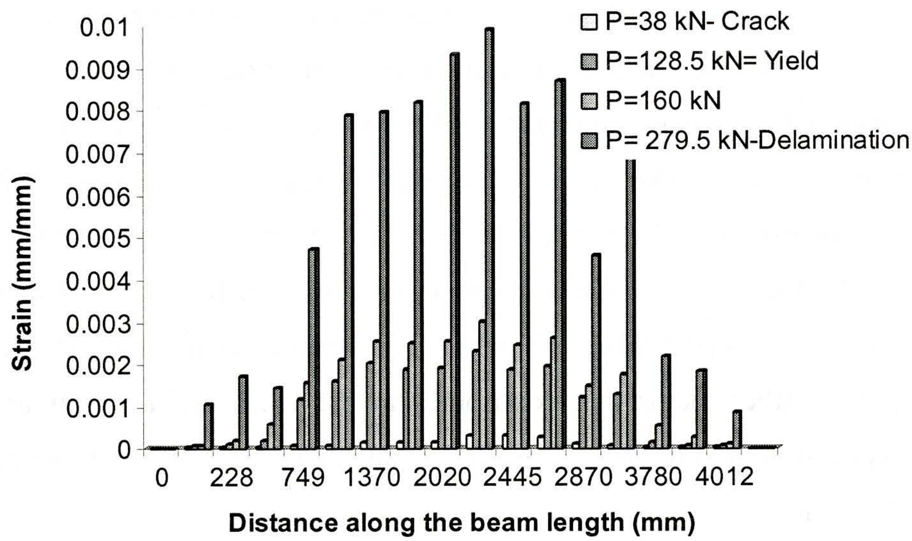

Fig.4-109: CFRP strain variation along beam B1-F4-M9-E3

In this beam, rupture of the anchor near the roller support was observed. The anchor rod sheared off at the anchor plate-rod junction. Thereafter, the laminate began slipping and another anchor in the midspan also ruptured as shown in Figure 4-110. It can be claimed that the maximum load in this beam was limited by the strength of the anchor. The calculated shear stress variation along the CFRP laminate is shown in Fig.4-111. The maximum shear stress was 6.23MPa, but only one point shows this high shear stress. This indicates the concentration of shear stresses in the anchor located in the vicinity of this point.

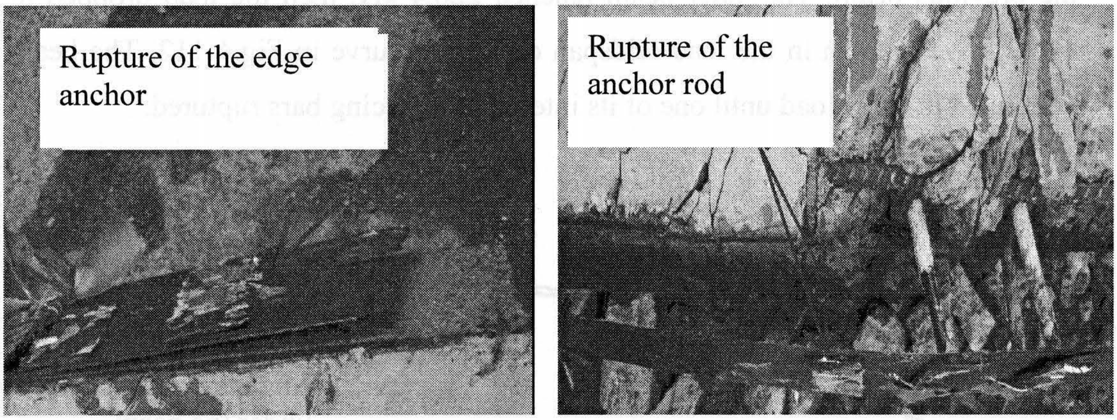

Fig.4-63110: Failure of the anchor in beam B1-F4-E3-M9

Although the other shear stress values are smaller compared to the highest calculated value, nevertheless they are generally higher than the values in the beams without anchors or with only end anchors. The results of this beam clearly demonstrate the advantage of distributed anchors along the length of the beam. Although simple beam theory dictates lack of shear in the constant moment zone and therefore, the lack of need for anchors in this zone, in reality the behaviour of such retrofitted beams is more complex than indicated by the simple beam theory.

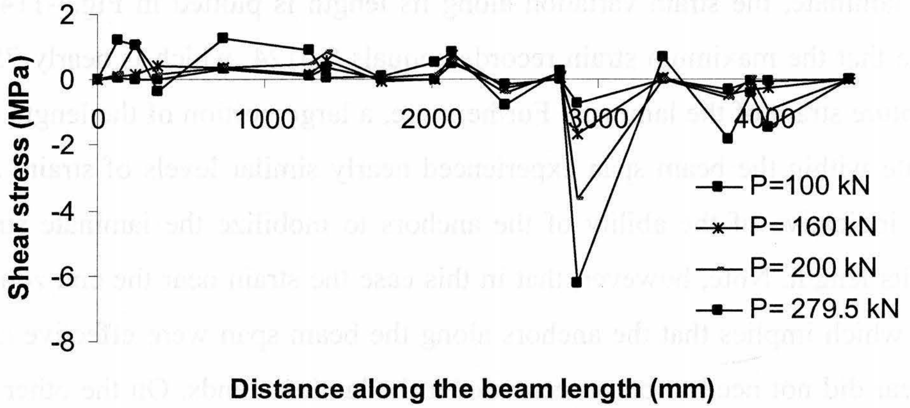

Fig.4-111: Shear stress distribution along beam B1-F4-E3-M9

4.6.10 Beam B1-F2-E3-M9

It was decided not to test replicate of the previous beam since the anchor could not mobilize the full strength of the four laminate layers. Thus, it was decided to test another beam with only two laminate layers but with an identical anchor layout as the previous beam. The latter beam reached 226.4 kN, then the load dropped to 146.7 kN as shown in the load midspan deflection curve in Fig.4-112. The beam continued to carry load until one of its internal reinforcing bars ruptured.

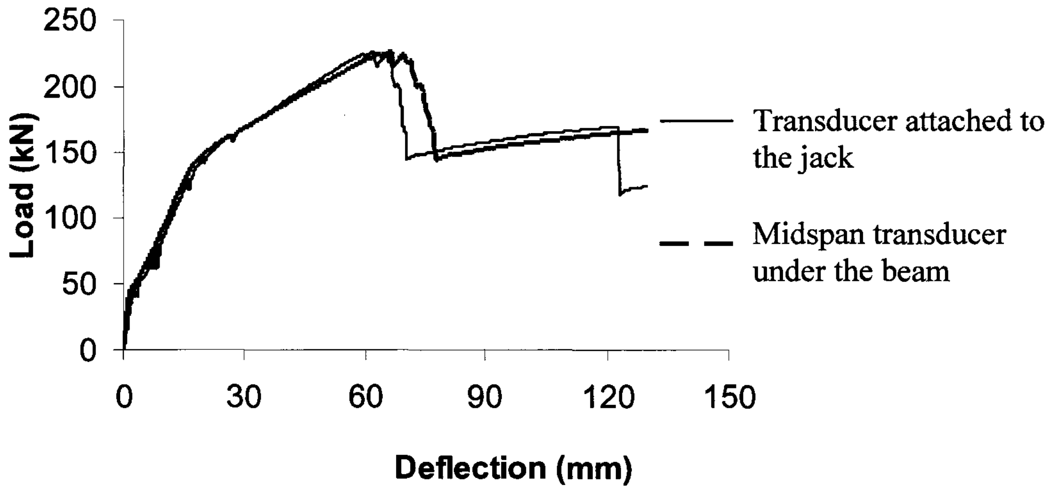

Fig.4-112: Load midspan deflection curve of beam B1-F2-E3-M9

The strain gauges along the internal steel failed functioning after a certain load level therefore, readings up to 180 kN load only could be recorded as shown in Fig.4-113. The maximum recorded strain was approximately 0.0037. As for the CFRP laminate, the strain variation along its length is plotted in Fig.4-114. One can see that the maximum strain recorded equals 0.0124, which is nearly 75% of the rupture strain of the laminate. Furthermore, a large portion of the length of the laminate within the beam span experienced nearly similar levels of strain. Again this is indicative of the ability of the anchors to mobilize the laminate strength along its length. Note, however, that in this case the strain near the end zones are small, which implies that the anchors along the beam span were effective and all the shear did not need to be concentrated a the laminate ends. On the other hand, the maximum load carried by this beam is practically the same as the load in the beam with two layers and with no anchors. It could be argued that due to the presence of the holes drilled into the laminate to allow the anchors legs to pass through, the net cross-section of the laminate is at least 10 % lower than that of the laminate in the former beam.

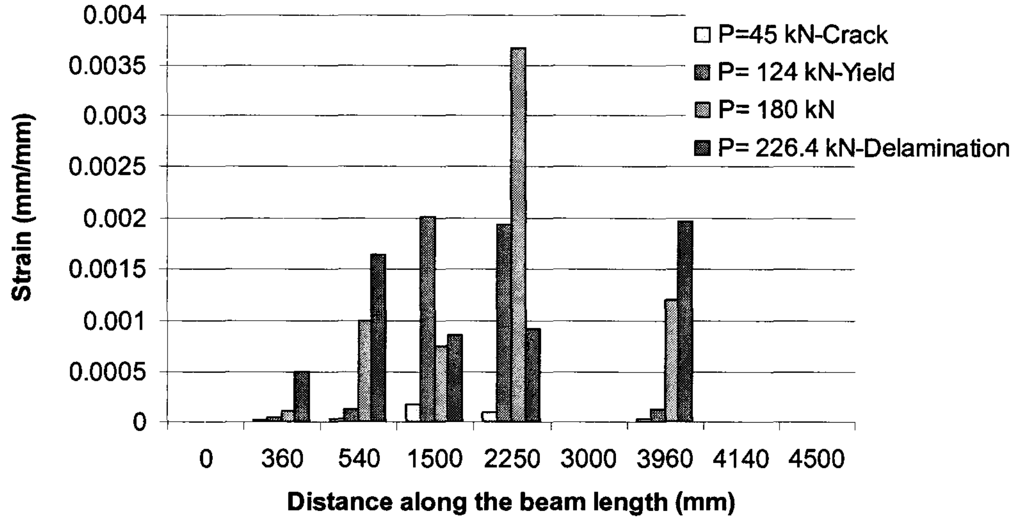

Fig.4-113: Steel reinforcement strain variation beam B1-F2-E3-M9

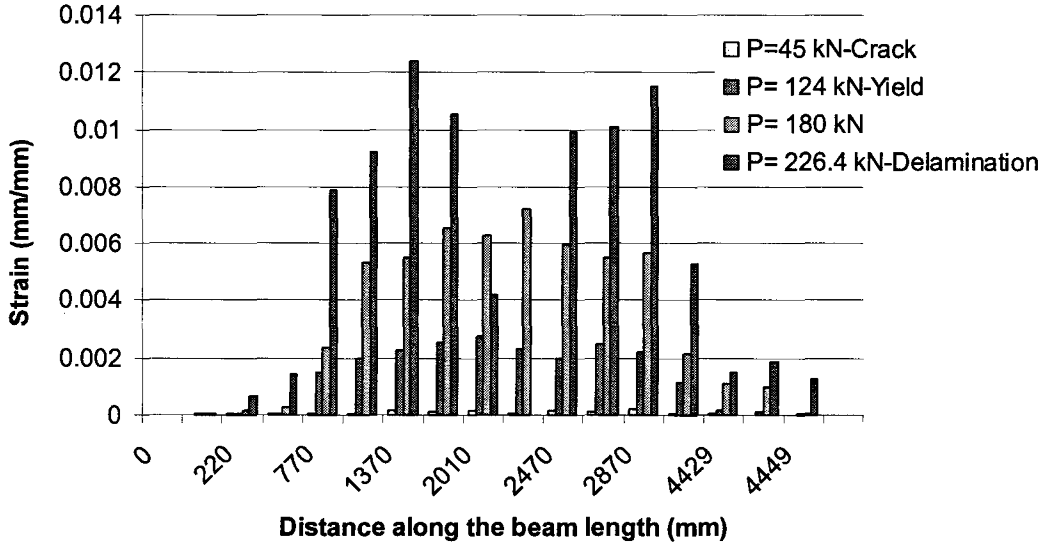

Fig.4-114: CFRP strain variation along beam B1-F2-E3-M9

In this beam, the CFRP laminate split longitudinally in the region between the hinge support and the anchors under the loading points as shown in Fig.4-115. After initial delamination, the laminate began to rupture at the location of the anchor heads in the midspan zone. This may be due to the fact that at the anchor locations, the laminate could not accommodate the beam curvature and was subjected to transverse forces causing it to rupture prematurely. One way to mitigate this effect may be to use more anchors along the span.

The calculated shear stress variation along the CFRP laminate is shown in Fig.4-116. Although a maximum shear stress of 11.4 MPa was calculated, it is unlikely that the concrete could resist such high shear stresses. The forces resisted by the anchor must have contributed to stress transfer and this stress reflects the combined resistance due to bond, or adhesion, and to the mechanical resistance of the anchor. This beam shows almost the same distribution as the beam with 4 layers since both have the same anchor uniform distribution.

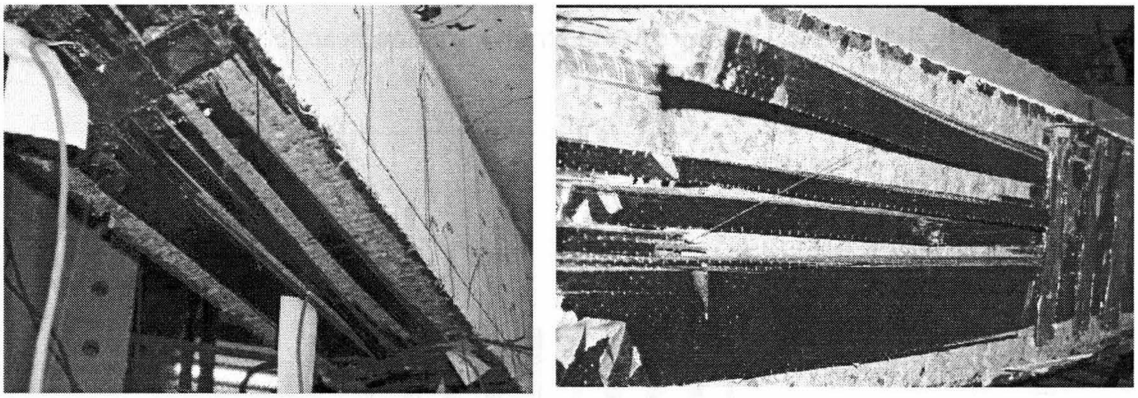

Fig.4-115: Delamination of the CFRP laminate between the anchors in beam B1-F2-M9-E3

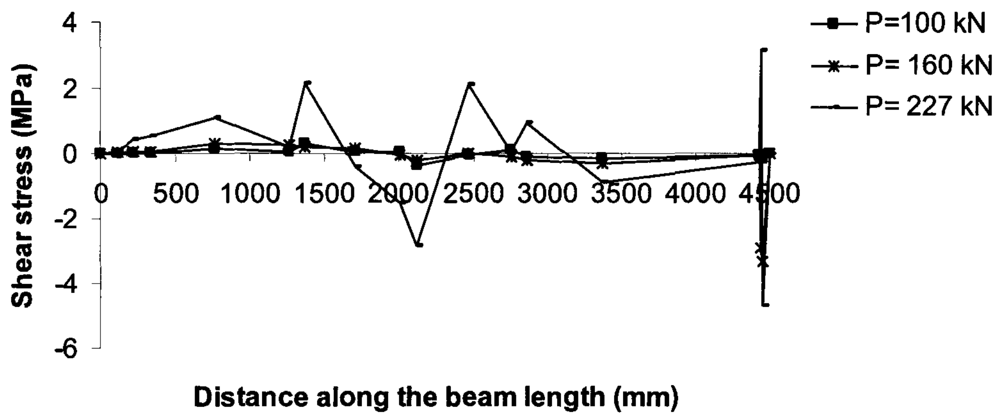

Fig.4-116: Shear stress distribution along the CFRP laminate in beam B1-F2-E3-M9

4.6.11 Beam B1-F2-E4-M11

Since the previous beam did not achieve its theoretical capacity with two layers of CFRP and it was believed the CFRP was ruptured partially by transverse forces, it was decided to reduce the effect of the transverse forces by increasing the number of anchors at midspan and at the ends. Eleven anchors with 200 mm spacing were used in the midspan region and four anchors at 100 mm spacing were used at each end.

This beam reached a maximum load of 234.5 kN, which is only 3.5% higher than that of the previous beam with nine anchors at midspan. The load dropped to 147.5 kN then the load increased again until one of the internal steel bars ruptured as shown in Fig.4-117. The second drop in the load-deflection diagram of the beam in Fig.4-117 is due to the rupture of the steel.

Only one strain gauge on the internal steel was functioning up to 200 kN, thereafter it failed, the steel strain at delamination was not recorded as can be seen in Fig. 4-119. The strain in the CFRP laminate showed a quite uniform distribution along a large portion of its length and it reached a maximum value of 0.013, which is 78% of its rupture strain, Fig.4-119. It is clear from the latter figure that the anchors allowed the laminate to achieve more uniform stress, but its strength is still governed by its maximum strain. Also since the anchors do not prevent the delamination of the portions of the laminate width lying outside the anchor head, the advent of delamination immediately reduces the available CFRP cross-section resisting the applied loads by at least 10%. Furthermore, the drilling of the holes through the laminate reduces its cross-sectional area by at least another 10%. These reductions in the effective area clearly affect the laminate load-carrying capacity. Therefore, one strategy would be to place all the laminate between the anchor legs and to not drill any holes through it.

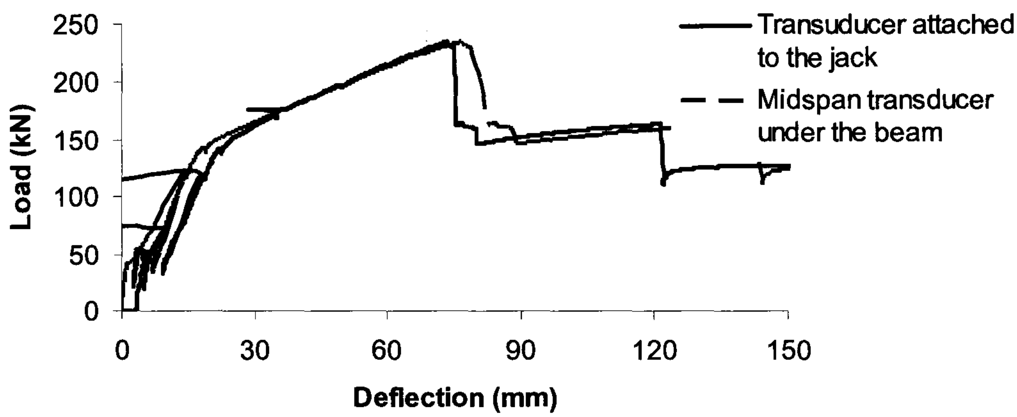

Fig.4-117: Load midspan deflection curve of beam B1-F2-E4-M11

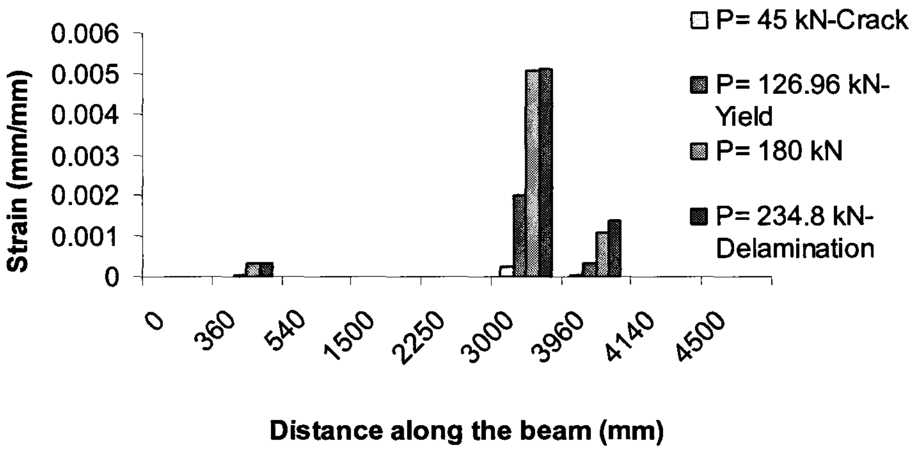

Fig.4-118: Steel reinforcement strain variation beam B1-F2-E4-M11

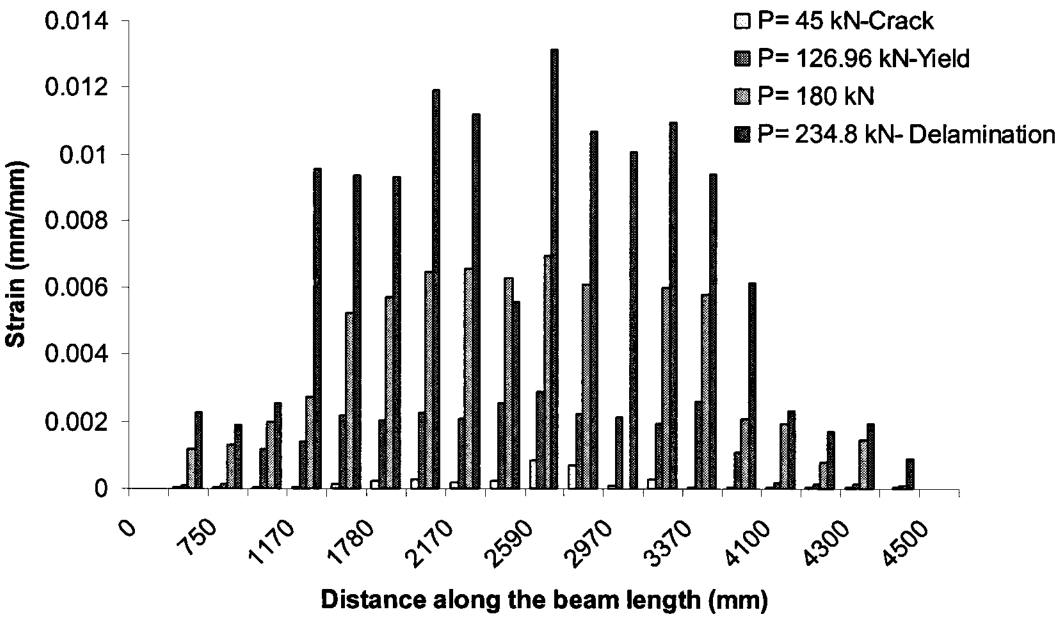

Fig.4-119: CFRP strain variation along beam B1-F2-E4-M11

It is important to mention that in this case while drilling the holes for the anchors, it was found that the distance between the 2 steel bars was not enough to pass the anchor rod through it, therefore, the anchors had to be placed on a slant. This caused a greater width to lie outside the anchor head and it was noticed upon visual inspection that this part delaminated first as shown in Fig.4-120. In this beam, the CFRP laminate ruptured between the anchors and split in the longitudinal direction. After delamination, the end anchors remained intact and no slippage was observed. Only the laminate outside the anchor head delaminated as can be seen in Fig.4-121. The calculated shear stress distribution along the CFRP laminate is shown in Fig.4-122. The maximum shear stress is 3.5 MPa and the abrupt changes are likely due the presence of the anchors.

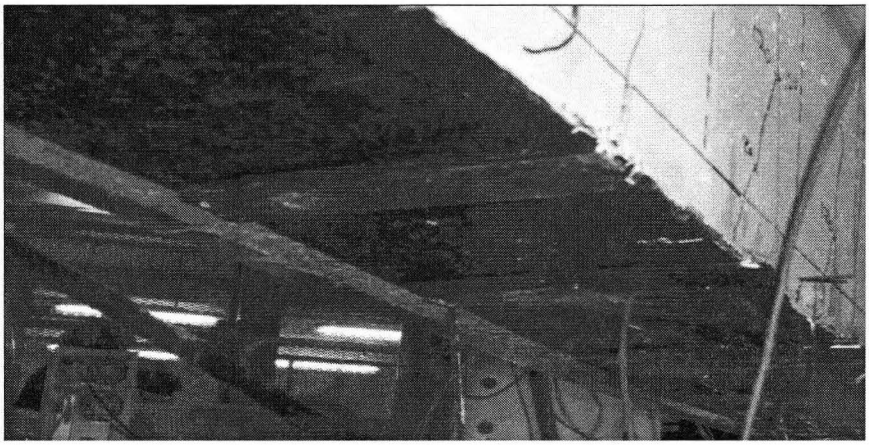

Fig.4-120: Delamination of the CFRP laminate outside the anchor head in beam B1-F2-E4-M11

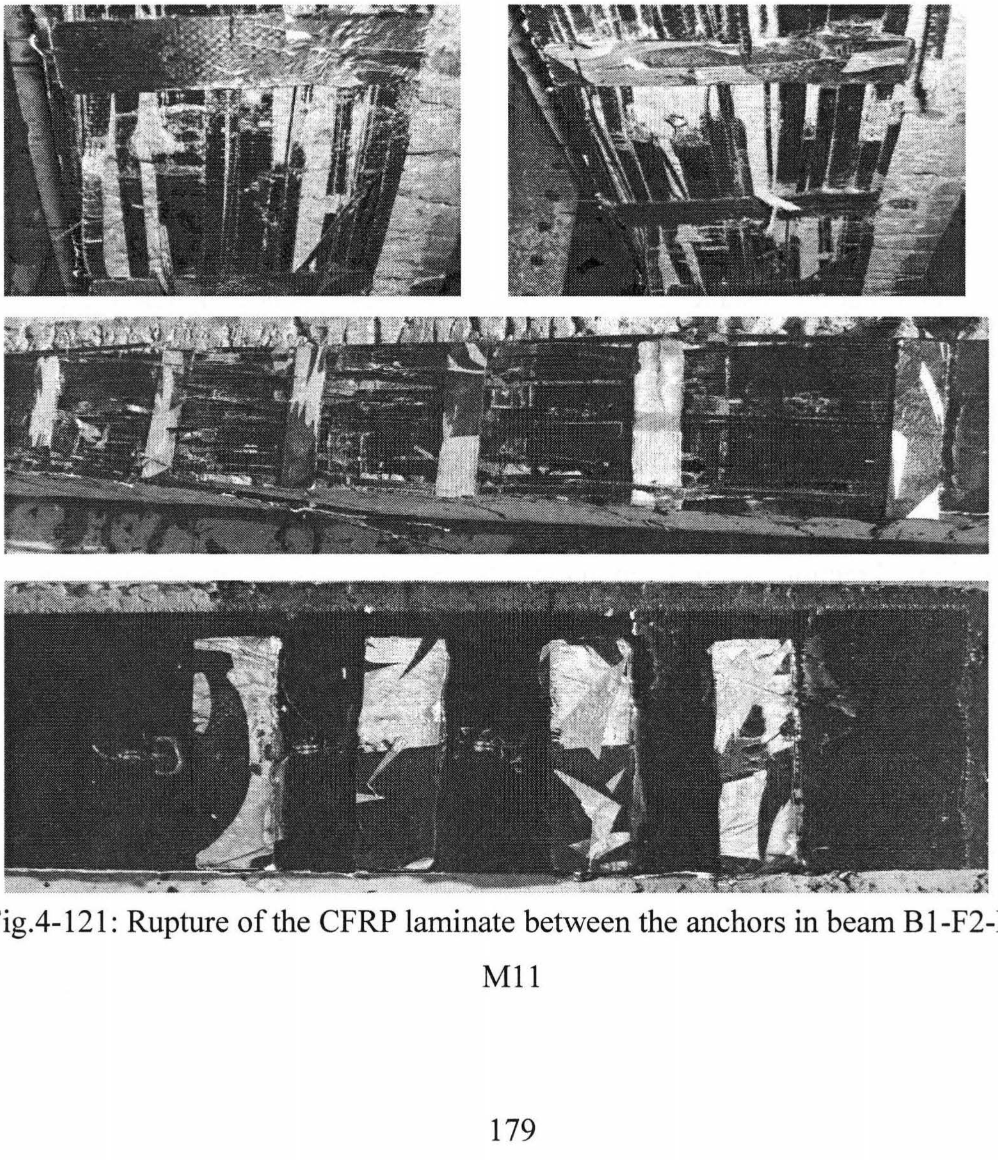

Fig.4-121: Rupture of the CFRP laminate between the anchors in beam B1-F2-E4-M11

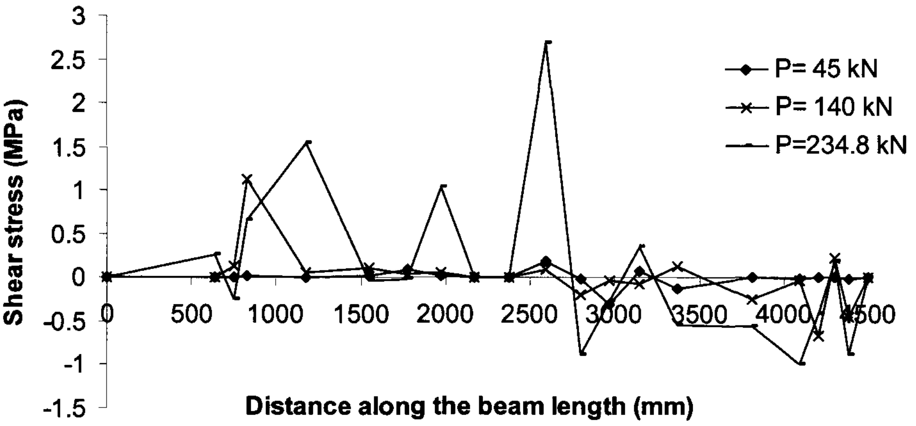

Fig.4-122: Shear stress distribution along the CFRP laminate in beam B1-F2-E4-M11

4.6.12 Beam B1-F4-N-b90

As stated earlier, it was discovered that drilling holes in the laminate or placing the laminate outside the anchor heads reduces the load resistance of the laminate. To avoid these problems, it was decided to place the FRP laminate within the anchor leg spacing. This beam was retrofitted with 4 layers of CFRP laminate each 90 mm wide. The laminate width was selected to fit within the anchor legs. Figure 4-123 shows the load deflection curve for this beam. The load reached 199.6 kN when the CFRP delaminated. This value is similar to the maximum load achieved in all the beams with 1 layer of 220 mm wide laminate and in one of the 2 beams strengthened with 2 layers of 220 mm wide laminate.

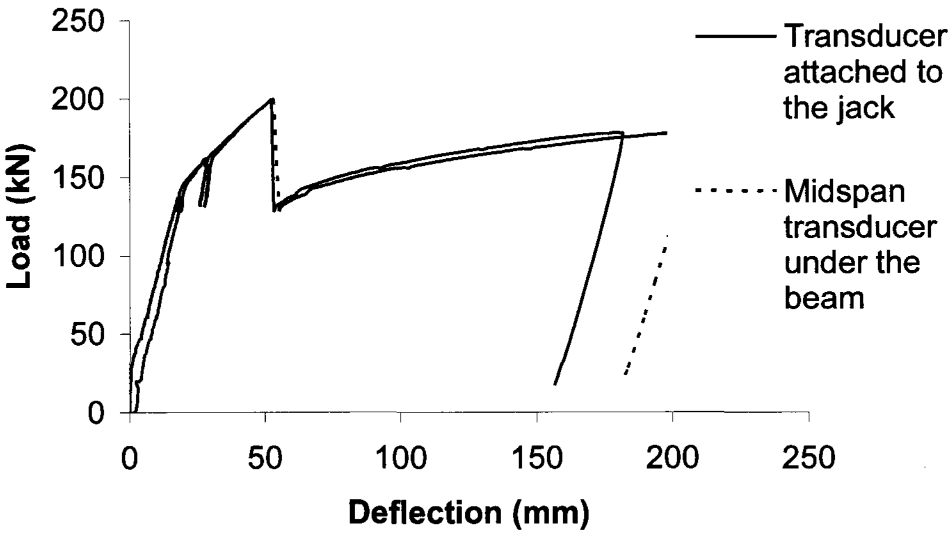

Fig.4-123: Load deflection curve for beam B1-F4-N-b90

After delamination, the load dropped to 132.9 kN and increased again until the concrete failed in compression. If we compare the maximum load achieved by this beam which is 199.6 kN, it is clear that it is marginally higher than the ultimate load capacity of the unretrofitted beam. Practically, the only benefit of this retrofit is that the maximum load before delamination occurs at a relatively smaller deflection. The strain profiles along the internal reinforcement and the CFRP laminate are shown in Figs.4-124 and 4-125. The maximum strain recorded just before delamination was 0.00875, which is 52.4 % of its ultimate strain. The shear stress profile along the CFRP laminate is shown in Fig.4-126. The maximum shear stress was 1.2 MPa. The plotted shear stress follow the shear force diagram and it goes to zero in the mid-span. The shear stress shows a more uniform stress at failure since the delamination occurred from the mid-span towards the ends. Figures 4-127 (a) and (b) shows beam B1-F4-N-b90 after delamination.

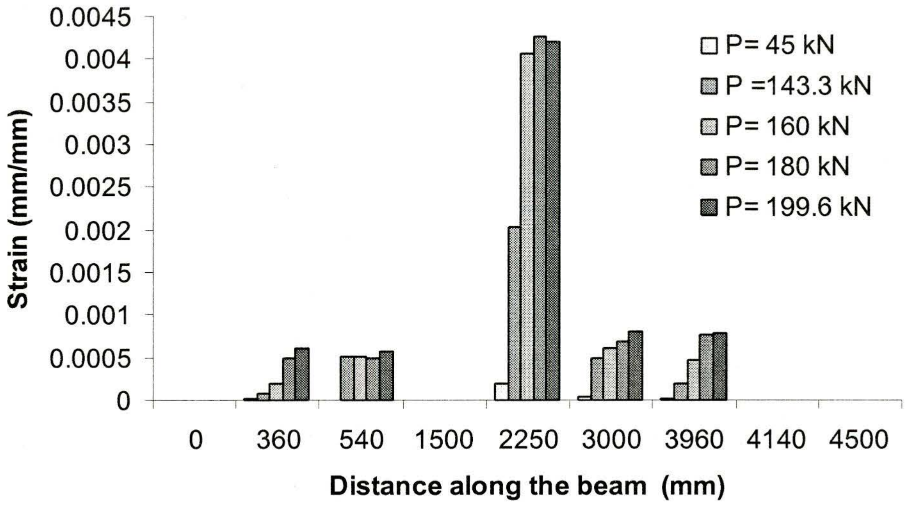

Fig.4-124: Strain variation on the internal reinforcement along beam B1-F4-N-b90

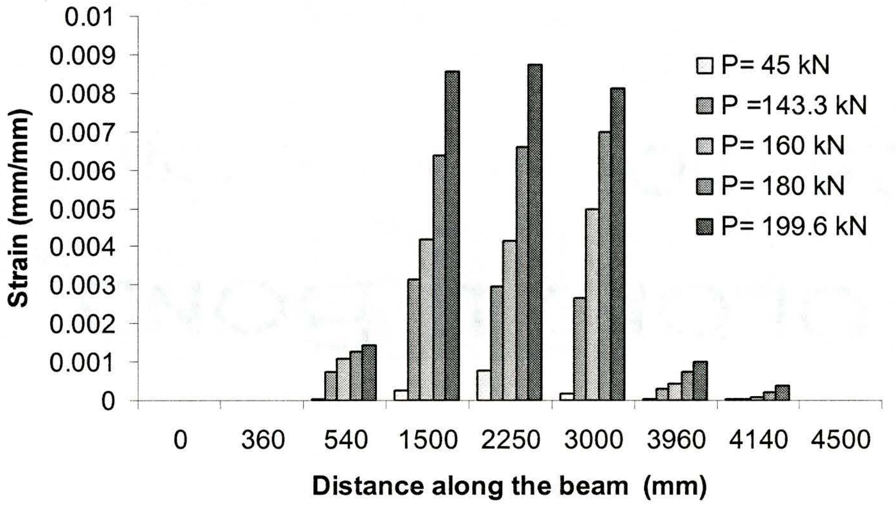

Fig.4-125: Strain variation on the CFRP laminate along beam B1-F4-N-b90

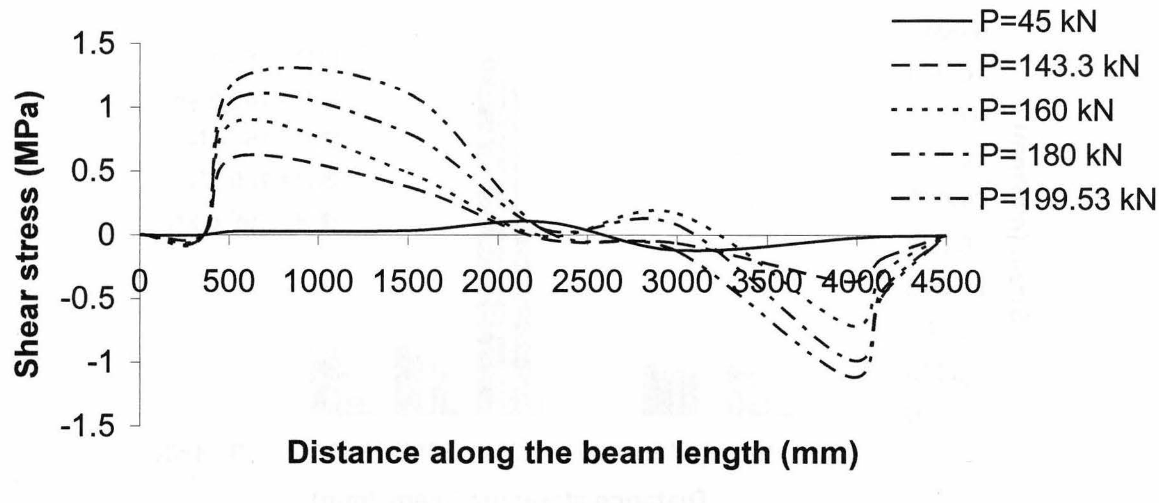

Fig.4-126: Shear stress distribution along the CFRP laminate for beam B1-F4-N-b90

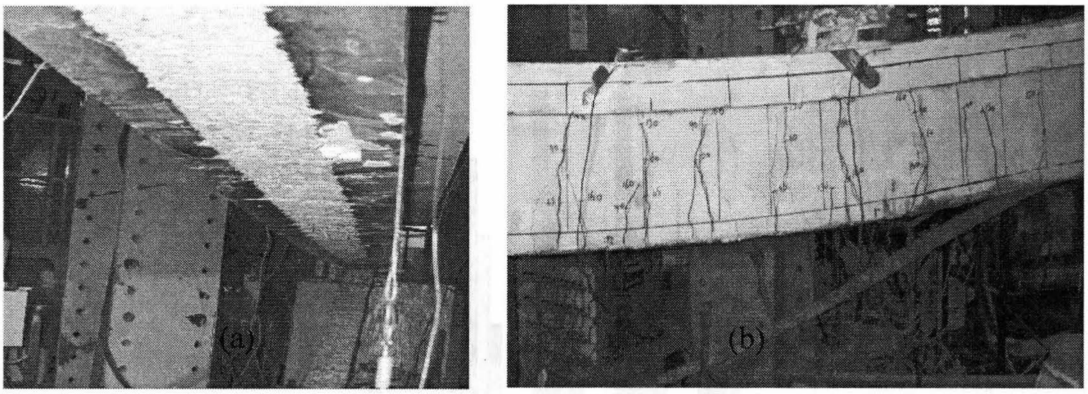

Fig.4-127: Beam B1-F2-N-b90 after delamination

4.6.13 Beam B1-F4-E2-M15-b90

In this beam, four layers of 90 mm wide and 0.165 mm thick laminate were used. Hence, the cross-sectional area of these four layers is 59.4 mm^2 versus 72.6 mm^2 when two 220 mm wide layers used in the previous few beams. Thus the CFRP area was reduced by 20%. The laminate width was chosen such that it could be placed in the 100 mm wide space between the anchor legs. Figure 3-20 (f) illustrates the anchor locations and the laminate disposition in this case, while Fig.4-128 shows an actual view of the bottom of the beam.

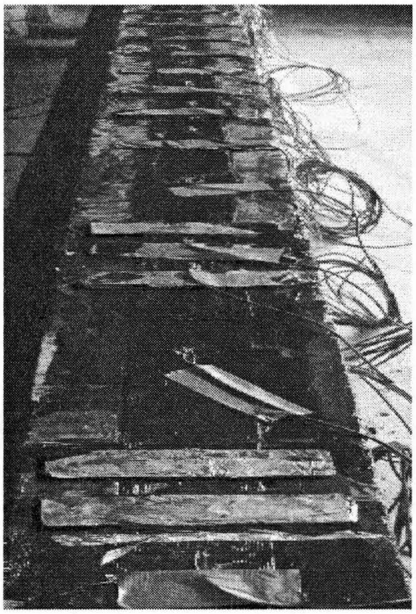

Fig.4-128: Anchor arrangement for beam B1-F4-E2-M15-b90

Figure 4-129 shows the load-midspan deflection for this beam. After loading, the first crack in the beam was observed at 50 kN as in most of the other beams and the beam reached a maximum load of 241 kN when delamination occurred between the end anchors and the next set of anchors. The load dropped slightly to 239 kN and then increased to 244 kN as can be seen in Fig.4-129. After the latter load, the load dropped to 145 kN due to delamination, but it subsequently increased to 174.2 kN at which point one of the internal reinforcing bars ruptured. The other two bars were also ruptured shortly after and the beam failed and broken into two halves.

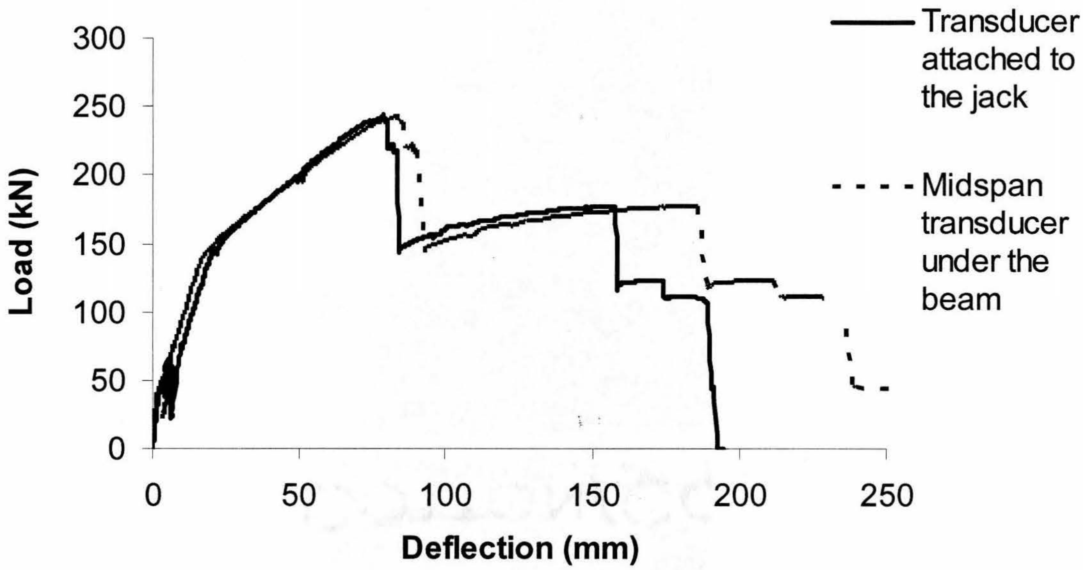

Fig.4-129: Load midspan deflection curve for beam B1-F4-E2-M15-b90

The strain variations along the internal reinforcement and along the CFRP laminate are shown in Figs.4-130 and 4-131. As shown in Fig.4-130, most of the strain gauges on the internal steel rebars malfunctioned except the two strain gauges near the midspan. The maximum strain recorded was 0.006 even through in reality the steel ruptured.

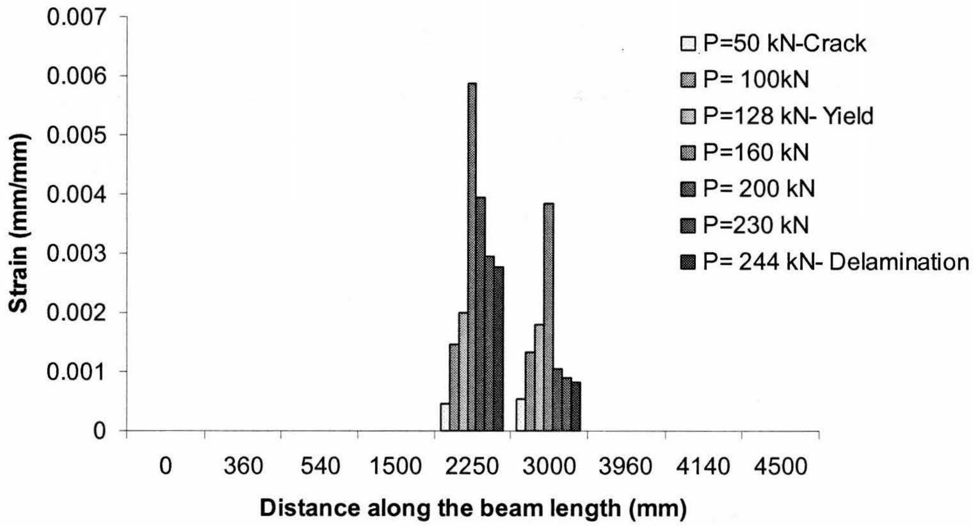

Fig.4-130: Steel reinforcement strain variation along beam B1-F4-E2-M15-b90

As for the laminate, as can be seen in Fig.4-131, the strain variation along the CFRP length approximately follows the moment diagram of the beam and the maximum strain recorded is 0.0157, which is 95% of the laminate specified rupture strain. The maximum strain occurred near midspan and in the neighbourhood of the point load and it was observed during the test that rupture occurred in these locations. In fact the CFRP in this beam ruptured, thus it can be stated that it achieved its full strength. Figure 4-132 shows the beam during the test and Fig.4-133 shows the ruptured CFRP laminate between the anchors. This beam actually surpassed its theoretical load capacity based on full bond until failure. Hence, the anchors enable it to achieve its full capacity.

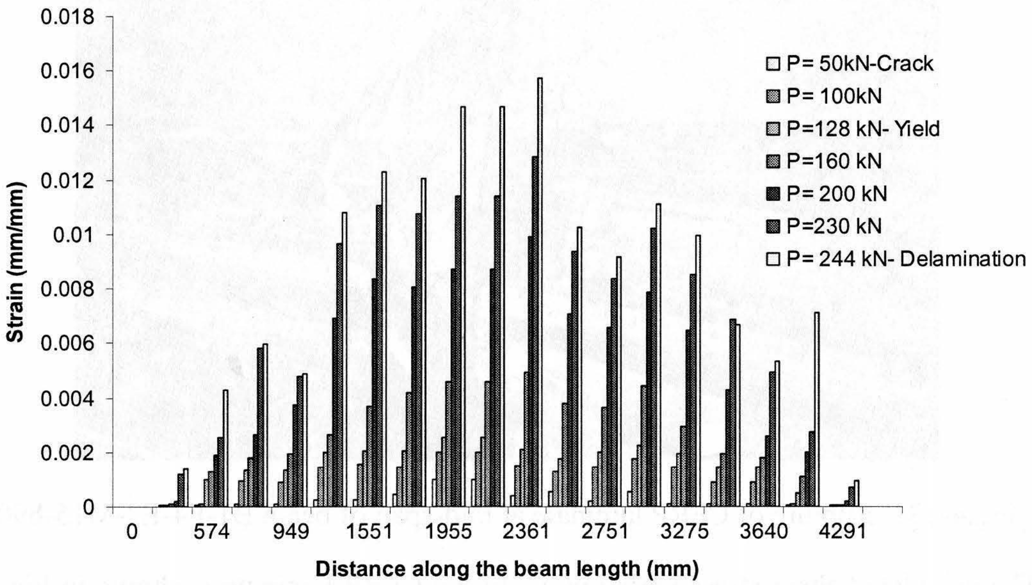

Fig.4-131: Strain variation of the CFRP laminate along beam B1-F4-E2-M15-b90

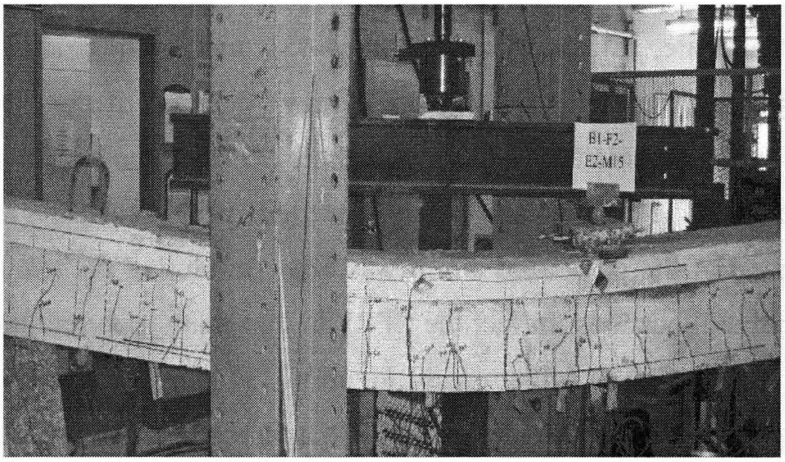

Fig.4-132: Beam B1-F4-E2-M15-b90 during the test

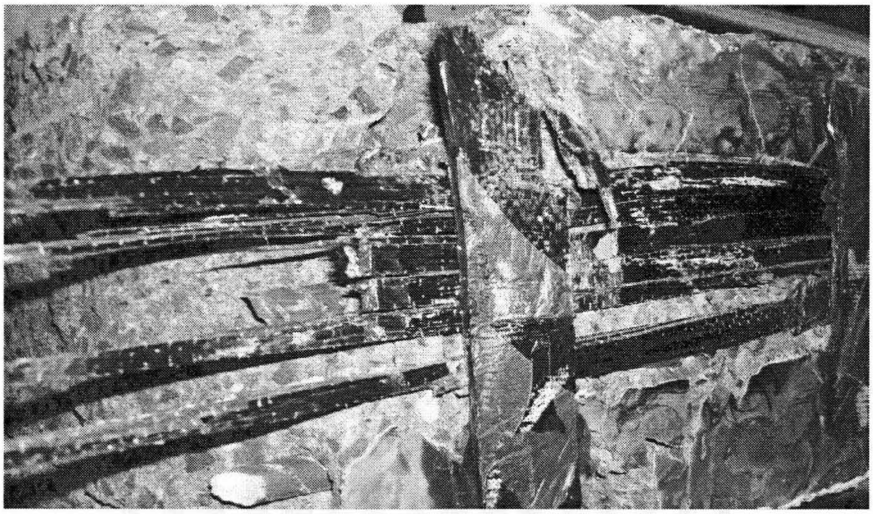

Fig.4-133: Rupture of CFRP laminate at mid-span of beam B1-F4-E2-M15-b90

The calculated shear stress variation along the CFRP laminate is shown in Fig.4-134. The maximum shear stress is 2.2 MPa, however, the shear stress diagram exhibits multiple peaks which occur in the vicinity of the anchors. This means that due to the presence of the anchors, the shear stresses are no longer concentrated in a small region because a number of anchors contribute to the total interfacial shear resistance of the beam. Without the anchors, once the shear stress at the point exceeds the interfacial shear strength of the concrete, delamination begins and the maximum shear stress point shifts to the neighbouring point again causing delamination, the anchors tend to arrest this uncontrolled delamination process.

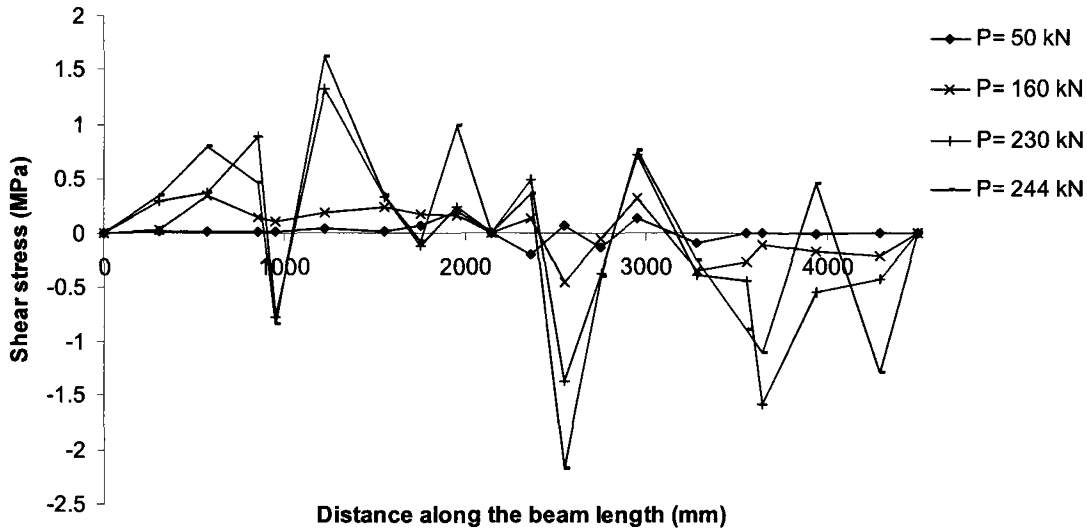

Fig.4-134: Shear stress distribution along the CFRP laminate in beam B1-F4-E2-M15-b90

4.6.14 Beam B1-F8-N-b90

This beam was retrofitted with eight layers of 90 mm wide CFRP laminate but the laminate was not anchored anywhere along its length. The beam reached a maximum load of 214.6 kN when delamination occurred. The load-midspan deflection curve of the beam is shown in Fig.4-135. After delamination, the load dropped to 121.5 kN but subsequently it increased to 176.3 kN when the concrete failed in compression. Notice that delamination occurred at a relatively small load and after delamination the load dropped significantly and the beam behaviour reverted to that of the unretrofitted beam.

Fig.4-136 shows the strain variation along the CFRP laminate in this beam. The maximum strain recorded just before delamination was 0.0061, which is only 36.5% of its expected ultimate value. The maximum load reached in this beam was only 20% higher than the maximum load carried by the companion unretrofitted beam.

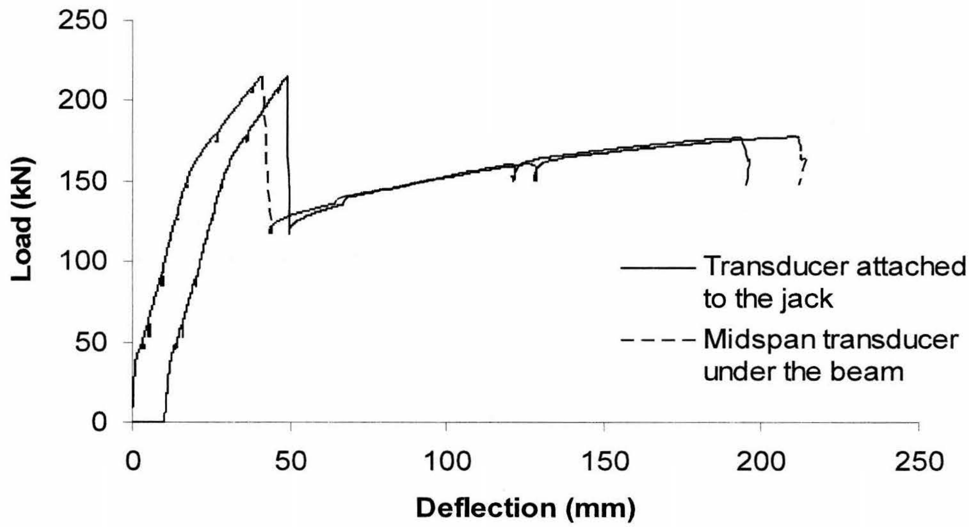

Fig.4-135: Load deflection curve for beam B1-F8-N-b90

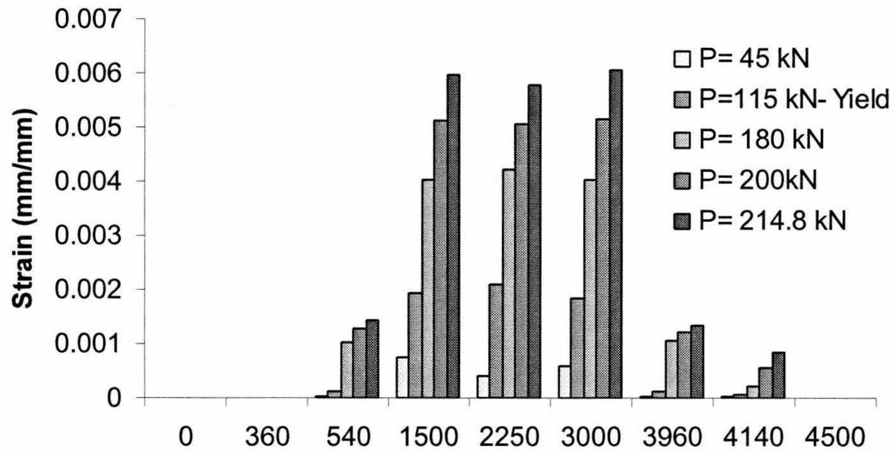

Fig.4-136: Strain variation along the CFRP laminate of beam B1-F8-N-b90

Figures 4-137 (a), (b), (c) and (d) show the delamination of beam B1-F8-N-b90. As can be seen in Fig.4-137 (c), the delaminated CFRP laminate has a thin layer of concrete attached to it. It is important to mention that the crack pattern was traced and it was found that the crack spacing in the midspan region closely follows the spacing of the internal stirrups. The internal stirrups had 200 mm spacing in the midspan zone. Figure 4-138 shows the location of the cracks and the stirrups.

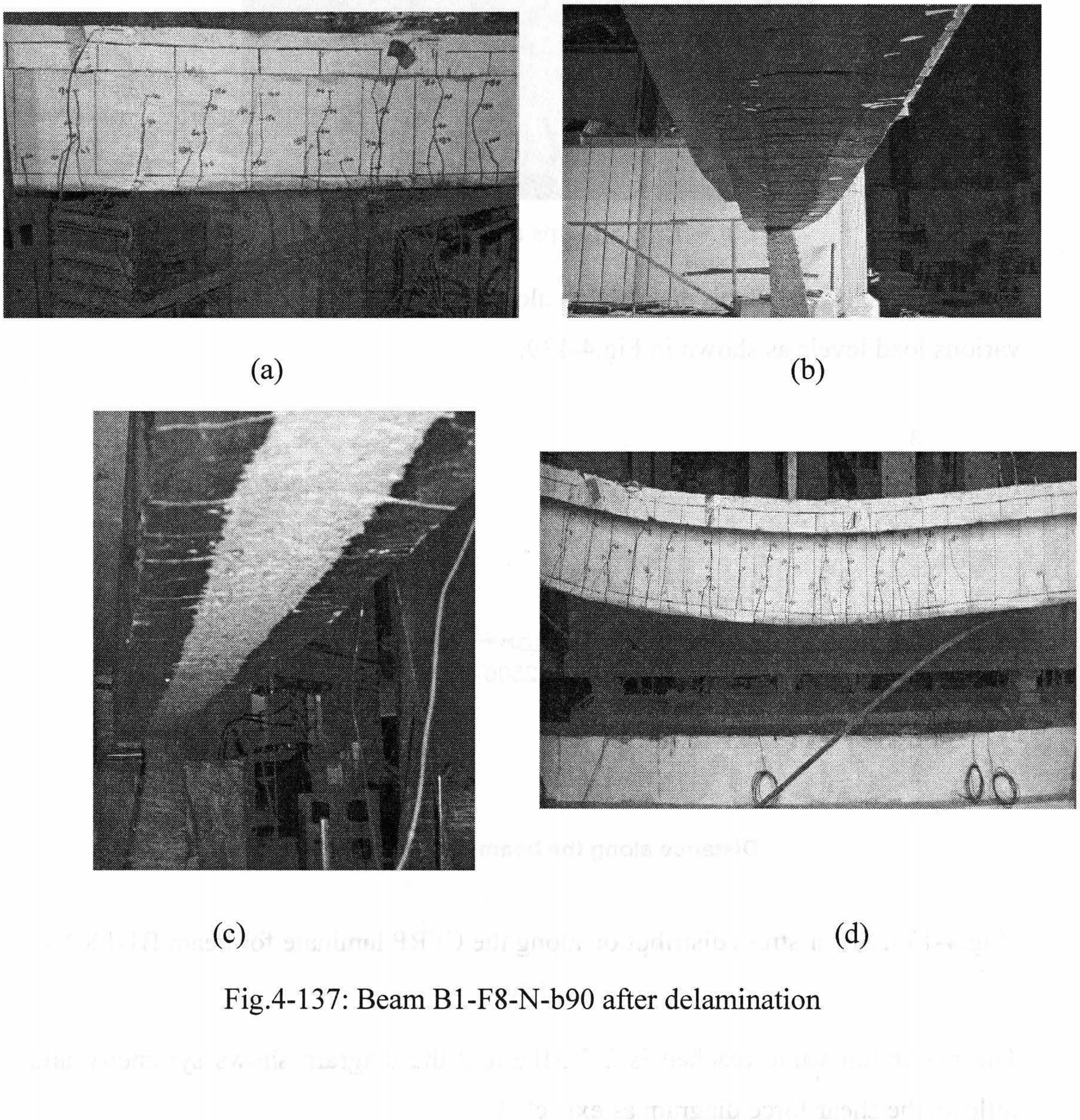

(a) (b) (c) (d)

Fig.4-137: Beam B1-F8-N-b90 after delamination

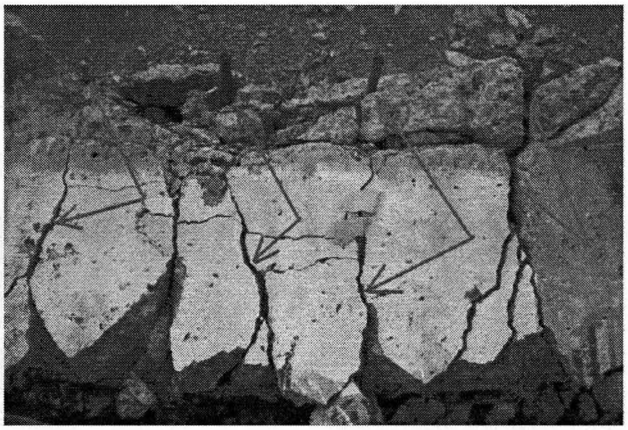

Fig.4-138: Stirrups and crack locations

The calculated shear stress distribution along the CFRP laminate is plotted at various load levels as shown in Fig.4-139.

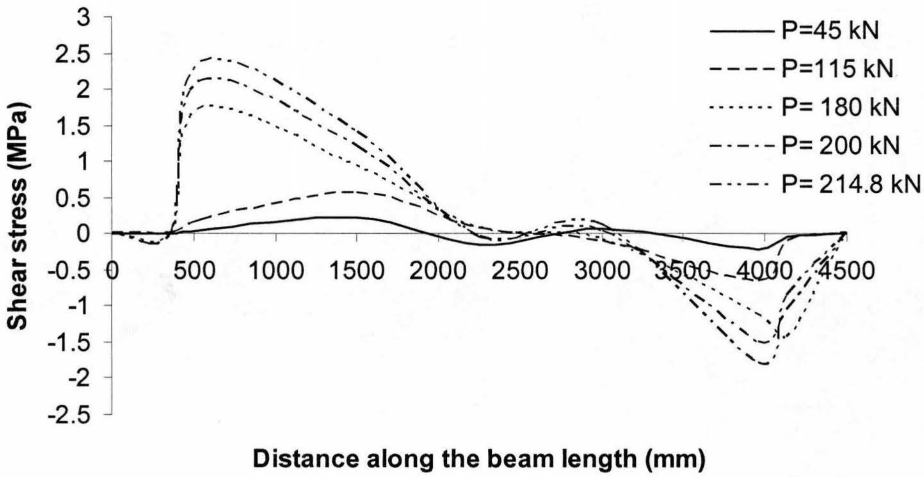

Fig.4-139: Shear stress distribution along the CFRP laminate for beam B1-F8-N-b90

The maximum value reached is 2.5 MPa and the diagram shows symmetry and follows the shear force diagram as expected.

4.6.15 Beam B1-F8-E3-M17-b90

Figure 4-140 shows the arrangement of the strain gauges and anchors for beam B1-F8-E3-M17-b90. This is the companion beam to beam B1-F8-N-b90 and the only difference between the two beams is the presence of the anchors in the current beam. In this case, three anchors were used at the end with 100 mm spacing from each end, and another 17 anchors were distributed along the beam length at 200 mm spacing. Eight layers of CFRP laminate was used, with each layer being 90 mm wide. The laminate strips were placed between the anchor rods as illustrated in Fig.3-20 (g) while the actual dispositions of the anchors and the CFRP laminate strips are shown in Fig.4-140.

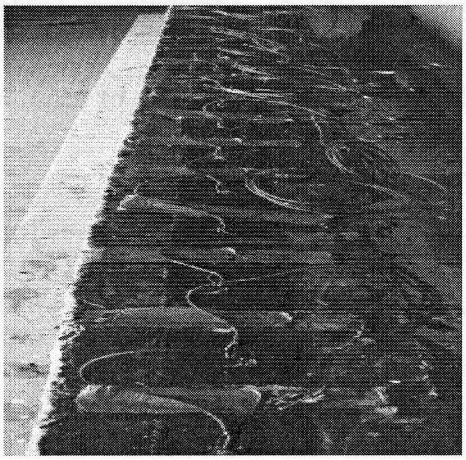

Fig.4-140: Strain gauges and anchor arrangement for beam B1-F8-E3-M17-b90

The load reached 50 kN when the first crack appeared. The internal reinforcement started to yield at 140 kN. The load was increased until it reached 309 kN at which point the CFRP laminate ruptured near the midspan as shown in Fig.4-141. Thereafter, as usual the load dropped dramatically to 148.6 kN but subsequently increased again and reached 177 kN when the concrete on the compression side crushed. The load-midspan deflection curve of this beam is shown in Fig.4-142. This beam achieved its full theoretical strength even though it contained eight layers of CFRP laminate. The beam strength nearly doubled and the CFRP experienced rupture without any evidence of delamination.

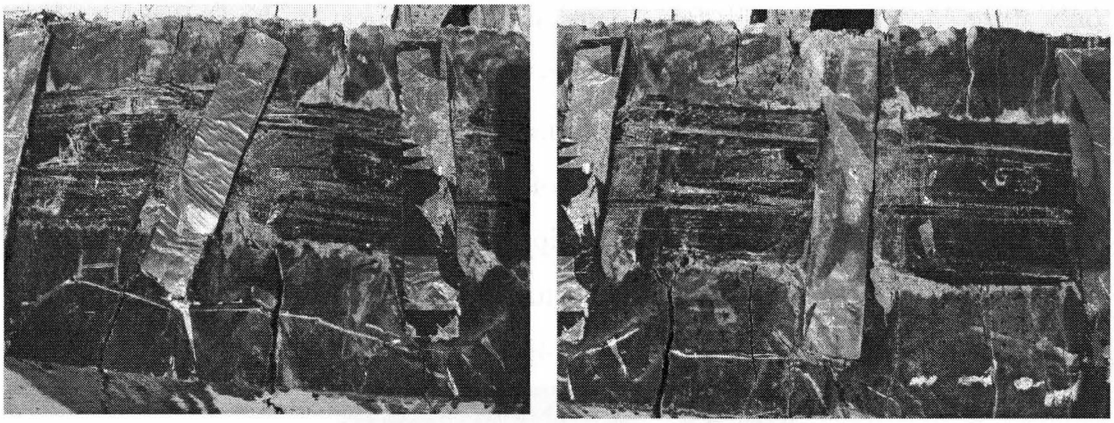

Fig.4-141: CFRP laminate rupture at midspan of beam B1-F8-E3-M17-b90

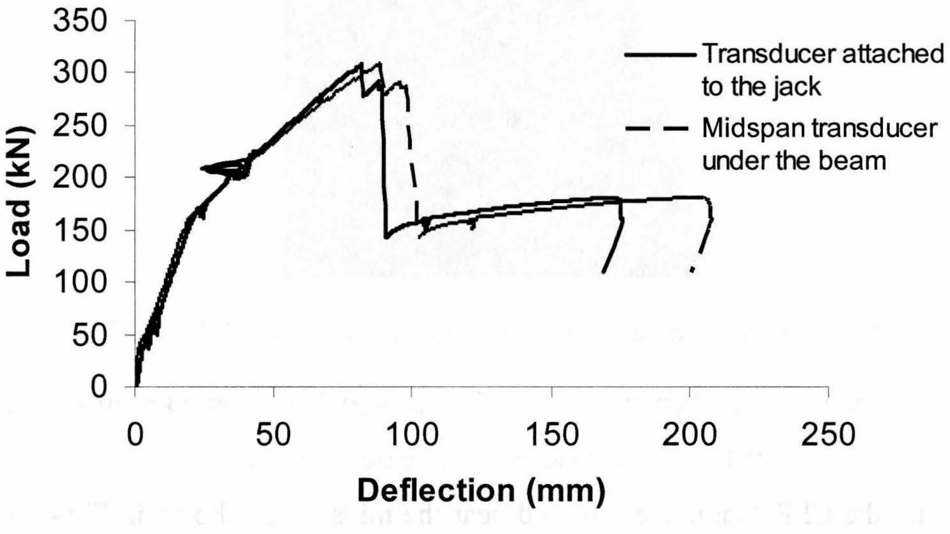

Fig.4-142: Load midspan deflection curve of beam B1-F8-E3-M17-b90

The strain variation along the internal reinforcement is plotted in Fig.4-143. Only three strain gauges were used under the load and in the mid-span. The maximum strain in the reinforcement reached 0.013 when the CFRP laminate ruptured at the midspan. This strain is nearly five times the yield strain of the bars. However, the strain distribution is not symmetric and this may be due to the fact that near the points adjacent to the flexural cracks the steel strain is generally much higher than between the cracks.

Figure 4-144 shows the strain variation along the laminate. As shown, the maximum strain recorded in the CFRP laminate was 0.0142 which is 85 % of its rupture strain; however, the laminate experienced rupture at midspan; therefore, the gauges may not have captured the actual rupture strain. Notice the nearly uniform strain distribution along the middle half of the laminate. It is quite clear that the anchors were able to distribute the stresses quite evenly along the interface and to avert stress concentrations. Figure 4-145 shows the crack spacing of the tested beam. The calculated shear stress variation along the CFRP laminate can be seen in Fig.4-146. The maximum shear stress is 5.0 MPa. As stated earlier, placing the anchors evenly along the beam length could be the reason for the multiple peaks in the vicinity of the anchors similar to the previous beam.

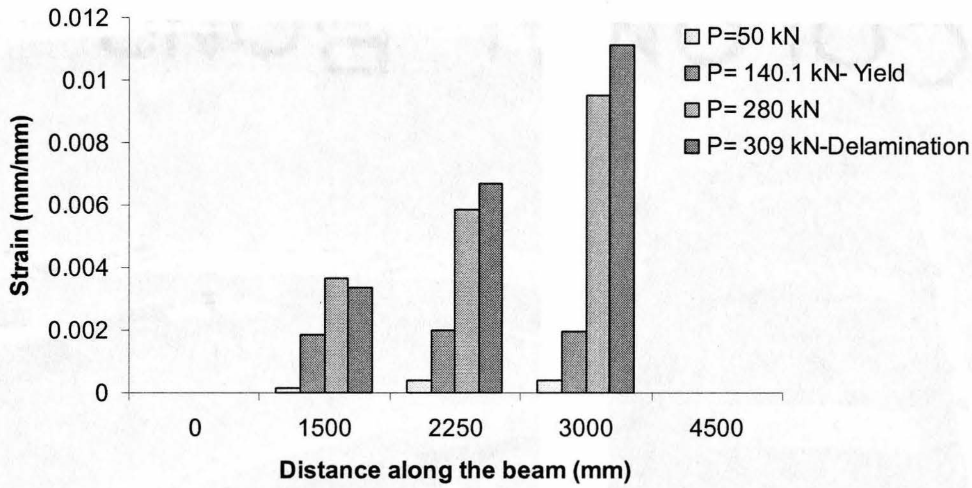

Fig.4-143: Strain profile on the internal reinforcement along the length of beam B1-F8-E3-M17-b90

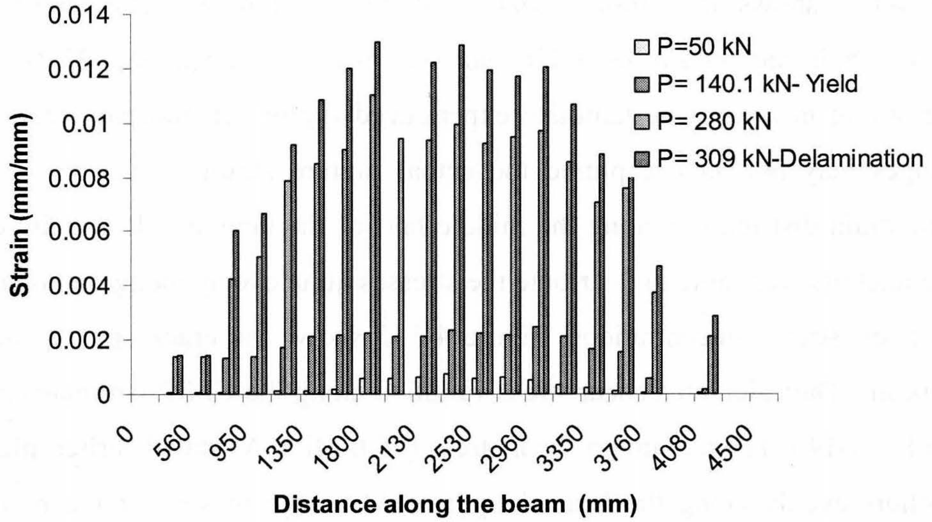

Fig.4-144: Strain profile on the CFRP laminate along the length of beam B1-F8-E3-M17-b90

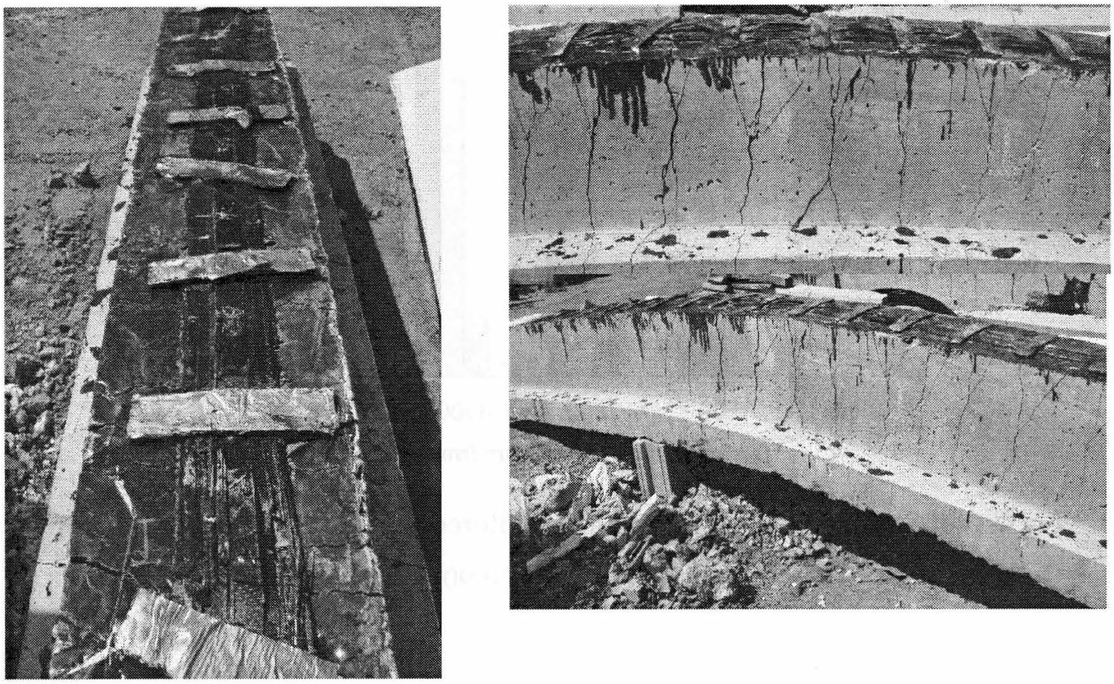

Fig.4-145: Beam deflection, crack spacing for beam B1-F8-E3-M17-b90

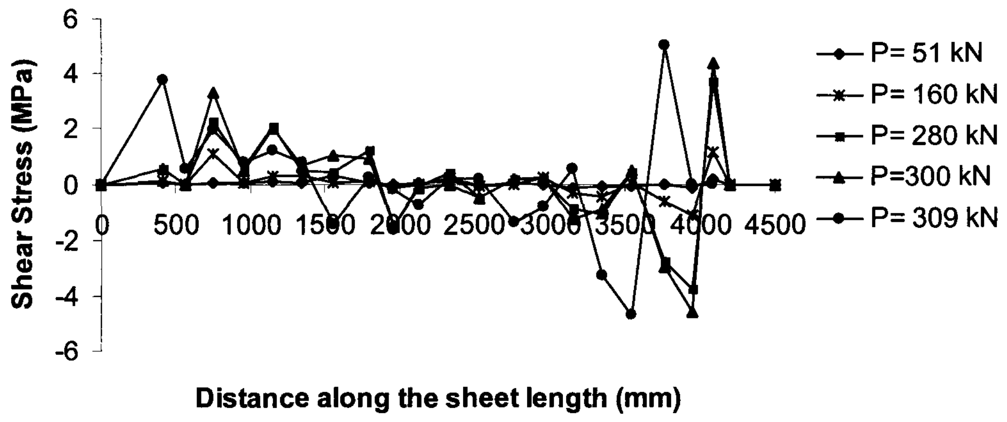

Fig.4-146: Shear stress distribution along the CFRP laminate of beam B1-F8-E3-M17-b90

4.7 Summary

Twenty one full scale beams, some external strengthened with CFRP laminates and anchored with the proposed anchors, were tested in externally flexure to investigate the effectiveness of the anchor to delay/prevent delamination. Test results showed that the proposed anchor has the potential to prevent delamination and to allow the FRP laminate to reach its ultimate rupture strain. It is important to mention that changing the CFRP laminate width to 90 mm, which allowed it to be placed between the anchor legs, such as in beams **B1-F4-E3-M15-b90** and **B1-F8-E3-M17-b90,** increased the capacity of the beams more compared to other beams with the full width of the web strengthened. This may be attributed to the fact that the CFRP laminate outside the anchor head could easily delaminate and thus trigger the delamination in other locations, rendering the laminate ineffective and causing a drop in its capacity. On the other hand, keeping the laminate within the anchor legs prevented the previous mode of failure and increased the beam capacity. Also, it was noticed that increasing the number of anchors in the mid-span region increases the capacity because it prevents premature delamination. In Beam **B1-F4-E3-M15-b90,** the spacing between the anchors at the end was maintained at 100 mm centre to centre. Maintaining the spacing as 200 mm in the mid-span region and 100 mm near the ends of the laminate proved effective in the present tests. Table 4-3 shows a summary of the key test results.

Table 4-3 : Summary of test results at failure

Beam designation	Experimental and theoretical results			
	FRP strain	Con. strain	Del. load	Ultimate load capacity (kN)
B1-F1-N	0.0167	0.0017	203.5	183.3
B2-F1-N	0.0167	0.0007	209	
B1-F1-E3	0.0167	0.0007	199.7	
B2-F1-E3	0.0167	0.001	198.2	
B1-F2-N	0.014	0.0009	230.1	252.8
B2-F2-N	0.01	0.0009	205.4	
B1-F2-E3	0.0093	0.0007	224.5	
B2-F2-E3	0.012	0.0015	216.7	
B1-F2-E3-M9	0.0124	0.0004	226.4	240.2
B1-F2-E4-M11	0.013	0.0005	234.5	
B1-F4-N-b90	0.0088	0.0007	199.6	227.6
B1-F4-E3-M15-b90	0.0157	0.0012	244	
B1-F4-N	0.0093	0.0008	252.7	390.1
B2-F4-N	0.01	0.0009	213	
B1-F4-E3	0.0095	0.0011	256.5	
B1-F4-E3-M9	0.01	0.0005	279.5	365.4
B1-F8-N-b90	0.0061	0.0008	214.6	340.5
B1-F8-E3-M17-b90	0.0142	0.0011	309	

It is quite clear from these test results that in order to prevent intermediate crack debonding failure mode in beams externally strengthened with FRP laminates of certain thicknesses, one must use anchors and the anchors must be evenly distributed. In the current tests, using the proposed anchor and by placing the laminate between the anchor rods, an anchor spacing of 200 mm was found to be adequate. Of course, this needs to be confirmed for other beam sizes and loading configurations, but before additional tests are performed; an analytical method must be developed to estimate the magnitude and distribution of interfacial stresses. Based on these stresses values, one may be able to determine the anchor spacing. In the next chapter an analytical method will be discussed which has the potential for developing a rational design method to prevent premature intermediate crack debonding.

CHAPTER 5
ANALYSIS

5.1 General

This chapter will focus on the analysis and discussion of the test results for the beams in phase III. In this phase, twenty one RC beams were designed, fabricated and tested in flexure. All the beams had the same dimensions and internal steel reinforcement, with the main test parameters being:

1. Amount of CFRP reinforcement.
2. Number/spacing of anchors.
3. Anchors distribution along the beam.
4. The width of the CFRP laminate.
5. The number of layers of the laminate.

Comparisons between the test results of the beams with and without anchors will be presented to investigate the effectiveness of the proposed anchor. The discussion will include the load at delamination, the drop in the load immediately after delamination, the ductility and energy absorption of the beams. The experimentally recorded FRP strain before debonding and at maximum load will be compared with the predictions of debonding strain equations or specified strain limits proposed in the literature. Finally, the theoretical ultimate capacity of the beams based on different guidelines and code provisions will be compared to the corresponding experimental values. To be able to propose a design equation for averting premature delamination, the FRP strain variation along the interface will be quantified, using a relatively simple but rigorous theoretical method based on composite beam theory. The results of this method will be compared with those obtained from a nonlinear finite element method (FEM), and based on the results of the beam theory, a procedure will be suggested for predicting the delamiantion load.

5.2 Analysis of Test Results

To investigate the effectiveness of the proposed anchor as to whether it enables the test beams to reach their theoretical strength, first the strength of each beam will be determined using the CSA A23.3-04 (CSA 2004) specifications. From the design point of view, this will be the maximum expected strength of each beam assuming failure is initiated by the rupture of the FRP. In the CSA method the following assumptions are made:

1- The stress strain relation of the CFRP laminate is linear elastic.
2- The stress strain relation of the tension reinforcement is elasto-plastic.
3- Strain compatibility and full bond between the FRP laminate and the concrete exist up to the failure load.

To gauge the effect of strain hardening on the ultimate capacity of these beams, their strength will be calculated using a simple strain-hardening behaviour for the reinforcing tension steel and the results will be compared with those obtained by the CSA method.

5.2.1 Ultimate Flexural Capacity

It may be recalled that after delamination the test beams reverted to regular under-reinforced RC beams and they failed due to the crushing of concrete at the extreme compression fiber. Once delamination occurred, the load dropped due to loss of stiffness caused by the ineffectiveness of the CFRP laminate, but the load subsequently increased, albeit not significantly, due to the upward movement of the beam neutral axis and the consequent increase in the internal lever arm. Table 5-1 shows the maximum load reached before delamination in the CFRP retrofitted beams or at failure in the control beams without CFRP. For the control beams, the predicted values including strain hardening are in better agreement with the experimental data. For the retrofitted beams, the predicted values based on the assumption of strain hardening are much higher than the corresponding maximum load measured. This is not unexpected because prior to delamination the maximum strain is the steel reinforcement is not expected to be within the strain hardening region, while after delamination the CFRP cannot resist any load, a fact that is ignored in the theoretical load calculation. Hence, in the case of the retrofitted beams, it is more logical to compare the delamination load with the corresponding theoretical load calculated without strain hardening. Based on the preceding argument, it can be seen that beams with one layer of FRP reached their theoretical capacity with or without end anchors. The slightly higher capacity of the beams without anchors may be due to the fact that the holes in the concrete made for inserting the anchor legs also go through the FRP laminate, which reduces the net FRP area and diminishes its tensile strength. Once delamination occurs in the FRP anchored at its ends only, the force throughout its length becomes equal, akin to an unbonded prestressed tendon, and due to the smaller cross-sectional area of the FRP at its ends, the maximum forces resisted by it is controlled by the capacity of its end sections.

None of the beams with two layers of FRP attained its theoretical strength. One of the beams without end anchors reached a maximum load of 230.1 kN which is 91% of its theoretical strength, while the maximum load in the beams with anchors reached 224.5 kN, or 88.8% of their theoretical capacity. It is obvious that the end anchors were unable to prevent slippage of the FRP in the anchor zone and enable the beams to reach their theoretical capacity.

Next we consider the beams with two layers of FRP and with both end and middle zone anchors. One of these beams with nine middle zone anchors reached a maximum load of 226.4 kN, which is 94.2% of its theoretical capacity based on the CSA method, while the beam with eleven middle zone anchors reached a maximum load of 234.5 kN, which is 97.6% of its theoretical ultimate capacity based on the CSA method. It is obvious that the placement of more anchors in the middle zone of the beams allowed them to achieve a higher load.

Table 5-1: Delamination load of retrofitted beams or ultimate load capacity of the control beams versus their theoretical ultimate load capacity

Beam designation	Delamination load (kN)	Ultimate load based on CSA A23.3		Observed mode of failure
		Without strain hardening (kN)	With strain hardening (kN)	
CB1	163.7	110.1	190.5	Yielding of steel followed by crush of concrete
CB2	192.7			
CB3	180.2			
B1-F1-N	203.5	183.3	219.3	CFRP rupture
B2-F1-N	209.0			
B1-F1-E3	199.7			
B2-F1-E3	198.2			
B1-F2-N	230.1	252.8	288.4	Yielding followed by delamination and concrete crushing
B2-F2-N	205.4			
B1-F2-E3	224.5			
B2-F2-E3	216.7			
B1-F2-E3-M9	226.4	240.2	275.8	Yielding followed by delamination and concrete crushing
B1-F2-E4-M11	234.5			
B1-F4-N-b90	199.6	227.6	263.3	Yielding followed by delamination and concrete crushing
B1-F4-E3-M15-b90	244.0			CFRP rupture
B1-F4-N	252.7	390.1	424.7	Yielding followed by delamination and concrete crushing
B2-F4-N	213.0			
B1-F4-E3	256.5			
B1-F4-E3-M9	279.5	365.4	400.1	Yielding followed by delamination and concrete crushing
B1-F8-N-b90	214.6	340.5	375.4	Yielding followed by delamination and concrete crushing
B1-F8-E3-M17-b90	309.0			CFRP rupture

Next let us consider the beams with four full width layers of FRP. The maximum load reached in one of the beams without any anchors was 252.7 kN or approximately 64.8% of its theoretical strength, while the beam with only end anchors reached a maximum load of 256.5 kN, or 65.7% of its theoretical capacity. On the other hand, the beam with nine middle zone anchors reached 76.5% of its theoretical capacity. Once again the middle anchors allowed the beam to carry higher load than the beams with no anchors or with only end anchors.

One of the observations during the test was that drilling holes through the FRP not only reduces its cross section, but it also disturbs the fibers adjacent to the holes and causes reduction in the beam resistance; hence, to avoid this problem, it was decided to place the laminate layers between the anchor legs. This has at least two advantages: first no hole is made through the laminate and second the anchor head is partially bonded to the concrete, which increases the anchor shear transfer capacity. To test the above hypothesis, first a beam with four layers of 90 mm wide laminate without any anchors was tested as a control specimen. This beam delaminated at 199.6 kN or 87.7% of its theoretical capacity. Its companion beam with both end and middle zone anchors, i.e. B1-F4-E3-M15-b90, delaminated at 244 kN, which is 7.2% higher than its theoretical capacity. The maximum load carried by the latter beam clearly demonstrated the effectiveness of the proposed anchor in this new configuration. In order to corroborate the latter configuration, two additional beams were tested. Beam B1-F8-N-b90 was retrofitted with eight layers of 90 mm wide FRP laminate without any anchors; it delaminated at 214.6 kN, or 63.1% of its maximum theoretical value. Its companion beam, B1-F8-E3-M17-b90, had the same amount and disposition of FRP reinforcement but was retrofitted with three anchors at each end and 17 evenly spaced middle zone anchors. This beam reached a maximum load of 309 kN, or 90.7% of its theoretical strength. However, it was observed during the test that the FRP ruptured; therefore, the cause of failure was not delamination. It is hypothesized that in the presence of anchors, the laminate may be subjected to some stresses perpendicular to the direction of its fibers in the vicinity of the edges of the anchor head. This may be the reason for the slightly premature rupture of the laminate. Considering the above results, particularly the high resistance of the beams retrofitted with either four or eight layers of the 90 mm wide laminate with anchors, it is obvious that the proposed anchor is effective in allowing the retrofitted beams to practically reach their theoretical capacity. However, this goal can only be achieved if the anchors are evenly distributed along the length of the laminate. Based on the current study, it would appear that 200 mm anchor spacing is sufficient to achieve FRP rupture rather than delamination. More study is needed to check the adequacy of this value for beams with different geometry, loading and FRP dispositions.

5.2.2 Load Drop after Delamination

The drop in load after delamination signifies the loss in the flexural stiffness of the beam caused by debonding. The magnitude of this drop is indicative of the extent of delamination and of the relative contribution of the external FRP to the flexural strength of a beam. Table 5-2 summarizes the maximum load sustained by each beam before delamination, P_{del}, and the load resisted by the beam immediately after delamination or rupture of the FRP, P_{drop}. The difference between these loads, designated by ΔP_{drop}, is the FRP contribution to the maximum load resisted by the beam. The magnitude of ΔP_{drop} for all the retrofitted beams is shown in column 4 of Table 5-2. Comparing beams B1-F1-N, B2-F1-N, B1-F1-E3 and B2-F1-E3 we observe in Table 5-2 that their loads dropped 64 kN, 61.9 kN, 64.9 kN and 23.6 kN respectively. Hence, as remarked earlier, in the case of beams strengthened with one layer of FRP, the anchors did not contribute either to a higher delamination load or to a greater stiffness. As for beams strengthened with two layers, with or without end anchors, their loads dropped 103.9 kN, 83.1 kN, 81.9 kN and 85.7 kN, respectively.

Table 5-2: Summery of delamination load and the drop in load after delamination for the tested beams

Beam Designation	$P_{del.}$ (kN)	P_{drop} (kN)	ΔP_{drop} (kN)	$\frac{\Delta P_{drop}}{P_{delm.}}$ %
B1-F1-N	203.5	139.5	64.0	31.4
B2-F1-N	209.0	147.1	61.9	29.6
B1-F1-E3	199.7	134.8	64.9	32.5
B2-F1-E3	198.2	174.6	23.6	11.9
B1-F2-N	230.1	126.2	103.9	45.2
B2-F2-N	205.4	122.3	83.1	40.5
B1-F2-E3	224.5	142.6	81.9	36.5
B2-F2-E3	216.7	131.0	85.7	39.5
B1-F2-E3-M9	226.4	146.7	79.7	35.2
B1-F2-E4-M11	234.5	147.4	87.1	37.1
B1-F4-N-b90	199.6	131.9	67.7	33.9
B1-F4-E3-M15 -b90	244.0	147.2	96.8	39.7
B1-F4-N	252.7	112.8	139.9	55.4
B2-F4-N	213.0	102.3	110.7	52.0
B1-F4-E3	256.5	118.7	137.8	53.7
B1-F4-E3-M9	279.5	154.5	125.0	44.7
B1-F8-N-b90	214.6	121.0	93.6	43.6
B1-F8-E3-M17 -b90	309.0	148.3	160.7	52.0

Hence due to the anchors, as column 5 of Table 5-2 indicates, the drop in load, relative to the delamination load, i.e. $\frac{\Delta P_{drop}}{P_{del}}$, for these beams was 45.2%, 40.5%, 36.5% and 39.5%, respectively, which indicates that the presence of the anchors did not prevent sudden delamination in these beams. However, when adding anchors in the zone of maximum moment, the drop in the load relative to the delamination was 35.2% and 37.1 % for beams B1-F2-E3-M9 and B1-F2-E4-M11, respectively, which shows that the performance of the beams was improved by adding more anchors in the midspan zone. Comparing beams B1-F4-N-b90 and

B1-F4-E3-M15-b90, the FRP in the former resisted 67.7 kN at delamination versus 96.8 kN in the latter, while their corresponding percent drop in loads were 33.9% and 39.7%, respectively. The same observation can be made for the two beams with 8 layers of CFRP laminate. The laminate in beams B1-F8-N-b90 and B1-F8-E3-M17-b90, resisted 93.6 kN and 160.7 kN load at delamination or rupture of the FRP. The percent drop in load after delamination was 43.6% and 52% respectively. It can be noticed from column 4 in Table 5-2, for beams strengthened with four layers, that for the beam with anchors at midspan, the drop was 44.7% compared to 55.4%, 52% and 53.7% for the companion beams with or without end anchors, respectively. Based on the above observations, the presence of the anchors did not lead to gradual delamination, but in the case of beams retrofitted with small width laminates and containing evenly distributed anchors in the middle zone of the beam, it essentially eliminated delamination. Although the failure was still brittle and sudden, accompanied with a big bang, these beams practically achieved their theoretical capacity.

5.2.3 Ductility

Ductility is a measure of the ability of a structure to undergo deformation without loss of significant strength. For an elasto-plastic response it is often measured in terms of deformation at ultimate to the deformation at yield while for responses that are not ideally plastic, there is no unique definition. In the case of FRP reinforced concrete, the response after the yielding of the internal steel reinforcement is due to the combination of the elastic response of the FRP and the plastic response of the reinforcing steel. Therefore, the post-yield response is neither completely elastic nor purely plastic. In this investigation, we will define ductility as the ratio of the beam maximum deformation at delamination to its maximum deformation at yield of the internal reinforcement, and this ratio is designated as μ. This definition of ductility is useful for assessing the level of deformation, relative to deformation at yield, that a beam can undergo before delamination. Beams with reasonably high μ values will give adequate warning of impending delamination and will be capable of absorbing sufficient energy before its occurrence. For the current test beams, the deflections at yield and delamination will be determined as shown in Fig.5-1.

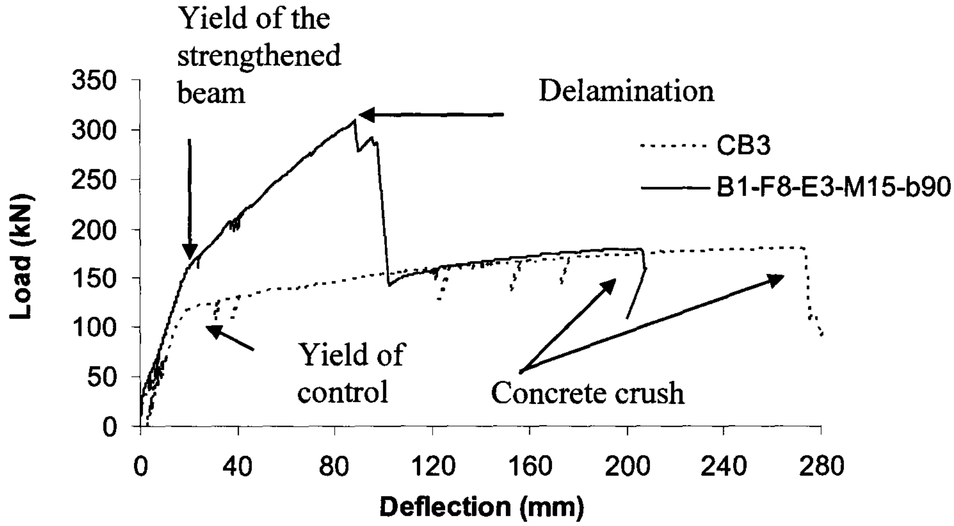

Fig.5-1: Load deflection curves of strengthened and un-strengthened beams

The figure shows typical load-midspan deflection curves for the control and one of the strengthened beams. Note that the strengthened beam reverts to the control beam after delamination and its ultimate deformation is only slightly less than that of the control beam, but the corresponding load is significantly lower than the delamination load. Practically, any loss of strength larger than 20% is often deemed to be detrimental to the effective performance of a member. Consequently, if the strengthened beam strength is only a maximum of 20% higher than the original unstrengthened beam, one can assume a negligible change in ductility, otherwise the ductility maybe based on the ratio of the maximum deformation at yield.

Table 5-3 shows the relevant deflection values necessary for calculating the ductility ratio for the beams tested here and the corresponding μ values. It is clear that all the strengthened beams have a noticeably lower ductility than the control beams, which is not unexpected. On the other hand, with the exception of beam B1-F2-N, all the strengthened beams without anchors have lower ductility than the beams with anchors, irrespective of the number and disposition of the anchors. More importantly, for the two beams strengthened with either four or eight layers of 90 mm wide laminate and with sufficient middle zone anchors, i.e. beams B1-F4-E3-M15-b90 and B1-F8-E3-M7-b90, the ductility ratios are 4.19 and 4.18, respectively, compared to their companion beams without anchors which had ductility ratios of 2.74 and 2.14. Thus the anchors increased these beams ductility ratio by 53% and 95%, while concurrently increasing their delamination loads by 22.5% and 44%, respectively.

Although the strengthening caused a reduction in ductility compared to the unstrengthened beams, in practice a ductility ratio larger than 4 is deemed acceptable even in seismic zones (Park and Paulay 1973)

5.2.4 Energy Absorption

The area under the load deflection curve of a beam is indicative of the total energy absorbed by it. The energy is generally comprised of elastic and plastic portions, with the latter being irrecoverable. Structures with a high plastic energy component are more ductile; however, in real structures, the high plastic energy is only beneficial if it is not accompanied by large reduction in the load capacity of the structure.

In this context, the energy absorption index, η, will be defined as the area under the load-deflection curve for the strengthened beams up to the delamination load divided by the area up to yielding of its reinforcement. The quantity η is indicative of energy based ductility. To calculate the area under the load-deflection curve, the curve will be approximated by two linear segments, one from zero load to the yield point and the other from the yield point to the delamination load. The data in Table 5-3 will be used to define the coordinates of the end points of these segments. Column 9 in Table 5-3 shows the energy absorption index of the strengthened beams. As mentioned earlier, beams retrofitted with one layer of FRP laminate, regardless of the presence of the anchors, had practically the same strength and stiffness and therefore, they did not require any anchorage system. As the last column in Table 5-3 shows, the presence of anchors increased the observed energy in every case and consequently increased the energy ductility of beams with anchors compared to their companion beams without anchors.

Table 5-3: Summary of the yield, delamination, failure loads and the corresponding deflections

Beam designation	Yield load (kN)	Defl.at yield (mm)	Del. load (kN)	Defl.at del. (mm)	Failure load (kN)	Defl.at failure (mm)	μ %	η kN.mm
CB1	119.9	27.4	-	-	163.7	186.2	6.79	14.7
CB2	128.7	32.8	-	-	192.7	220.5	6.72	-
CB3	122.9	25.1	-	-	180.2	179.9	7.16	-
B1-F1-N	133.5	29.2	203.5	84.2	176.9	228.0	2.88	13.15
B2-F1-N	136.0	20.3	209.0	90.7	175.7	213.5	4.46	14.65
B1-F1-E3	134.8	16.3	199.7	62.9	168.1	220.8	3.86	10.21
B2-F1-E3	134.3	20.0	198.2	98.2	174.0	211.0	4.91	16.02
B1-F2-N	136.7	16.4	230.1	75.5	165.8	203.0	4.61	10.97
B2-F2-N	147.6	24.9	205.4	56.1	170.7	199.9	2.25	7.14
B1-F2-E3	146.2	19.3	224.5	78.6	167.9	223.4	4.07	15.80
B2-F2-E3	148.75	19.5	216.7	67.6	182.8	215.3	3.47	11.18
B1-F2-E3-M9	149.2	20.0	226.4	69.6	168.6	142.9	3.49	13.24
B1-F2-E4-M11	144.8	19.7	234.5	76.7	163.9	142.4	3.90	15.10
B1-F4-N-b90	143.6	19.4	199.6	53.2	177.6	208.1	2.74	7.85
B1-F4-E3-M15-b90	147.2	19.9	244.0	83.4	177.2	185.9	4.19	15.84
B1-F4-N	156.2	15.5	252.7	51.0	174.5	238.0	3.29	8.35
B2-F4-N	150.2	17.2	213.0	35.3	179.1	276.1	2.06	5.58
B1-F4-E3	161.8	19.8	256.5	50.5	175.2	237.6	2.55	9.33
B1-F4-E3-M9	158.4	18.0	279.5	60.8	185.9	153.3	3.38	11.44
B1-F8-N-b90	158.0	19.2	214.6	41.0	176.4	211.5	2.14	6.72
B1-F8-E3-M17-b90	165.3	21.2	309.0	88.6	177.7	206.3	4.18	18.70

If we focus on the strengthened beams with 90 mm wide laminates, we observe that in beam B1-F4-E3-M15-b90 the energy ductility index increased by 69% compared to its companion beam without anchors while in beam B1-F8-E3-M17-b90 it increased by 275% compared to its companion beam B1-F8-N-b90.

5.2.5 Maximum FRP Strain

The most important aspect of the design of structures is their ability to satisfy the safety, or strength, and the serviceability requirements, but economic design is also a major goal. When using CFRP laminates for strengthening, brittle failure due to delamination may occur which will cause the strengthened member to fail well before the FRP reaches its tensile strength, and consequently it will prevent full utilization of the strength of the FRP. CFRP is considered an expensive material and delamination normally occurs when FRP strain is only between 40-60% of its ultimate strain, which means that at least 40% of the capacity of the material is wasted.

In this section, the increase in the CFRP laminate strain achieved due to the presence of anchors will be discussed. Table 5-4 provides a summary of the maximum recorded strains in the midspan zone for concrete (ε_c), bottom steel reinforcement (ε_s) and CFRP laminate (ε_f) at delamination for all the tested beams. It is clear from column 4 of the table that the recorded strains in the CFRP laminate in three of the four beams strengthened with one layer of FRP reached their ultimate strain as specified by the manufacturer, regardless of the presence of the anchors.

Table 5-4: Summary of recorded strains for the tested beams at delamination

Beam designation	Strain (mm/mm)			$\frac{\varepsilon_F}{\varepsilon_{Fu}}$
	ε_c	ε_s	ε_{FRP}	
CB1	0.00290	0.0450	-	-
CB2	0.00260	0.0200	-	-
CB3	0.00320	0.0840	-	-
B1-F1-N	0.00170	0.0110	0.01670	1.00
B2-F1-N	0.00070	0.0100	0.01670	1.00
B1-F1-E3	0.00070	0.0080	0.01670	1.00
B2-F1-E3	0.00100	0.0130	0.01430	0.86
B1-F2-N	0.00089	0.0070	0.01400	0.84
B2-F2-N	0.00089	0.0065	0.01000	0.60
B1-F2-E3	0.00007	0.0131	0.00930	0.56
B2-F2-E3	0.00146	0.0070	0.01200	0.72
B1-F2-E3-M9	0.00044	0.0016	0.01240	0.74
B1-F2-E4-M11	0.00050	0.0070	0.01300	0.78
B1-F4-N-b90	0.00140	0.0042	0.00860	0.51
B1-F42-E3-M15 -b90	0.00120	0.0028	0.01570	0.94
B1-F4-N	0.00077	0.0082	0.00934	0.56
B2-F4-N	0.00086	0.0078	0.01000	0.60
B1-F4-E3	0.00110	0.0062	0.00950	0.57
B1-F4-E3-M9	0.00047	0.0121	0.00988	0.59
B1-F8-N-b90	0.00075	-	0.00600	0.36
B1-F8-E3-M17 -b90	0.00100	0.0100	0.0130	0.85

The two beams strengthened with two layers of laminate and without anchors delaminated when the strain in the laminate reached 84% and 60% of its ultimate strain, respectively. Adding three anchors at the end zone did not contribute to the increase of the laminate strain at delamination. However, adding nine anchors in the zone of maximum moment, as in beams, B1-F2-E3-M9 and B1-F2-E4-M11, allowed the laminate to achieve 74% and 78% of its ultimate strain, which is slightly higher than the beams with only end anchors.

Beam B1-F4-N-b90, which had four layers of FRP but no anchors, delaminated when the strain in the FRP reached 51% of its ultimate value while in its companion beam, B1-F4-E3-M15-b90, with anchors the maximum strain it reached 94% of its ultimate value. In fact, based on visual inspection during the test, it was noticed that the CFRP laminate had ruptured, and it is quite possible that the strain gauges had failed before the actual maximum strain occurred. Therefore, it can be argued that the anchors allowed the CFRP laminate reach its ultimate strain.

In the case of the beams with four layers of full width FRP and no anchors, the delamination occurred at 56% and 60% of the laminate ultimate strain capacity; adding anchors at the end and the midspan zones did not significantly contribute to increased strain at delamination.

Beam B1-F8-N-b90 delaminated when the FRP strain was only 36% of its ultimate value versus 85% in its companion beam (B1-F8-E3-M17-b90) with anchors. However, based on visual inspection during the test, it was noticed that the FRP had ruptured. Notice that beams without anchors, except for the beams with only one layer if FRP, delaminated at strain values ranging between 60-80% of the FRP ultimate strain, which agree with the values reported in the literature. The fact that the anchors, when properly disposed, allowed the FRP to reach its ultimate strain makes it possible to exploit the full strength of the FRP.

Table 5-4 also shows the maximum concrete and internal steel reinforcement strains at delamination. In the strengthened beams, the concrete strain is less than 0.0015 and in most cases less than 0.001. These values are substantially less than the ultimate strain capacity of concrete, which is in the range of 0.0035-0.004. In the present context, the strain value does not have much significance other than the fact that as far as concrete is concerned, the beam has significantly higher capacity for strengthening than executed in the current investigation. The steel strain values are all greater than its nominal yield strain value of 0.002, and in many cases four times or greater than the yield strain. This means that in none of the beams the FRP delaminated before the steel yielded.

In the light of the above discussion about the effectiveness of the proposed anchor in delaying/preventing delamination, it is reasonable to state that delamination could be essentially prevented and the FRP laminate could practically reach its ultimate strength in the presence of properly disposed anchors. Since in this study the anchor position, distribution and spacing were investigated here, it was found that having anchors in the midspan is vital and end anchors alone can not prevent delamination and FRP slippage in beams where delamination initiates in the midspan zone. To date there is no robust method available for designing anchorage systems in FRP retrofitted beams and the available guidelines or code provisions normally specify limits for the strain or the stress of the FRP laminate to calculate the delamination load.

To check the applicability of these guidelines to the beams tested here, recommendations for preventing intermediate crack debonding in structures externally strengthered with FRP laminate will be reviewed. Reference can be made to Table 2-1 in Chapter 2 for more details about these methods. Notice that the ACI 440.08 Committee (2008) debonding strain limits will be used instead of the older ACI 440.02 Committee (2002) limit that has been generally used in the literature.

Table 5-5 summarizes the various parameters which normally appear in the available debonding strain limit equations. Note that the CSA Standard A23.3-04 defines the concrete flexural tensile strength, f_t, as modulus of rupture and as assumes it equal to $0.6\sqrt{f_c^{'}}$, where $f_c^{'}$ is the concrete compressive strength. Notice that the current test beams were made of two different concrete batches with a compressive strength of either 54 MPa or 59.5 MPa.

Table 5-5: Summary of parameters used in all the guidlines and proposed equations for the tested beams

Beam Designation	n	E (GPa)	t (mm)	f'_c (MPa)	f_t (MPa)	b_f (mm)	b_c (mm)	β(Teng et al. 2003)	β (Lu 2004)	A_{FRP} (mm^2)
CB1	-	-	-	54.0	4.4	-	250	-	-	-
CB2	-	-	-	59.5	4.6	-	250	-	-	-
CB3	-	-	-	59.5	4.6	-	250	-	-	-
B1-F1-N	1	227	0.165	54.0	4.4	220	250	0.772	0.802	36.3
B2-F1-N	1	227	0.165	59.5	4.6	220	250	0.772	0.802	36.3
B1-F1-E3	1	227	0.165	54.0	4.4	220	250	0.772	0.802	36.3
B2-F1-E3	1	227	0.165	59.5	4.6	220	250	0.772	0.802	36.3
B1-F2-N	2	227	0.165	54.0	4.4	220	250	0.772	0.802	72.6
B2-F2-N	2	227	0.165	59.5	4.6	220	250	0.772	0.802	72.6
B1-F2-E3	2	227	0.165	54.0	4.4	200	250	0.816	0.841	66
B2-F2-E3	2	227	0.165	59.5	4.6	220	250	0.772	0.802	72.6
B1-F2-E3-M9	2	227	0.165	54.0	4.4	200	250	0.816	0.841	66
B1-F2-E4-M11	2	227	0.165	54.0	4.4	200	250	0.816	0.841	66
B1-F4-N-b90	4	227	0.165	59.5	4.6	90	250	1.098	1.083	59.4
B1-F4-E3-M15-b90	4	227	0.165	59.5	4.6	90	250	1.098	1.083	59.4
B1-F4-N	4	227	0.165	54.0	4.4	220	250	0.772	0.802	145.2
B2-F4-N	4	227	0.165	59.5	4.6	220	250	0.772	0.802	145.2
B1-F4-E3	4	227	0.165	54.0	4.4	220	250	0.772	0.802	145.2
B1-F4-E3-M9	4	227	0.165	54.0	4.4	200	250	0.816	0.841	132
B1-F8-N-b90	8	227	0.165	59.5	4.6	90	250	1.098	1.083	118.8
B1-F8-E3-M17-b90	8	227	0.165	54.0	4.4	90	250	1.098	1.083	118.8

The capacity of all the beams were calculated based on their actual compressive strength, but the difference in the calculated delamination load would be less than 1% if one were to use the actual concrete strength versus its specified strength of 54 MPa. Therefore, for simplicity it was decided to use $f_c^{'} = 54$ MPa in all the calculations. In the latter table, n, t_f , b_f and A_f refer to the number of layers, thickness, width and cross-sectional area of the FRP laminate, respectively. The quantity β was defined earlier in section 2.3.3, while b_c is the width of the beam web.

Table 5-6 summarizes the expected FRP delamination strains for the current test beams based on some well known methods or recommendations. Note that the strain limits for the same beams based on the different recommendations vary by almost 300% in some cases. Clearly, they can not be all correct and some may be on the unconservative side while others maybe highly conservative.

The predicted capacities of the tested beams based on the strain limits in Table 5-6 are shown in Table 5-7. These capacities are calculated based on the assumption of full bond between the CFRP laminate and the concrete. To be able to calculate these loads based on the strain compatibility approach, the compression strain in the concrete top fiber or the depth of the neutral axis has to be known. Since neither is known in advance and since the corresponding compression strain in the concrete is expected to be far less than its maximum value of 0.0035 specified by the Canadian Standard CSA A.23.3-04, a trial and error procedure involving strain compatibility and the constitutive relations of concrete and steel reinforcement need be applied to satisfy the equilibrium requirements at delamination. Here, the process was started by assuming the location of the neutral axis and setting the strain in the FRP equal to the pertinent limit strain in Table5-6.

Next, based on strain compatibility, the maximum compressive strain in the concrete was determined. Since in each case the maximum compressive strain in the concrete was less than 0.0035, the values of the rectangular compression block parameter α_1 and β_1, corresponding to the calculated maximum concrete strain had to be determined.

Table 5-6: Calculated strain limits (millistrain) in FRP at delamination based on different guidelines and proposed methods in the literature

<table>
<tr><th>Beam Designation</th><th>ACI (08)</th><th colspan="2">Fib 14-1 (01)</th><th>JSCE (01)</th><th>SIA 166 (03)</th><th>TR55 (04)</th><th>CNR (02)</th><th>S806-02</th><th>Werner et al. (03)</th><th>Teng et al. (03)</th><th>Lu (04)</th><th>Said and Wu (08)</th><th>Neale et al. (09)</th></tr>
<tr><td>CB1</td><td>-</td><td>-</td><td>-</td><td>-</td><td>-</td><td>-</td><td>-</td><td>-</td><td>-</td><td>-</td><td>-</td><td>-</td><td>-</td></tr>
<tr><td>CB2</td><td>-</td><td>-</td><td>-</td><td>-</td><td>-</td><td>-</td><td>-</td><td>-</td><td>-</td><td>-</td><td>-</td><td>-</td><td>-</td></tr>
<tr><td>CB3</td><td>-</td><td>-</td><td>-</td><td>-</td><td>-</td><td>-</td><td>-</td><td>-</td><td>-</td><td>-</td><td>-</td><td>-</td><td>-</td></tr>
<tr><td>B1-F1-N</td><td rowspan="4">15.0</td><td rowspan="18">6.5</td><td rowspan="18">8.5</td><td rowspan="4">5.2</td><td rowspan="18">8.0</td><td rowspan="18">8.0</td><td rowspan="4">10.9</td><td rowspan="18">7.0</td><td rowspan="18">6.5</td><td rowspan="4">5.2</td><td rowspan="4">13.1</td><td rowspan="4">12.8</td><td rowspan="4">8.9</td></tr>
<tr><td>B2-F1-N</td></tr>
<tr><td>B1-F1-E3</td></tr>
<tr><td>B2-F1-E3</td></tr>
<tr><td>B1-F2-N</td><td rowspan="6">11.0</td><td rowspan="6">3.7</td><td rowspan="4">7.7</td><td rowspan="4">3.7</td><td rowspan="4">9.2</td><td rowspan="4">10.0</td><td rowspan="4">8.0</td></tr>
<tr><td>B2-F2-N</td></tr>
<tr><td>B1-F2-E3</td></tr>
<tr><td>B2-F2-E3</td></tr>
<tr><td>B1-F2-E3-M9</td><td rowspan="2">7.8</td><td rowspan="2">3.9</td><td rowspan="2">9.6</td><td rowspan="2">10.0</td><td rowspan="2">8.2</td></tr>
<tr><td>B1-F2-E4-M11</td></tr>
<tr><td>B1-F4-N-b90</td><td rowspan="6">7.8</td><td rowspan="6">2.6</td><td rowspan="2">5.8</td><td rowspan="2">3.7</td><td rowspan="2">8.6</td><td rowspan="2">7.9</td><td rowspan="2">8.3</td></tr>
<tr><td>B1-F4-E3-M15-b90</td></tr>
<tr><td>B1-F4-N</td><td rowspan="3">5.4</td><td rowspan="3">2.6</td><td rowspan="3">6.4</td><td rowspan="3">7.9</td><td rowspan="3">6.1</td></tr>
<tr><td>B2-F4-N</td></tr>
<tr><td>B1-F4-E3</td></tr>
<tr><td>B1-F4-E3-M9</td><td>5.5</td><td>2.7</td><td>6.7</td><td>7.9</td><td>6.5</td></tr>
<tr><td>B1-F8-N-b90</td><td rowspan="2">5.5</td><td rowspan="2">1.8</td><td rowspan="2">4.1</td><td rowspan="2">2.6</td><td rowspan="2">6.0</td><td rowspan="2">6.2</td><td rowspan="2">6.8</td></tr>
<tr><td>B1-F8-E3-M17-b90</td></tr>
</table>

Table 5-7: Experimental versus predicted ultimate capacity of test beams

Beam designation	Test results	ACI (08)	Fib 14-1		JSCE (01)	SIA 166 (03)	TR55 (04)	CNR (02)	S806-(02)	Werner et al. (03)	Teng et al. (03)	Lu (04)	Said et al. (08)	Neale et al. (09)
			0.65 %	0.85 %										
CB1	163.7	-	-	-	-	-	-	-	-	-	-	-	-	-
CB2	192.7	-	-	-	-	-	-	-	-	-	-	-	-	-
CB3	180.2	-	-	-	-	-	-	-	-	-	-	-	-	-
B1-F1-N	203.5	175.8	137.8	146.9	131.7	144.6	144.6	157.5	140.1	137.8	131.8	167.5	166.0	148.9
B2-F1-N	209.0													
B1-F1-E3	199.7													
B2-F1-E3	198.2													
B1-F2-N	230.1	203.7	164.7	182.1	139.4	177.7	177.7	175.1	169.0	164.7	139.6	188.0	195.5	177.8
B2-F2-N	205.4													
B1-F2-E3	224.5													
B2-F2-E3	216.7													
B1-F2-E3-M9	226.4	195.5	159.8	175.9	136.7	171.7	171.7	169.8	163.8	159.8	138.6	184.7	187.9	173.2
B1-F2-E4-M11	234.5													
B1-F4-N-b90	199.6	164.2	132.9	169.3	125.8	165.7	165.7	149.6	158.5	154.9	134.3	170.3	164.9	168.2
B1-F4-E3-M15-b90	244.0													
B1-F4-N	252.5	239.8	217.9	251.9	150.4	243.4	243.4	199.8	226.4	217.9	150.5	216.2	241.5	211.9
B2-F4-N	213.0													
B1-F4-E3	256.5													
B1-F4-E3-M9	279.5	228.0	208.3	239.3	146.6	231.5	231.5	192.4	216.0	208.3	149.2	211.5	229.7	208.0
B1-F8-N-b90	214.6	184.6	198.6	226.6	131.5	219.6	219.6	164.4	205.6	198.6	143.2	191.2	194.0	203.2
B1-F8-E3-M17-b90	309.0													

This was accomplished by assuming the concrete compressive stress-strain relationship to vary according to the Hognestad parabolic relationship (Park and Paulay 1973) and the rectangular stress block parameters were calculated by integrating the area under this curve and by finding its centroid as described by

Collins and Mitchell (1999). Note that the resultant compression force in concrete, C, is given by $\alpha_1 f_c^{'} \beta_1 c b_f$,where c is the depth of the neutral axis. The force C acts at $\frac{\beta_1 c}{2}$ from the extreme compressive fiber.

In this manner, the location of the neutral axis and the top compression strain were determined. Fig.5-2 shows schematically the stress (force) and strain distribution along the beam height.

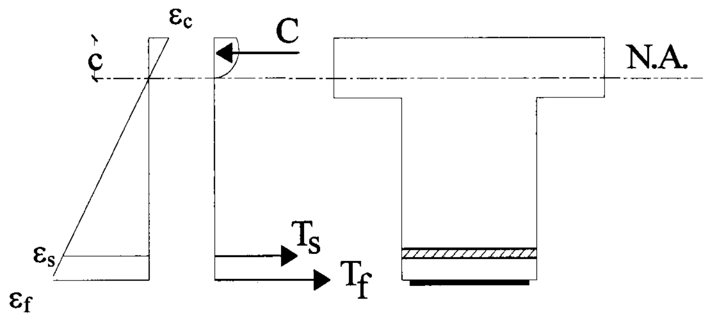

Fig.5-2: Strain profile along the beam height

Note that all the available guidelines/methods specify the strain limit for beams without any anchorage system, therefore, the predicted delamination load based on these limits should be compared to the observed delamination load in beams without anchors. For beams without anchors and with up to four layers of laminate, most of the available methods, except the JSCE (2001) and Teng et al.(2003) methods, give similar results, albeit the ACI method gives overall more accurate results. The JSCE and Teng et al. methods consistently underestimate the actual strength of the beams. The ACI method tends to give less accurate results for the beams with reduced laminate width. Methods which specify a single strain limit, regardless of the number of FRP layers or the geometry of the laminate, such as the CSA S806-02 method, tend to underestimate the actual strength of the beams retrofitted with one or two layers of FRP. On the basis of these results, the specifications of a single strain limit for all retrofit cases are not appropriate.

For the beams with anchors and with up to four layers of full width FRP, the same level of accuracy as in the case of the beams without anchors is observed.

However, all the methods severely underestimate the actual strength of beams B1-F4-E3-M15-b90 and B1-F8-E3-M17-b90. The highest predicted strengths of these beams are 170 kN (Lu's method) and 226.6 kN (fib method) versus their actual strength of 244 kN and 309 kN, respectively, while their lowest predicted values are 125.8 kN and 131.5 kN (JSCE method). It is obvious that the existing strain limits cannot be applied to beams with effective anchorage system, and a revised method is required to include the effect of anchors on the delamination load of retrofitted beams.

5.3 Interfacial Stresses

The development of a stress-based design method for beams externally reinforced with FRP is generally considered problematic because the determination of the stresses at the FRP-concrete interface can be very complex due to the advent of cracking and the associated slip and stress concentrations which follow. Therefore, for simplicity most of the available standards/guidelines make the delamination load a function of the maximum strain in the FRP laminate. The maximum strain is either limited to a specified value or made a function of the axial rigidity of the laminate and the concrete compressive strength. However, by limiting the FRP strain to values well below its tensile rupture strain, the full capacity of the material will not be fully utilized. The available methods for predicting the interfacial shear and normal stresses are based on many assumptions, including linear elastic behaviour and uncracked sections, neither of which is generally true at delamination; therefore, this issue requires more investigation. The fact that delamination can start near midspan in the zone of maximum moment makes it difficult to predict the delamination load. Whereas the plate end delamination can be related to the maximum interfacial shear using approximate analytical methods, the delamination in the midspan zone occurs in regions that are theoretically under constant moment and according to the Euler-Bernoulli beam theory, free of any shear stress. Therefore, based on conventional methods of analysis, delamination should not occur in this region. Yet, in the beams tested in this investigation, the delamination always initiated in this region. Therefore, in this study, the delamination due to intermediate crack debonding (ICD) will be further investigated since it is one of the failure modes which require more attention.

In the zone of maximum moment, the beam experiences more flexural cracks and the external reinforcement in the form of CFRP laminate has to accommodate the increase in the curvature caused by cracking. The fact that the crack spacing is not known makes it hard to determine the location where the delamination might initiate. The distribution of stresses at the laminate concrete interface between flexural cracks is complex because the cracks act as stress risers and accelerate delamination. To properly predict delamination in the midspan or constant moment zones, one must include in the analysis the cracks or their effect on the interfacial stresses. To be able to come up with a design method, the shear and normal stress distribution along the interface as well as the strain variation need to be computed. In this investigation, two approaches will be considered to deal with the latter phenomena.

First, a model based on non-linear finite element analysis procedures will be described. The well known softwear LS- DYNA (2007) will be used to determine the interfacial strain variation before delamination and the load deflection curves for the tested beams. Furthermore, the predicted load versus strain diagrams will be compared with the experimental results.

The second model is an analytical model based on beam theory, but it considers slippage at the FRP-concrete interface. This model has been used by a number of investigators in the past, including Roberts (1989) and Taljsten (1997), but these earlier versions are based on the assumptions of linear elasticity, without any consideration of inelasticity, even in the case of a reinforced concrete beam which may experience significant nonlinearity due to concrete cracking and internal steel reinforcement yielding. Recently, Youssef (2006) showed a procedure for the extension of the previous models to beams undergoing inelastic deformations. More specifically, he analyzed the response of a steel section reinforced with GFRP laminate along its tension flange and showed good agreement between the observed delamination load and its corresponding calculated value. Unlike concrete, steel sections do not involve cracking; nevertheless, the approach has the potential for extension to RC members and this will be explored in the current study.

5.4 Overview of the Finite Element Analysis

The finite element method (FEM) as a general method of analysis can be theoretically used to obtain a more accurate distribution of the strains and stresses at the FRP laminate-concrete interface. Practically, however, the degree of accuracy of such an analysis will depend on the extent to which the finite element model can predict the actual location and movements of cracks in reinforced concrete members and on the accuracy of the constitutive laws for cracks. Cracks in concrete are modelled in two ways, smeared or discrete cracks. The former cannot predict the actual crack location and movements, but their effects are accounted for in an average sense by adjusting the constitutive matrix of the concrete and reinforcement tributary to the point where stresses and strains are evaluated. Normally, the stress evaluation points are the Gauss quadrature points.

On the other hand, discrete cracks can be modelled by FEM if the initial crack locations and geometries are known. In reinforced concrete, the cracks are caused either by applied loads or by shrinkage and thermal stresses, but the latter type of cracks cannot be defined, either in terms of location or geometry, their approximate locations and geometries can be only estimated. Once the concrete tensile stress is found to exceed its tensile strength, a crack is preassumed to have formed, and the elements topology is modified by remeshing the finite element model. This is still an approximate method and is rarely used in reinforced concrete FEM analysis programs; the most common method is the smeared crack model. Hence, in this study a smeared crack model will be used. It is expected that this will provide an approximate distribution of interfacial strains, but it may not be able to predict the stress concentrations in the vicinity of actual cracks, which often trigger delamination. Nevertheless, getting a sense of the accuracy of this distribution by comparing it with experimental data and the beam theory model results would be useful. Many researchers [Teng et al., 2002, Yang et al, 2003, Hsuan et al. 2004, Seyed et al., 2007,Abdel Baky et al., 2007, Mostafa and Razaqpur 2008] have used the finite element method to predict the delamination load and the beam post-peak response as well as the interfacial strain variation, with various degrees of success.

The majority of the finite element analyses to date have failed to predict the post-peak load or descending portion of the response due to the complex behaviour of these interfaces, and the lack of suitable constitutive relations for them. The post-peak load response may involve negative stiffness; consequently, the stiffness matrix would no longer be positive definite. This phenomenon creates difficulty in most FEM programs and as a result the solution is often terminated once the load has reached its peak value. Although from the strengthening point of view, the peak load is the main quantity of interest, from the energy absorption and ductility perspective, the total response of the structure is important. The post-peak response is indicative of the type of delamination, i.e. partial or total delamination. Partial delamination may lead to a reduction in strength, but it may allow the member to continue to carry substantial load at the expense of gradual strength reduction. This type of behaviour is of particular interest in the case of structures subjected to seismic or blast loads. Consequently, in this investigation, the nonlinear dynamic analysis approach is adopted to analyze the T beams tested here. The analysis is performed using dynamic analysis in conjunction with velocity control. The velocity is imposed in such a manner that its time variation is essentially insignificant. The solution of the dynamic equations of equilibrium prevents the numerical instability problems caused by the negative stiffness of a member. The distinguishing feature of the present analysis is that it can capture the initiation and propagation of the delamination process, the post-peak load response, the crack pattern, and the failure load of the member. Furthermore, the strain profile along the interface will be compared with the recorded strain values measured during the test.

LS-DYNA (2007) is designed to analyze the large deformation static and dynamic response of structures, including the interaction between fluids and structures. The main solution methodology is based on explicit time integration. In the explicit approach, the internal and external forces are summed at each node, and a nodal acceleration is computed by dividing the computed force by the nodal mass. The solution is advanced by integrating this acceleration in time. The maximum time step size is limited, producing an algorithm which typically requires many relatively inexpensive time steps. Explicit analysis is well suited to dynamic simulations such as impact and crash, but it can become extremely expensive to conduct long duration or static analyses. The disadvantage of using the implicit solution is the large numerical effort required to form, store and factorize the stiffness matrix since the global stiffness matrix is computed, inverted and applied to the nodal out of balance force to obtain a displacement increment. The advantage of this approach is that the time step size may be selected by the user.

5.4.1 Finite Element Idealization

Finite Element Mesh

All the beams were modeled using a 3D-8 node solid element with three translational degrees of freedom (DOF). As indicated in Fig.5-3, each beam was discretized by twenty elements along its height, ten elements across its width and 192 elements along its length. The elements aspect ratio was maintained as 1:1 in the x -z directions and 1:1.25 in the x-y directions where x,y and z are Cartesian axes running parallel to the beam length, height and width, respectively. The internal transverse and longitudinal reinforcement were modeled using bar or truss elements, with two end nodes and three displacement DOF. The beam elements were fully connected with the solid element at the nodes. The FRP laminate was modeled using the 4-node 3D shell element. Each node has six DOF, three translations and three rotations. Due to its back connection with the solid element, the program automatically takes care of the incompatibility between the DOF of the solid and shell elements. The interface between the concrete surface and the CFRP laminate was modeled using the 4 point cohesive elements with offset for use with shell elements.

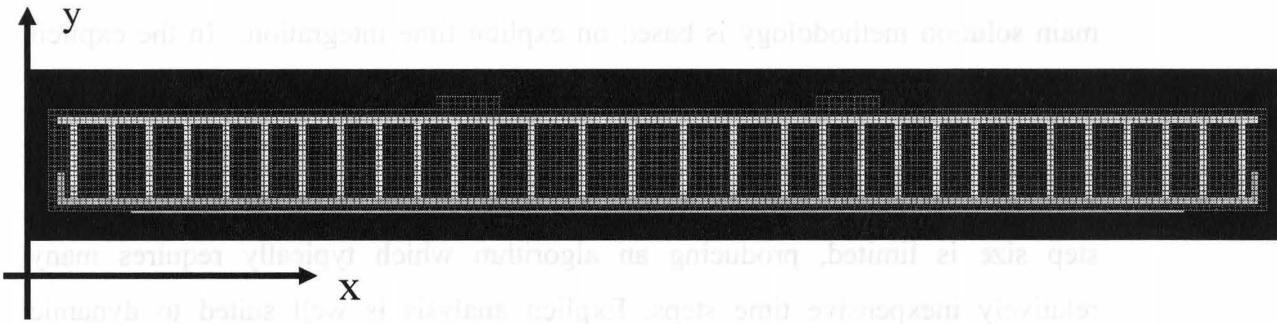

Fig.5-3: 2D view for typical modeled beam

To avoid artificial stress concentrations under the loading points, the steel loading plates were discretized as rigid elements. The supporting plates were not modelled because there were no expectations of failure at the supports and the laminate was cut-off at some distance from these plates. Finally, full bond between the concrete and the internal reinforcement was assumed throughout the loading range until failure.

Material Constitutive Laws

The concrete material model in LS-DYNA selected in the present analysis is termed *Mat_Winfrith_Concrete* (Broadhouse and Neilson 1987, Broadhouse 1995). As described in the LS-DYNA manual, this model is known as a smeared crack or pseudo crack model. The concrete is initially treated as a linear material within a defined yield surface that is expressed in terms of the invariants of the stress tensor, and which in the principal stress space has the form of a paraboloid oriented on the hydrostatic axis. After yielding in compression, the material is assumed to undergo plastic flow, but is allowed to crack in the tensile principal stress directions. After cracking, to account for the tension resisted by the concrete between the cracks, tension stiffening is assumed. The input parameters used in this concrete model include the concrete mass density, initial tangent modulus, Poisson's ratio, uniaxial compressive and uniaxial tensile strength, crack width at which tensile stress normal to the crack becomes zero, aggregate size and strain rate effect, if any.

The material model used for steel reinforcement is termed *MAT_PIECEWISE_LINEAR_PLASTICITY_TITLE*. In this model, the stress-strain relationship of steel is assumed to be piecewise linear with the first linear segment starting at zero stress and terminating at the yield point. In the present analyses, the stress-strain relationship of the reinforcement obtained from the ancillary tests [See section 3.4.4.] was used to construct the piecewise linear model. The material model used for the CFRP laminate is called *MAT_ELASTIC_TITLE* which assumes linear elastic behaviour until failure. The input parameters are elastic modulus, density and Poisson's ratio of the CFRP.

The model *MAT_COHESIVE_GENERAL_TITL*E in LS-DYNA was used for the cohesive element. The cohesive element was used to model the CFRP- concrete interface. In fact, this element is essentially made of three nodal springs which can be used to model separation and slippage in the directions normal and tangent to the interface. The model includes three general irreversible mixed-mode iteration cohesive formulations with arbitrary normalized traction-separation. The interaction between fracture modes I and II is considered in this model and irreversible conditions are enforced via a damage formulation. Details are provided in the LS-DYNA user manual (2007). Notice that whenever possible the input values used were based on the data from the coupon tests on the steel rebars, and the concrete cylinders in compression and tension. The material properties for the FRP laminate were taken from the data sheet provided by the manufacturer. The interface parameters were basically the traction- separation curve in the normal and tangential directions. The values for the shear and normal stresses were selected based on the suggested values found in the literature [El-Mihilmy and Tedesco 2001] and are shown in Fig.5-4, where t is the traction and δ is the separation. These quantities are normalized to their maximum permissible values in Fig.5-4.

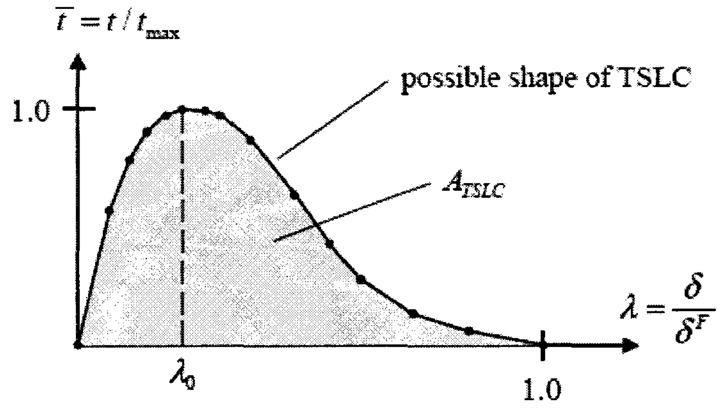

Fig.5-4: Normalized traction separation law

Input-Data, Loading and Boundary Conditions

As mentioned earlier, the material input-data used in the current investigation were based on the experimental values or on the values provided by the manufacturer of the FRP laminate. The material properties used for the concrete model are as follow: mass density = 2400 kg/m^3, concrete elastic modulus = 33068 MPa, Poisson's ratio=0.18, concrete compressive strength = 54 MPa, Concrete tensile strength= 5.4 MPa. The material properties for the longitudinal and transverse reinforcement are as follow: yield strength = 400 MPa, Poisson's ratio=0.30, mass density = 7850 kg/m^3,. a linear elastic material model is used for the FRP laminate defined by the FRP laminate elastic modulus = 227 GPa, mass density = 1800 kg/m^3 and Poisson's ratio=0.30. As for the cohesive elements, which represent the adhesive material, the material properties are defined as follow: mass density = 1.9 kg/m^3 , fracture toughness/energy release rate for mode I and mode II = 0.16, peak traction in normal (mode I) and tangential (mode II) directions = 4 and 10 MPa, respectively.

All the beams were loaded in four point bending. The solution was obtained using velocity control by defining a velocity curve rising over a long time to simulate the static applied on the loading plates. To be able to simulate the hinge and the roller supports, the nodes at these locations were appropriately restrained. The time step was allowed to be automatically chosen by the program and no damping was used because initial trials with different damping ratios had little effect on the final results. In this investigation, only the control beam and the beams externally strengthened with CFRP laminate without anchors were modeled. Modelling of the anchors is easy in theory, but obtaining suitable constitutive relations for the anchors is a task that needs more investigation.

5.4.2 Results and Discussion

As stated before, delamination is caused primarily by the shear stresses at the FRP-concrete interface. Therefore, these stresses are of particular interest, both in terms of their magnitude and distribution. While stresses can vary greatly from one point to another, and their precise variation may be difficult to predict in concrete structures, the load-deflection curve is far less sensitive to the exact location and size of individual cracks. Therefore, plotting the load-midspan deflections curve of a beam and comparing it with the corresponding experimental data, one can get a sense of the accuracy of the finite element analysis at the global level.

With the preceding discussion in mind, in the following the load-midspan deflection curves, the strain variation in the FRP and the load-strain curves for the tested beams will be shown.

Load-Deflection Curves

Figure 5-5 (a) shows the deflected shape of the T-beam externally strengthened with one layer of the CFRP laminate and its crack pattern as predicted by the FEM while Fig.5-5 (b) shows the longitudinal stresses distribution in the beam. The crack pattern in Fig.5-5 (a) indicates heavy concentration of cracks in the neighbourhood of the applied loads and extensive cracking throughout the length of the beam. Cracks are also shown along the web-flange junction although such cracks were not observed in the test.

Fig.5.5 (b) shows extensive tension within the constant moment zone and slightly less tension in the shear span zone. This is unexpected because one would expect the maximum longitudinal stress to occur in the constant moment zone. It is interesting to note the tensile stresses near the extreme bottom fibre of the beam. These stresses appear to be intermittent and are due to tension stiffening.

Table 5-8 shows the delamination load and corresponding midspan deflection of the beams analyzed by FEM as well as the corresponding experimental values, while Figure 5-6 (a) to (f) show the comparison between the predicted load-midspan deflection curves for the different test beams by the finite element analysis and the corresponding experimental curves for each beam.

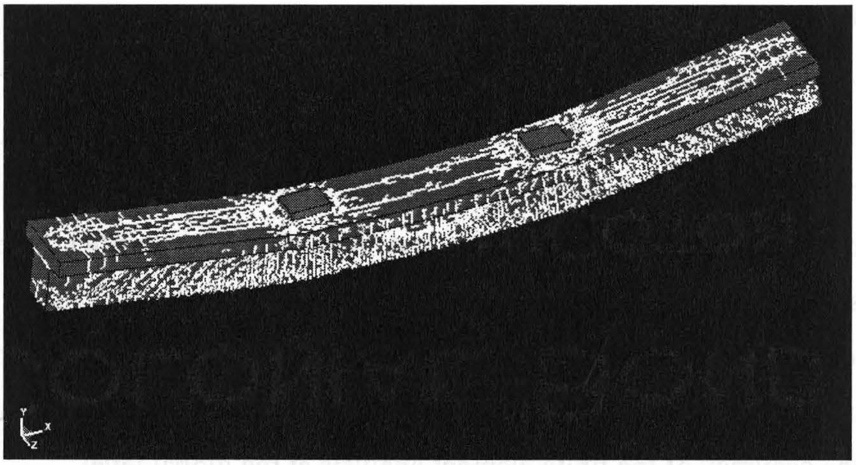

(a)

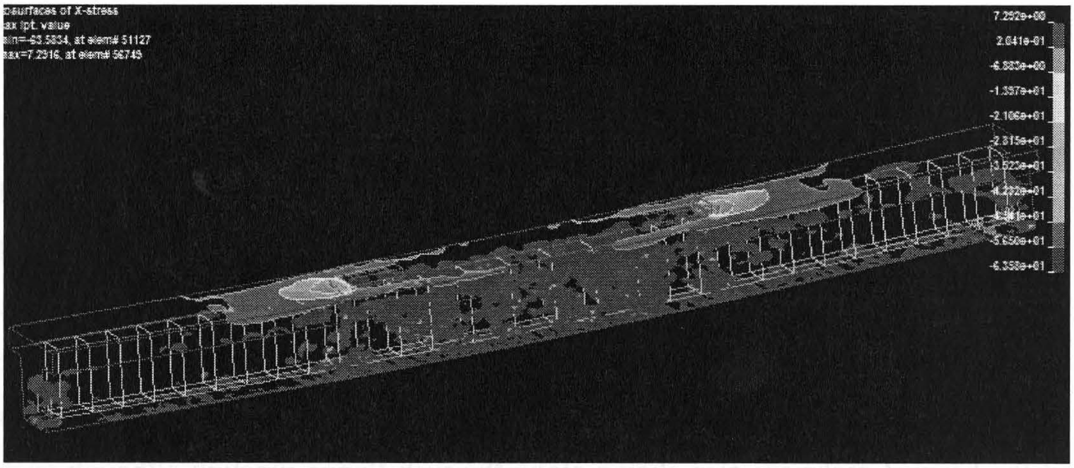

(b)

Fig.5-5(a): Deflected shape, crack pattern and (b) longitudinal stresses for beam B-F1-N

Fig.5-6 (a) shows the comparison for the three control beams. Since the experimental results varied noticeably among the three beams, the FEM results compare better with the results of beam CB2, but not so well with those of the other two beams.

Table 5-8: Comparison of FEM predicted delamination load and midspan deflection of some test beams without anchors and the corresponding experimental values

Beam #	Beam designation	Experimental results		Finite element results		$\frac{P_{Exp.}}{P_{FEM}}$	$\frac{\delta_{Exp.}}{\delta_{FEM}}$
		Del.load (kN)	Defl. at del. (mm)	Del.load (kN)	Defl. at del. (mm)		
1	CB1	163.7	181.1	184.0	145	0.89	1.25
2	CB2	192.7	193.7			1.05	1.34
3	CB3	180.2	250.2			0.98	1.73
4	B1-F1-N	203.5	89.9	213.3	89	0.95	1.01
5	B2-F1-N	209.0	97.6			0.98	1.10
6	B1-F2-N	230.1	69.7	220.5	52.3	1.04	1.33
7	B2-F2-N	205.4	56.1			0.93	1.07
8	B1-F4-N-b90	199.6	53.2	206.8	42.4	0.97	1.25
9	B1-F4-N	252.5	51.0	216.8	47	1.16	1.09
10	B2-F4-N	213.0	35.5			0.98	0.76
11	B1-F8-N-b90	214.6	41.0	207.0	35.6	1.04	1.15

The load-deflection curves of the strengthened beams in the latter figure clearly indicate that the FEM method is capable of predicting the delamination load and the corresponding deflection quite well. Also, it is able to predict reasonably well the post-delamination response of the beams analyzed. This is most probably due to two reasons: first, the finite element analysis is capable of predicting the interfacial stresses reasonably accurately; secondly, the interface traction-separation parameters that were used must have been reasonable. As will be discussed later, a maximum shear stress of 7.9 MPa at the interface, as used in this analysis, can be justified by available data in the literature.

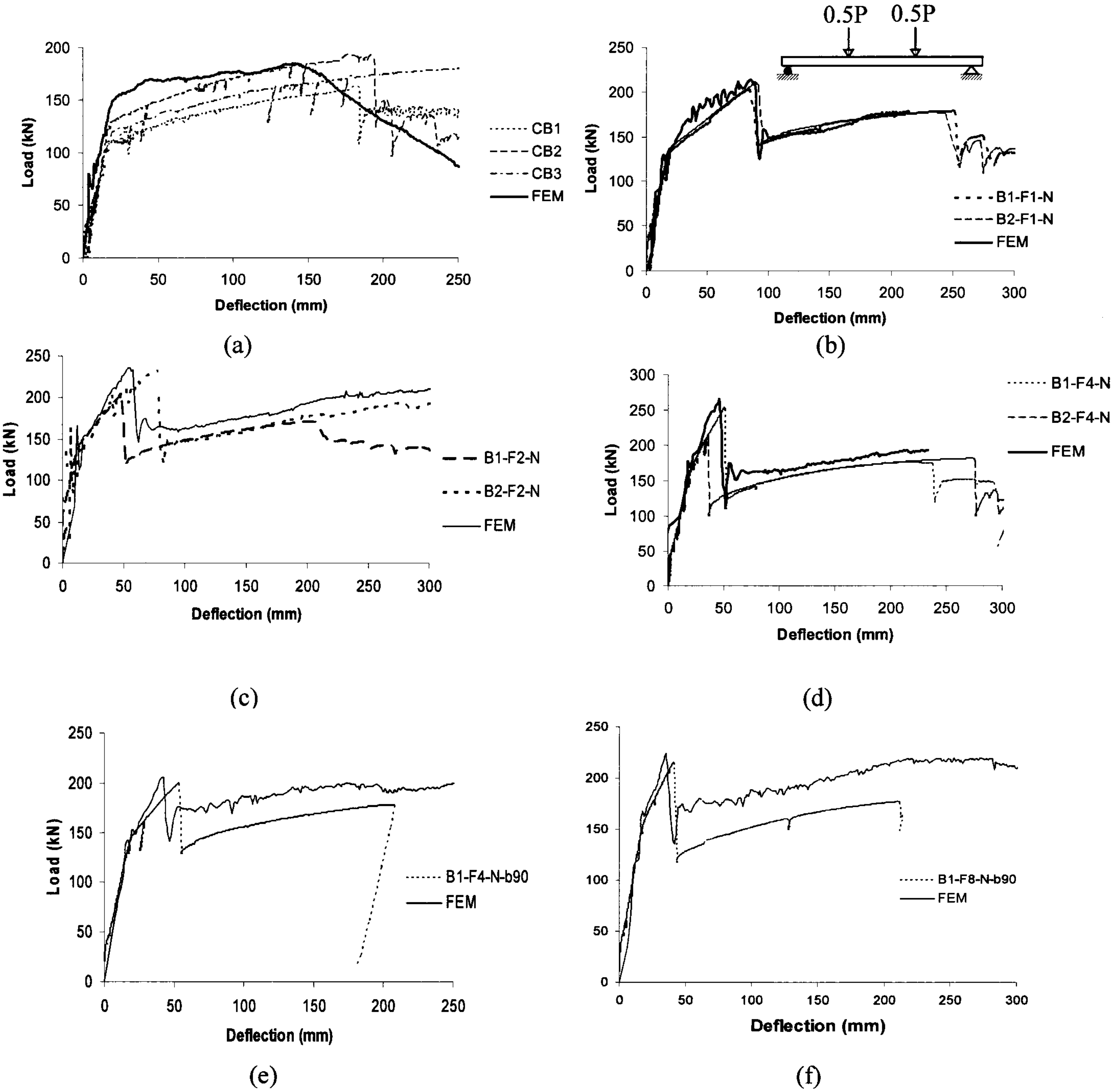

Fig.5-6: Experimental and FEM load midspan deflection curves of the tested beams

The sudden drop in load resistance after delamination which can be observed in each load-deflection curve indicates that delamination is an abrupt process and it does not occur in a gradual manner. This is indicative of a brittle response, which does not allow for stress redistribution. Consequently, the use of average stress values to predict delamination may not be a fruitful exercise.

With reference to the results in Table 5.8, we can see that the FEM predicted delamination load are within ± 7% of the experimental values. Thus the FEM results are quite accurate given that the experimental values for replicate beams differ by a wider margin. On the other hand, the predicted midspan deflection values at delamination are not as accurate, but again the experimental values for replicate beams also vary quite noticeably in some cases. These differences are due to random variations in materials properties and quality of construction. Considering these facts, once again it is concluded that the FEM predicted delamination loads and deflections are acceptable from the design point of view.

Load-Strain Diagrams

The FEM predicted load-FRP strain diagrams are compared with their experimental counterparts. The strains are plotted for a point at 1500 mm from the left support, as in Fig.5-7 or at midspan as in Fig 5-8. The point at 1500 mm was chosen because in the vicinity of this point the longitudinal and shear stresses combination may lead to diagonal cracks and high strain in the FRP. Notice that good agreement exists between the predicted and experimental curves in Fig.5-7 while in Fig.5-8 in some cases the comparison is not as good. Except for the beams strengthened with one layer of FRP laminate, all the load strain diagrams based on the experimental data show a trilinear behaviour as expected, representing the cracking, post-cracking and post-yield stages. The predicted curves show good agreement in the post-yield stage but the agreement is less favourable prior to yielding. This disagreement could be due to the fact that the strain gauges measure strain over relatively small gauge lengths and it is well known that in cracked reinforced concrete members both concrete and reinforcement strains can vary greatly over relatively small distances. Since these variations are caused by the cracks and since exact crack location cannot be predicted by the finite element method, the observed differences are not entirely unexpected. Overall, the predicted load-strain diagrams appear acceptable and in most cases sufficiently accurate.

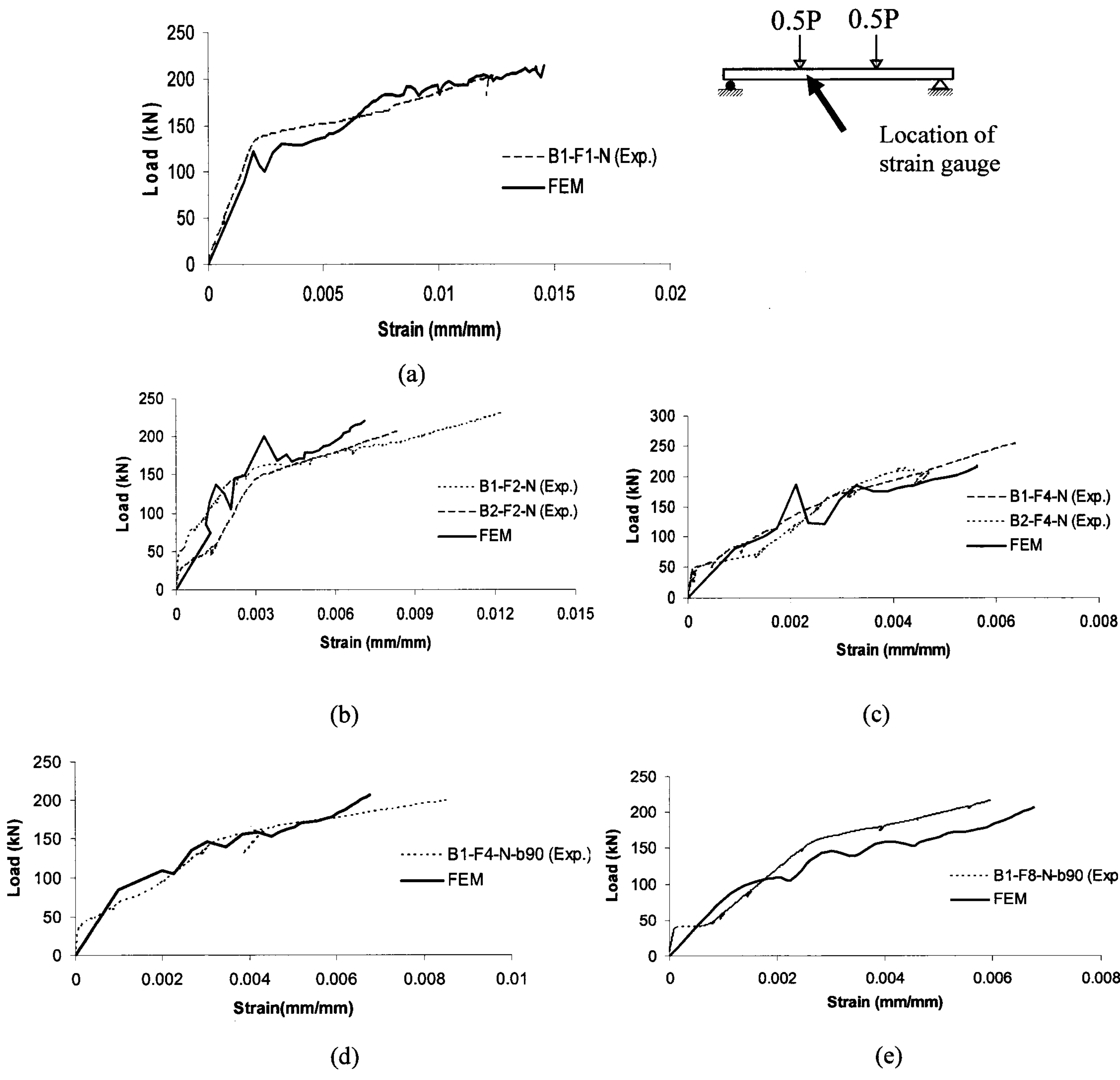

Fig.5-7: Load-FRP strain diagrams at 1500 mm from the left support

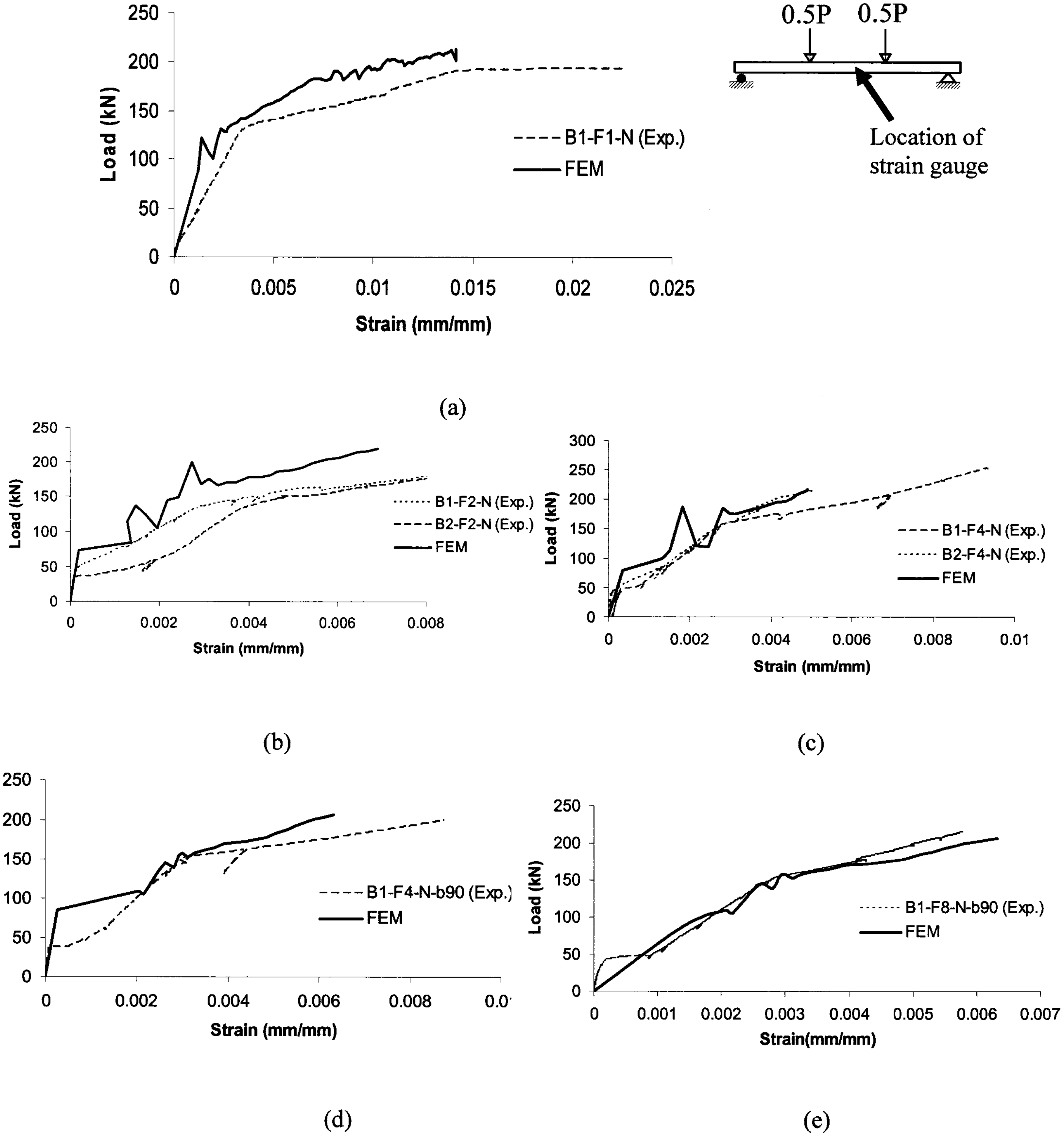

Fig.5-8: Load-FRP strain diagrams at midspan

Strain Variation along the FRP Laminate

To be able to design against delamination, the distribution of the FRP-concrete interfacial stresses and their magnitude should be quantified. As mentioned earlier, the interfacial shear stresses may vary greatly from one point to another, and their actual variation may be difficult to predict. In this section, the predicted strain variation along the laminate by FEM is plotted for two different load levels. Furthermore, for the same load levels, the recorded strain values from the test as well as the predicted strain values using an analytical model are also plotted. The predicted strain variation based on the analytical model will be discussed in detail later in this chapter. The main objective is to investigate the ability of these methods in predicting the interfacial strain variation at the FRP-concrete interface.

Figures 5-9 (a) to (f) show the predicted FEM strain variations versus their experimental values at the delamination load while Fig. 5-10 (a) to (f) show the same strain variation at 160 kN, which is less than the delamination load of all the beams. The predicted strain variations along the laminate based on the FEM follow the bending moment variation along the beam and they exhibit reasonable agreement with the corresponding experimental values at both load levels. The agreement is much better at the delamination load level than at 160 kN, which is somewhat surprising given the fact that at the lower load level the beam has fewer cracks and it is expected to behave more closely to its theoretical behaviour. The one important point to observe is the locally oscillating nature of the strain variation by the finite element method. Since the interfacial shear strains and stresses are related to the slope of the longitudinal strain diagram, these local oscillations, although globally insignificant, can lead to severely high interfacial shear strains and stresses as will be shown later.

The strain variations predicted by the analytical method generally compare better with the corresponding experimental results than the FEM result, particularly at the delamination load level. The analytical method over-predicts the experimental values at the 160 kN load level in some cases. Practically, the strain values before the delamination load are not of much interest; therefore, the larger differences between the experimental and analytical results in the latter case are not important.

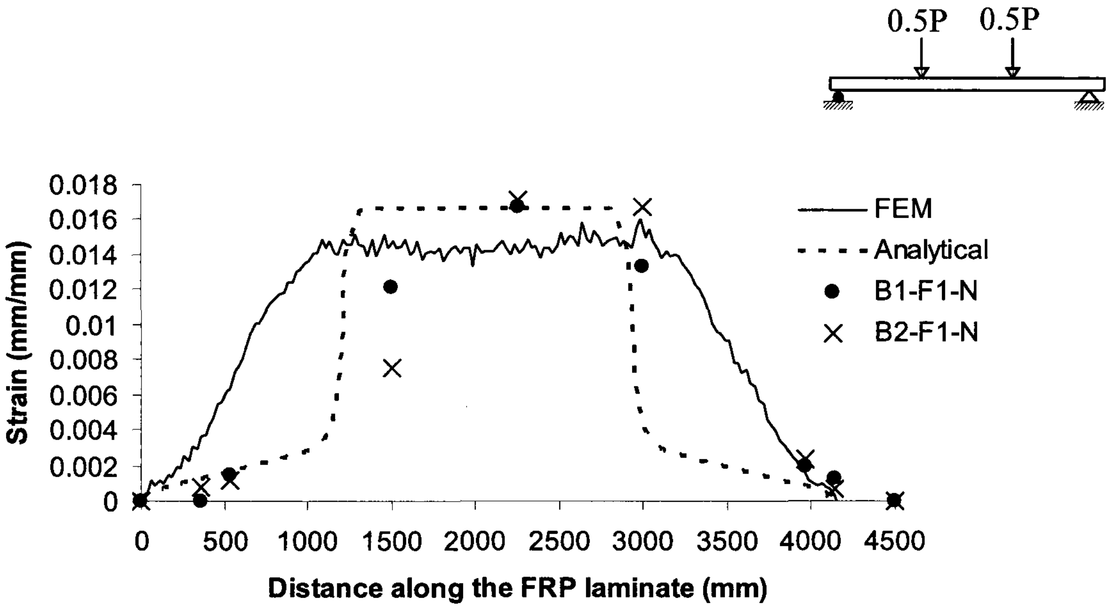

(a)

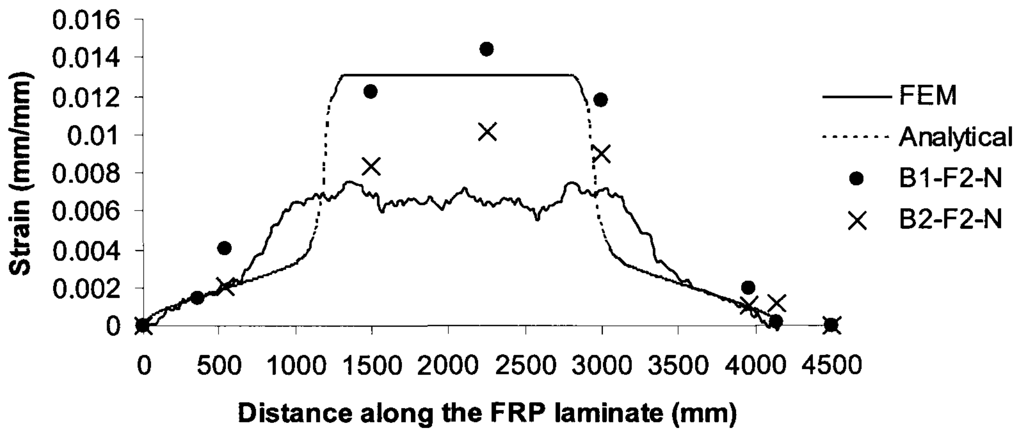

(b)

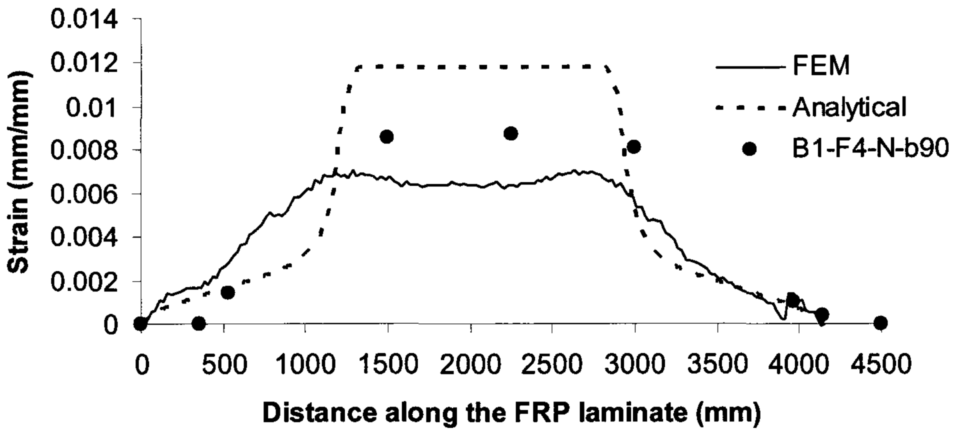

(c)

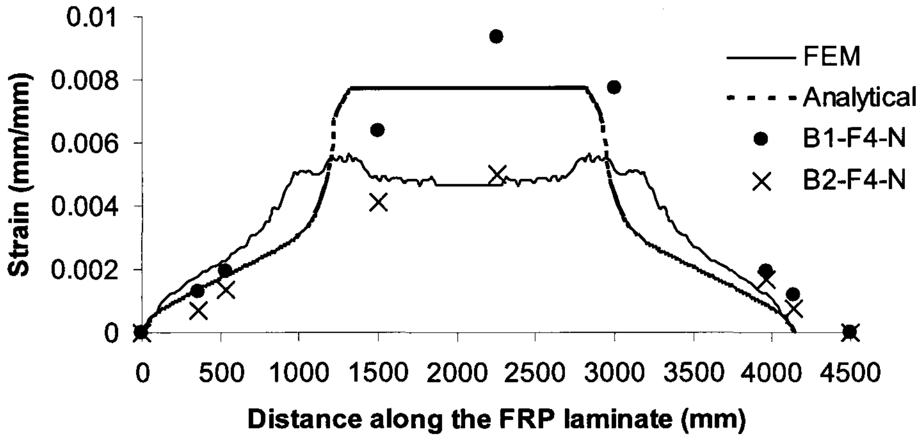

(d)

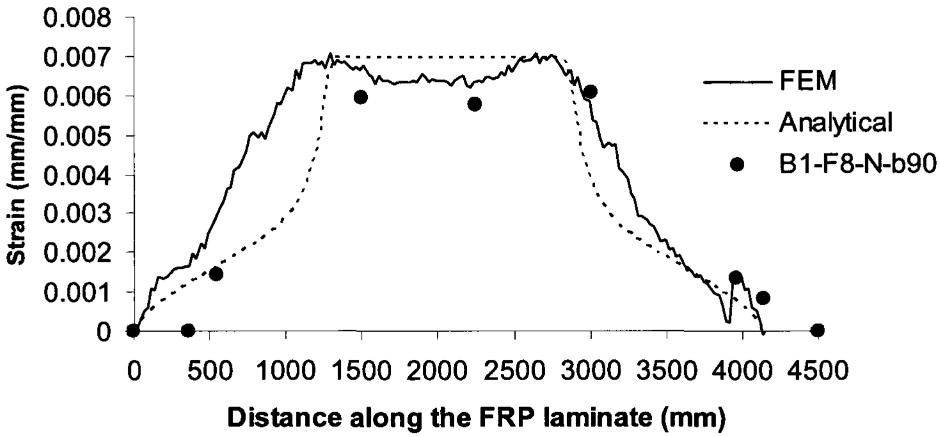

(e)

Fig.5-9: Strain variation along the FRP laminate at delamination

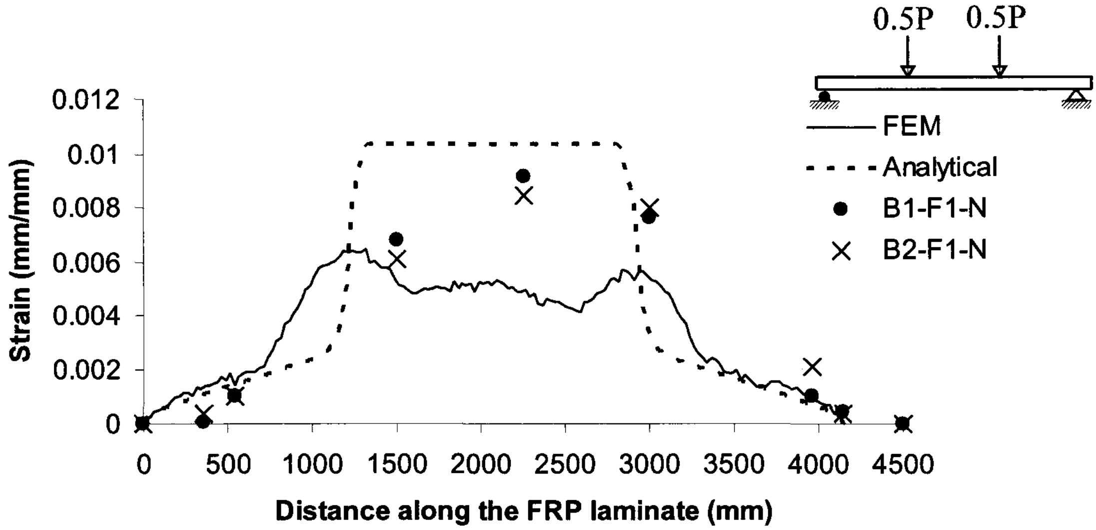
0.5P
0.5P
FEM
Analytical
B1-F1-N
B2-F1-N
Strain (mm/mm)
0.012
0.01
0.008
0.006
0.004
0.002
0
0 500 1000 1500 2000 2500 3000 3500 4000 4500
Distance along the FRP laminate (mm)

(a)

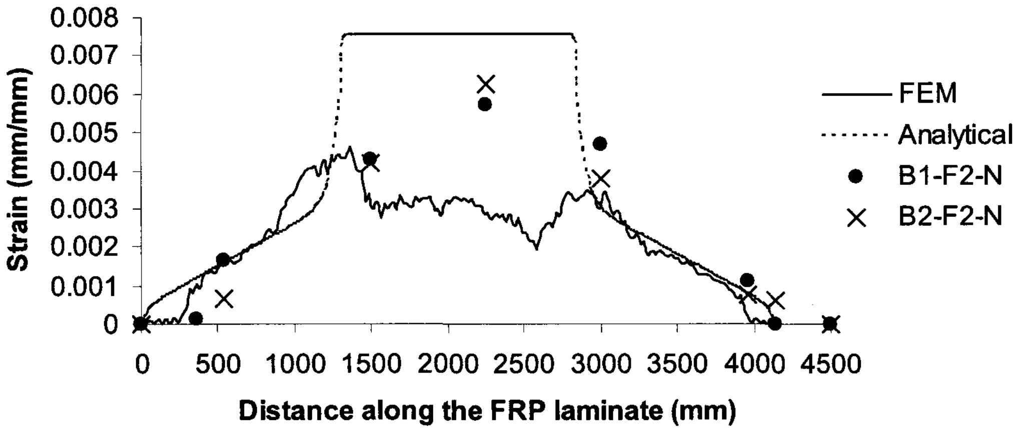
FEM
Analytical
B1-F2-N
B2-F2-N
Strain (mm/mm)
0.008
0.007
0.006
0.005
0.004
0.003
0.002
0.001
0
0 500 1000 1500 2000 2500 3000 3500 4000 4500
Distance along the FRP laminate (mm)

(b)

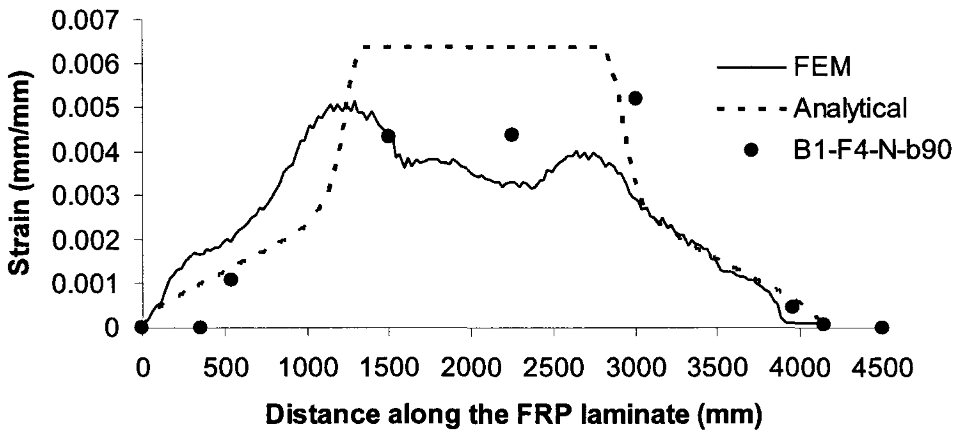
FEM
Analytical
B1-F4-N-b90
Strain (mm/mm)
0.007
0.006
0.005
0.004
0.003
0.002
0.001
0
0 500 1000 1500 2000 2500 3000 3500 4000 4500
Distance along the FRP laminate (mm)

(c)

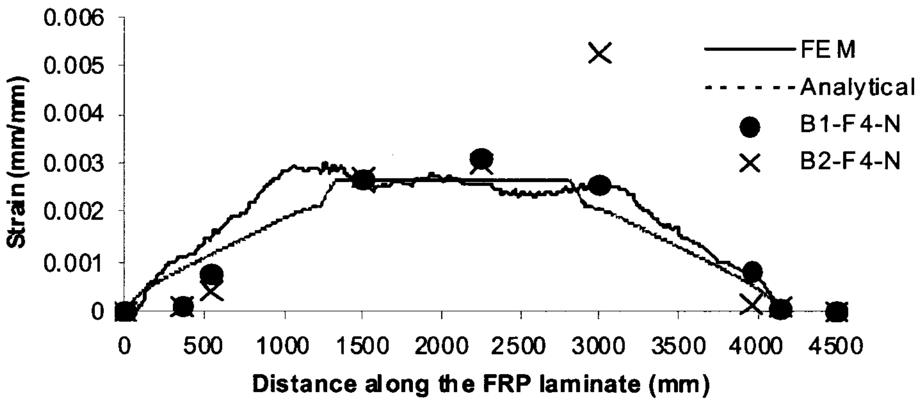

(d)

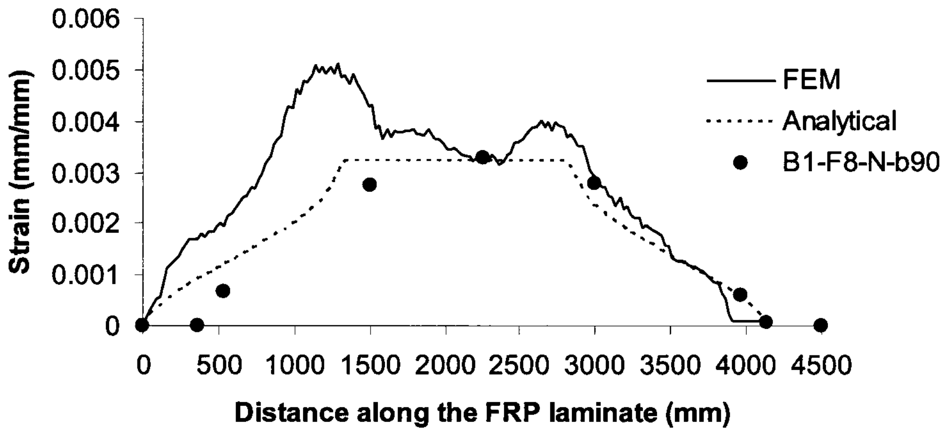

(e)

Fig.5-10: Strain variation along the FRP laminate at 160 kN load acting in the beam

In the opinion of the author, the problem of delamination in midspan zone is a local or stress concentration problem that arises due to the abrupt changes in FRP strain in the vicinity of the loading points or cracks. As stated earlier, in the midspan zone many cracks form and these cracks cause high local shear stresses to develop in their neighbourhood. To check the validity of this hypothesis, the predicted shear stresses at the interface based on the FEM analysis are plotted in Figs. 5-11. These stresses correspond to the delamination load. Notice the multiple peaks and oscillation along the interface. It is difficult to judge whether these sharp variations are a consequence of the FEM analysis method or a true reflection of the actual state of stress at the interface. Similar shear stress variation was reported by Abdel Baky et al. (2007) and they attributed it to the location of flexural cracks. Since the FRP-concrete interface has a brittle behaviour using average value of shear stresses to determine the delamination load may not be reasonable. Ideally, one should find a method that can predict the maximum shear stress at the interface and then this value should be compared to the interface shear strength, which is governed by the strength of the concrete. In the following section, such a method is discussed.

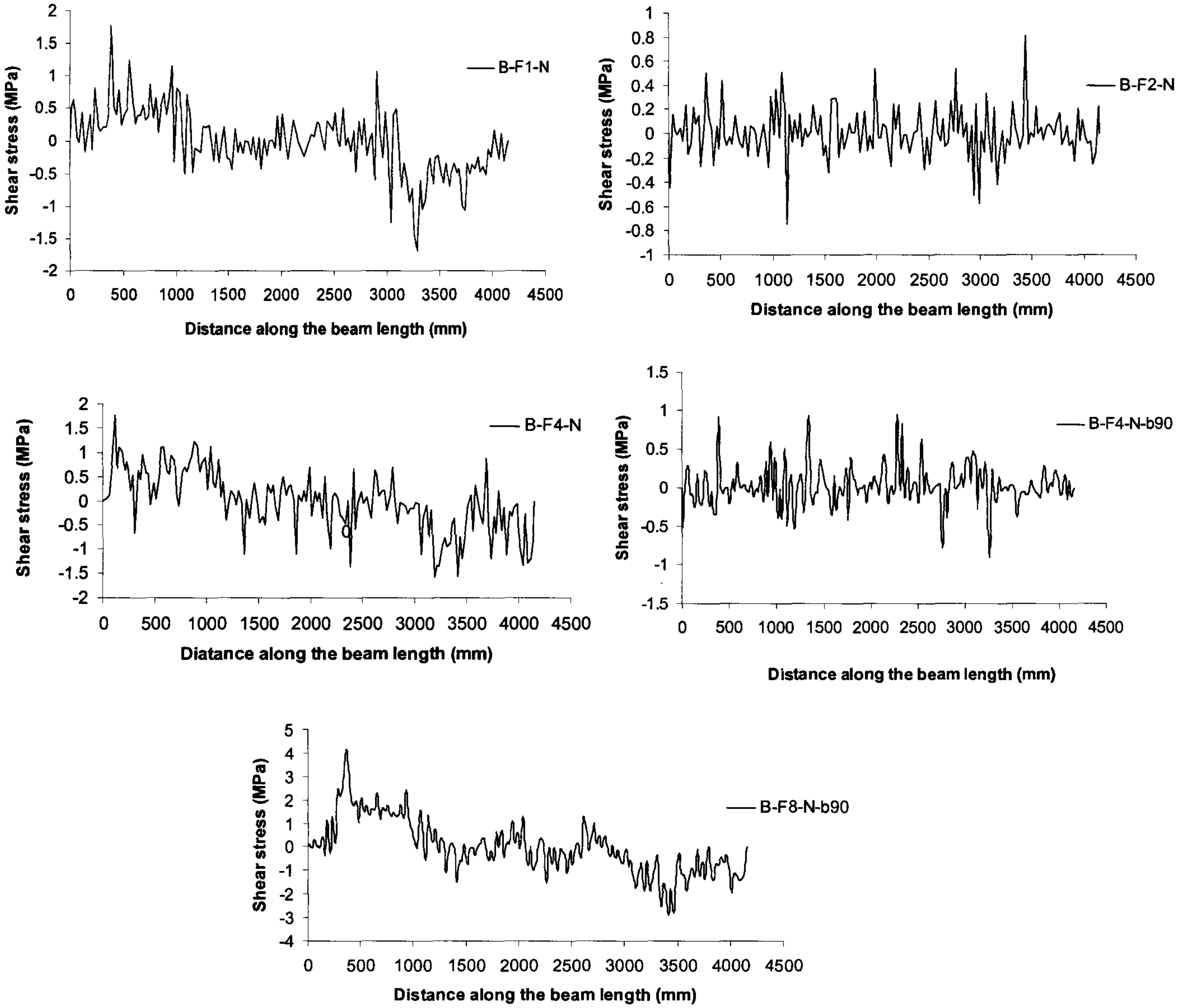

Fig.5-11: Predicted shear stress distribution along the interface for the tested beams

5.5 Analytical Model Based on Partially Composite Beam Theory

In this section an analytical model is described which can be used to determine the shear and normal stresses at the FRP-concrete interface. The model is based on composite beam theory where slippage at the FRP-concrete interface is permitted. This model was applied to steel beams strengthened with GFRP laminate by Youssef (2006) and he reported good agreement between the experimental and predicted delamination load. However, he did not present any comparison between the measured longitudinal strain variation along the interface and the corresponding computed values. In this study, such a comparison was made earlier in Figs. 5-9 and 5-10, with acceptable agreement between the two sets of values which indicates that this model has the potential of predicting the delamination load with relatively smaller effort compared to the FEM.

5.5.1 Model Description

Consider the simply supported steel beam in Fig.5-12 loaded in four point bending and externally strengthened with FRP laminate along its bottom surface. An infinitesimal element of the beam, located at distance x from the beam centreline, is shown in Fig.5-13. The axial displacements of the steel beam and the FRP at their interface are assumed to be u_1 and u_2 , respectively, where, u_1 is assumed to be higher than u_2 because of the flexibility of the adhesive material. Before we develop the necessary relationships between the applied load and the interfacial stresses, it is important to point out that any nonlinearity in this analysis is limited to the beam and not to the interface or the FRP. All FRP's are known to be linear elastic, and it is reasonable to assume that the adhesive bonding the FRP to the beam also behaves elastically. As far as inelasticity of the beam is concerned, it can be represented in terms of its moment-curvature or moment-strain relationship. Youssef assumed a bilinear moment-strain relationship as shown in Fig.5-14, where the strain ε in this figure refers to the extreme tension fiber in the steel section.

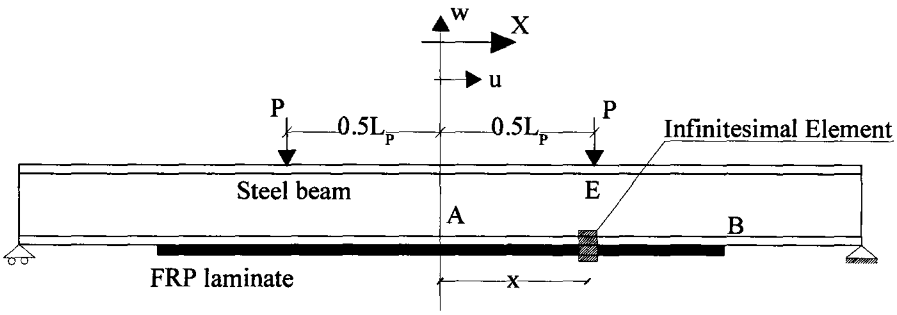

Fig.5-12: W-shape steel beam strengthened with GFRP laminate (Youssef 2006)

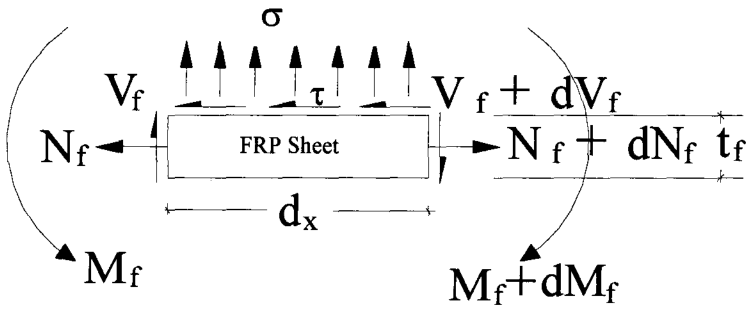

Fig.5-13: Straining actions acting on the infinitesimal element of the FRP laminate (Youssef 2006)

This relationship can simulate the response of a steel beam undergoing strain hardening. The moment M_p in this case corresponds to the yield moment of the section and K_1 represents ES where E is the elastic modulus of steel and S is the section modulus. The slope K_2 represents equivalent quantities in the post-yield range. For reinforced concrete beam a similar relationship can be developed as will be shown later in this chapter.

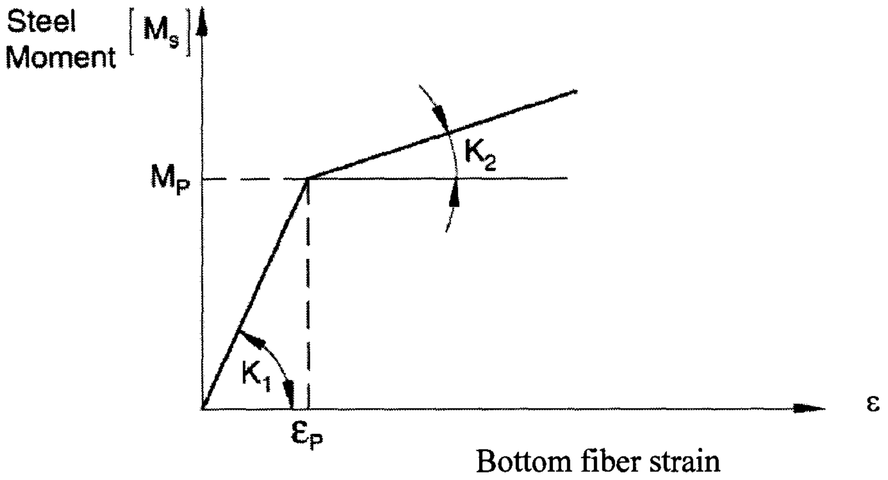

Fig.5-14: Relationship between moment and axial strain of steel section (Youssef 2006)

With reference to Fig.5-13, the relation between the moment and the axial strain can be written as:

Elastic stage:

$$\left(\frac{du_1}{dx} \leq \varepsilon_p\right):$$

$$M_s = K_1 \frac{du_1}{dx} \qquad \text{Eq.5-1(a)}$$

Plastic stage:

$$\left(\frac{du_1}{dx} \geq \varepsilon_p\right):$$

$$M_s = M_p + K_2\left(\frac{du_1}{dx} - \varepsilon_p\right) \qquad \text{Eq.5-1(b)}$$

The shear stress, τ, in the adhesive can be expressed by :

$$\tau = K_s\,(u_1\text{-}u_2) \qquad \text{Eq.5-2}$$

where K_s is the shear stiffness of the adhesive.

Considering the horizontal equilibrium of the forces shown in Fig.5-13, the following differential equation can be written

$$\tau dx = t_F E_F \frac{d^2 u_2}{dx^2}$$ Eq.5-3

Substituting for τ from Eq.5-2 in Eq.5-3 gives

$$u_1 = u_2 - \frac{t_f E_f}{K_s} \frac{d^2 u_2}{dx^2}$$ Eq.5-4

where E_f and t_f are the modulus of elasticity and the thickness of the FRP laminate, respectively. The external moment, M , acting on the strengthened section is equal to the sum of the moment resisted by the steel section, M_s, and the moment resulting from the axial forces in the FRP laminate, M_{FRP} , and can be written as

$$M = M_s + M_{FRP} = M_s + b_f t_f (h+t_f).E_f \varepsilon_f$$ Eq.5-5

where b_f , h and ε_f are the width of the FRP laminate, the height of the steel section, and the axial strain in the FRP laminate, respectively. Taking the first derivative of Eq.5-4 with respect to x and setting $\varepsilon_f = \frac{du_2}{dx}$, the differential equation which relates the axial strain at the extreme fibre of the steel section and the FRP laminate can be written as:

$$\frac{du_1}{dx} = \varepsilon_f - \frac{t_f E_f}{K_s} \frac{d^2 \varepsilon_f}{dx^2}$$ Eq.5-6

Simplifying Eqs. 5-1, 5-5, 5-6 results in the following differential equations that govern the shear stress at the interface:

<u>Elastic stage:</u>

$$\frac{d\varepsilon_f^2}{dx^2} - \omega_E^2 \varepsilon_f = \frac{K_s M}{K_1 E_f t_f}$$ Eq.5-7(a)

<u>Plastic stage:</u>

$$\frac{d\varepsilon_f^2}{dx^2} - \omega_P^2 \varepsilon = \frac{K_s \left(M - M_p + K_2 \varepsilon_p\right)}{K_2 E_f t_f}$$ Eq.5-7(b)

where

$$\omega_E^2 = \frac{K_s}{E_f t_f} + \frac{K_s b_f (h+t_f)}{K_1} \qquad \text{Eq.5-8}$$

$$\omega_P^2 = \frac{K_s}{E_f t_f} + \frac{K_s b_f (h+t_f)}{K_2}$$

The differential equation governing the normal behaviour in the adhesive material can be determined from the equilibrium of vertical forces and moment shown in Fig.5-13.

$$\frac{dV_f}{dx} = -K_p w b_f \qquad \text{Eq.5-9}$$

$$V_f = \frac{dM_f}{dx} + \frac{b_f t_f}{2}\tau \qquad \text{Eq.5-10}$$

$$M_f = E_f I_f \frac{d^2 w}{dx^2} \qquad \text{Eq.5-11}$$

where V_f and M_f are the shear force and the moment acting on the FRP, w is the beam vertical displacement and K_P is the normal stiffness of the adhesive in the transverse direction. By substituting for V_f from Eq.5-10 into Eq.5-9 and by replacing M_f in the resulting equation according to Eq.5-11, the following differential equation can be obtained.

$$\frac{d^4 w}{dx^4} + \lambda^4 w = \frac{b_f t_f^2}{2I_f}\frac{d^2\varepsilon}{dx^2} \qquad \text{Eq.5-12}$$

where I_f is the moment of inertia of the FRP laminate and

$$\lambda^4 = \frac{b_f K_P}{E_f I_f} \qquad \text{Eq.5-13}$$

Note that Eq.5-12 is similar to the equation of a beam on elastic foundation. To solve these equations, the beam is divided into two zones since the moment is constant between the loading points and varies linearly in the shear span. Zone AE (see Fig.5-12) covers from x=0 to x=0.5L_p, where x is measured from the midspan and L_p is the distance between the loading points while zone BE covers the domain $0.5L_p < x \leq 0.5\,L_f$ where L_f is the length of the FRP sheet. The solution of the relevant governing equations, Eq.5-7 and Eq.5-12, are then obtained for these zones as follows

Zone AE: $0 \leq x \leq 0.5L_p$

The moment in this zone is constant and can be written as:

$$M_{AE}=M_0=0.5P(L-L_p) \qquad \text{Eq.5-14}$$

The solution of the differential equations Eq.5-7 (a) and Eq.5-11 can be written as:

$$\varepsilon_{AE} = A_1 \sinh(\omega_E x) + B_1 \cosh(\omega_E x) + \frac{K_s M_0}{K_1 E_f t_f \omega_E^2} \qquad \text{Eq.5-15}$$

$$\begin{aligned} w_{AE} &= A_3 \cos(\lambda x)\cosh(\lambda .x) + B_3 \cos(\lambda x)\sinh(\lambda x) \\ &+ C_3 \sin(\lambda x)\cosh(\lambda x) + \frac{b_f t_f^2 \omega_E^2}{2I_f\left(\omega_E^4 + \lambda^4\right)}\left[A_1 \sinh(\omega_E x) + B_1 \cosh(\omega_E x)\right] \end{aligned}$$

Eq.5-16

Zone BE: $0.5L_p \leq x \leq 0.5L_f$

The moment in this zone is can be written as

$$M_{BE} = \frac{2M_0\left(0.5L - x\right)}{\left(L - L_p\right)} \qquad \text{Eq.5-17}$$

Therefore, the solution of the differential equations Eq.5-7(b) and Eq.5-12 can be written as:

$$\varepsilon_{BE} = C_1 \sinh(\omega_E x) + D_1 \cosh(\omega_E x) + \frac{K_s M_{BE}}{K_1 E_f t_f \omega_E^2} \qquad \text{Eq.5-18}$$

$$\begin{aligned} w_{BE} &= E_3 \cos(\lambda x)\cosh(\lambda x) + F_3 \cos(\lambda x)\sinh(\lambda x) \\ &+ G_3 \sin(\lambda x)\cosh(\lambda x) + H_3 \sin(\lambda x)\sinh(\lambda x) \qquad \text{Eq.5-19} \\ &+ \frac{b_f t_f^2 \omega_E^2}{2I_f\left(\omega_E^4 + \lambda^4\right)}\left[C_1 \sinh(\omega_E x) + D_1 \cosh(\omega_E x)\right] \end{aligned}$$

Due to symmetry, constants, A_1, B_3 and C_3 are equal to zero. The rest of the constants can be evaluated by applying the following boundary or compatibility conditions

$\varepsilon_{AE} = \varepsilon_{BE}$ at $x=0.5L_p$ (Continuity of strains)

$\varepsilon_{BE} = 0$ at $x=0.5L_f$ (FRP strain is zero at its end)

$\dfrac{d\varepsilon_{AE}}{dx} = \dfrac{d\varepsilon_{BE}}{dx}$ at $x=0.5L_p$ (Continuity of curvature) Eq.5-20(a)

$w_{AE} = w_{BE}$ at $x=0.5L_p$ (Continuity of displacement)

$\dfrac{dw_{AE}}{dx} = \dfrac{dw_{BE}}{dx}$ at $x=0.5L_p$ (Continuity of slope or rotation)

$\dfrac{dw_{AC}}{dx} = 0$ at $x=0.5L_f$ (FRP moment is zero at its end)

$(V_f)_{CE} = 0$ at $x=0.5L_f$ (FRP shear is zero at its end)

$(V_f)_{AE} = (V_f)_{BE}$ at $x=0.5L_p$ (Continuity of shear)

$(M_f)_{AE} = (M_f)_{BE}$ at $x=0.5L_p$ (Continuity of moment) Eq.5-20(b)

In the case of the plastic zone, the length of the strengthened beam was divided into three zones. Zone AP with x varying from 0 to $0.5L_p$, zone BP with x varying from $0.5L_p$ to x_p, and zone CP with x varying from x_p to $0.5L_f$, where x_p is defined to be the distance measured from the beam midspan to the point where the moment of the steel section (M_s) begins to be less than M_p,

<u>Zone AP: $0 \le x \le x_p$ (Applied moment > M_p)</u>

The moment in this zone is equal to M_0 and the differential equations governing the shear behaviour can be determined by solving the two equations Eq.5-7(b) and Eq.5-12. The solution of the equations can be expressed as:

$$\varepsilon_{AP} = A_2 \sinh(\omega_P x) + B_2 \cosh(\omega_P x) + \frac{K_s\left(M_0 - K_1\varepsilon_p + K_2\varepsilon_p\right)}{K_2 E_f t_f \omega_P^2} \qquad \text{Eq.5-21}$$

$$w_{AP} = A_4\cos(\lambda x)\cosh(\lambda x) + B_4 c\mathrm{os}(\lambda x)\sinh(\lambda x) + C_4\sin(\lambda x)\cosh(\lambda x) + D_4\sin(\lambda x)\cosh(\lambda x) + \frac{b_f t_f^2\omega_P^2}{2I_f\left(\omega_P^4+\lambda^4\right)}\left[A_2\sinh(\omega_P x) + B_2\cosh(\omega_P x)\right] \qquad \text{Eq.5-22}$$

Zone BP: $0.5L_p \le x \le x_p$ (Applied moment $\ge M_p$)

The moment in this zone is similar to M_{BE} and The solution of the differential equations Eq.5-7b and Eq.5-12 can be written as:

$$\varepsilon_{BP} = C_2\sinh(\omega_P x) + D_2\cosh(\omega_P x) + \frac{K_s\left(M_{BP} - K_1\varepsilon_p + K_2\varepsilon_p\right)}{K_2 E_f t_f \omega_P^2} \qquad \text{Eq.5-23}$$

$$w_{BP} = E_4\cos(\lambda x)\cosh(\lambda x) + F_4\cos(\lambda x)\sinh(\lambda x) + G_4\sin(\lambda x)\cosh(\lambda x) + H_4\sin(\lambda x)\sinh(\lambda x) + \frac{b_f t_f^2\omega_P^2}{2I_f\left(\omega_P^4+\lambda^4\right)}\left[C_2\sinh(\omega_P x) + D_2\cosh(\omega_P x)\right] \qquad \text{Eq.5-24}$$

Zone CP: $x_p \le x \le 0.5L_f$ (Applied moment $\le M_p$)

The moment in this zone is similar to M_{BE} and the solution of the differential equations Eq.5-7(b) and Eq.5-12 can be written as:

$$\varepsilon_{CP} = E_2\sinh(\omega_E x) + F_2\cosh(\omega_E x) + \frac{K_s M_{CE}}{K_1 E_f t_f \omega_E^2} \qquad \text{Eq.5-25}$$

$$w_{CP} = I_4\cos(\lambda x)\cosh(\lambda x) + J_4\cos(\lambda x)\sinh(\lambda x) + K_4\sin(\lambda x)\cosh(\lambda x) + L_4\sin(\lambda x)\sinh(\lambda x) + \frac{b_f t_f^2\omega_E^2}{2I_f\left(\omega_E^4+\lambda^4\right)}\left[E_2\sinh(\omega_E x) + F_2\cosh(\omega_E x)\right] \qquad \text{Eq.5-26}$$

From symmetry of the problem, the constants B_4, C_4 and A_2 are equal to zero. The rest of the constants could be determined using the following procedure:

1. Assume a reasonable value for x_p

2. Enforce the five boundary conditions given below to solve for constants B_2, C_2, D_2. E_2 and F_2.

$\varepsilon_{AP} = \varepsilon_{BP}$	at $x=0.5L_p$	(Continuity of strains)
$\varepsilon_{BP} = \varepsilon_{CP}$	at $x=x_p$	(Continuity of strains)
$\varepsilon_{CP} = 0$	at $x=0.5L_f$	(FRP strain is zero at its end)

$\frac{d\varepsilon_{AP}}{dx} = \frac{d\varepsilon_{BP}}{dx}$ at $x=0.5L_p$ (Continuity of curvature)

$\frac{d\varepsilon_{BP}}{dx} = \frac{d\varepsilon_{CP}}{dx}$ at $x=x_p$ (Continuity of curvature)

3. Eq.(5-4) is applied to evaluate two values for $\frac{du_1}{dx}$ at $x=x_p$. The first value is evaluated using ε_{BP} (Eq.5-23) and the second using ε_{CP} (Eq.5-25).

4. If the difference between the two values in step 3 is greater than a predefined tolerance, then the assumed x_p has to be revised and steps 1 thought 4 have to be repeated.

5. The remaining constants are evaluated by applying the following ten kinematic and static conditions:

$W_{AP} = W_{BP}$ at $x=0.5L_p$ (Continuity of displacement)

$W_{BP} = W_{CP}$ at $x=x_p$ (Continuity of displacement)

$\frac{dw_{AP}}{dx} = \frac{dw_{BP}}{dx}$ at $x=0.5L_p$ (Continuity of rotation)

$\frac{dw_{BP}}{dx} = \frac{dw_{CP}}{dx}$ at $x=x_p$ (Continuity of rotation)

$\frac{d^2 w_{CP}}{dx^2} = 0$ at $x=0.5L_f$ (FRP moment is zero at its end)

$(V_f)_{CP} = 0$ at $x=0.5L_f$ (FRP shear is zero at its end)

$(V_f)_{AP} = (V_f)_{BP}$ at $x=0.5L_p$ (Continuity of shear)

$(V_f)_{BP} = (V_f)_{CP}$ at $x=x_p$ (Continuity of shear)

$(M_f)_{AP} = (M_f)_{BP}$ at $x=0.5L_p$ (Continuity of moment)

$(M_f)_{BP} = (M_f)_{CP}$ at $x=x_p$ (Continuity of moment)

Using the above steps, the shear τ and normal (peeling) stress σ_w at the interface can be determined using $\tau = K_s(u_1 - u_2)$ and $\sigma_w = K_p w$, respectively. Youssef applied this approach to a steel section reinforced with a GFRP laminate and calculated the shear and normal stress variations as shown in Figs.5-15 and 5-16. The figures show the stresses at two load levels, with the greater of the two corresponding to the delamination load and the smaller are due a load less than the delamination load.

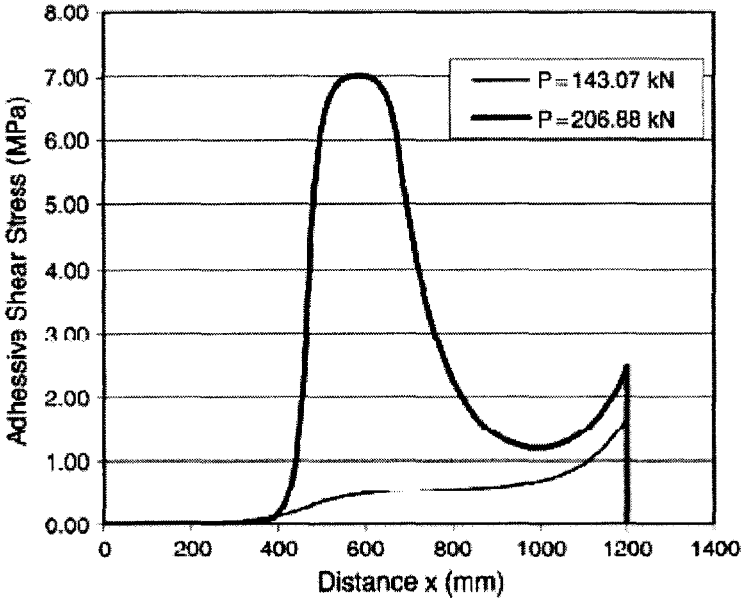

Fig.5-15: Shear stress variation along the interface measured from the midspan (Youssef 2006)

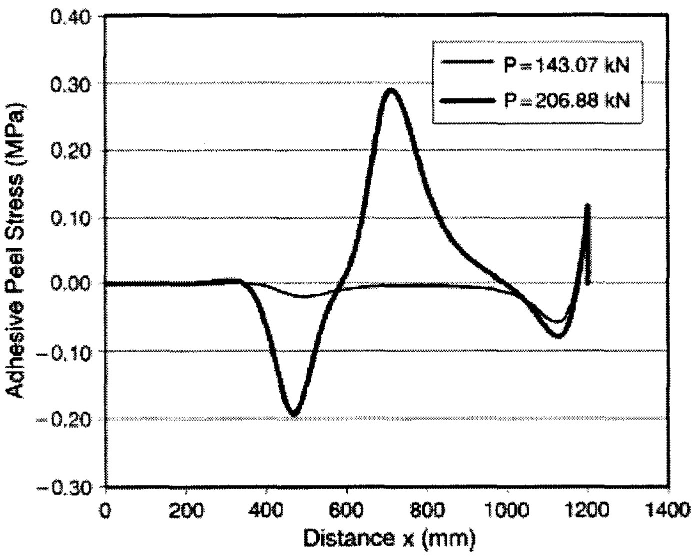

Fig.5-16: Normal stress variation along the interface measures from the midspan (Youssef 2006)

As can be noticed, just before delamination, a high shear stress of 7MPa was predicted in the zone of maximum moment versus 2.5 MPa at the laminate end. This clearly shows that a high shear stress can exist in the zone of maximum moment even if according to simple beam theory the shear stress is supposed to be zero in this zone. Furthermore, the shear at the laminate end is not as high as at the midspan, which could be the reason for the initiation of delamination in the constant moment zone as observed in the beams tested in this study. The variation of the normal stress (Fig.5-16) at failure shows a maximum tensile stress of 0.3 MPa at the point located a distance x_p from midspan. It is also important to mention that a high tensile stress of almost 0.12 MPa was predicted at the laminate end. These stresses could be combined with an interfacial failure criterion to determine the delamination load and location along the interface. For reinforced concrete members, the interface strength is governed by concrete.

5.5.2 Model Modifications

As mentioned earlier, Youssef applied the above model to steel beams externally strengthened with GFRP laminates. To be able to apply the model to the RC T-beams tested here, a moment-strain curve similar to Fig.5-14, need be constructed. The curve is similar to the moment curvature diagram; therefore, for simplicity the theoretical moment and corresponding strain at concrete cracking, steel yielding and ultimate moment could be used to define the moment strain diagram. In this case the curve would be trilinear with slopes K_1, K_2 and K_3 shown in Fig.5-17.

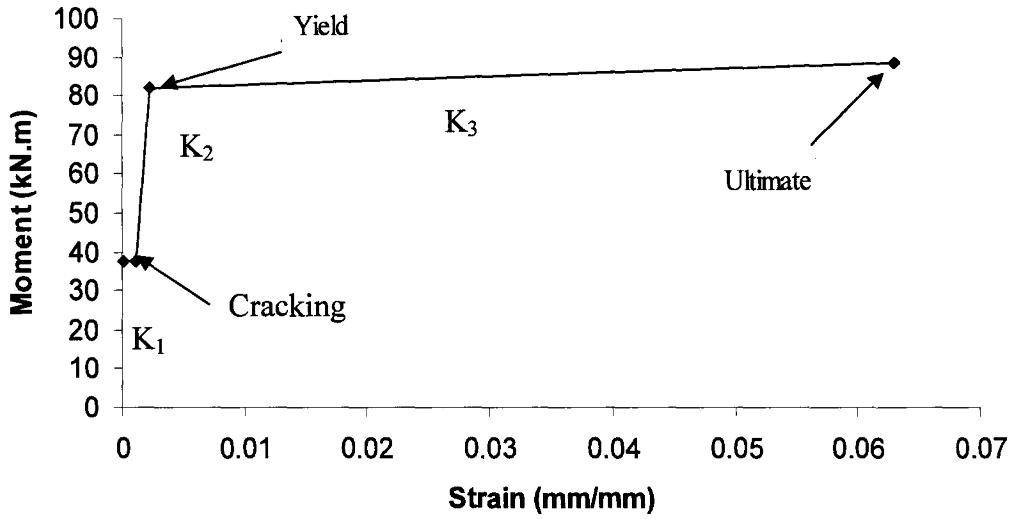

Fig.5-17: Theoretical moment strain diagram for the unstrengthened T-beam

This curve ignores the effect of tension carried by the concrete between the cracks, the so-called tension stiffening effect, which will be considered later. When applying the previous model in conjunction with the moment-strain diagram in Fig.5-17, the solution can be divided into three stages: uncracked, cracked not yielded, yielded not failed. The elastic solution was implemented before cracking while after cracking only K_2 and K_3 were used.

The theoretical moment-strain diagram is trilinear as in Fig.5-17, which shows discontinuity at cracking. The slopes K_1 , K_2 and K_3 based on the theoretical moment strain diagram in Fig.5-17 are 282331, 37000 and 103.63 kN.m respectively. To be able to check the veracity of this theoretical curve, in Fig.5-18, the actual moment-strain curves of the three control beams are plotted. These diagrams are based on the experimentally measured strain values. Note that CB1 and CB3 were made of the same concrete batch, while CB2 was made of another batch. It is clear from this figure that the experimental curves do not exhibit an uncracked stage and are essentially bilinear. The reason may be that they were pre-cracked due to either shrinkage or lifting before concrete had gained adequate tensile strength. This means that the use of a bilinear moment-strain diagram in this case may be justified. Based on experimental data, the slope K_2 might vary depending on the beam but K_1 does not vary too much among the three beams.

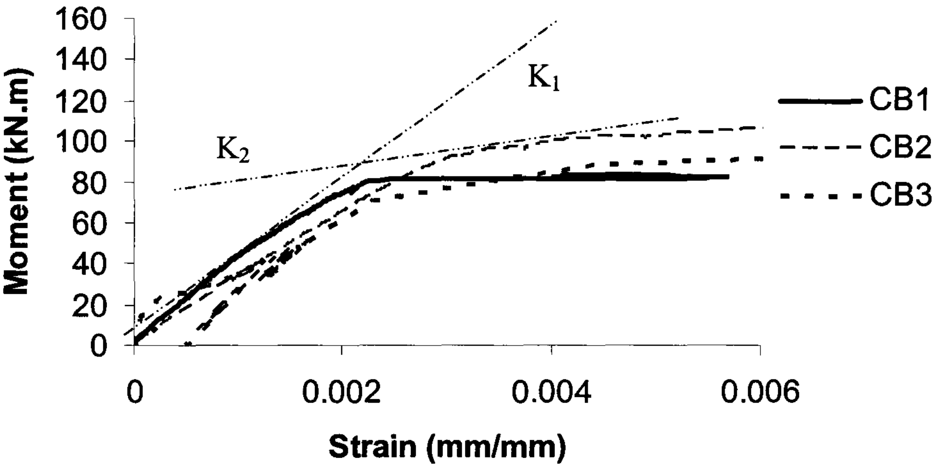

Fig.5-18: Moment strain curves for the control beam

Let us consider Fig.5-19 which presents a comparison between the theoretical and experimental moment-strain curves for the control beam CB1. First it is clear that the experimental curve does not exhibit a response pertaining to an uncracked section, therefore, the theoretical uncracked stage is not actually pertinent in the present case. Secondly, the experimental curve can be represented by a bilinear curve using either the initial tangent line or the secant line to the yield point as the first linear segment and the line connecting the yield point to the ultimate moment point as the second segment. For this beam, the slopes of the initial tangent line K_1 and secant line K_2 differ by only 3.5%, therefore, it would make little practical difference whichever slope is used. Accordingly, in this analysis a moment-strain diagram based on the secant line will be used. Note that this diagram belongs to the original unstrengtheend beam, akin to the steel section used by Youssef.

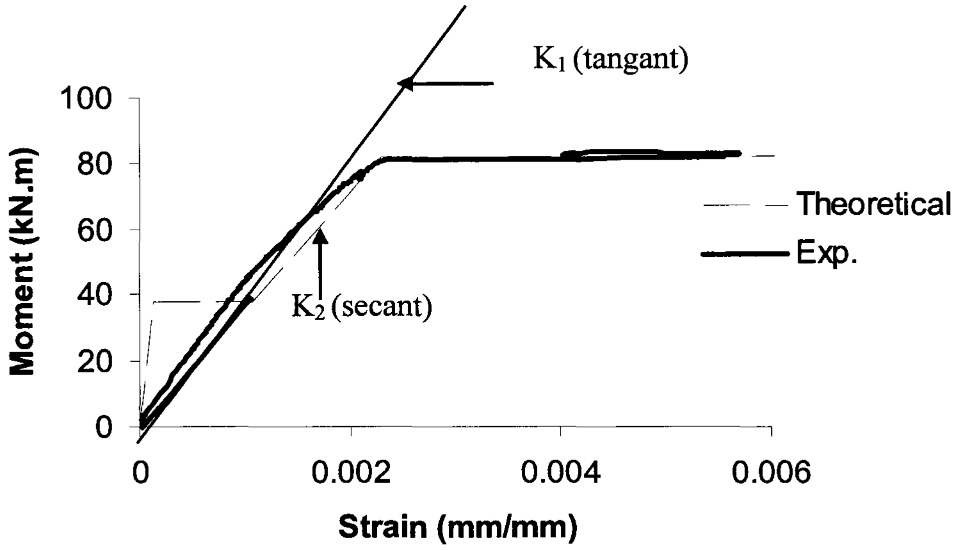

Fig.5-19: Comparison between the theoretical and experimental moment strain for CB

For the current beams, in theory K_s and K_p should be determined experimentally, but this requires a special test set-up (El Damatty and Abushagur 2003) which was not available to the writer, therefore, the values suggested by Youssef will be used. The effect of K_s on the shear stress will be examined later in this chapter, while K_p is expected to have little effect given the relatively small magnitude of the normal stresses at the interface.

5.5.3 Analysis Model

The results of this analysis are exhibited in two forms. First, the variation of the longitudinal strain along the CFRP laminate is plotted at two different load levels as shown earlier in Fig.5-9 and Fig.5-10 for beams B1-F1-N, B2-F1-N, B1-F2-N, B2-F2-N, B1-F4-N, B2-F4-N, B1-F4-N-b90, B1-F8-N-b90, and the results are compared with the corresponding experimental data and with the FEM analysis results. Secondly, the shear and normal stresses distributions along the interface are presented.

Strain Variation

The strain variation along the FRP laminate was plotted in Figs.5-9 and 5-10 for two different load levels. The strain distributions along the FRP laminate for 160 kN applied load and the delamination load were selected and compared with the experimental values and the FEM. It is clear from those figures that the predicted strain variations agrees remarkably well with the experimental data and with the FEM prediction both at midspan and at the laminate ends. In fact, overall the results of this analysis are in closer agreement with the experimental data than the FEM results. Notice in these figures the sudden change in the slope of the strain curve in the vicinity of the loading point which is indicative of a high shear stress at this location. The strain curve at midspan shows zero slope and consequently zero shear stress, which agrees with beam theory and the requirements of symmetry.

The high shear stress predicted in the vicinity of the loading point is the reason for the initiation of delamination in the zone of maximum moment, and indicates that the problem of delamination in the constant moment zone is basically a local or stress concentration problem. Also notice that the model predicts the value of the FRP rupture strain for beams B1-F1-N and B2-F1-N, which agrees with the recorded strain values and the rupture of the FRP observed during the test. In general the predicted strain variations are in a good agreement with the recorded strain, which reflects the appropriateness of the assumptions made in this analysis, including the idealization of the actual moment-strain curves by a bilinear curve.

Normal Stresses

Table 5-9 summarizes the predicted maximum shear and normal stresses at midspan and at laminate ends with and without tension stiffening. The tension-stiffening phenomenon and its importance will be discussed later. As can be seen in this table, and in Fig.5-20, which shows a typical normal stress distribution for beam B1-F8-N-b90, the normal stresses acting on the interface are generally very small, compared to the tensile strength of the 54 MPa concrete used in this investigation. This concrete is expected to have a tensile strength of approximately

5 MPa. The distribution of the normal stress appears rather complicated, and shows a jump from tension to compression at the location where the slope of the strain changes or the expected location of the peak shear stress. The normal stress at the laminate ends follows the same type of variation reported by other investigators (i.e. Teng 2002, Oehlers 2004). Due to the lack of a suitable measurement technique, the actual distribution of this stress, or more precisely its corresponding strain, cannot be accurately measured, but given its relatively small magnitude, it should not be of much concern.

Table 5-9: Maximum predicted shear and normal stress values at the midspan and plate end zones at delamination

Beam	No tension Stiffening					With tension Stiffening				
	Shear stress (MPa)		Normal Stress (MPa)			Shear stress (MPa)		Normal Stress (MPa)		
	Midspan	Plate end	Midspan (+)	Midspan (-)	Plate end	Midspan	Plate end	Midspan (+)	Midspan (-)	Plate end
B-F1-N	8.7	0.48	0.017	0.034	0.008	11.9	0.59	0.023	0.045	0.009
B-F2-N	9.7	0.86	0.040	0.089	0.018	13.4	1.03	0.041	0.089	0.018
B-F2-E3-M9	14.5	0.58	0.034	0.065	0.015	13.9	1.06	0.040	0.080	0.018
B-F4-N-b90	12.0	1.20	0.150	0.060	0.030	15.9	1.41	0.060	0.150	0.030
B-F4-N	6.7	1.32	0.030	0.050	0.030	8.3	1.56	0.030	0.060	0.030
B-F4-E3-M9	10.3	0.72	0.040	0.080	0.030	11.8	1.77	0.046	0.095	0.036
B-F8-N-b90	9.3	1.85	0.050	0.070	0.045	12.0	2.18	0.062	0.100	0.050

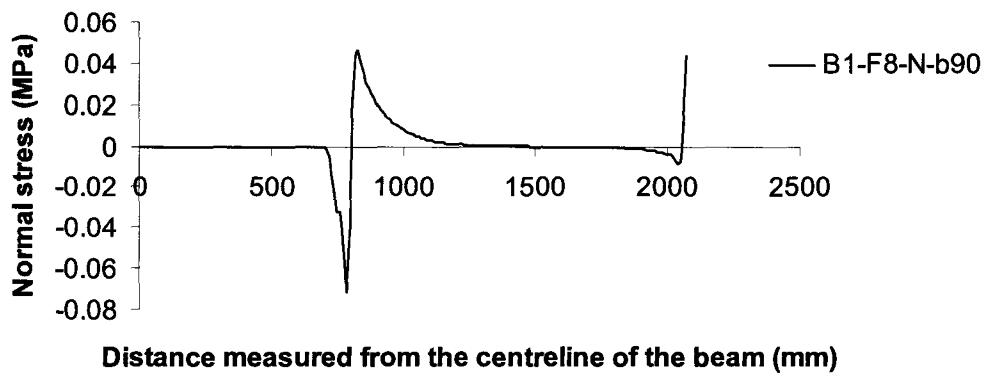

Fig.5-20: Predicted normal stress distribution along the CFRP-concrete interface for beam B1-F8-N-b90

Shear Stresses

With refrence to Table 5-9, beam B-F1-N, which was strengthened with one layer of laminate, experienced 8.7 MPa shear stress before rupture. The corresponding shear stress at the laminate end was only 0.48 MPa. It is difficult to judge if the interface could have sustained more shear stress since the FRP laminate reached its rupture strength in this beam. However, Beam B-F2-N reached a 9.7 MPa shear stress when delamination initiated in the maximum moment zone. Since the laminate did not reach rupture in this case, it means that the interface shear capacity in the absence of anchors was 9.7 MPa. When anchors were used in the maximum moment zone in the companion beam B-F2-E3-M9, the FRP cross section was reduced due to the presence of the holes made through the laminate for passing the anchor legs. Theoretically, the reduction in the cross sectional area will result in a higher shear stress since the contact area is reduced. This agrees with the predicted shear value of 14.5 MPa, which is 49.5 % higher than the companion beams without anchors in the midspan zone. Notice that in these theoretical calculations the load was set equal to be the maximum load reached in the test, therefore, the 14.5 MPa is theoretically the maximum shear resisted by the interface if nine anchors were used in the maximum moment zone. Hence, the presence of the anchors allowed the beam to resist 49.5 % higher shear stress than the beam without midspan anchors.

Since the model does not take into account the presence of the anchors, it is not possible to predict the actual shear stress resisted by them, but the beam with 11 evenly distributed anchors in the zone of maximum moment achieved 98% of its ultimate strength, which corresponds to a maximum shear stress of 14.5 MPa. When a laminate with smaller width of 90 mm was used in beam B1-F4-N-b90, the maximum shear before delamination was calculated to be 12 MPa. This value is 24% higher than that in a similar beam retrofitted with two layers of 220 mm wide laminate. The ratio of the FRP laminate width in the former beam to that in the later was 0.41. This reflects the fact that the smaller the width, the higher the interfacial shear stress since the shear stress is concentrated over a smaller width. The same observation can be made in the case of beam B-F8-N-b90 where the maximum shear stress reached was 9.3MPa when eight layers of 90 mm wide laminate were used compared to 6.7 MPa in the case of four layers of 220 mm wide laminate.

Clearly, in addition to the width of the laminate, its thickness or number of layers, have to be taken into account when predicting the shear stress distribution. When four layers of FRP and midspan anchors were used, the predicted shear stress was 10.3 MPa, which is 53.7% higher than the companion beam B-F4-N that did not have anchors. Therefore, this beam theoretically transferred 10.3 MPa shear stress along the interface, but it did not reach its theoretical ultimate flexural capacity based on full bond.

Figures 5-21 (a) to (g) show the predicted shear stress distribution along the FRP-concrete interface from midspan to laminate one end for the different retrofit configurations. As explained earlier, the sudden steep change in the strain variation in the vicinity of the loading point [See Fig.5-9] is indicative of high shear stress and we observe this high stress in each case. These figures show that the basic shape of the shear stress distribution does not change noticeably with change in either the number of FRP layers or the presence of anchors. However, the magnitude of the maximum shear stress before delamination changes significantly as indicated earlier in Table 5-9. Based on the shape of the interfacial shear stress distribution and the fact that both the concrete and the FRP at the interface are brittle materials, it is not possible to predict the delamination load based on an average shear stress. The delamination is triggered by the peak stress once it exceeds the interface shear strength. The peak value is several times higher than the average interface shear stress value, thus the average value has little practical significance. The average would be only meaningful if it is obtained through the integration of the actual shear stress distribution. To date no simple expression is available for determining the actual shear stress distribution at the FRP-concrete interface. Therefore, the solution procedure based on modified Youssef model as described earlier may be a relatively simple method for calculating the interfacial shear stress.

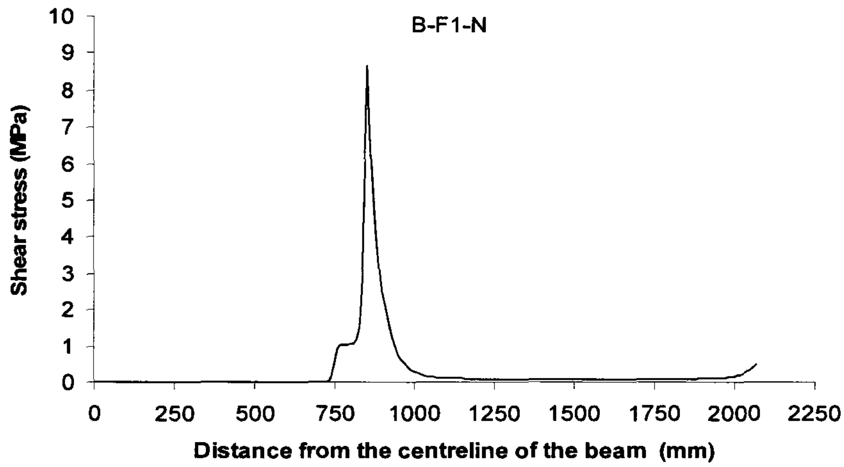

(a)

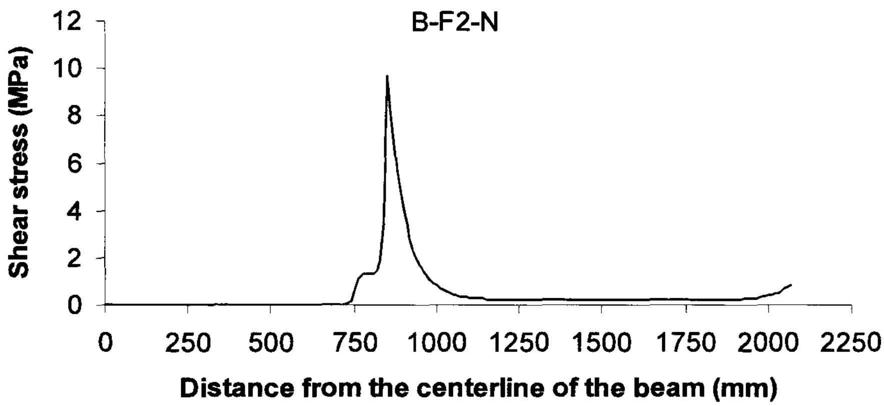

(b)

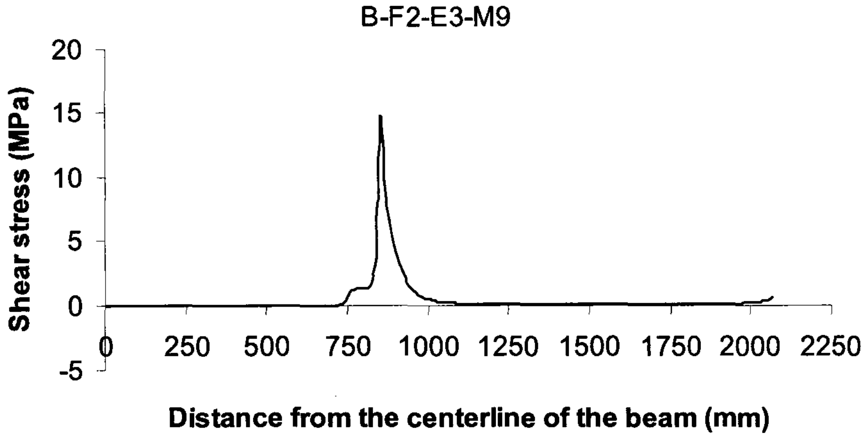
B-F2-E3-M9
Shear stress (MPa)
20
15
10
5
0
-5
0
250
500
750
1000
1250
1500
1750
2000
2250
Distance from the centerline of the beam (mm)

(c)

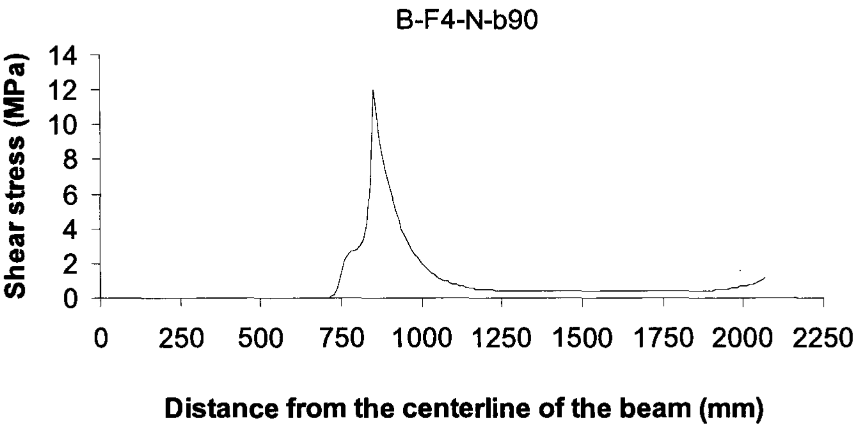
B-F4-N-b90
Shear stress (MPa)
14
12
10
8
6
4
2
0
0
250
500
750
1000
1250
1500
1750
2000
2250
Distance from the centerline of the beam (mm)

(d)

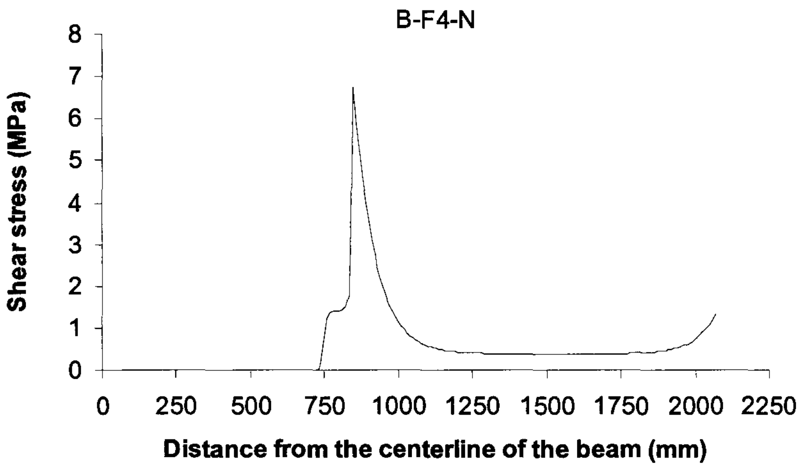
B-F4-N
Shear stress (MPa)
8
7
6
5
4
3
2
1
0
0
250
500
750
1000
1250
1500
1750
2000
2250
Distance from the centerline of the beam (mm)

(e)

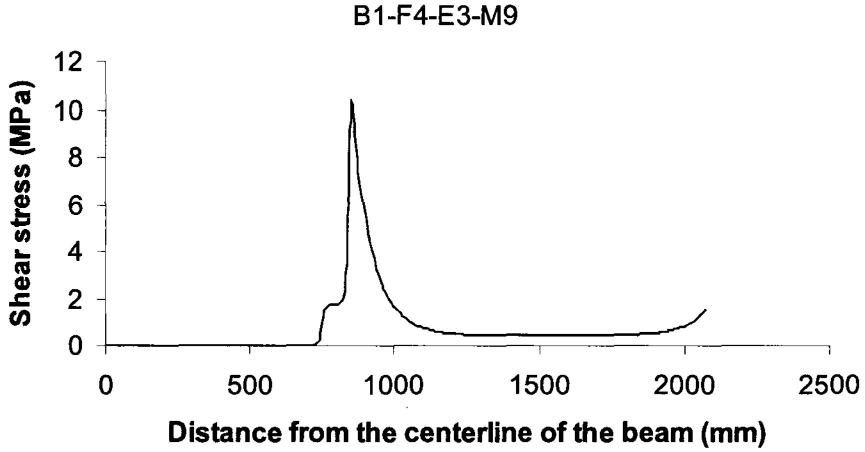

(f)

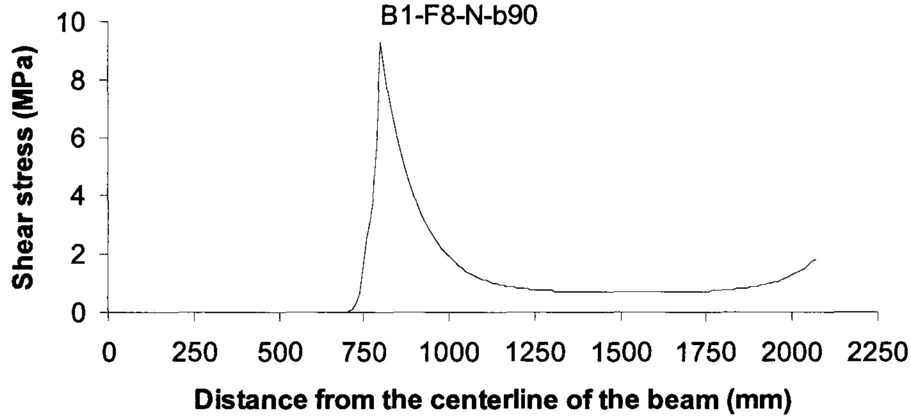

(g)

Fig.5-21: Predicted shear stress distribution along the CFRP-concrete interface for the tested beams

5.5.4 Tension Stiffening

Notice that all the above calculations are based on the assumption of no tension stiffening in the concrete beam. Tension stiffening refers to the presence of tensile stresses in concrete segments between two flexural cracks in a reinforced concrete beam. These stresses are known to exist and they will influence the moment-strain curve of the beam. It is useful to check the predicted interfacial stresses using the modified Youssef model, including tension stiffening. In this case the moment-strain diagram for the T-beam should be developed including the tension stiffening effect. It is known (Bazant and Oh 1984) that reinforced concrete exhibits tensile strain softening, i.e., a gradual reduction of tensile stresses with the increase of strain after cracking as shown in Fig.5-22.

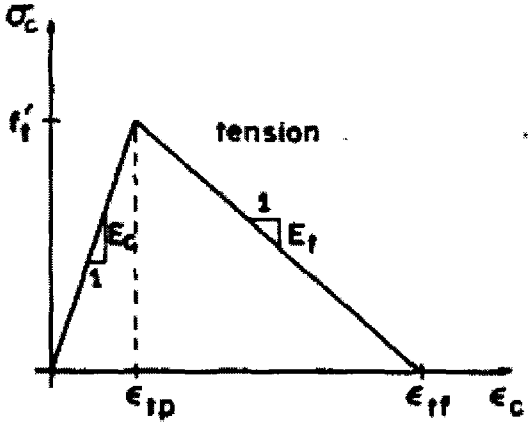

Fig.5-22: Stress strain relationship of concrete in tension (Bazant and Oh 1984)

This behaviour is idealized by a bilinear stress-strain diagram characterized by

$$\begin{aligned}
&\text{For } \varepsilon_c \le \varepsilon_{tp}', && \sigma_c = E_c\varepsilon_c \\
&\text{For } \varepsilon_{tp} < \varepsilon_c < \varepsilon_{tf}', && \sigma_c = f_t' - (\varepsilon_c - \varepsilon_{tp})(-E_t) \\
&\text{For } \varepsilon_c > \varepsilon_{tf}', && \sigma_c = 0
\end{aligned} \qquad \text{Eq.5-27}$$

in which σ_c, ε_c = uniaxial tensile stress and strain of concrete, E_c = elastic modulus of concrete, f_t' = tensile strength of concrete, ε_{tp}=strain at tensile strength or the cracking strain, ε_{tf} is the final strain when the tensile stress in concrete drops to zero. In this investigation, the strain at which the tensile stress goes to zero will be taken as 5 time the cracking strain. E_t = tangent strain-softening modulus and can be approximated (Bazant and Oh 1984) as

$$E_t = \frac{-70E_c}{57 + f_t'} \qquad \text{Eq.5-28}$$

By integrating the above stress-strain relation for concrete in tension, the moment-strain diagram can be developed as usual and it is plotted in Fig.5-23. Notice that the cracking moment is the same in both cases yet the concrete continues to show a high stiffness in the post-cracking stage. The yield moment is higher in this case compared to the yield moment calculated when tension stiffening was not included. Also notice that the after yield, the moment-strain curve shows a descending branch since the concrete in tension experiences softening, therefore, both curves, with and without tension stiffening, tend to have similar slopes and as expected give the same ultimate moment. In other words, tension stiffening does not affect the ultimate moment capacity of a RC section. To be able to consider the effect of tension stiffening, the following approximations will be made:

1. The stiffness, or the slope K_1, in the uncracked zone is the same regardless of the effect of tension stiffening.
2. The slope of the post-cracked zone will be approximated as indicated in Fig.5-23 and in this case, K_2 would be higher than in the case of no tension stiffening.
3. After yielding the behaviour is not significantly affected by tension stiffening, therefore it will be approximated as indicated by K_3 in Fig.5-23.

The author is well aware that the above approximations are made to avoid numerical problems and to avoid making the problem overly complex. Table 5-9 shows the predicted shear and normal stresses for some of the tested beams. As expected, using the tension stiffening leads to higher interfacial shear stresses at delamination. Since precise inclusion of tension stiffening in the analytical model would make it overly complex, a reasonable approach to dealing with the problem is to ignore it, but at the same time to assume a lower interfacial shear strength. It should be emphasized that in theory the inclusion of the tension stiffening in the model is not difficult, but practically it would make the solution more complex and more prone to numerical problems due to the many changes in the shape of the moment-strain curve. Since many of these, changes take place well before delamination; their precise effect on the delamination load needs more investigation.

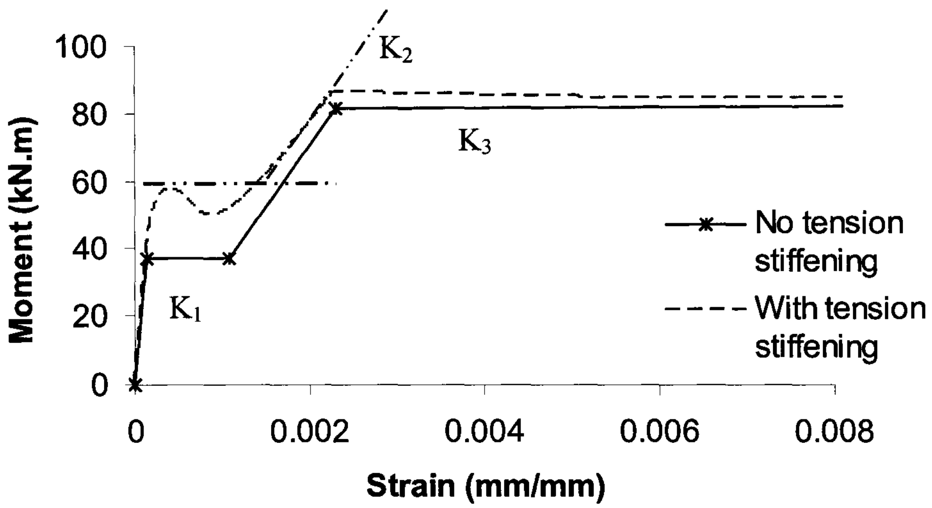

Fig.5-23: Moment-strain diagram with and without tension stiffening

5.6 Failure Criteria

It was shown in the previous section that the analytical model can predict the shear and normal stress at the FRP-concrete interface. To be able to predict the delamination load, one needs to establish a failure criterion. As mentioned before, delamination in FRP strengthened concrete members involving epoxy adhesive in practically every case occurs due to concrete failure at the interface. Consequently, the failure criterion must be based on the strength of concrete under combined stresses. In theory the concrete at the interface is subjected to biaxial tension and shear, but the maximum values of these stresses do not occur at the same location. It would appear that failure is caused mainly by interfacial shear stresses; therefore, it would suffice in practice to determine the interfacial shear strength of concrete and to compare the maximum computed shear with the latter strength. Failure would be assumed if the maximum shear stress exceeds the interfacial concrete shear strength.

Table 5-10 summarizes some available interfacial shear strength values. As can be seen in column 3 of Table 5-10, only two of these methods show shear stress limits that are close to the maximum shear stresses at delamination in the current test beams. Fib14-3 (2001) gives a limit of 7.9 MPa assuming a 54 MPa concrete. This value, however, could be considered a lower bound for most of the beams with no anchors except for beam B-F4-N, which reached a maximum shear stress of 6.7 MPa in the analysis. Notice that according to Fib 14-3 (2001) the maximum shear stress should not be greater than 1.8 f_{ctk} where f_{ctk} is the characteristic value of the tensile strength of concrete. The tensile strength of concrete is a function of the compressive strength of concrete and is given by Fib 14-3 as f_{ctk}. In this study, for $f_c' = 54$ MPa , the shear stress thus calculated would be 7.9 MPa. For the second group of beams with $f_c' = 59$ MPa, it would be 8.3 MPa. The relationship proposed by Nakaba et al. (2001) based on experimental data yields interfacial shear strength of 7.5 and 7.6 MPa for the 54 MPa and 59 MPa concrete, respectively. Notice that the lower shear stress limits in Table 5-10 ranging between 0.8 and 2.2 MPa are based on average shear stress along the interface. However, the average stress concept can not be used in the current situation since the shear stress shows a high peak value which rapidly drops over a small length. This peak stress may in fact be responsible for the initiation of delamination and it is this stress that needs to be limited to prevent premature delamination.

Table 5-10: Summary of the shear stress limitations

Codes and guidelines	Delamination criteria	Shear stress limit for the beams in this study (MPa)
Fib14-3 (2001)	$\tau = \dfrac{\Delta T_f}{b_f \Delta x} \leq 1.8 f_{ctk}$	7.9
SIA166 (2003)	$\tau \geq 0.3\sqrt{f_c}$	2.2
TR55 (2004)	$\tau \leq 0.8 \text{N/mm}^2$	0.8
Werner et al. (2003)	$\tau \geq 1.6 \text{MPa}$	1.6
Nakaba et al. (2001)	$\tau \geq 3.5 f_c'^{0.19}$	7.5

Let us use the Fib, 14-3 shear stress limit of 7.9 MPa and determine the corresponding load producing this level of stress in some of the current test beams.

Towards this end, the maximum interface shear stress in the midspan zone and near the laminate end are plotted against the applied load in Fig.5-24. We noticed that the end shear stresses are small and therefore inconsequential in the case of the present beams. The midspan zone shear stresses vary in a non-linear fashion with the applied load. Based on these figures, the delamination load of each beam can be found by determining the load corresponding to a shear stress of 7.9 MPa as indicated in each of the shear stress-load diagrams in Fig.5-24. The delamination loads calculated in this manner are shown in columns 3 of Table 5-11 and the ratio of these theoretical load values to the corresponding experimental values are given in column 4 of the table. We observe that this procedure yields reasonable results for practically all the beams except for the two beams with many anchors in which the laminate practically reached its rupture strain and which did not fail due to delamination. For the remaining beams, the ratio of the theoretical to the measured delamination load ranges from 0.85 to 1.25.

The beam with the ratio of 1.25, beam (B1-F4-N), must have had some flaw because its companion beam (beam B1-F4-N) has a more reasonable ratio of 1.05. This level of accuracy is quite reasonable for practical applications, given the complexity of this problem and the variability which one observes in the actual shear strength of concrete. Furthermore, in the majority of the cases, the predicted values are on the conservative side, which is desirable from the safety point of view. Since for the two beams with many evenly distributed anchors and laminate width of 90 mm, the predicted delamination loads are low and rather inaccurate, it means that the Fib, 14-3 shear limit cannot be applied to these beams without further analysis. The reason is that in the case of these beams, part of the interfacial shear stress is transferred by the anchors and therefore the anchors contribution increases the total interfacial shear resistance of these beams. This issue will be dealt with in a subsequent section in this chapter.

Table 5-11: Summary of test results and the predicted delamination load

Beam Designation	Test Results (kN)	Theory (kN)	$\frac{P_{Th.}}{P_{Exp}}$
B1-F1-N	203.5	184.0	0.90
B2-F1-N	209.0		0.88
B1-F1-E3	199.7		0.92
B2-F1-E3	198.2		0.93
B1-F2-N	230.1	215.0	0.93
B2-F2-N	205.4		1.05
B1-F2-E3	224.5		0.96
B2-F2-E3	216.7		0.99
B1-F2-E3-M9	226.4	207.0	0.91
B1-F2-E4-M11	234.5		0.88
B1-F4-N-b90	199.6	170.0	0.85
B1-F4-E3-M15-b90	244.0		0.70
B1-F4-N	252.5	266.0	1.05
B2-F4-N	213.0		1.25
B1-F4-E3	256.5		1.04
B1-F4-E3-M9	279.5	250.0	0.89
B1-F8-N-b90	214.6	205.0	0.96
B1-F8-E3-M17-b90	309.0		0.66

5.6.1 Parametric Study

Since both the FE and the analytical model predicted the FRP strain variation with a reasonable accuracy, a parametric study will be carried out to examine the effect of laminate width and thickness on the maximum interfacial shear stress. The variation in the laminate thickness will be simulated by the number of layers in the laminate. This parametric study was preformed using the analytical model described earlier. Figure 5-25 shows the maximum interfacial shear stress plotted versus the number of FRP layers for different laminate widths. As can be seen from the figure, the interfacial shear stress would be theoretically higher than the limiting value of 7.9 MPa and therefore all beams would fail due to delamination since none of the beams would achieve their theoretical capacity based on full bond. Furthermore, and based on Fig.5-26, the shear stress at the laminate end would be always less than concrete shear strength and therefore it is not expected that failure due to end delamination would occur.

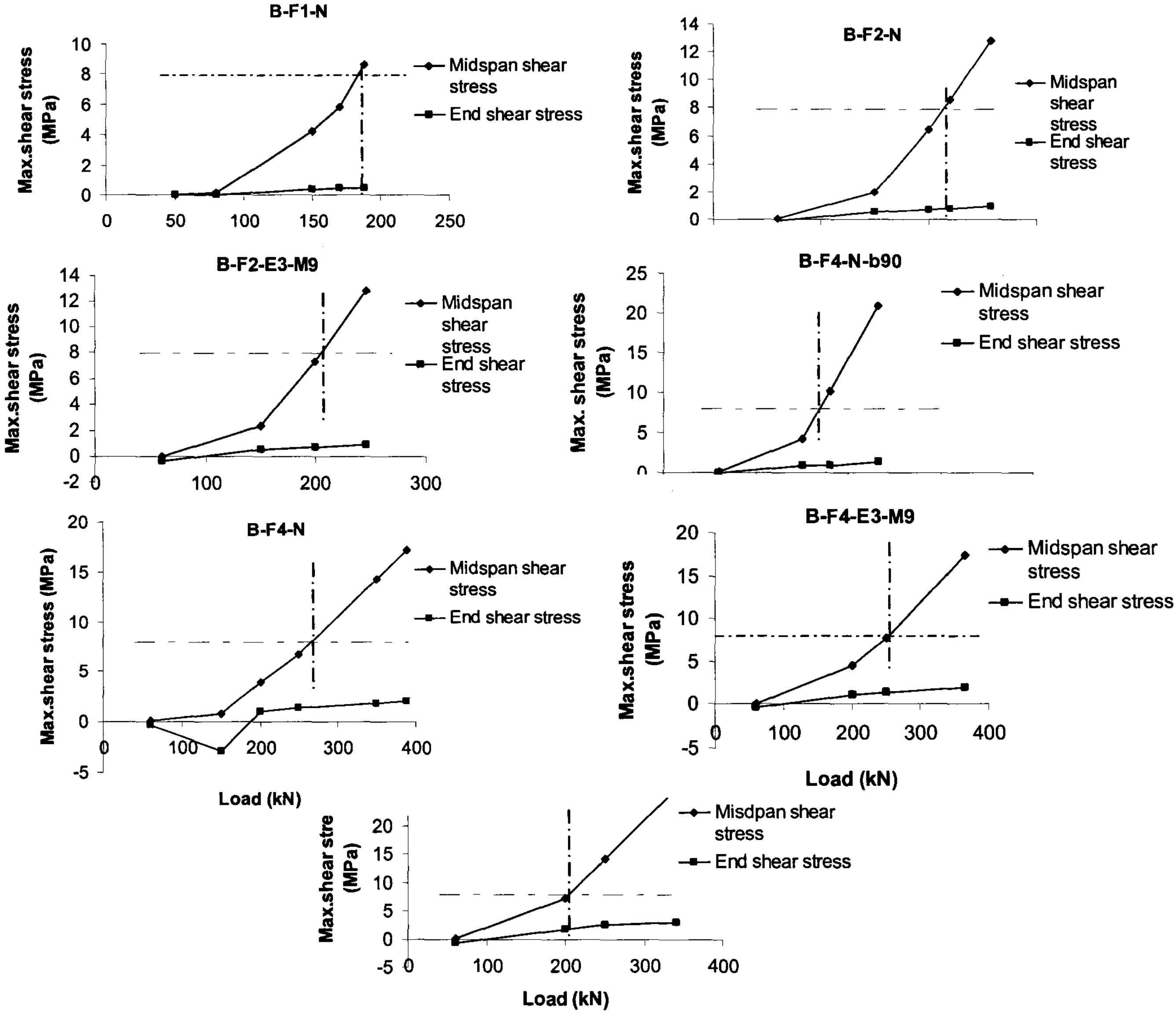

Fig.5-24: Delamination load of tested beams based on Fib.14-3 interfacial shear stress limit

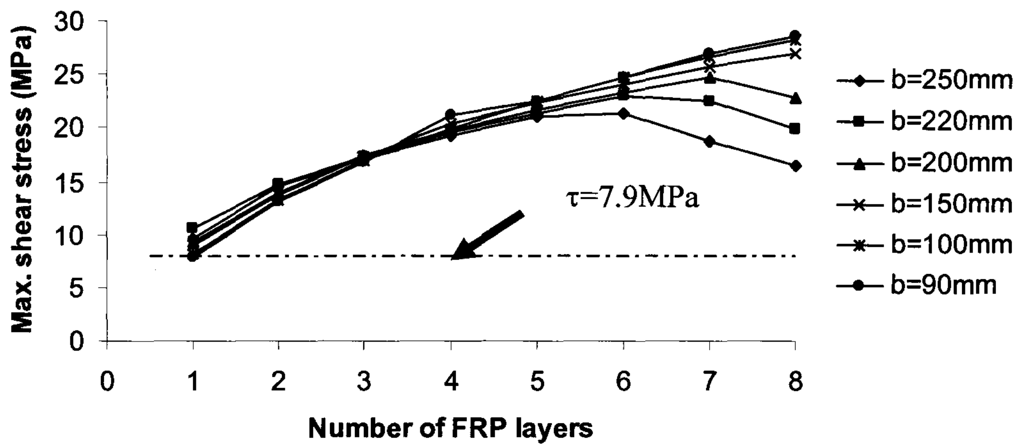

Fig.5-25: Maximum shear stress versus the number of FRP layers with different laminate widths at midspan

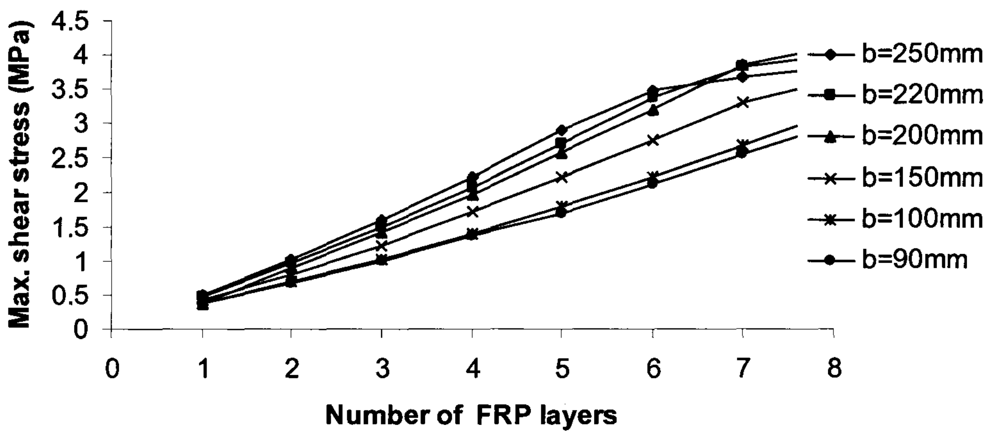

Fig.5-26: Maximum shear stress versus the number of FRP layers at different laminate widths at laminate end

As mentioned earlier, the problem of delamination at the constant moment zone cannot be treated using the average shear stress concept since the predicted shear stress shows a peak shear stress in the vicinity of the loading points over a small bonded length. The area of the shear stress diagram is equal to the axial force that can be carried by the FRP laminate. Since the peak shear stress occurs over a small distance, and since the interface between the concrete and the FRP laminate can not sustain this shear stress alone, an additional bonded surface is required to transfer the extra shear stress which could be provided by the proposed anchorage system. The maximum distance over which the peak shear stress occurs was found to be 300 mm. This distance will be referred to as the effective bond length. This means that an additional area is required to carry an interfacial shear stress in excess of that carried by the beam without anchors.

In the following calculation the bonded length of 300 mm as predicted from the model will be used. Since the modified model and the limiting shear stress value of 7.9 MPa gives a good prediction of the capacity of beams without anchors, these values will be used to estimate the contribution of the interface without anchors to the delamination load of the test beams.

<u>Case Study:</u>

As shown in Table 5-11, Beam B1-F4-N-b90 reached a maximum load of 199.6 kN while the predicted value based on 7.9 MPa shear strength is 170 kN, which is 85% of the delamination load. The companion beam with anchors reached 244 kN, which is 44% higher than the predicted value using a limiting shear stress of 7.9 MPa. Since the anchors were evenly distributed at 200 mm centre to centre over the span length, the number of anchors over the 300 mm would be 2. Based on the anchor geometry (anchor head being 200x50), the contact width of the FRP laminate with the anchor head is 90 mm whereas the total anchor head length is 200 mm. Therefore, the part of the anchor head surface directly bonded to the concrete surface is 110 x50 mm^2 . The area of the FRP laminate bonded to the concrete over the same length is 300x90 mm^2. Therefore, this anchor head provides an additional bonded surface of 11000 mm^2 versus the 27000 mm^2 surface directly provided by the laminate. Let us define the factor ξ as the ratio of the total bonded area of FRP, including the anchors, to the bonded area of the FRP laminate alone.

$$\xi = \frac{L_b b_f + n l_a b_a}{L_b b_f} = \frac{300\text{x}90+2\text{x}110\text{x}50}{300\text{x}90} = 1.41 \qquad \text{Eq.5-29}$$

where L_b is the laminate bonded length, b_f is the FRP laminate width, n is the number of anchors in the bonded length, l_a is the anchor plate length bonded to the concrete and b_a is anchor plate width bonded to the concrete. If we multiply the previously predicted delamination load of this beam based on the Fib.14-3 shear limit as shown in Table 5-11, i.e. the 170 kN, by the factor ξ , we will obtain a delamination load of 238 kN, which is 97.5% of its experimental value.

Next let us consider beams B1-F8-N-b90 and its companion beam B1-F8-E3-M17-b90. In this case the beam without anchors reached 214.6 kN versus its predicted value of 205 kN, which is 96% of its actual value, while the beam with anchors reached 309 kN, which is much higher than its predicted value. If we calculate the factor ξ for this beam, it will turn out to be the same value as in Eq.5-27. Therefore, the delamination load f this beam can be approximated as 1.41x205=289.05 kN, which is 93.5% of its corresponding experimental value. Consequently, the delamination load for the beams with anchors depends on the amount of bonded surface are between the anchor plate and the concrete, and the above procedure yields a reasonable estimate of these beams.

Effect of Ks

Recall that the spring constant simulating the shear stiffness (K_s) of the adhesive and the spring constant simulating the peeling stiffness(K_p) should be determined experimentally, but this requires a special set-up which was not available to the author; therefore, the values suggested by Youesef (2006) were used. Since the normal stresses are not significant in this case, it was decided to investigate the effect of K_s on the shear stress magnitude. Towards this end, different values of K_s, ranging from 15 to 40 N/mm^3,with an increment of 5 N/mm^3 ,were used. For illustration, the effect of changing K_s will be considered for beam B1-F8-N-b90, where the predicted shear stresses versus different K_s values for this beam are plotted in Fig.5-27. As can be seen in this figure, the maximum shear stress at the delamination load increased with increase of K_s, but the rate of increase is relatively small. For example, changing K_s from 15 N/mm^3 to 25 N/mm^3, a 67% increase, increased the maximum shear stress by only 25%. Nevertheless, this issue will need further investigation in the future.

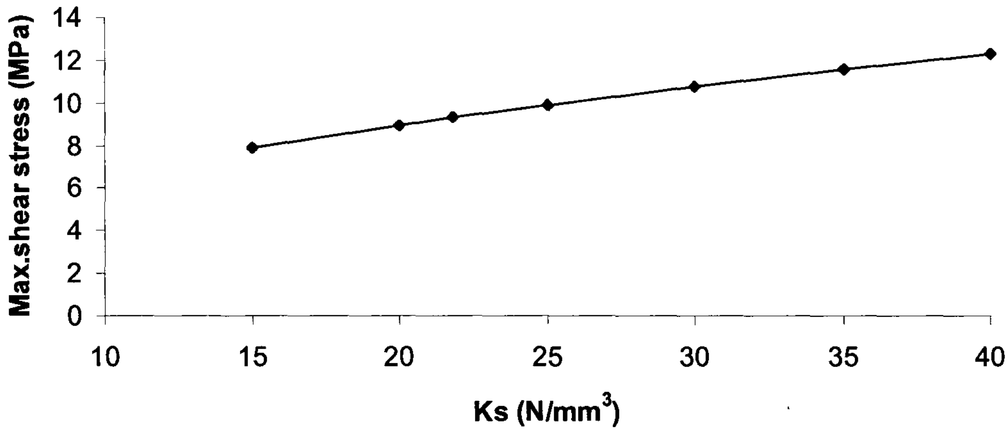

Fig.5-27: Effect of K_s on the shear stress

5-7 Summary

In this chapter the experimental results were analyzed using different analytical and numerical techniques. It was discovered that the nonlinear finite element analysis can predict both the delamination load and the strain variation in the FRP laminate reasonably well. However, it could not provide an accurate estimate of the interfacial shear stresses. On the other hand, the analytical model based on composite beam theory with partial interaction at the FRP-concrete interface yielded more satisfactory results. This model is able to predict the delamination load and the strain in the FRP relatively accurately. Its results could also be modified to obtain the delamination load of beams with anchors, provided the anchor head is partially bonded to the concrete. The method has potential for further improvement and for eventual adoption in design standards.

CHAPTER 6
SUMMARY, CONCLUSIONS AND RECOMMENDATIONS FOR FUTURE WORK

6.1 Summary

In this study, a new FRP anchor is developed and tested to substantially delay/prevent delamination in beams externally strengthened with FRP laminates. The main objective of the current experimental work is to investigate the effectiveness of the proposed new anchorage system and to find the appropriate anchor arrangement which can be used to achieve the foregoing π- shape objective. The anchor comprises a wide CFRP plate that services as the head and two CFRP rods serving as the legs. The head plate with dimensions of 200 mm long , 50 mm wide and 3 mm thick is designed to provide a relatively large surface for resisting interfacial shear stresses. The cylindrical anchor legs are 90 mm long and 10 mm in diameter and are designed for embedment inside the concrete to resist shear and normal stresses. Each anchor is made from a carbon fibre tow immersed in an epoxy resin and then shaped and cured inside a metal mould. During the retrofit, the anchor legs are inserted into pre-drilled holes filled with epoxy adhesive and the head plate is bonded by epoxy to the surface of the FRP laminate and the adjacent concrete. Anchors can be placed at any location along the length of the FRP laminate.

To be able to investigate the effectiveness of the proposed anchor, first, the anchors were tested by anchoring CFRP laminate strips bonded to a concrete prism and subjected to direct tension (Phase I and Phase II). The results of these tests demonstrated the potential of the proposed anchor in preventing premature delamination. To further investigate this potential in real structures, twenty one large scale RC T-beams were constructed and tested. All the beams had the same dimensions and internal steel reinforcement and, except for the control beams, were retrofitted with one or more layers of CFRP laminate strips to increase their flexural resistance. The main test parameters were:

1. Amount of CFRP reinforcement, using three FRP reinforcement ratios.
2. Presence / absence of mechanical CFRP anchors.
3. Number/spacing of anchors.
4. Anchors along the beam length

Due to the preliminary nature of the study and due to lack of any design guidelines for such anchors, the number and spacing of the anchors were based on some trial and error and on practical considerations. Ultimately, an anchor arrangement was found which allowed beams with this arrangement to achieve over 90 % of their theoretical capacity, even if up to eight layers of the laminate were applied to the soffit of the beam.

All the methods available in the literature for designing against intermediate crack debonding were reviewed and the accuracy of the design methods was evaluated via comparison with the experimental results. The theoretical capacities of these beams were also calculated based on the different design guidelines and were compared with the experimental data.

Finally, an existing theoretical model was modified and applied to the current RC beams. The modified model was used to predict the interfacial shear and normal stresses along the laminate. A parametric study was carried out to investigate the effects of the number of layers and the laminate width on the maximum interfacial shear stress. Limiting shear stress values based on the Fib 14-3 (2001) recommendation were used in conjunction with the aforementioned theoretical model to calculate the ultimate load capacity of each beam. Good agreement between the predicted values and the delamination loads measured in the test was observed. Furthermore, a simple procedure was developed to determine the effect of the anchors on the delamination load and the procedure gave a reasonable estimate of the delamination or failure loads of the tested beams.

6.2 Conclusions

From the experimental results and their analysis, the following conclusions can be stated:

Phase I: Prisms with continuous steel reinforcement.

1- Prisms with anchors achieved 14.5 % and 41.8 % higher delamination load compared to the prisms without anchor.

2- The CFRP laminate reached approximately 90% of its ultimate strain in the prisms with anchors.

3- Contrary to the prisms without anchors, the prisms with anchors did not experience full delamination but they did experience slippage at one end.

4- None of the anchors experienced pull out.

5- None of the prisms experienced rupture of the CFRP laminate. Only local rupture in the vicinity of the anchors was observed.

6- The two steel reinforcement bars going through the mid-length of the test prisms often made it difficult to ascertain the ability of the anchor to delay/prevent the delamination. It was obvious from the prisms load elongation curves that these bars experienced yielding and rupture.

Phase II: Prisms without continuous steel reinforcement

1- The proposed anchor proved effective in increasing the load carrying capacity of the test prisms and in delaying delamination, however, the anchor could not prevent the end slippage.

2- The load in the prisms containing one anchor at each end of the laminate strips was 32% higher than the companion prisms without anchors.

3- The load in the prisms containing two anchored at each end of the laminate strips was about 98% higher than the companion prisms without anchors and 50% higher than the primes with one anchor at each end of the laminate.

4- The maximum axial displacement reached in the case of the prisms with one anchor at each end was about double the corresponding displacement in the prisms without anchors.

5- The maximum displacement reached in the prisms with 2 anchors at each end was double the corresponding displacement in the prisms with one anchor at each end.

6- Two prisms with anchors experienced substantial slip exceeding 50 mm, however, neither prism experienced anchor pullout. The prisms experienced a ductile behavior until failure.

7- In prisms P12 and P13, the anchors prevented the laminate from slippage until the concrete totally crushed.

8- The CFRP laminate in none of the prisms reached the rupture strain; only local rupture could be visually seen around the anchor.

9- In the prisms with anchors, the longitudinal strain profile in the laminate showed a more uniform distribution close to the failure load. Once delamination initiated at a certain point, the strain at that point abruptly increased and propagated to adjacent sections causing abrupt increases in strain. In the delaminated portions, all points experience more or less the same strain value which is reflected by the uniform distribution profile.

10- Initial or pre-debonding of a portion of the laminate before application of the load caused reduction in the ultimate load capacity; therefore, it is not recommended.

<u>Phase I</u>: Based on the outcomes and findings from the test results, the following conclusions could be drawn:

1- Anchors have to be used throughout the zone of maximum moment to prevent the intermediate crack debonding failure mode in beams externally strengthened with FRP laminates and designed to fail in flexure.

2- Using anchors with 90 mm long legs in the current beams with concrete cover of 40 mm, none of the anchors pulled out the concrete cover peel off. Therefore, the anchor leg length should be at least double the concrete cover. However, the anchor must always extend at least 50 mm into the concrete beyond the stirrups.

3- When using end anchorage only, different modes of failures were observed in the current investigation:

a) Bearing failure at the location of the anchor leg

b) Slippage of the laminate

c) Failure of the anchor

It is believed that the reason for these failure modes was the way the CFRP anchor legs were inserted through the laminate which disturbed the fibers and caused stress concentration at the location of the anchor legs. Therefore, it is recommended not to drill through the laminate instead, always place the CFRP laminate between the anchor legs.

4- The anchor head was 200 mm long and it was constant in this investigation. The width of the beam was 250 mm and the width of the CFRP laminate used in some of the beams was 220 mm. Therefore, 20 mm of the CFRP laminate was outside the anchor head. It is concluded that any portion of the CFRP laminate width lying outside the anchor head would delaminate early and it would trigger delamination at other locations. Therefore, it is recommended that the full width of the laminate be always bonded to the anchor head to avoid premature delamination.

5- Anchors evenly distributed at 200 mm centre-to-centre along the length of the bonded FRP laminate allowed the beams to practically achieve their full theoretical capacity.

6- Placing the laminate within the anchor legs and using evenly distributed anchors allowed the beams to achieve practically their full theoretical capacity.

7- The anchors allowed the laminate to achieve its ultimate strain as reported by the manufacturer.

8- The beams strengthened with 90 mm wide laminate strips and anchors achieved more than double the ductility and the energy absorption than their companion beams without anchors.

9- Beams with anchors reached their delamination load at a higher deflection compared to their companion beams without anchors.

10- The portion of the anchor head plate surface bonded directly to the concrete in the vicinity of the maximum interfacial shear stress enhanced the anchor ability to prevent delamination.

11- The anchor is easy to apply but it needs some practical considerations, such as knowing the location of the internal reinforcement, including the stirrups. The anchor geometry is easy to change; however, it needs a better manufacturing process to be able to produce a sufficient number of anchors in a short time period.

12- The theoretical model used to predict the interfacial shear and normal stresses indicates extremely high shear stresses in the vicinity of the applied concentrated load in the constant moment zone. The fact that delamiantion initiated in that zone shows that the problem of intermediate crack debonding cannot be predicted by the conventional beam theory assuming full bond between the FRP laminate and the concrete substrate. Due to the highly uneven distribution of interfacial stresses, the concept of average shear stress cannot be used to predict the delamination load. Limiting the maximum interfacial shear stress calculated by the theoretical model to 7.9 MPa, based on fib recommendations for the concrete used in these beams, showed good agreement with the experimental delamination load of the beams without anchors.

6.3 Recommendations for Future Work

1- Test beams with different numbers of FRP laminate layers placed between the anchor leg to determine its effect on the delamination load, ultimate strength and ductility of beams externally strengthened with FRP.

2- In order to obtain an optimum embedment depth, test anchors with different embedment depths.

3- Investigate the extension of the theoretical delamination model to beams with anchors and different load configurations.

4- The theoretical model can be further modified to account more accurately for the effects of tension stiffening and concrete racking on the moment-strain diagram and the interfacial stresses.

5- Test beams strengthened with GFRP or GFRP anchors to explore the applicability of the proposed anchor system to other FRP materials, particularly GFRP, which is widely used in practice.
6- Test beams with different FRP development lengths and unsheeted
7- It may be beneficial to test some much larger beams to determine whether the anchor geometry and dimensions would be suitable for full size members.
8- The proposed anchor is universal and it could be used to prevent delamination of shear reinforcement, but this needs to be proven by proper testing.
9- These anchors should be tested in retrofitted reinforced concrete and masonry walls subjected to cyclic loads to see if they can prevent delamination in such walls under seismic excitation.

References

El Damatty, A.A.and Abushagur, M. (2003),"Testing and Modeling of Shear and Peel Behaviour for Bonded Steel/FRP Connections", *Journal of Thin Walled Structures*, Vol. 41, No.11, pp. 987-1003.

Abdel Baky, H., Ebead, U.A. and Neale, K. (2007),"Flexural and Interfacial Behaviour of FRP-Strengthened Reinforced Concrete Beams", *Journal of Composites for Construction*, ASCE , Vol.11, No. 6, pp. 629-639.

Abdelouahed, T. (2006),"Improved Theoretical Solution for Interfacial Stresses in Concrete Beams Strengthened with FRP Plate", *International Journal of Solids and Structures*, Vol. 43, No.14-15, pp. 4154–4174.

ACI 440.2R (2002), *Guide for the Design and Construction of Externally Bonded FRP Systems for Strengthening Concrete Structures*, American Concrete Institute, Farmington Hills, MI.

ACI 440.2R (2008), *Guide for the Design and Construction of Externally Bonded FRP Systems for Strengthening Concrete Structures*, American Concrete Institute, Farmington Hills, MI.

Aram, M. R., Czaderski, C. and Motavalli, M. (2008)," Debonding Failure Modes of Flexural FRP-Strengthened RC Beams", *Journal of Composites: Part B*, Vol. 39, pp. 826-841.

Arduini, M. and Nanni (1997),"Behaviour of Pre-Cracked RC Beams Strengthened with Carbon FRP Sheets", *Journal of Composites for Construction*, ASCE, Vol.1, No.2, pp. 63-70.

Ascione, F. (2009)," Mechanical Behaviour of FRP Adhesive Joints: A Theoretical Model", *Journal of Composites: Part B.*, Vol. 40, No. 2, pp.116-124.

Bazant, Z.P. and Oh, B.H. (1984)," Deformation of Progressively Cracking Reinforced Concrete Beams", *ACI Structural Journal*, Vol. 81, No. 3, pp. 268-278.

Bonfiglioli, B., Pascale, G., Ibarra and Perez, J. (2003),"Flexural Behaviour of Reinforced Concrete Beams Repaired with Externally Bonded FRP", *Journal of Composites for Construction*, ASCE, pp. 295-300.

Broadhouse, B.J. and Neilson, A.J. (1987),"Modeling Reinforced Concrete Structures in DYNA3D", Safety and Engineering Science Division, United

Kingdom Atomic Energy Authority, Winfrith, AEEW-M 2465. Paper presented at DYNA3D User Group Conference, London.

Buykozturk, O., Gunes, O. and Karaca, E. (2004),"Progress on Understanding Debonding Problems in Reinforced Concrete and Steel Members Strengthened Using FRP Composites", *Construction and Building Materials*, Vol.18, pp. 9-19.

Ceroni, F., Pecce, M., Matthys, S. and Taerwe, L. (2008),"Debonding Strength and Anchorage Devices for Reinforced Concrete Elements Strengthened with FRP Sheet", *Journal of Composites Part B: Engineering*, Vol. 39, No. 3, pp.429-441.

Chahrour, A. and Soudki, K.(2005)," Flexural Response of Reinforced Concrete Beams Strengthened with End-Anchored Partially Bonded Carbon Fiber-Reinfoced Polymer Strips", *Journal of Composites for Construction,* ASCE, Vol. 9, No. 2, pp. 170-177.

Chajes, M.J., Thomson, T.A., Januszka, T.F. and Finch, W.W.(1994)," Flexural Strengthening of Concrete Beams Using Externally Bonded Composite Materials", *Construction and Building Materials*, Vol. 8, No. 3, pp.191-201.

Chen, F. and Qiao, P. (2009),"Debonding Analysis of FRP-Concrete Interface Between Two Balanced Adjacent Flexural Cracks in Plated Beams", *International Journal of Solids and Structures*, Vol. 46, No.13, pp. 2618-2628.

Chen, J. F., and Teng, J. G. (2001), "Anchorage Strength Models for FRP and Steel Plates Bonded to Concrete", *Journal of Structural Engineering*, ASCE, Vol. 127, No.7, pp.784–791.

Chen, J. F., Yuan, H. and Teng, J. G.(2005),"Analysis of Debonding Failure Along a Softening FRP-to-Concrete Interface Between Two Adjacent Cracks", Proc., Int. Symp. on Bond Behavior of FRP in Structures, (BBFS 2005), *International Institute for FRP in Construction*, pp. 103–111.

CNR-DT 200 (2004), *Guide for the Design and Construction of Externally Bonded FRP Systems for Existing Structures*, Italian National Research Council, Rome.

Collins, M. P. and Mitchell, D.(1999), *Reinforced and Prestressed Concrete Structures*, Prentice Hall, N.J., 766 pp.

CSA. (2002), *Design and Construction of Building Components with Fiber-Reinforcement Polymers, CSA Standard S806-02*, CSA, Rexdale (Toronto). Ontario.

El-Mihilmy, M. and Tedesco, J. (2001), "Prediction of Anchorage Failure for Reinforced Concrete Beams Strengthened with Fiber-Reinforced Polymer Plates", *ACI Structural Journal*, Vol. 98, No. 3, pp. 301-314.
Elsayed, W., Ebead, U. and Neale, K.(2009),"Studies on Mechanically Fastened Fiber-Reinforced Polymer Strengthening Systems", *ACI Structural Journal*, Vol. 106, No.1, pp.49-59.

Federation internationale du beton (fib) (2001), *Design and Use of Externally Bonded Fiber Reinforced Polymer Reinforcement (FRP EBR) for Reinforced Concrete Structures*, Technical Report, Bulletin No.14, Paris.

Galal K. and Mofidi A.(2009),"Strengthening RC Beams in Flexure Using New Hybrid FRP Sheet/Ductile Anchor System", *Journal of Composites for Construction*, ASCE, Vol. 13, No. 3, pp. 217-225.

Gardent, H.N. and Hollaway, L.C. (1998),"An Experimental Study of the Influence of Plate End Anchorage of Carbon Fibre Composite Plates Used to Strengthen Reinforced Concrete Beams", *Composite Structures*, Vol. 42, No.2, pp. 175-188.

Harmon, T. G., Kim, Y. J., Kardos, J., Johnson, T., and Stark, A. (2003), "Bond of Surface Mounted Fiber-Reinforced Polymer Reinforcement for Concrete Structures", *ACI Structural Journal*, Vol. 100, No.5, pp 557–564.

Heffernan, P.J. and Erki, M.A.(1996),"Equivalent Capacity and Efficiency of Reinforced Concrete Beams Strengthened with Carbon Fiber Reinforced Plastic Sheets", *Canadian Journal of Civil Engineering*, Vol. 23, No.1, pp. 21-29.

Hu, H.T., Li, F.M. and Jan, Y.Y (2004),"Nonlinear Finite Element Analysis of Reinforced Concrete Beams Strengthened by Fiber-Reinforced Plastics", *Composite Structures*, Vol. 63, No.3, pp 271-281.

ISIS. (2001), *Strengthening Reinforced Concrete Structures with Externally Bonded Fiber Reinforced Polymers*, The Canadian Network of Centers of Excellence on Intelligent Sensing for Innovative Structures, Winnipeg, Manitoba.

Teng, J.G., Zhang, J.W. and Smith, S.T. (2002)," Interfacial Stresses in Reinforced Concrete Beams Bonded with a Soffit Plate: A Finite Element Study", *Construction and Building Materials*, Vol. 16, No.1, pp. 1-14

JSCE (2001), *Recommendations for Upgrading of Concrete Structures with Use of Continuous Fiber Sheets*, JSCE Concrete Engineering Series, 41, 31-34, Tokyo.

Juvandes, L., Figueiras, J.A. and Marques, A.T.(1998)," Performance of Concrete Beams Strengthened with CFRP Laminates", Proc. of 2nd International Conference on Composite in Infrastructure, ICC 98, University of Arizona, Tucson, pp. 126-137.

Nakaba, K., Kanakubo, T., Furuta, T. and Yoshizawa, H. (2001)," Bond Behaviour between Fiber-Reinforced Polymer Laminates and Concrete", *ACI Structural Journal*, Vol. 98, No. 3, pp. 359-367.

Lamanna, A.J, Bank, L.C., and Scott, D.W.(2001)," Flexural Strengthening of RC Beams using Fasteners and FRP Strips", *ACI Structural Journal*, Vol. 93, No. 3, pp. 368-376.

Leung, C.K.Y., and Tung, W.K.(2001), "A Three Parameter Model for Debonding of FRP from Concrete Substrate", Proc., Int. Conf. on FRP Composites in Civil Engineering, Hong Kong, China, pp. 373–379.

Li, L.J., Guo, Y.C., Liu, F. and Bungey, J.H. (2006)," An Experimental and Numerical Study of the Effect of Thickness and Length of CFRP on Performance of Repaired Reinforced Concrete Beams", *Construction and Building Materials*, Vol. 20, No.10, pp. 901-909.

Liu, I., Oehlers, D.J. and Seracino, R.(2007),"Study of Intermediate Crack Debonding in Adhesively Plated Beams", *Journal of Composites for Construction*, ASCE , Vol. 11, No. 2, pp. 175-183.

LS-DYNA Keyword User's Manual, Version 971, http://www.lstc.com/index.htm

Lu, X.Z. (2004), "Studies of FRP-Concrete Interface", Ph.D. thesis, Tsinghua University, Bejing.

Lu, X.Z., Teng J.G. and Jiang, J.J.(2007)," Intermediate Crack Debonding in FRP-Strengthened RC Beams: FE Analysis and Strength Model", *Journal of Composite for Construction*, ASCE, Vol. 11, No. 2, pp.161-174.

Youssef, M.A. (2006),"Analytical Prediction of the Linear and Nonlinear Behaviour of Steel Beams Rehabilitated using FRP Sheets", *Journal of Engineering Structures*, Vol. 28, No. 6, pp. 903-911.

Maeda, T., Asano, Y., Sato, Y., Ueda, T., and Kakuta, Y.(1997)," A Study on Bond Mechanism of Carbon Fiber Sheet", Proc., 3rd Int.Symp.on Non-Metallic (FRP) reinforcement for Concrete Structures (FRPRCS3), Sapporo, Japan, pp. 279-286.

Malek, A.M., Saadatmanesh, H. and Ehsani, M.R.(1998),"Predication of Failure Load of R/C Beams Strengthened with FRP Plate due to Stress Concentration at the Plate End", *ACI Structural Journal*, Vol. 95, No.2, pp. 142-152.

Martin, J., Lamanna, A.(2008),"Performance of Mechanically Fastened FRP Strengthened Concrete Beams in Flexure", *Journal of Composites for Construction*, Vol. 12, No. 3, pp. 257-265.

Matthys, S. (2000),"Structural Behaviour and Design of Concrete Members Strengthened with Externally Bonded FRP Reinforcement", Doctoral thesis, University of Ghent. Ghent, Belgium.

Meier, U. (1995),"Strengthening of Structures Using Carbon Fiber/Epoxy Composites", *Construction and Building Materials*, Vol. 9, No. 6, pp. 341-351.

Mostafa, A. (2005),"Development of a New FRP anchor for Externally Bonded CFRP Sheet/Laminate to Beams", M.A.Sc. Thesis, Carleton University. Ottawa, Canada.

Mostafa, A. and Razaqpur, A.G.(2008),"Modelling the Delamination Process and Load in RC Beams Externally Strengthened with CFRP Laminate", Proc. of the 5th International Conference on Advanced Composite Materials in Bridges and Structures (ACMBS-V), Winnipeg, Manitoba. (on CD).

Neale, K.W., Godat, A. and Abdel Baky, H. (2009)," Design Equations for Debonding strains in FRP Strengthening Concrete Structures", Proc., 4th Int. Conference on Construction Materials: Performance, Innovations and Structural Implications, Nagoya, Japan. (on CD).

Neubauer U. and Rostasy F.S.(2001),"Debonding Mechanism and Model for CFRP Plates as External Reinforcement for Concrete Members", In: Proceeding of the International Conference Composites in Construction. Porto, Portugal, Balkema Publishers, Portugal; pp. 467–72.

Oehlers, D.J. and Seracino, R.(2004), *Design of FRP and Steel Plated RC Structures*, Elsevier, UK. 228 pp.

Oehlers, D.J., Liu, I.S.T., Seracino, R. and Ali, M.S.(2004)," Prestress Model for Shear Deformation Debonding of FRP-and Steel-Plated RC Beams", *Magazine of Concrete Research*, V. 56., No. 8., pp. 475-486.

Oller, E., Salcedo, D.Cobo and Mari, A.(2001),"Flexural Strengthening of Reinforced Concrete Beams with Externally Bonded CFRP Laminates", Proc. of Composite in Constructions, Porto, Portugal, Balkema Publishers, pp. 473-478.

Orton, S.L., Jirsa, J.O. and Bayrak, O.(2008),"Design Consideration of Carbon Fiber Anchors", *Journal of Composites for Construction*, ASCE, Vol. 12, No. 6, pp. 608-616.

Pham H. and Al-Mahaidi, R. (2006),"Prediction Models for Debonding Failure Loads of Carbon Fiber Reinforced Polymer Retrofitted Reinforced Concrete Beams", *Journal of Composites for Construction*, ASCE, Vol. 10, No.1, pp. 48-59.

Poulsen, E., Bendtsen, L., Mortensen, J. and Ottosen, N.S. (2001), "Anchorage and Laps of CFRP Strips for the Strengthening of RC Structural Components", Proc. of Composite in Construction, Porto, Portugal, Balkema Publishers, pp. 205-209.

Qiao, P., Chen, F.(2008),"An Improved Adhesively Bonded Bi-Material Beam Model for Plated Beams", *Journal of Engineering of Structures*, Vol. 30,No. 7, pp.1949-1957.

Park, R. and Paulay, T. (1973), *Reinforced Concrete Structures*, Wiley-Interscience, John Wiley and Sons, N.Y., 768 pp.

Rasheed, H. A. and Pervaiz, S.(2002),"Bond Slip Analysis of Fiber-Reinforced Polymer-Strengthened Beams", *Journal of Engineering Mechanics*, Vol. 128, No. 1, pp. 78-86.

Rashid, R., Oehlers, D.J., Seracino, R.(2008)," IC Debonding of FRP NSM and EB Retrofitted Concrete: Plate and Cover Interaction Tests", *Journal of Composites for Construction*, ASCE, Vol.12, No. 2, pp.160-167.

Ritchie, P.A., Thomas, D.A., Lu, L.W., and Connely, G.M.(1991),"External Reinforcement of Concrete Beams Using Fiber Reinforced Plastics", *ACI Structural Journal*, Vol. 88, No. 4, pp. 490-550.

Roberts,T.M.,(1989)"Approximate Analysis of Shear and Normal Stress Concentration in the Adhesive Layer of Plated RC Beams", *Structural Engineer*, Vol. 67, No.12, pp. 228-233.

Rosenboom O. and Rizkalla S. (2008),"Experimental Study of Intermediate Crack Debonding in Fiber- Reinforced Polymer Strengthened Beams", *ACI Structural Journal*, Vol.105, No.1, pp.41-50.

Rosenboom, O. and Rizkalla, S. (2008),"Modelling of IC Ddebonding of FRP-Strengthened Concrete Flexural Members", *Journal of Composites for Construction*, ASCE , Vol.12, No.2. pp. 168-179.

Ross, C.A., Erome, D.M., Tedesco, J.W. and Hughes, M.L.(1999),"Strengthening of Reinforced Concrete Beams with Externally Bonded Composite Laminates", *ACI Structural Journal*, Vol. 96, No. 2, pp. 212-220.

Saadatmanesh, H. and Malek, A.M. (1998),"Design Guidelines for Flexural Strengthening of RC Beams with FRP Plates", *Journal of Composites for Construction*, ASCE, Vol. 2, No. 4, pp. 158-164.

Said, H. and Wu Z. (2008)," Evaluating and Proposing Models of Predicting IC Debonding Failure", *Journal of Composites for Construction*, ASCE, Vol. 12, No.3, pp. 284-299.

Saxena, P., Toutanji, H. and Noumowe, A. (2008),"Failure Analysis of FRP-Strengthened RC Beams", *Journal of Composites for Construction*, ASCE, Vol. 12, No.1. pp. 2-14.

Hashemi, A.H., Rahgozar, R. and Maghsoudi, A.A. (2007), "Finite Element and Experimental Serviceability Analysis of HSC Beams Strengthened with FRP Sheets", *American Journal of Applied Sciences,* Vol. 4, No. 9, pp. 725-735.

Sharif, A., Al-Sulaimani, Basunbul, G.J., Baluch, M.H. and Ghaleb, B.N.(1994), " Strengthening of Initially Loaded Reinforced Concrete Beams Using FRP Plates", *ACI Structural Journal*, Vol. 91, No. 2, pp.166-168.

SIA166, Klebebewehrungen (Externally Bonded Reinforcement). Schweizerischer Ingenieur und Architektenverein SIA; 2003.

Smith, S.T and Teng, J.G. (2001),"FRP-Strengthened RC Beams I: Review of Debonding Strength Models", *Engineering Structures*, Vol. 24, No. 4, pp. 385-395.

Smith, S.T and Teng, J.G. (2002),"FRP Strengthened RC Beam. II Assessment of Debonding Strength Models", *Engineering Structures*, Vol. 24, No. 4, pp. 397-417.

Smith, S.T. and Kim, S.J. (2008),"Shear Strength and Behaviour of FRP Spike Anchors in FRP-to-Concrete Joint Assemblies ", Proceedings (CD Rom), Proc. of Advanced Composite Materials in Bridges and Structures, Winnipeg, Canadian Society for Civil Engineering,Montreal.(on CD).

Smith,S.T.(2009),"FRP Anchors: Recent Advances in Research and Understanding", Proc. of Aisa-Pasific Conference on FRP in Structures , Seoul, South Korea.(on CD).

Takahashi, Y., Sato, Y.,Ueda, T., Maaeda, T. and Kobayashi, A. (1997)," Flexural Behaviour of RC Beams with Externally Bonded Carbon Fiber Sheet", Proc. of the 3rd International Symposium on non-Metallic (FRP) Reinforcement for Concrete Structures, Sapporo, Japan, Concrete Institute Publisher, Vol. 1, pp. 327-334.

Takeda, K., Mitsui, Y., Murakami, K., Sakai, H. and Nakamura, M. (1996)," Flexural Behaviour of Reinforced Concrete Beams Strengthened with Carbon Fiber Sheets", *Composite Part A*, Vol. 27, No.10, pp. 981-987.

Taljsten, B. (1997),"Strengthening of Beams by Plate Bonding", *Journal of Materials in Civil Engineering*, Vol. 9, N.4, pp.206-212.

Taljsten, B. (1999),"Concrete Beams Strengthened for Bending Using CFRP-Sheets", Proc.of the 8th International Conference on Advanced Composites for Concrete Repair. MC Ford (editor), London, UK.(on CD.)

Teng, J.G., Chen, J.F., Smith, S.T. and Lam, L.(2002), *FRP Strengthening RC Structures*, John Wiley and Sons, NY.245 pp.

Teng, J.G., Lu, X.Z., Ye, L.P., and Jiang, J.J. (2004),"Recent Research on Intermediate Crack-Induced Debonding in FRP Strengthened RC Beams", Proc., Advanced Composite Materials in Bridges and Structures (ACMBS), Calgary, Alta., Canada, 1–12.

Teng, J.G., Smith, S.T., Yao, J., and Chen, J.F.(2003),"Intermediate Crack-Induced Debonding in RC Beams and Slabs", *Construction and Building Materials*, Vol. 17, No. 6, pp. 447–462.

Teng, J.G. and Yao, J.(2007), " Plate End Debonding in FRP-Plated RC Beams-II: Strength Model", *Journal of Engineering Structures*, Vol. 29, No.10, pp. 2472-2486.

Teng, J.G., Lam, L.(2001)," Strengthen of RC Cantilever Slabs Bonded with GFRP Strips", *Journal of Composites for Construction*, ASCE, Vol. 5, No.4, pp. 221-227.

Teng, J.G., Yuan, H. and Chen, J.F.(2006),"FRP-to-Concrete Interfaces Between Two Adjacent Cracks: Theoretical Model for Debonding Failure", *International Journal of Solids and Structures* , Vol. 43, No.18-19, pp. 5750-5778.

Tounsi, A., Daouadji, T.H., Benyoucef, S. and Adda bedia, E.A.(2009)," Interfacial Stresses in FRP-Plated RC Beams: Effect of Adhered Shear Deformation", *International Journal of Adhesion & Adhesives*, Vol. 29, No.4, pp .343-351.

Toutanji, H., Zhao, L. and Zhang, Y. (2006),"Flexural Behaviour of Reinforced Concrete Beams Externally Strengthened with CFRP Sheets Bonded with An Inorganic Matrix", *Engineering Structures*, Vol. 28, No.4, pp. 557-566.

TR55 (2003), *Design Guidance for Strengthening Concrete Structures Using Fibre Composite Materials*, Technical report No. 55 of the Concrete Society, UK, 2nd edition; 2004.

Triantafillou, T.C. and Plevris, N. (1992),"Strengthening of RC Beams with Epoxy-Bonded Fiber-Composite Materials", *Materials and Structures*, Vol. 25, pp. 201-211.

Ulaga, T., Vogel, T., and Meier, U.(2003),"Bilinear Stress–Slip Model: Theoretical Background and Significance", Proc., 6th Int. Symp. On Fiber-Reinforced Polymer Reinforcement for Reinforced Concrete Structures, Singapore, pp.153–162.

Varastehpour, H. and Hamelin, P.(1997),"Strengthening of Concrete Beams Using Fibre-Reinforced Plastics", *Material and Structures*, Vol. 30, pp.160-166.

Werner, S., Vasquez, A., Karbhari, V. and Seible, F. (2003)," Poststrengthening of Concrete Slabs: Full-Scale Testing and Design Recommendations", *Journal of Structural Engineering,* ASCE, Vol.129, No.6, pp.743-752.

Wu, Z.S., and Niu, H.D.(2007),"Prediction of Crack-Induced Debonding Failure in R/C Structures Flexurally Strengthened with Externally Bonded FRP Composites", *JSCE, Journal of Materials, Concrete Structures, and Pavements*, Vol.63, No.4, pp. 620–639.

Xiong G.J., Jiang X., Liu J.W. and Chen L.(2007),"A Way for Preventing Tension Delamination of Concrete Cover in Midspan of FRP Strengthened Beams", *J. Construction and Building Materials*, Vol.21, No.2, pp. 402-408.

Yao, J. and Teng J.G. (2007),"Plate End Debonding in FRP-Plated RC Beams-I: Experiments", *Journal of Engineering Structures*, Vol. 29, No.10, pp. 2457-2471.

Yuan, H., Teng, J. G., Seracino, R., Wu, Z. S., and Yao, J.(2004),"Full Range Behavior of FRP-to-Concrete Bonded Joints: A Closed-Form Analytical Solution", *Journal of Engineering Structures,* Vol. 26, No. 5, pp. 553–564.

Yang, Z.J., Chen, J.F. and Proverbs, D. (2003)," Finite Element Modeling of Concrete Cover Separation Failure in FRP Plated RC Beams", *Construction and Building Materials*, Vol.17, No.1, pp. 3-13.

Zaghloul A. (2002),"Behaviour and Strength of CFRP Reinforced Flat Plate Interior Column Connections Subjected to Shear and Unbalanced Moments", M.A.Sc. Thesis, Carleton University, Ottawa, Canada.